A GENERAL FINITE ELEMENT SYSTEM WITH SPECIAL REFERENCE TO THE ANALYSIS OF CELLULAR STRUCTURES

A thesis submitted for the degree of

Doctor of Philosophy in the

Faculty of Engineering of

the University of London

by

Lionel Paul Russell Lyons BSc, MSc, DIC

Imperial College of Science and Technology
London

January 1977

To my relatives

ABSTRACT

A need existed in the Civil Engineering Department of Imperial College for the development of a computer based analysis procedure to provide solutions to a wide range of structural and continuum problems. A general finite element system was developed for the static linear analysis of one, two and three dimensional problems. The computer system incorporates flexible input and output facilities, an extensive library of finite element types, and an efficient solution processor, which are broadly described. The element library includes two new families of elements which are especially suitable for the analysis of thin plates in flexure and cellular structures in flexure and torsion. Details of the elements are given and the validity of the formulations is established by reference to the patch test. The accuracy and efficiency of the elements is demonstrated by extensive theoretical convergence studies and comparisons with model test results.

I N D E X

Page

Page

A C K N O W L E D G E M E N T S

The research described herein was undertaken in the Civil Engineering Department of Imperial College. During the course of the research the author received helpful suggestions from many persons. In particular the author wishes to express his gratitude to the following:

To Professor B.G. Neal for the helpful way in which he accommodated the project as Head of the Engineering Structures Section and Head of Department.

To the late Professor S.R. Sparkes who granted the initial permission for the project to proceed as previous Head of the Engineering Structures Section.

To Dr. A.C. Cassell for acting as supervisor for this work, for his encouragement and guidance throughout the duration of the project. The author is also extremely grateful to him for arranging the initial bursary, without which this work would not have been possible.

To Dr. K.R. Moffatt for his generous and constructive advice on many aspects of this project.

To Miss F. Javadi for her suggestions which were helpful especially during the finite element research and development.

To Messrs. S. Budd, M.R. Lewis, J. Greenaway and other staff of the Imperial College Computer Centre who provided much valuable advice on the computing aspects of this work.

To my many research colleagues, who employed the finite element system for other research and made many helpful suggestions.

To CRD/Freeman Fox and Partners who provided financial support in the initial stages.

To Miss C.D.M. Collins who typed the manuscript and Mrs. R. Thake who typed the tables.

To Mrs. P. Guile who traced the figures.

Finally, but in no way least, to the author's wife who helped and provided support in so many ways.

NOTATION

C_{crit}	diagonal decay criterion
D_n	extensional modulus matrix
D_f	flexural rigidity matrix
E	modulus of elasticity for an isotropic material
E_x, E_y	modulus of elasticity for an orthotropic material in the x and y directions respectively
e	eccentricity of a plate measured from the plane of the plate to the reference plane
F^e	element nodal force vector
I	unit matrix
J	the Jacobian matrix
$\vec{J}$	vector of covariant base vectors
$\vec{j}$	vector of contravariant base vectors
K	structure stiffness matrix
K^e	element stiffness matrix
K'	stiffness matrix with respect to the local axes
L	area coordinates for a triangle
M	flexural moment components
M_x, M_y	flexural moments per unit width perpendicular to the x and y axes, respectively
M_{xy}	twisting moment per unit length perpendicular to the x axis

M_A, M_B	constraint matrices referring to the wanted and unwanted variables respectively
M_{xi}, M_{yi}	nodal moments about the x and y axes respectively
N	shape functions
P	vector of applied nodal loads
q	distributed pressure acting on the surface of an element
T	superdiagonal transformation matrix
T_e	transformation matrix for a plate with eccentricity
t	thickness of plate
u,v,w	global displacement components at a point
W	shape function array
W_A, W_B	partitions of the shape function array which refer to the wanted and unwanted variables respectively
W_c	constrained shape function array
B	strain matrix
γ_{xy}	shearing component of strain in the xy plane
γ_{xz}, γ_{yz}	transverse shear strain components in the xz and yz planes respectively
δ	vector of global displacements
δ^e	vector of global displacements for an element
δ_A, δ_B	element displacements associated with the wanted and unwanted variables

δ^*	vector of displacements and derivatives at any point within an element
ε	strain vector
$\varepsilon_x, \varepsilon_y$	normal components of strain in the x and y directions respectively
ε_y	extensional strain components
ε_s	transverse shear strain components
ε_f	flexural strain components (curvatures)
ζ	natural coordinate in the zeta direction
η	natural coordinate in the eta direction
θ_x, θ_y	rotations of normals to the mid-surface about the x and y axes respectively
θ_z	rotation about the z axis
ν	Poisson's ratio
ν_{xy}	Poisson's ratio for induced strain in the y direction due to a strain in the x direction for an orthotropic material
ν_{yx}	Poisson's ratio for induced strain in the x direction due to a strain in the y direction for an orthotropic material
ξ	natural coordinate in the xi direction
π	external potential energy
σ	stress vector
σ_x, σ_y	normal components of stress in the x and y directions respectively
σ_n	extensional stress components

σ_f	flexural stress components (moments)
$\tilde{\sigma}$	smoothed stress components
σ_B	bending stress
σ_{DB}	distortional bending stress
σ_{DW}	distortional warping stress
τ	shearing stress

CHAPTER 1

GENERAL INTRODUCTION

1.1 INTRODUCTORY REMARKS

In recent years there has been an increasing tendency for designers to employ cellular structural forms in, for example, the construction of offshore production platforms and medium and long span elevated highway bridges. This trend has been primarily due to the economic and functional advantages of cellular structures over other types of structure, together with a greater understanding of the structural behaviour.

The procedure employed for the design of cellular structures, is to first perform a global analysis based on some static linear theory. In the case of plated steel structures, stiffeners and plate panels are then proportioned to exclude instability, or for concrete cellular structures, concrete and steel reinforcement sizes are then checked for allowable stress levels. A global static linear analysis[†] is usually required for consideration of the unserviceability limit states of stress, fatigue, deflection and dynamic response. It is important that the analysis technique chosen enables the design engineer to

---

[†] A global ultimate load analysis is also required but as yet is not feasible with existing analysis techniques using the present generation of computing machines.

carry out an analysis economically with an accuracy sufficient for design purposes.

Cellular structures have been analysed using techniques based on thick orthotropic plate theory,[B7,P8] the grillage analogy,[L7] thin walled beam theory,[V4] folded plate theory,[S9] the finite strip method,[C7] and the finite element method.[Z1] Of these approaches the finite element method is the most general requiring a minimum of assumptions. In principle, it is applicable to the special features encountered in cellular structures, such as varying cross-sectional properties, longitudinal and transverse stiffening, random spacing of diaphragms and supports, and complex loading conditions. For these reasons the finite element method has been employed exclusively in the research into the analysis of cellular structures presented in this thesis.

The basic theory and the application of the finite element method are well established,[B8,F1,M1,Z1] but some detailed development is required for the analysis of certain static linear elastic structures. For example, cellular structures which are subjected to overall flexural and torsional perturbations and are idealized as an assemblage of thin extensional-flexural finite elements. For these idealizations, existing element formulations may not be able to represent such a structure efficiently, and convergence to the correct solution as the mesh is refined may not be guaranteed. Accordingly, this thesis is concerned in part with the development of extensional-flexural elements that are especially applicable for the analysis of cellular structures. The formulation for these elements is based on the Displacement Method with assumed displacement and strain variations. The elements are justified theoretically by the patch test, *vide* section 1.4.

The finite element method is general and can also, in principle, be applied to any other type of structural and continuum problem. Solutions can be obtained for problems that are of arbitrary geometry, and include complex boundary and loading conditions. The finite element formulation can be extended to take account of, for example, dynamic response,[C8] geometric and material non-linearities,[O1,Z1] and problems which may include all of these effects simultaneously. The versatility and power of the finite element method is clearly valuable to engineers for the solution of a wide range of problems.

In an environment such as the Civil Engineering Department of Imperial College, there are many structural and continuum problems to be solved. It is unlikely that these will ever be a mathematical substitute for all model experiments, but compared with other mathematical techniques, the finite element method is capable of making the greatest impact and providing the solution to many problems.

The development of a finite element capability involves four principle subject areas. These are:

(i) Mechanics - derivation of finite element theory for new element models, convergence, spurious mechanisms and material behaviour.

(ii) System engineering - efficient system design and programming techniques for the development of finite element computer system(s).

(iii) Numerical methods - efficient numerical algorithms and error analysis for the computation of the finite element results.

(iv) Applications - comparisons with theoretical and experimental results for the verification of the finite element theory and computer system(s), and for information on the idealization of a problem to produce the required accuracy of results.

Each of these subject areas is necessary to achieve an effective finite element capability as required in the Civil Engineering Department of Imperial College. An effective strategy is the development of a general purpose finite element computer system as opposed to many individual programs. Accordingly, this thesis is in part concerned with the development and implementation of such a computer system which incorporates flexible input and output facilities, an efficient solution technique, and a comprehensive range of finite element types. Furthermore, although at present restricted to static linear analysis, the modularity of the system would permit additional facilities to be easily incorporated and the system could be developed to take account of many other types of structural behaviour.

1.2 FINITE ELEMENT FORMULATION

The analysis of structural and continuum problems by the finite element method, involves approximating a region with an infinite number of variables by an assemblage of sub-regions or elements. Each element may accommodate a simple displacement or stress variation, is of a simple geometric shape, and is connected to adjacent elements by nodes located at the vertices and sometimes along the element boundary. Each node may have several variables, thus the total number of variables for the whole structure is finite and can be solved numerically. The concept of the finite element method was introduced in 1956 by Turner et al.[T4]

A basis for constructing a finite element approximation is the principle of minimum potential energy, which involves one displacement field u. The total potential energy π can be expressed as

$$\pi = \frac{1}{2} \int_V \varepsilon^T D \varepsilon \, dv - \int_V u^T F \, dv - \int_S u^T T ds = \min \tag{1.1}$$

where ε is the strain tensor, D the elasticity tensor, F is the vector of body forces, and T is the vector of surface tractions. The first term of eqn. 1.1 is the strain energy of the structure, whilst the remaining terms are the potential energy of the external loads. Eqn. 1.1 is subjected to the strain displacement relationship

$$\varepsilon = \frac{1}{2}(\nabla u + (\nabla u)^T) \tag{1.2}$$

where ∇ is the gradient operator, and to the geometric (kinematic) boundary conditions

$$u = u_s \tag{1.3}$$

where u_s are prescribed displacements on the surface boundary.

The finite element displacement method involves constructing approximate solutions to eqn. 1.1 by dividing the volume V into elements, and approximating the displacement field u by interpolations within each element.

For equilibrium to be ensured the total potential energy π must be stationary for variations of admissible displacements requiring

$$\Delta\pi = 0 \tag{1.4}$$

where $\Delta\pi$ is the total potential energy increment. It can be shown that this total potential energy increment can be expressed as

$$\Delta\pi = \int_v \Delta\varepsilon^T D\,\varepsilon\, dv - \int_v \Delta u^T F\, dv - \int \Delta u^T T\, ds \tag{1.5}$$

The displacement field within any element can be interpolated in terms of the generalised nodal displacements δ by use of suitable shape functions N as

$$u = N\delta \tag{1.6}$$

By differentiation according to eqn. 1.2, the strains can be expressed in terms of the generalised displacements as

$$\varepsilon = B\delta \tag{1.7}$$

and B is the strain matrix. The displacement and strain increments can be obtained directly from eqns 1.6 and 1.7 as

$$\Delta u = N\Delta\delta \tag{1.8}$$

and

$$\Delta\varepsilon = B\Delta\delta \tag{1.9}$$

Combining eqns 1.4, 1.5, 1.8 and 1.9 after some manipulation leads to

$$\Delta\delta^T(\int_v B^T DB\, dv)\delta - \Delta\delta^T \int_v N^T F\, dv - \Delta\delta^T \int_s N^T T\, ds = 0 \tag{1.10}$$

and setting

$$K = \int B^T DB\, dv \text{ and } F = \int_v N^T F\, dv + \int_s N^T T\, ds \tag{1.11}$$

and dividing through by $\Delta\delta^T$ gives the general form of stiffness equation

$$K\delta = F \tag{1.12}$$

where K is defined as the stiffness matrix and F is the vector of nodal forces. This procedure for the formulation of the force-displacement equations for an element is termed the Displacement Method.

It can be shown that for equilibrium, the total potential energy π is not only stationary but a minimum. Therefore an approximate finite element solution based on the Displacement Method, will always give a value of total potential energy as an upperbound on the true total potential energy of the structure.

In addition to the Displacement Method for the formulation of the force-displacement equations for an element, there are other methods which can be broadly catagorized as the Equilibrium, Mixed, and Hybrid methods. These approaches are summarised in Table 1.1 which was originally compiled by Pian and Tong.[P6] Of all these approaches the Displacement Method is the most simple and general to employ for the formulation of finite elements, and for these reasons has been adopted exclusively for the work in this thesis.

1.3 NUMERICAL INTEGRATION

The integrations of eqn. 1.11 can be highly complex and indeed often impossible to perform explicitly. As an alternative, the integrations can be computed numerically by a weighted summation of the matrix products at the appropriate integration points. Numerical integration is straightforward to implement, makes for clear concise computer programs, and thus considerably reduces the likelihood of a coding error. Furthermore, it does not necessarily reduce computational efficiency, particularly if higher order numerical integration can be avoided. Zienkiewicz et al[Z2] have noted that for certain elements, performance can be considerably improved by using reduced order numerical integration rules. For these reasons numerical integration is an invaluable fundamental technique in finite element work and is employed in the proposed element formulations in this thesis.

1.4 CONVERGENCE AND THE PATCH TEST

Classically, for convergence to the exact solution, the assumed displacement field for an element should be continuous within the element domain and across the element boundaries, and should include rigid body motions. Also as a mesh of elements is refined the strain in each element will become nearly constant, the displacement field within each element should therefore be able to accommodate constant strain. If these classical requirements were to be fulfilled, finite element formulations would be restricted to fully conforming elements only. However, it has recently been established that a necessary and sufficient condition for convergence is that an element should pass the patch test.[I7,I10,S8] This test guarantees convergence for any type of finite element formulation including, for example, non-conforming elements, elements with singularities, and elements with discrete Kirchhoff constraints. Obviously, any element which satisfies both the compatibility and constant strain criteria would always pass the patch test.

The patch test is simple to apply, and involves prescribing displacements to the external nodes of a patch of elements which correspond to a known but arbitrary state of constant strain. If the displacements of the unrestrained internal nodes correspond to the assumed displacement field, and the strains (or stresses) are constant at every point within the patch, the element will converge in the limit. In the author's opinion it is unwise to carry out an analysis with elements that do not pass the patch test for element geometries akin to those required in the finite element idealization.

The patch test can also be employed to test for spurious mechanisms†. Again it is simple to apply and involves restraining a minimum of deflections to prevent rigid body motions, and applying to the patch boundary the force components computed in the previous test. If an element formulation can give a singular assembled stiffness matrix, then it is likely to occur during this test as opposed to later during an important analysis. However, even if this test is passed it may still be possible for mechanisms to occur and propagate throughout a large structure.

The patch testing procedure that was adopted for the finite element research in this thesis can be summarised as follows:

(i) Select a patch of elements with rectangular geometry and unequal size. Prescribe the appropriate displacements for constant strain (stress) at all nodes. If the patch is in equilibrium the reactions at the internal nodes should be zero, and the strains (stresses) should be constant††.

(ii) Remove the prescribed displacements at the internal nodes and check that the displacement results are in accordance with the externally

---

† A perturbation that carries no strain energy

†† Say to six significant figures

prescribed displacement field, and that the strains (stresses) are constant[††] everywhere.

(iii) Constrain sufficient displacements to prevent rigid body motions, apply the forces computed in (ii), and check that the strains (stresses) are again constant[††].

(iv) Repeat (i) to (iii) for various element geometries including, square, parallelogram, trapezoidal and quadrilateral shapes. For a family of elements repeat (i) to (iii) for a mixed patch of elements consisting of several members of the family. Note that this stage is important since some elements may, for example, pass a quadrilateral patch test for constant strain, but contain mechanisms for square element geometry.

(v) If it is expected that the element can accommodate a linear or higher order strain (stress) variation then a higher order or super patch test can be performed. The strain (stress) resultants throughout the patch will now be position dependent in accordance with the chosen strain variation. Repeat (i) to (iv).

---

† A perturbation that carries no strain energy

†† Say to six significant figures

The importance of the patch test both in research and in practice cannot be over-emphasised. The primary roles that it performs are:

(i) It establishes the range of element geometry for which fine mesh convergence is guaranteed for an element.

(ii) To a certain extent it establishes the range of element geometry for which spurious mechanisms are not present.

(iii) To a certain extent it establishes the validity of a computer program if an element is known to pass the patch test.

(iv) It encourages adventurous research, justifies formulations in which variational crimes have been committed, and leads to a great deal of productive thought when a new formulation does not pass the patch test.

For these reasons the patch test is important to all engineers who use the finite element method.

1.5 OUTLINE OF THESIS

Chapter 1 broadly introduces the requirement for the analysis of cellular structures by finite elements, the requirement for a general purpose computer system and finite element theory.

Chapter 2 gives a brief description of the general purpose finite element computer system, and the application thereof to the analysis of two models.

Chapter 3 describes in detail a new family of thin plate flexure elements, and several numerical examples are provided to establish the validity of the formulation.

Chapter 4 describes in detail a new family of extensional elements. These elements are combined with the elements of the previous chapter to form extensional-flexural elements that are particularly efficient in representing the behaviour of cellular structures subjected to overall flexural and torsional pertabations. Several numerical examples are provided to establish the validity of the formulation.

Chapter 5 gives brief conclusions of an overall nature.

CHAPTER 2

IMPLEMENTATION OF THE FINITE ELEMENT COMPUTER SYSTEM

2.1 INTRODUCTION

The finite element displacement method is a powerful analytical technique that can provide the solution to a wide range of complex structural and continuum problems. The basic theory is general and well established[A1,Z1], and the matrix notation is convenient for the implementation of the method on digital computing machines. A virtue of the finite element method is the similarity of computer code required for various types of problems, thus the method can form a basis for the development of a general purpose structural analysis system. However, the computer implementation of the basic algebraic formulations requires many decisions which play a decisive role in the utility and longevity of the final computer system. These decisions require knowledge and experience in structural mechanics, numerical methods and system engineering.

This chapter aims to describe some of the fundamental concepts behind the computer implementation of a general purpose finite element system, and the application thereof to the analysis of the two models. The system, developed by the writer, is referred to as LUSAS which is an acronym for the London University Structural Analysis System. LUSAS has been developed for the linear static analysis of one, two and three dimensional structures, and contains a comprehensive range of elements which permit a wide range of modelling capabilities. The modularity of the LUSAS system enables new capabilities to be introduced quickly and easily. From this point LUSAS forms a sound basis for future research and development requirements within the Civil Engineering department of Imperial College.

2.2 REQUIREMENTS FOR A FINITE ELEMENT COMPUTER SYSTEM

The requirements for a finite element computer system can be summarized as follows:

(i) The development of a computer system is time consuming and laborious so independence from a particular operating system and computer installation must be essayed. Ideally the design of the computer system should be such that it could operate efficiently and be easily implemented on a wide range of computing machines, including for example, the new generation of mini computers.

(ii) Most computing machines now operate in the multiprogramming mode, so it is desirable if the organisation of the computer system is such that it occupies a minimum of central memory.

(iii) The design of the computer system should be modular and the coding clear and concise so that it can be quickly modified, updated or extended to incorporate new facilities.

(iv) The computer system should incorporate a range of external options so that the user has a measure of control over the internal computations.

(vi) The computer system should have a comprehensive range of error diagnostics embedded in the computer code. These diagnostics should provide information on the validity of the data input, and give advice which may guide the user in his assessment of the suitability of the idealization.

(vii) The computer system should be able to solve as wide a range of problems as possible, so that the user, knowing how to use the system for one class of problem, can easily solve any other.

(viii) The versatility of the finite element method enables highly complex structural forms to be analysed, and this can require the solution of a large set of symmetric positive definite load-deflection equations. For large problems the solution of these equations becomes the most time consuming computational step, so it is important that the computer system includes an efficient solution scheme. Iterative procedures have not yet been developed sufficiently for the solution of static linear elastic equations encountered in the finite element method. The main problems with iterative solutions are that they can be slow to converge, require non-productive trial runs to determine the correct acceleration factor and require the complete solution to be repeated for additional load cases. A direct solution scheme would be preferred because it is automatic and trouble free.

(ix) The maintenance of a large computer system is time consuming so facilities should be provided to reduce this burden to a minimum.

2.3 SOME FACILITIES PROVIDED IN THE FINITE ELEMENT COMPUTER SYSTEM

In addition to the usual facilities provided in finite element computer systems the LUSAS system incorporates a number of special facilities some of which are described below.

2.3.1 *Machine independence and requirements*

A high degree of machine independence has been achieved by the use of ANSI[†] fortran for all but a very small part of the computer system. The use of machine dependent functions and machine language subroutines was necessary to obtain a high degree of computational efficiency, but since these have been restricted to only a few critical sections the revisions required for implementation on an alternative computer installation would be minimal.

The LUSAS computer system requires a minimum central memory equivalent to 25K of 60 bit words, within which a wide range of problems can be solved. The computer system has been successfully implemented on CDC 3300/6400/6500 machines using the Scope and Kronas operating systems and FUN, MNF and FTN fortran compilers.

2.3.2 *Modular internal data structure and dynamic vector array*

The internal data is organised in a modular way by the use of a single dynamic vector array which is divided into a string of data records. The lengths of the data records are determined automatically during execution according to the

---

†American National Standards Institute

individual problem requirements, and the positions of the first and last location of each record are recorded in a pointer table. This technique ensures an economical use of the available central memory and enables control information and numerical data to be transferred from one module of subroutines to another by a simple common statement containing the single dynamic vector array. This dynamic array also permits restart facilities to be easily incorporated by a simple transfer statement which saves the whole core image on secondary storage at any stage of the computations. A further advantage is that since the length of the dynamic vector array can easily be adjusted by the user according to the problem size, a minimum usage of central memory can be achieved at all times.

2.3.3 *Modular computer system structure*

The computer system is organised in a modular way by grouping subroutines into overlay modules each of which carries out a logical well defined task. The computer system consists of several of these overlay modules which are stored in a library on permanent disc file and brought in turn into the computer central memory. This overlay procedure allows consecutive modules to occupy the same area of central memory and therefore considerably reduces the total central memory requirements. The minimal core storage requirement of LUSAS has proved valuable in that it can operate within the limits of the Imperial College Instant Turnaround Computer Service of 25K central memory words, and within 18 seconds of central processing time on the CDC 6400 computer.

2.3.4 *Internal user control options*

The user has a measure of control over the internal computations of the computer system by the use of several options. For example, the user can specify the extent of data checking and terminate the problem immediately after the data processing, choose an exact or reduced numerical integration rule for the calculation of the element characteristic matrices and specify the amount and type of output.

2.3.5 *Flexible free format input*

LUSAS has been programmed to accept alphanumeric data input records in a free format field. Free format input has the advantage that it reduces the human effort in the preparation of data, obviates the need for special coding forms, and minimises input errors. Furthermore, free format is convenient for both time-sharing and remote batch access, and gives flexibility in the design of a self-explanatory data input command structure. Since the LUSAS command structure is consistent for all problem types,the user does not have to learn a different command structure for each new problem.

Automatic data generation facilities are incorporated within the computer system, and these permit a wide range of structural forms to be input for analysis with a substantial reduction in the quantity of data input required. It is permissible, at no penalty, for elements or nodes to be numbered with gaps in the numbering. For changes during the design loop or construction sequence it is possible to overwrite areas of existing data and add new data if required without spending excessive human effort renumbering the whole mesh.

This is made possible by the incorporation of a facility whereby the user can specify the order in which the solution of the load-deflection equations takes place. Both the overwrite and specified solution order facilities also provide greater flexibility in the use of the data generation facilities.

2.3.6 *Comprehensive error diagnostics*

As the analysis proceeds the user is kept in communication with the computer system by a comprehensive range of error diagnostics. The computer system checks for sequencing of input, improbable input, wrong input, and issues advisory messages on the validity of the structure idealization and a map of the storage locations used in the dynamic vector array. If a non-fatal error is discovered the computer system will continue to process the remaining data to check for further errors, automatically suppress the solution and exit to the next problem. The total lengths, areas, and volumes of elements and the structure are output as an additional check on the problem idealisation.

2.3.7 *User program interface facility*

At any stage during the processing of the data input the computer system can be instructed, by the use of simple commands, to receive data from external fortran subroutines supplied by the user. Thus the integral system data generators can be supplemented by special purpose data generators which enable the user to quickly tackle complex modelling of any mathematically describable structure.

External subroutines can also be supplied to post-process the stresses, displacements and reactions, and to output these results in an alternative format which may be more suitable for the user's particular requirements. It would also be possible to write external subroutines that could convert the computer system for the analysis of simple non-linear or dynamic problems and multilevel substructure analysis.

2.3.8 *Flexible output facilities*

The user can suppress or call for certain areas of the output from an analysis, for example, the averaged nodal point stresses. The output of results can be either stress or force components and these can be relative to either the local element axis or the global system axis. The output of results for LUSAS has been designed to be compact, clear and self-explanatory.

2.3.9 *Integral maintenance facilities*

The maintenance of a computer system is time consuming and is required when changes occur in the software or hardware of a particular computer installation, or if a failure occurs at the installation or in the computer system code. LUSAS contains integral diagnostics which protect the user from software or hardware failures. For example, when data is retrieved from secondary storage certain variables are always tested to ensure that their values lie within an expected range. If a failure does occur the progress of the computations can be easily monitored by the systems engineer by the use of the integral maintenance options and the failure point can be quickly located and corrected.

2.3.10 *Incorporation of new facilities*

The modular structure of the internal data and computer system enables existing facilities to be quickly modified and updated to take account of unforseen applications, and new facilities to be easily added as new techniques become available.

2.4 DESCRIPTION OF THE COMPUTER SYSTEM

The computer system[L8] is divided into nine primary overlay modules, one of which is optional. Each overlay module, which consists of a group of subroutines that carry out a well defined task, is called in turn into the central memory by a simple main program, which remains in core throughout problem execution and contains the single dynamic vector array, *vide* Fig. 2.1. The length of the dynamic vector array is determined by two statements in this main program, and is easily adjusted by the user to suit each particular problem. The first four overlays process the data input, the fifth computes the segment lengths of the dynamic vector array required for the problem, the sixth retrieves data and computes the characteristic matrices for each element, the seventh assembles the structure stiffness matrix and solves the displacements for each load case by the frontal technique[I1], and the eighth uses the displacements to compute and output the stresses for each element, and the displacements and reactions for the structure. The ninth overlay module is optional and can be supplied by the user to post-process the results according to his particular requirements. The sixth overlay module is served by a subset of thirteen secondary overlay modules each of which contains a family of finite element subroutines for each particular structure type. A simplified flow chart of the primary and secondary overlay modules of LUSAS are given in Fig. 2.2 and the subdivisions of the dynamic vector during each phase of the analysis are shown in Figs 2.3 to 2.7.

2.4.1 *Data processors*

The data input for LUSAS has been designed to be compact, self-explanatory and in a free format field. A free format subroutine and a data generation subroutine reside in the central memory during the data processing phase. The alphanumeric characters in each column of an input record are read by the free format subroutine and assembled into complete numbers, words and special characters. The free format routine therefore accepts any combination of numbers, words and special characters and provides for flexibility in the design of the input record formats.

The first data input card for any problem must be a PROBLEM header card which is followed in turn by chapters of numerical data each of which is identified by the appropriate header cards. Any number of problems can be solved in the same computer run, and the last card of a series of problems must be and END card. The problem card is followed by the specification of the STRUCTURE type, the UNITS to be used throughout the problem and any OPTIONS which may be required by the user. The first chapter data input requires the header card < type > ELEMENT NODES followed by a list of element numbers and node numbers for that element type. For structures which are idealized with mixed element types the header card and numerical data are repeated for each element type. A list of the element types for the various classes of structure which are currently available in LUSAS are given in Appendix 1. The node numbers of any element can be overwritten by the node numbers of a new element even if the number of nodes is different, and gaps can be left in the element numbering sequence if required with no penalty in central memory requirements.

The main generation routine which resides permanently in the central memory during the data processing phase, can be used to generate data for any input chapter. This scheme, hereafter referred to as incremental generation, is based on the ASKA[A7] topological generation procedure for elements, but is more powerful, applies to all types of data input records, and has been reorganised in a simplified format as follows:

FIRST	n_1	...	n_m, R
INC	$\Delta_1 n_1$	...	$\Delta_1 n_m$, R_1
II	$\Delta\Delta_1 n_1$	...	$\Delta\Delta_1 n_m$
INC	$\Delta_2 n_1$	...	$\Delta_2 n_m$, R_2, $\Delta_2 R_1$
II	$\Delta\Delta_2 n_1$	...	$\Delta\Delta_2 n_m$
INC	$\Delta_3 n_1$	...	$\Delta_3 n_m$, R_3, $\Delta_3 R_1$, $\Delta_3 R_2$
II	$\Delta\Delta_3 n_1$	...	$\Delta\Delta_3 n_m$
III	$\Delta\Delta\Delta_3 n_1$	...	$\Delta\Delta\Delta_3 n_m$
I3I2	$\Delta_3\Delta_2 n_1$	...	$\Delta_3\Delta_2 n_m$
INC	$\Delta_4 n$	...	$\Delta_4 n_m$, R_4

where

n_m are a list of integer or real numbers

$\Delta_i n_m$ are a list of increments to be added at the ith level

$\Delta\Delta_i n_m$ are a list of increments of increments to be added at the ith level

$\Delta\Delta_i n_n$ are a list of increments of increments of increments to be added at the ith level

R_i is the number of repetitions at the ith level

$\Delta_j R_i$ is the increment at the jth level to be added to the repetition at the ith level

This scheme has been previously described with examples by Lyons, Cassell and Hobbs[L6] and can generate, for example, an array of element and node numbers, a stack of node coordinate lines with quadratic or cubic spacing, and element properties, support conditions and loading which may have linear, quadratic or cubic variations.

The solution of the structure load deflection equations in LUSAS is carried out by a random access frontal solution technique. This solution technique, as with many others, requires that the equations are reduced in a certain order to keep the front width (akin to bandwidth), and thus the total number of arithmetic operations, to a minimum. For the frontal solution, this is controlled by the order in which the elements are presented. A useful facility is provided in LUSAS in the next data chapter, whereby the ordering of the elements may be controlled by the user according to any one of the following procedures.

(i) For most structures it is possible to number the elements across the narrow direction of the structure and the solution can be carried out according to ascending element order. In this case the header card SOLUTION ORDER ASCENDING is inserted or assumed as the default procedure if no card is provided.

(ii) For certain structures it may be convenient for the solution to be carried out according to the order in which the elements were presented or generated. In this case the header card SOLUTION ORDER PRESENTED is inserted.

(iii) For other structures it may be convenient to assign certain numbers to elements to simplify the data input for automatic generation or to add new element numbers for mesh refinement without renumbering the whole mesh. In this case the header card SOLUTION ORDER is inserted and the element solution order can then be specified as data. The data supplied by the user, is in accordance with the horizontal looping facility which expresses the series

$$i,\ i + k,\ i + 2k,\ i + 3k,\ \ldots\ j,$$

where i and j are positive integer element numbers and k is a positive or negative integer, as

i, j, k

As a special case, the series may consist of only i.

The next data chapter is for the specification of the coordinates of each nodal point and the header card required is NODE COORDINATES. The input that follows this header card can include numerical data such as a node number and its coordinates punched on each card , alphanumeric data as required by the coordinate generation schemes provided in LUSAS, or numerical data as required by a user-supplied subroutine. The incremental generation scheme mentioned previously can be employed here, and can generate, for example, lines of nodes with equal, quadratic or cubic spacing between the nodes with straight, quadratic or cubic shapes. The coordinates of any node can be overwritten by new coordinates, dummy nodes not associated with elements can be specified, and gaps can be left in the node numbering sequence if required with no penalty in central memory requirements. These facilities have proved valuable for mesh refinement and give flexibility in the generation of data.

The main feature of the coordinate generation facilities is the Zienkiewicz and Phillips' scheme for curvilinear mapping of parabolic quadrilaterals[Z3]. This scheme allows a unique coordinate mapping of curvilinear and cartesian coordinates in two and three dimensions by using the shape functions of the eight node isoparametric quadrilateral element.[Z1] The input data required is the header card QUADRILATERAL SPACING, the node number and coordinates of each corner point, and the coordinates of a point along each side of the quadrilateral. The side points control the grading of the mesh in any direction and can distort the quadrilateral to have curved parabolic sides. It should be noted that the side points are not necessarily coincident with a node. If the coordinates of the side points are not specified the computer system assumes the coordinates for the centre of each side and the corresponding mesh generated is a quadrilateral with straight sides and equal spacing. The distortion of the quadrilateral can be quite severe, even to the point of two sides lying on a straight line. However, corner angles must not be greater than 180° otherwise non-uniqueness of mapping may result. This arrangement of data input for curvilinear mapping has been described previously by Lyons, Cassell and Hobbs.[L6]

The next data chapter is for the specification of element elastic properties or rigidities and requires header cards such as PLATE PROPERTIES or BEAM RIGIDITIES. The horizontal looping facility is employed here for the specification of several elements with identical properties or rigidities. The incremental generation facility can also be employed and can be useful for generating element properties or rigidities that have linear, quadratic or cubic variations. Overwriting is permitted, as is the specification of dummy element properties or rigidities.

The penultimate data chapter is for the specification of support node conditions and requires the header card SUPPORT NODES. The support conditions for each variable at a node may be specified as free (F), restrained (R) with a prescribed displacement of zero or a positive or negative value, and spring (S) with a positive spring stiffness constant. The horizontal looping facility is employed here for the specification of several nodes with identical support conditions. The incremental generation facility can also be employed and can be useful for generation prescribed displacement or spring constants that have linear, quadratic or cubic variations. Overwriting is permitted, as is the specification of dummy support nodes.

The ultimate data chapter is for the specification of the load conditions and requires the header card LOAD CASE. The computer system will accept any number of load cases providing there is sufficient central memory available. The load types incorporated at present are concentrated loads, uniformly distributed loads, constant body forces and body force potentials. The horizontal looping facility is employed here for the specification of several nodes or elements with identical loads. The incremental facility can also be employed for the generation of loads that have linear, quadratic or cubic variations. If the same node or element number is specified more than once the computer system takes the sum of these values as the load case. The specification of dummy loads is permitted.

The data card following the last load case item must be an END card or a PROBLEM and for the next problem. However, both of these cards instruct the computer system to output a summary of the data and, providing there are no errors, to proceed with the sequence of computations required to solve the problem.

After the data input has been read and stored in the dynamic vector array, *vide* Fig. 2.3 to Fig. 2.5., the computer system computes the segment lengths of the dynamic vector required for the pre-solution, solution and post-solution phases. For the information of the user a map of the various segment lengths is provided, together with the maximum length of dynamic vector required. If the length of the dynamic vector specified by the user is insufficient for the problem, the computer system issues an error message, terminates execution and exits to the next problem.

The computer system now proceeds to form a list of active node numbers, equation numbers and front destinations, and a list of active support node numbers as shown in Fig. 2.3. The array of element node numbers is coded to contain the appearance code numbers for the node and variables, and the array of node coordinate numbers is coded to include the number of variables at each node and the position of the node in the array of active node numbers. All of these arrays include single computer words which contain several integer values. This technique, referred to here as integer compaction, is shown in Fig. 2.5 and saves valuable central memory without any significant effect on the computational efficiency of the computer system. The compact structure of the data storage scheme permits all data for a large number of elements to be stored in the central memory, as opposed to secondary storage devices. This has the advantage of high speed data retrieval during the formation of the individual element records.

For a dynamic vector array size of 27K, the maximum number of elements that the computer system could accommodate with respect to data storage requirements would be, for example:

4	node Isoparametric plane stress elements	≃	1900
4	node ISOBEAM flat shell elements	≃	1400
8	node semiloof doubly curved shell elements	≃	600
20	node Isoparametric solid elements	≃	300

2.4.2 *Pre-solution processor*

The pre-solution processor simply retrieves data stored in the dynamic vector array and assembles each of the individual element records in turn. Each element record includes arrays of the element node numbers, number of variables at each node, node destinations, support node destinations, node appearance codes, node coordinates, elastic properties, thermal properties, support values, support codes whether free,restrained or spring, constant body forces, body force potentials, nodal initial stresses and strains, node numbers for each variable, equation numbers, front destinations and variable appearance codes, *vide* Fig.2.3. This data is then transferred to the appropriate secondary element overlay module where the element stress matrices are computed and written onto tape, the stiffness matrix is computed, and the element load vector due to constant body forces and body force potentials is calculated. Control is then returned to the primary overlay module where the stiffness matrix and element load vectors are modified in accordance with the support conditions. The concentrated loads for nodes making their last appearance are added into the element load vector, and the second element record which contains the solution data, including the element load vector, is transferred to tape followed by the element stiffness matrix.

2.4.3 *Random access front processor*

The computational procedure of the finite element displacement method requires the solution of the matrix equation

$$K\delta = P \qquad (2.1)$$

where K is the coefficient or structure stiffness matrix, δ is the vector of unknown displacements, and P is the vector of applied loads. This matrix equation constitutes a set of perhaps several thousand simultaneous equations, the coefficient matrix of which is symmetrical, positive-definite and banded about the diagonal. Theoretically the various direct solution algorithms that have been developed to date are similar, but their computer implementation differs significantly. Thus the principle scientific discipline involved is that of system engineering, and it is in this area that considerable research has been carried out in the quest for efficient equation solvers.[F2,I2,M3,M4,W1]

The algorithm which solves a set of linear algebraic equations with the minimum of arithmetic operations is Gaussian elimination, or one of its closely associated techniques. For symmetric positive-definite equations, Gaussian elimination is guaranteed to be numerically stable irrespective of the order in which the equations are eliminated, and with floating point arithmetic a pivotal search is unnecessary.

Virtually all structure stiffness matrices, as found in the finite element method, are not only banded about the diagonal but exhibit areas of sparsity within this band. The fundamental requirement for the efficient solution of these structure equations is to avoid superfluous arithmetic operations on the zeros. Basically there are two ways of handling sparsity:

(i) In the data structure by exluding all zero coefficients from storage.

(ii) In the computations by excluding all operations on zero coefficients.

Each approach has its advantages, but it is not clear which is to be preferred in general.

An elegant solution procedure for avoiding the zero coefficients within the band of a structure stiffness matrix is frontal technique,as developed by Irons[I1] and Bamford[M1]. The computer algorithm is based on Gaussian elimination and takes advantage of both the symmetry and sparsity found in structural stiffness matrices. Large variations of local bandwidth are handled in a compact area of central memory, and numerical operations on zeros are essentially avoided. Consequently, the method is particularly efficient for finite elements with side nodes, or for bifurcated structures, when re-entrant sparseness occurs. The solution proceeds according to the ordering of the elements for which there is an optimum, and the node numbering is irrelevant. In general, element ordering is more natural and straightforward to use than node ordering, especially when a computer system is enhanced with a reordering option. For these reasons, the frontal technique has been incorporated into the general finite element computer system described here, together with a user specified solution order facility. Irons[I1] has presented a detailed description and Fortran listing of the frontal technique and it is from this that the present solution routine has been developed.

The principle of the frontal solution is indicated by the Gaussian algorithm itself. The elimination of δ_r for row r of a system of equations leads to a modification of the coefficients in the remaining rows according to

$$K_{ij}^* = K_{ij} - \frac{K_{ir}K_{rj}}{K_{rr}} \tag{2.2}$$

$$P_i^* = P_i - \frac{K_{ir}P_r}{K_{rr}} \tag{2.3}$$

where the modifications are only for non-zero admissible pairs i, j. The elimination reduces the matrix K to an upper triangular matrix. The terms K_{ij} for the overall stiffness matrix and P_i for the overall load vector are the sum of the individual element contributions, and need not be fully summed when the above modification is executed. However, it can be seen from the expressions that the terms K_{ir} (which is equal to K_{ri} by symmetry), K_{rj}, K_{rr} and P_r of row r, must be fully summed before δ_r can be eliminated. It therefore does not matter in which order the element contributions are added to K_{ij} and P_i, or in which order the δ_r are eliminated provided that row r is fully summed. Also the only variables required in the central memory are the active coefficients of K_{ij} and the active terms of P_i which are to be modified. The coefficients of K_{ij} form a densely populated triangular array which excludes the zeros outside the band and this is often smaller than the corresponding triangle of coefficients required for a band algorithm.

These coefficients continually change but the frontal technique avoids disturbing the active variables residing in core by using the rows and columns vacated by recently eliminated equations. Thus the frontal technique continuously alternates between the assembly of the element contributions to form the overall stiffness matrix, and the elimination of completed equations. The reduced equations are saved on secondary storage to be retrieved later for the back-substitution phase. The dimension of the triangle of stiffness coefficients is termed the front width, and this changes as the solution proceeds. It is important that the element stiffness matrices and load vectors are introduced into the central memory in an optimum order to keep the front width to a minimum. The maximum area of central memory required for a solution is dependent on the maximum front width.

The back-substitution phase reads the element records and reduced equations from tape in reversed order and calculates the displacements according to

$$\delta_n = \frac{P_n^*}{K_{nn}^*} \qquad (2.4)$$

and $$\delta_i = \left(P_i^* - \sum_{j=i+1}^{j=n} K_{ij}^* \delta_j\right) / K_{ii}^* \quad \text{for } i < n \qquad (2.5)$$

where n is the total number of unknown displacements.

The housekeeping for the frontal solution procedure can be briefly illustrated by reference to the simple structure shown in Fig. 2.8, which has only one variable at each node.

Element number 1 with variables 1,2,6 is introduced into the central memory and its coefficients are assembled into locations in the overall stiffness and load vectors in accordance with its destination vector (1,2,3). Since variable 1 appears for the last time it is eliminated and the reduced equation preserved on backing storage. The positions of the active variables remaining in core are [0,2,6].

Element number 2 with variables 2,3,7 is now introduced. Variable 2 already has a place in the second location, variable 3 is new so is given the vacant place in the first equation, and variable 7 is also new so is given a place in the fourth location. The destination vector for element number 2 is thus (2,1,4). Since variable 3 appears for the last time it is eliminated and the reduced equation preserved on backing storage. The position of active variables remaining in core are [0,2,6,7].

Finally, element number 3 with variables 2,7,6 is introduced and since all of these variables are already active the destinations are obviously (2,4,3). All of these variables appear for the last time and accordingly are eliminated.

From the preceding example it can be seen that the maximum size of problem is limited by the amount of central memory available for the overall stiffness and load vector arrays. The random access front processor implemented in LUSAS is organised to provide a maximum amount of storage for these arrays, by segmenting the dynamic vector array for each phase of the solution as shown in Fig. 2.6. The elimination phase for the first solution is critical and the only arrays used in addition to the overall stiffness and load arrays are the arrays for the current active nodes and variables, the array for element record 2 which consists essentially of element loads, and the buffer array which is used for element stiffness matrices and reduced equation coefficients consecutively. The latter action is possible since the element stiffness coefficients are immediately assembled into the overall stiffness matrix as they appear in core, leaving the equation buffer free to receive the next set of reduced equation coefficients. For elements with large stiffness matrices, for example, the 32 node isoparametric solid element with 4656 stiffness coefficients, the buffer length is minimised by fragmenting the stiffness record into several shorter records. With these core saving arrangements up to 95% of the dynamic vector array is available for the overall stiffness matrix and load vectors.

The frontal solution processor implemented can take account of elements with different numbers of variables at each node. This has been achieved by operating with the destination and appearance code for each variable instead of each node of the element. This approach is more efficient in that there is a greater likelihood of finding a vacant position in the front for a single variable than a vacant position for a node with a particular number of variables. Also this approach has greater flexibility and can accommodate, for example, the coupling of individual variables. The implementation of such facilities involves modifications to only the pre-processing routines which must determine the appropriate destination and appearance codes of each variable.

Every tape reading operation after the initial forward elimination process, must access the records in reversed order.

The original version of the frontal program required the computer action BACKSPACE-READ-BACKSPACE, but this is costly both in peripheral and central processing time†. In the present program this action was avoided by a simple modification which involves the use of random access disc transfers. The frontal solution procedure requires the tape records to be accessed sequentially by both forward and backward reading. If during the creation of a series of records ,the random access position of each record is stored with the following record, and so on; then the series of records can be read backwards because as each record is read the position on disc of the next record is given. This procedure is completely dynamic because only the exact length of each record, which varies throughout the solution, is transferred to disc. This procedure has the advantage of being straightforward to implement and does not require the use of further valuable central memory locations.

The computational efficiency of the front processor was improved further by the incorporation of a machine code subroutine of the innermost reduction loop.

The success of implementing both the random access and machine code subroutine facilities can be judged from the following example. The problem was a shell roof which was idealised with a mixed mesh of beam and shell elements, and required the solution of 1512 equations with a maximum front width of 108. The computer

---

†Of the order of 30x the cost of a READ statement for a CDC6500 computer

used was a CDC6500 and the total problem costs included data pre-processing, the assembly of the element characteristic matrices, the solution of equations and the output post-processing phases. A comparison of computer costs with and without the machine code and random access facilities are given in Table 2.1.

The refined diagonal decay criterion for the estimation of round-off damage, as suggested by Irons, was incorporated into the frontal solution. During the forward elimination process the diagonal stiffness terms decrease monotonically but remain positive. If the final pivotal value is small compared with the proceeding values ill-conditioning would be suspected. In the program each time a diagonal term is modified during the elimination, its initial value squared is accumulated into an extra overall load vector. The criterion is that ratio of the square root of this sum divided by the final value of the diagonal should not exceed a certain value

$$C_{crit} = \frac{\{\Sigma(K_{ii})^2\}^{\frac{1}{2}}}{K_{ii}\ (\text{final})} \tag{2.6}$$

If C_{crit} is greater than 10^4 then ill-conditioning is suspected but the solution continues. If C_{crit} is greater than 10^{11} fatal ill-conditioning is assumed, and the solution is terminated. The program prints out the node number and variable which caused the problem to enable the user to perhaps correct the fault.

2.4.4 *Post-solution processor*

The post-solution processor retrieves from tape, the overall solution vector of displacements, and calculates and outputs the element stresses, displacements at each node and reactions to earth, for each load case. There are several output options available which may be required by the user including, element stresses with respect to the element local coordinates, as opposed to system coordinates, averaged nodal stresses, and force components as opposed to stress components. The output is concise and self-explanatory with many texts.

External user supplied subroutines can be incorporated into the computer system to post-process and output the results in accordance with the user's particular requirements. Since the element records, reduced equations and element results for a problem are stored on disc, it would be possible for the user to update the element load vectors or stiffness matrices and resolve. This would enable simple non-linear or dynamic problems to be tackled.

2.5 THE FINITE ELEMENT LIBRARY

The finite element types implemented in the computer system include joint elements, spar and beam elements, extensional elements, flexural elements, axi-symmetric elements, extensional-flexural plate elements, doubly curved thin shell elements, doubly curved thick shell elements and solid three dimensional elements. A list of the element types currently available, together with, details of the permitted data input is given in Appendix 1.

2.5.1 *Standard elements*

The characteristic matrices of nearly all of the standard elements incorporated in the computer system are computed using numerical integration. A detailed description of most of the elements can be found in the text by Zienkiewicz[Z1].

2.5.2 *Special elements*

LUSAS contains several elements that have been specially developed for use in the analysis of plates in flexure and cellular structures. These are:

(i) A simple quadrilateral element ISOFLEX 4† which is efficient for the analysis of thin plates in flexure.

(ii) A simple triangular element ISOFLEX 3† which, in conjunction with the elements of type (i), is suitable for use in the analysis of thin

---

†See Chapter 3

plates in flexure which require mesh refinement or have irregular boundaries.

(iii) A curvilinear quadrilateral element ISOFLEX 8[†] which is efficient for the analysis of thin plates in flexure with curved boundaries.

(iv) A curvilinear triangular element ISOFLEX 6[†] which, in conjunction with the elements of type (iii), is suitable for use in the analysis of thin plates in flexure which require mesh refinement or have irregular boundaries.

(v) A quadrilateral extensional-flexural element ISOBEAM 4[††] which is efficient in representing the overall behaviour of cellular structures in flexure.

(iv) A triangular extensional-flexural element ISOBEAM 3[††*] which, in conjunction with the elements of type (v), may be suitable for the analysis of skewed cellular structures in flexure.

(vii) A curvilinear quadrilateral extensional-flexural element ISOBEAM 6[††] which in addition to being very efficient in representing the overall behaviour of cellular structures in flexure, is particularly suitable for curved structures

---

[†] See Chapter 3, [††] See Chapter 4

*It should be emphasised that although the formulation is given, this element has not been tested numerically or for use in rapidly varying stress fields.

(viii) A curvilinear triangular extensional-flexural element ISOBEAM 5[††*] which, in conjunction with elements of type (vii), may be suitable for use in the analysis of skewed cellular structures in flexure.

2.5.3 *Incorporation of new elements*

New improved finite element formulations are continually appearing in the literature. The flexibility and modularity of the computer system is such that new elements can be quickly and easily incorporated and tested. Since the computer system is based on a dynamic vector array principle there are no limitations to the maximum number of element nodes, size of stiffness matrix, number of geometric properties, and number of material properties, providing a sufficient area of computer central memory is available. Also the number of variables can vary from node to node but must be in the range 0 to 7 inclusive.

---

†† See Chapter 4

* It should be emphasised that although the formulation is given, this element has not been tested numerically

2.6 VERIFICATION OF THE COMPUTER SYSTEM

The verification of LUSAS has been made by reference to results obtained from the patch test,[I7,I10] classical theory, other numerical techniques, and model experiments. This section briefly describes some applications of LUSAS.

2.6.1 *Doubly curved arch dam under hydrostatic pressure*

The El Altazar dam was the subject of theoretical and model studies at Imperial College.[W7] Details are shown in Figs 2.9 and 2.10.

The dam and valley socket was idealized with hexahedronal and pentahedronal elements, Fig. 2.11, and analysed using LUSAS. The results given for displacements and stresses, Figs 2.12 and 2.13, compare well with an alternative finite element analysis[B4] which employed the Ahmad thick shell element.

2.6.2 *The analysis of a thin intersecting cylindrical shell problem - T-joint*

The analysis of thin intersecting cylindrical shells presents problems in finite element analysis because of the geometric discontinuity at the junction. Early attempts included idealizations comprised of flat extensional-flexural elements with three translations and three rotations as the nodal variables.[G3] It was found that a large number of these elements were required to represent the curvature of the cylinders, and that inaccuracies occurred at the junction due to connecting artificial extensional rotation variables in one cylinder, to the flexural rotation variables of the other cylinder. Recently however, Irons[I4-I6] had developed a doubly curved thin shell element which overcomes these earlier difficulties, and this element has been incorporated in LUSAS.

The T-joint model, Fig. 2.14, was tested experimentally[C9] and analysed using LUSAS. For the analysis the model was idealized as an assemblage of 60 thin shell elements[J1] Fig. 2.15, and this coincides with a mesh used by other investigators. It can be seen that the finite element and experimental results are in close agreement.

2.6.3 *Other models*

Further models that have been analysed using LUSAS include a straight three cell box girder bridge model (section 4.8.5), a straight multicell bridge model (section 4.8.6), a curved single cell box girder bridge model (section 4.8.7), a shear wall,[L1] a stiffened diaphragm,[D3] a stiffened plate,[D1] and a composite bifurcated bridge.[O2]

2.7 CONCLUSIONS

A general computer system has been developed which can be used for the analysis of a wide variety of linear elastic structures. The computer system incorporates flexible free format input facilities which include powerful automatic data generation and comprehensive error diagnostics, an extensive range of finite element types, an efficient solution processor, and flexible output facilities. Its practical application has been illustrated by reference to the analysis of two models.

CHAPTER 3

THIN PLATE FLEXURE ELEMENTS

3.1 INTRODUCTION

In the finite element analysis of plates with arbitrary boundaries or shells comprised of flat plates, triangular and quadrilateral flexural elements having three variables at the vertices are commonly used. Elements with this simple nodal configuration have the advantage of being readily incorporated into computer systems which accept only elements with a constant number of variables at each node. They can also be used in conjunction with the standard grillage beam element for the analysis of, for example, a ribbed plate.

Elements with a linear stress response

$$M = f(1,x,y) \tag{3.1}$$

are known to have a good performance. A conforming plate flexure displacement element, with only the lateral displacement and its two first derivatives at the vertices, cannot accommodate this linear stress response because there is only sufficient information to define a linear variation of the tangential rotation along each side as opposed to the required quadratic variation. It is possible that a hybrid formulation could succeed, but as an alternative, a higher order element could be created by the introduction of a midside node at which a tangential rotation is specified.[B2,A4,R1] This additional rotation variable would have the minor disadvantage of producing an element with different numbers of nodal variables, but this is preferable to the use of higher order derivatives, which require special treatment for abrupt changes of plate thickness or properties. If the departure from linearity of the midside tangential rotation is used instead of the absolute value [R1], then such an element can still be used in conjunction with a standard grillage beam element, simply by constraining this variable to zero in the presence of a beam. A midside node can also be used to define curved element boundaries and this gives an improved geometric definition for many structures.

A unified formulation which includes triangular and quadrilateral elements with the aforementioned nodal configurations does not exist. Furthermore, nearly all individual formulations to date fail to satisfy the requirements for thin plate flexure elements.

The classical requirements for thin plate flexure elements are that the assumed displacements should be continuous within each element and across the element boundaries, and should provide every state of constant curvature including rigid body motions. Also, the Kirchhoff thin plate theory, in which normals to the middle surface remain straight and normal to the mid-surface during deformation, is required to exclude shear deformations. In the displacement formulation, if these requirements are fulfilled then the principle of minimum potential energy is valid, and convergence to the correct solution is ensured. However, Irons[I8] has shown that it is impossible to specify simple polynomial expressions for shape functions that ensure both displacement (C^0) and slope (C^1) continuity, when only three variables are prescribed at the element vertices. Consequently earlier attempts to produce satisfactory elements included formulations which either introduced complex functions to satisfy slope continuity, or violated this requirement precipitating precarious convergence characteristics. For example, the fully conforming triangles of Bazeley et al [B1] and Clough and Tocher[C4], and the fully conforming quadrilaterals of Clough and Felippa[C2] and Veubeke[V1,B3], all require complex computer code, whilst the simple non-conforming triangle also by Bazeley et al has limited convergence properties.

The hybrid method, pioneered by Pian[P4], avoids the difficulties encountered with the conventional displacement formulations, and some of the more notable work has been carried out by Allman[A4,A6], Severn and Taylor[S6], Wolf[W6], and Torbe and Church[T2]. However, hybrid elements are prone to spurious mechanisms[†C3,W6], and the formulation is often cumbersome, but it is generally recognised that they are capable of providing accurate solutions[P5].

In recent years, it has been established that a necessary and sufficient condition for convergence to the correct solution is that an element should pass the patch test.[I7,I10,S8] This test in itself does not remove the difficulties encountered with

---

† A purtabation which carries no strain energy

the formulation of plate flexure elements, but it does broaden the search to include for example, non-conforming elements, elements with approximately integrated energy, and elements in which the Kirchhoff requirement for thin plates is imposed discretely. Regrettably there are relatively few simple elements which pass the patch test.

Irons and Razzaque[I9,R1] have developed synthetic versions of Allmans triangular elements which are based on an incompatible displacement formulation with smoothed derivatives. These elements pass the patch test and are coded into a shape function subroutine, but the higher order element cannot accommodate curved boundaries.

A radical approach for the formulation of plate flexure elements is to proceed initially from the basic equations of elasticity and allow shear deformations to occur.[F4,K1,M6,S7,T2,U1] † The Kirchhoff hypothesis for thin plates is then invoked by applying constraints at discrete points within the element domain, for example, at the nodes, the boundaries, or the Gauss points.[I3-6,W5] Irons and Razzaque[I3,R2,B2] used this technique to formulate a higher order quadrilateral with a good performance, but this element does not pass the patch test for quadrilateral geometry.

In this chapter a formulation is given for a family of thin plate flexure elements, hereafter referred to as the ISOFLEX elements. These elements belong to the second generation

---

† Note also the extensive work based on Ahmads' stacked shell element.[A3,B4,C6,H1,P3,R2,T1]

of isoparametric elements and have an extensive ancestry. The formulation is based on the three-dimensional formulation originally given by Ahmad et al[A3], uses reduced integration techniques presented by Zienkiewicz et al[Z2], and employs an essential modification to invoke the Kirchhoff normality hypothesis at discrete points within the element, similar to that developed by Irons.[I3-6] The ISOFLEX elements may have tapering thickness and curved boundaries, and have the simplest nodal configurations Fig.3.1, which allow the standard grillage beam element to be incorporated into an idealisation. They fulfil the requirements for convergence because even a mixed mesh of triangular and quadrilateral elements of arbitrary geometry passes the patch test. Furthermore, there are no limitations such as low rank or spurious mechanisms. The performance of the ISOFLEX family is demonstrated by extensive convergence studies and comparisons with various classical solutions, and it is shown that the elements can be used with confidence even in rapidly varying stress fields. The ISOFLEX elements are a unified formulation which can be easily implemented from a single compact shape function subroutine, and compared with previous elements they are also computationally efficient.

3.2 REQUIREMENTS FOR THIN PLATE FLEXURE ELEMENTS

The requirements for thin plate flexure elements may be summarised as follows:

(i) The elements should be capable of being used in triangular and quadrilateral form and should be capable of representing tapering thickness and curved boundaries when necessary. In general quadrilateral elements are preferred requiring less data preparation and computer output and for a given number of variables can give greater accuracy. Triangular elements are occasionally required when the element size is refined in the vicinity of rapidly varying stress fields, or for irregular boundaries.

(ii) The nodal configuration should be simple and permit the standard grillage beam element to be incorporated into an idealization. Second or higher order derivatives should be avoided and low order elements should have a constant number of variables at each node.

(iii) As a mesh of arbitrarily shaped elements is refined, convergence to the correct solution should be ensured. With certain provisos, the existence of fine-mesh convergence for an element can be established by the patch test.[I7,I10]. The convergence of a mesh comprised of both triangular and quadrilateral elements should also be established.

(iv) The equations produced should not be ill-conditioned and fail for certain geometries.

(v) The coarse mesh performance should be such that if an idealization is in error the results are not unreasonable.

(vi) The element(s) should be easy to implement and computationally efficient. A shape function subroutine is easy to implement, and reduced numerical integration invites computational efficiency. Ideally, it should be possible to code a family of elements into a single compact shape function subroutine thus saving a substantial area of computer core.

(vii) The stresses should be available at the nodes to be consistent with the majority of finite element system output schemes. Sometimes stress output at the Gauss points is acceptable if the accuracy is improved.[B5]

3.3 THEORY FOR CONSTRAINED THIN PLATE ELEMENTS

The derivation commences with the three dimensional equations of elasticity which include shearing deformations. Thus the in-plane and lateral displacements u, v and w are specified independently, and are in coordinate directions shown in Fig. 3.2. The Kirchhoff hypothesis for thin plates without shearing deformations is then invoked discretely by applying constraints to the displacement field.

3.3.1 *Basic assumptions*

The basic assumptions for a plate including shearing deformations are

(i) The deflections are small

(ii) Lines originally normal to the mid-surface remain straight during the deformations

(iii) Stresses and strains normal to the mid-surface are always negligible

For thin plates the additional assumption required is

(iv) Lines originally normal to the mid-surface remain normal during the deformations, i.e. zero shear strain.

3.3.2 *Derivation of the thin plate theory*

From the basic assumptions for a plate with transverse shearing deformations, the displacements of any point x, y and z in the plate can be specified as

$$\delta = \begin{Bmatrix} u \\ v \\ w \end{Bmatrix} = \begin{Bmatrix} + z\,\theta_y \\ - z\,\theta_x \\ w \end{Bmatrix} \tag{3.2}$$

where θ_x and θ_y are the rotations of the normals to the mid-surface with the sign convention of Fig. 3.2.

From this definition of displacements the strain components can be expressed as

$$\varepsilon = \begin{Bmatrix} \varepsilon_n \\ \hline \varepsilon_s \end{Bmatrix} = \begin{Bmatrix} \varepsilon_x \\ \varepsilon_y \\ \gamma_{xy} \\ \hline \gamma_{xz} \\ \gamma_{yz} \end{Bmatrix} = \begin{Bmatrix} \frac{\partial u}{\partial x} \\ \frac{\partial v}{\partial y} \\ \frac{\partial u}{\partial y} + \frac{\partial v}{\partial x} \\ \hline \frac{\partial w}{\partial x} + \frac{\partial u}{\partial z} \\ \frac{\partial w}{\partial y} + \frac{\partial v}{\partial z} \end{Bmatrix} \tag{3.3}$$

where ε_n is the in-plane strain components and ε_s the transverse shear strain components.

Combining eqns 3.2 and 3.3 for the in-plane components of strain gives

$$\varepsilon_n = z \begin{Bmatrix} \dfrac{\partial \theta_y}{\partial x} \\ -\dfrac{\partial \theta_x}{\partial y} \\ \dfrac{\partial \theta_y}{\partial y} - \dfrac{\partial \theta_x}{\partial x} \end{Bmatrix} = z\,\varepsilon_f \qquad (3.4)$$

Noting that $\theta_x = -\dfrac{\partial v}{\partial z}$ and $\theta_y = \dfrac{\partial u}{\partial z}$, the rotational derivatives ε_f can be rewritten as

$$\varepsilon_f = \begin{Bmatrix} \dfrac{\partial^2 u}{\partial x \partial z} \\ \dfrac{\partial^2 v}{\partial y \partial z} \\ \dfrac{\partial^2 u}{\partial y \partial z} + \dfrac{\partial^2 v}{\partial x \partial z} \end{Bmatrix} \qquad (3.5)$$

The displacement field is now constrained to effectively exclude transverse shear strains as required by the Kirchhoff hypothesis, *vide* assumption (iv), by the technique described in a subsequent section. The evaluation of the element stiffness matrix now involves only in-plane stress and strain products. The in-plane stress components σ_n are given by the usual equation

$$\sigma_n = D_n\,\varepsilon_n \qquad (3.6)$$

where D_n is the conventional membrane modulus matrix where

$$D_n = \begin{bmatrix} dx & dl & o \\ dl & dy & o \\ o & o & dxy \end{bmatrix} \tag{3.7}$$

$$\text{with } dx = dy = \frac{E}{1-\nu^2}$$

$$dl = \frac{E}{1-\nu^2} \tag{3.8}$$

$$dxy = \frac{E}{2(1+\nu)}$$

for an isotropic material, in which E is the elastic modulus and ν Poisson's ratio.

From the variational principle of minimum potential energy the contribution of the internal stresses to the energy functional is the volume integral

$$\frac{1}{2} \int_v \varepsilon_n^T \ \sigma_n \ dv \tag{3.9}$$

Substituting eqns 3.4 and 3.6 into this integral, expanding and rearranging gives

$$\begin{aligned} \frac{1}{2} \int_v \varepsilon_n^T \sigma_n \ dv &= \frac{1}{2} \int\int\int \varepsilon_n^T \ \sigma_n \ dxdydz \\ &= \frac{1}{2} \int\int\int \ z\varepsilon_f^T \ D_n \ z \ \varepsilon_f \ dxdydz \\ &= \frac{1}{2} \int\int \ \varepsilon_f^T \int D_n \ z^2 \ dz \ \varepsilon_f \ dxdt \end{aligned} \tag{3.10}$$

The innermost integral contains the coordinate z which can be integrated explicitly before the integration with respect to x and y. Thus the energy integral may be rewritten as

$$\frac{1}{2} \iint \varepsilon_f^T \sigma_f \, dxdy \tag{3.11}$$

where $\sigma_f = D_f \varepsilon_f$ (3.12)

and $D_f = \int D_n z^2 \, dz$ (3.13)

so that the final integration may be carried out with respect to x and y only.

The generalised stress vector σ_f represents the conventional flexural stress resultants of thin plate theory

$$\sigma_f = \{M_y, M_x, M_{xy}\}^T \tag{3.14}$$

and the generalised strain vector ε_f represents the conventional curvatures. Since the transverse shear strains are only constrained to be approximately zero, these strains are more appropriately termed pseudo-curvatures. For approximately zero shear, $\frac{\partial u}{\partial z} \simeq -\frac{\partial w}{\partial x}$ and $\frac{\partial v}{\partial z} \simeq -\frac{\partial w}{\partial y}$, eqn. 3.5 becomes

$$\varepsilon_f = \left\{ \begin{array}{c} \dfrac{\partial^2 u}{\partial x \partial z} \\ \dfrac{\partial^2 v}{\partial y \partial z} \\ \dfrac{\partial^2 u}{\partial y \partial z} + \dfrac{\partial^2 v}{\partial x \partial z} \end{array} \right\} \simeq \left\{ \begin{array}{c} -\dfrac{\partial^2 w}{\partial x^2} \\ -\dfrac{\partial^2 w}{\partial y^2} \\ -2\dfrac{\partial^2 w}{\partial x \partial y} \end{array} \right\} \tag{3.15}$$

The integration of eqn. 3.13 gives the conventional flexural rigidity D_f where

$$D_f = \begin{bmatrix} Dx & D1 & 0 \\ D1 & Dy & 0 \\ 0 & 0 & Dxy \end{bmatrix} \qquad (3.16)$$

for orthotropy with respect to the x and y axes and in the case of an isotropic material reduces to

$$\begin{aligned} Dx = Dy &= \frac{Et^3}{12(1-\nu^2)} \\ D1 &= \frac{Et^3}{12(1-\nu^2)} \\ Dxy &= \frac{Gt^3}{12} = \frac{Et^3}{24(1+\nu)} \end{aligned} \qquad (3.17)$$

where t is the plate thickness and G the membrane shearing modulus.

The formulation now follows the standard displacement method[21]. The displacement field can be expressed in terms of a set of discrete nodal displacements δ^e by use of suitable shape functions N.

$$\delta = N\,\delta^e \qquad (3.18)$$

Suitable constraints are applied to exclude shear strains and from eqn. 3.15 the flexural strains are defined as

$$\varepsilon_f = B\delta^e \tag{3.19}$$

where B is the strain matrix which also includes shear constraints.

The element stiffness matrix can be derived from the principle of virtual work from eqns 3.11 and 3.19 as

$$K^e = \iint B^T D B \, dxdy \tag{3.20}$$

where D is the flexural modulus matrix, eqn. 3.16, with the suffix now removed for convenience.

3.3.3 *Unconstrained displacement fields*

The unconstrained nodal configurations and coordinate systems are shown in Fig. 3.3. The discrete nodal displacements for the ith node are chosen as the mid-surface displacement w_i and the two rotations of the normal θ_{xi} and θ_{yi}.

By employing suitable shape functions $\bar{N}_i$, the global displacement field, eqn. 3.18 , can be written as

$$\delta = \sum_{i=1}^{n} \bar{N}_i \, \delta_i \tag{3.21}$$

where n is the total number of nodes. For variable thickness elements, defined by nodal thicknesses t_i, the displacements at a point ξ,η and distance z above the mid-surface, can be given by expanding eqn. 3.21 as

$$\begin{Bmatrix} u \\ v \\ w \end{Bmatrix} = \sum_{i=1}^{n} \begin{bmatrix} 0 & 0 & \frac{z}{t} N_i t_i \\ 0 & -\frac{z}{t} N_i t_i & 0 \\ N_i & 0 & 0 \end{bmatrix} \begin{Bmatrix} w \\ \theta_x \\ \theta_y \end{Bmatrix}_i \tag{3.22}$$

where for midside and central nodes the discrete nodal displacements are changed as

$$\begin{Bmatrix} w \\ \theta_x \\ \theta_y \end{Bmatrix}_i \rightarrow \begin{Bmatrix} \Delta w \\ \Delta\theta_x \\ \Delta\theta_y \end{Bmatrix}_i \tag{3.23}$$

The symbol Δ refers to the departure from linearity of the value with respect to the values at the corner nodes. The departures from linearity are

$$\Delta\delta_j = \delta_j - \frac{1}{(\ell-m+1)} \sum_{i=\ell}^{m} \delta_i \tag{3.24}$$

where ℓ to m refers to the two corner nodes at the extremities of the side of the midside node j, or all corner nodes for the central node j.

3.3.4 *Hierarchical shape functions*

Hierarchical shape functions take account of the variables specified as the departure from linearity. For the triangle the shape functions are conveniently defined in area coordinates L at each node i as

$$\begin{aligned} N_i &= L_i && \text{for } i = 1,2,3 \\ N_i &= 4L_{i-3}\,L_{j-3} && \text{for } i = 4,5,6 \text{ and } j = 5,6,3 \\ N_i &= 27L_1L_2L_3 && \text{for } i = 7 \end{aligned} \qquad (3.25)$$

The area coordinates can be defined in terms of the natural coordinates as

$$\begin{aligned} L_1 &= \xi \\ L_2 &= \eta \\ L_3 &= 1 - \xi - \eta \end{aligned} \qquad (3.26)$$

For the quadrilateral elements the hierarchical shape functions are defined in natural coordinates as

$$\begin{aligned} N_i &= \tfrac{1}{4}(1+\xi_o)(1+\eta_o) && \text{for } i = 1,4 \\ N_i &= \tfrac{1}{2}(1-\xi^2)(1+\eta_o) && \text{for } i = 5 \text{ and } 7 \\ N_i &= \tfrac{1}{2}(1+\xi_o)(1-\eta^2) && \text{for } i = 5 \text{ and } 8 \\ N_i &= (1-\xi^2)(1-\eta^2) && \text{for } i = 9 \end{aligned} \qquad (3.27)$$

where $\xi_o = \xi\xi_i$ and $\eta_o = \eta\eta_i$.

With the definition of the functions N_i established eqns 3.21 and 3.22 define a unique variation of the displacements within the element and over any external face and full C^0 continuity between adjacent elements is maintained.

3.3.5 *Hierarchical mapping and the Jacobian matrix*

It is now necessary to establish the relationship between the Cartesian and natural curvilinear coordinate systems. The x and y coordinates and thickness t at a point ζ,η on the mid-surface can be given in a special form as

$$\left\{\begin{bmatrix} x \\ y \\ t \end{bmatrix}\right\} = \sum_{i=1}^{n} N_i \left\{\begin{bmatrix} x \\ y \\ t \end{bmatrix}\right\}_i \qquad (3.28)$$

where the hierarchical shape functions N are in terms of the natural ζ,η coordinates and the summation is taken over n nodes on the element periphery which are sufficient to define the element geometry. When midside nodes are require the nodal coordinates $\{x,y,t\}_i^T$ become the departures from linearity $\{\Delta x, \Delta y, \Delta t\}_i^T$ which are calculated simply as

$$\begin{Bmatrix} \Delta x \\ \Delta y \\ \Delta t \end{Bmatrix}_i = \begin{Bmatrix} x \\ y \\ t \end{Bmatrix}_i - \frac{1}{2} \begin{Bmatrix} x \\ y \\ t \end{Bmatrix}_\ell - \frac{1}{2} \begin{Bmatrix} x \\ y \\ t \end{Bmatrix}_m \qquad (3.29)$$

where i is now a midside node and ℓ and m are the adjacent corner nodes.

This special form of coordinate transformation, referred to here as hierarchical mapping, permits the same shape functions to be adopted for the definition of the displacement field as for the geometry. Furthermore, the same shape functions apply for the geometry of both the straight edged elements defined by corner nodes only, and the curvilinear elements defined by corner and midside nodes. This approach saves computer time compared with an alternative subparametric formulation[Z1] which would require the computation of two sets of shape functions.

The shape functions are in terms of the natural ξ,η coordinates and therefore it is now necessary to establish the analytical process for calculating the strain derivatives of eqn. 3.15 which are expressed in Cartesian x, y coordinates.

Since the thickness of these elements is variable and the mid-surface planar the geometry is a special case of a three-dimensional solid element. The transformation relationship can therefore be expected to contain zero products which could be avoided in the numerical process with an explicit derivation, and to be similar to the two-dimensional relationship. For comparison both the two-dimensional and special three-dimensional transformation relationships will now be derived.

From the chain rule the relationship between the natural and Cartesian derivatives in two-dimensions can be written in matrix notation as

$$\begin{Bmatrix} \dfrac{\partial}{\partial\xi} \\ \\ \dfrac{\partial}{\partial\eta} \end{Bmatrix} = \begin{bmatrix} \dfrac{\partial x}{\partial\xi} & \dfrac{\partial y}{\partial\xi} \\ \\ \dfrac{\partial x}{\partial\eta} & \dfrac{\partial y}{\partial\eta} \end{bmatrix} \begin{Bmatrix} \dfrac{\partial}{\partial x} \\ \\ \dfrac{\partial}{\partial y} \end{Bmatrix} = [J] \begin{Bmatrix} \dfrac{\partial}{\partial x} \\ \\ \dfrac{\partial}{\partial y} \end{Bmatrix} \tag{3.30}$$

where J is defined as the Jacobian matrix. The components of J can be found numerically for any position ξ,η within the element from eqn. 3.28 as

$$[J] = \sum_{i=1}^{n} \begin{bmatrix} \dfrac{\partial N_i}{\partial\xi} & \dfrac{\partial N_i}{\partial\xi} \\ \\ \dfrac{\partial N_i}{\partial\eta} & \dfrac{\partial N_i}{\partial\eta} \end{bmatrix} \begin{bmatrix} x_i & 0 \\ 0 & y_i \end{bmatrix} \tag{3.31}$$

where x_i, y_i are the x and y coordinates for corner node i or the Δx and Δy coordinates for midside node i. The summation is only for nodes on the element periphery.

Inverting the Jacobian in eqn. 3.30 gives the two-dimensional transformation relationship explicitly as

$$\begin{Bmatrix} \dfrac{\partial}{\partial x} \\ \\ \dfrac{\partial}{\partial y} \end{Bmatrix} = \frac{1}{\det[J]} \begin{bmatrix} \dfrac{\partial y}{\partial\eta} & -\dfrac{\partial y}{\partial\xi} \\ \\ -\dfrac{\partial x}{\partial\eta} & \dfrac{\partial x}{\partial\xi} \end{bmatrix} \begin{Bmatrix} \dfrac{\partial}{\partial\xi} \\ \\ \dfrac{\partial}{\partial\eta} \end{Bmatrix} = \begin{bmatrix} \dfrac{\partial\xi}{\partial x} & \dfrac{\partial\eta}{\partial x} \\ \\ \dfrac{\partial\xi}{\partial y} & \dfrac{\partial\eta}{\partial y} \end{bmatrix} \begin{Bmatrix} \dfrac{\partial}{\partial\xi} \\ \\ \dfrac{\partial}{\partial\eta} \end{Bmatrix} \tag{3.32}$$

where $\det[J] = \dfrac{\partial x}{\partial\xi}\dfrac{\partial y}{\partial\eta} - \dfrac{\partial x}{\partial\eta}\dfrac{\partial y}{\partial\xi}$

For the three-dimensional transformation relationship the natural coordinate ζ is introduced for convenience. The z coordinate at any point ξ,η,ζ is now given by

$$z = \frac{t}{2}\zeta \tag{3.33}$$

where the thickness t of the element at the same point is given numerically by eqn. 3.28. From the chain rule in matrix notation

$$\begin{Bmatrix} \frac{\partial}{\partial\xi} \\ \frac{\partial}{\partial\eta} \\ \frac{\partial}{\partial\zeta} \end{Bmatrix} = \begin{bmatrix} \frac{\partial x}{\partial\xi} & \frac{\partial y}{\partial\xi} & \frac{\partial z}{\partial\xi} \\ \frac{\partial x}{\partial\eta} & \frac{\partial y}{\partial\eta} & \frac{\partial z}{\partial\eta} \\ \frac{\partial x}{\partial\zeta} & \frac{\partial y}{\partial\zeta} & \frac{\partial z}{\partial\zeta} \end{bmatrix} \begin{Bmatrix} \frac{\partial}{\partial x} \\ \frac{\partial}{\partial y} \\ \frac{\partial}{\partial z} \end{Bmatrix} = [J] \begin{Bmatrix} \frac{\partial}{\partial x} \\ \frac{\partial}{\partial y} \\ \frac{\partial}{\partial z} \end{Bmatrix} \tag{3.24}$$

Inverting the Jacobian gives

$$[J]^{-1} = \frac{1}{\det [J]} \begin{bmatrix} \frac{\partial y}{\partial\eta}\frac{\partial z}{\partial\zeta} - \frac{\partial y}{\partial\zeta}\frac{\partial z}{\partial\eta} & \frac{\partial y}{\partial\zeta}\frac{\partial z}{\partial\xi} - \frac{\partial y}{\partial\xi}\frac{\partial z}{\partial\zeta} & \frac{\partial y}{\partial\xi}\frac{\partial z}{\partial\eta} - \frac{\partial y}{\partial\eta}\frac{\partial z}{\partial\xi} \\ \frac{\partial x}{\partial\zeta}\frac{\partial z}{\partial\eta} - \frac{\partial x}{\partial\eta}\frac{\partial z}{\partial\zeta} & \frac{\partial x}{\partial\xi}\frac{\partial z}{\partial\zeta} - \frac{\partial x}{\partial\zeta}\frac{\partial z}{\partial\xi} & \frac{\partial x}{\partial\eta}\frac{\partial z}{\partial\xi} - \frac{\partial x}{\partial\xi}\frac{\partial z}{\partial\eta} \\ \frac{\partial x}{\partial\eta}\frac{\partial y}{\partial\zeta} - \frac{\partial x}{\partial\zeta}\frac{\partial y}{\partial\eta} & \frac{\partial x}{\partial\zeta}\frac{\partial y}{\partial\xi} - \frac{\partial x}{\partial\xi}\frac{\partial y}{\partial\zeta} & \frac{\partial x}{\partial\xi}\frac{\partial y}{\partial\eta} - \frac{\partial x}{\partial\eta}\frac{\partial y}{\partial\xi} \end{bmatrix} \tag{3.35}$$

A geometrical interpretation of the Jacobian is that the rows of J constitute three vectors which are tangential to the coordinate curves ξ,η,ζ at the point of intersection and are known as the covariant base vectors; the columns of J^{-1} constitute three vectors which are normal to the coordinate surfaces ξ = constant, η = constant and ζ = constant and are known as contravarient base vectors.

Mathematically the relationship between the Jacobian J and its inverse can be written as

$$[J] = \begin{Bmatrix} \vec{J}_\xi \\ \vec{J}_\eta \\ \vec{J}_\zeta \end{Bmatrix} \tag{3.36}$$

and
$$[J]^{-1} = \frac{1}{\det [J]} [\vec{J}_{\eta} * \vec{J}_{\zeta}, \vec{J}_{\zeta} * \vec{J}_{\xi}, \vec{J}_{\xi} * \vec{J}_{\eta}]$$
$$= [\vec{j}_\xi, \vec{j}_\eta, \vec{j}_\zeta] \tag{3.37}$$

where $\vec{J}_\xi$, $\vec{j}_\xi$ etc. are the covarient and contravariant base vectors respectively, and the symbol * signifies a vector cross-product.

Since x and y are functions of ξ and η only, the derivatives $\frac{\partial x}{\partial \zeta}$ and $\frac{\partial y}{\partial \zeta}$ must be zero, and the inverse Jacobian can be simplified to

$$\therefore \quad [J]^{-1} = \frac{1}{\det [J]} \begin{bmatrix} \frac{\partial y}{\partial \eta}\frac{\partial z}{\partial \zeta} & -\frac{\partial y}{\partial \xi}\frac{\partial z}{\partial \zeta} & \frac{\partial y}{\partial \xi}\frac{\partial z}{\partial \eta} - \frac{\partial y}{\partial \eta}\frac{\partial z}{\partial \xi} \\ -\frac{\partial x}{\partial \eta}\frac{\partial z}{\partial \zeta} & \frac{\partial x}{\partial \xi}\frac{\partial z}{\partial \zeta} & \frac{\partial x}{\partial \eta}\frac{\partial z}{\partial \xi} - \frac{\partial x}{\partial \xi}\frac{\partial z}{\partial \eta} \\ 0 & 0 & \frac{\partial x}{\partial \xi}\frac{\partial y}{\partial \eta} - \frac{\partial x}{\partial \eta}\frac{\partial y}{\partial \xi} \end{bmatrix}$$

where $\det [J] = \frac{\partial z}{\partial \zeta} \left(\frac{\partial x}{\partial \xi}\frac{\partial y}{\partial \eta} - \frac{\partial x}{\partial \eta}\frac{\partial y}{\partial \xi} \right)$. (3.38)

On inspection, it can be seen that the first 2 x 2 partition is identical to the inverted two-dimensional Jacobian, eqn. 3.31. Noting from eqn. 3.33 that $\frac{\partial z}{\partial \zeta} = \frac{t}{2}$ and from eqn. 3.38 that $\frac{\partial z}{\partial x} = \frac{\zeta}{2} \frac{\partial t}{\partial x} = \frac{z}{t} \frac{\partial t}{\partial x}$ etc. and substituting these expressions into eqn. 3.38 gives

$$[J]^{-1} = \begin{bmatrix} \frac{1}{\det [J]} \frac{\partial y}{\partial \eta} & -\frac{1}{\det [J]} \frac{\partial y}{\partial \xi} & -\frac{2z}{t^2} \frac{\partial t}{\partial x} \\ -\frac{1}{\det [J]} \frac{\partial x}{\partial \eta} & \frac{1}{\det [J]} \frac{\partial x}{\partial \xi} & -\frac{2z}{t^2} \frac{\partial t}{\partial y} \\ 0 & 0 & \frac{t}{2} \end{bmatrix} \tag{3.39}$$

where the first 2 x 2 partition is identical to J^{-1} for the two-dimensional Jacobian. Noting that eqn. 3.39 gives $\frac{\partial}{\partial z} = \frac{t}{2} \frac{\partial}{\partial \zeta}$, the final relationship for the Cartesian x and y derivatives in terms of the natural ξ and η derivatives is

$$\begin{Bmatrix} \frac{\partial}{\partial x} \\ \frac{\partial}{\partial y} \end{Bmatrix} = \left[\begin{array}{c|c|c} \frac{1}{\det [J]} \frac{\partial y}{\partial \eta} & -\frac{1}{\det [J]} \frac{\partial y}{\partial \xi} & -\frac{z}{t} \frac{\partial t}{\partial x} \\ -\frac{1}{\det [J]} \frac{\partial x}{\partial \eta} & \frac{1}{\det [J]} \frac{\partial x}{\partial \xi} & -\frac{z}{t} \frac{\partial t}{\partial y} \end{array} \right] \begin{Bmatrix} \frac{\partial}{\partial \xi} \\ \frac{\partial}{\partial \eta} \\ \frac{\partial}{\partial z} \end{Bmatrix} \tag{3.40}$$

The physical interpretation of eqn. 3.40 is that for variable thickness an in-plane strain component, for example $\varepsilon_x = \frac{\partial u}{\partial x}$, includes a small strain contribution from the change of u over the thickness. When the plate is constant thickness this contribution vanishes.

For numerical convenience eqns 3.28 and 3.31 can be combined and expanded to include the necessary components to create the transformation relationship of eqn.3.40 as

$$\begin{bmatrix} x & y & t \\ \frac{\partial x}{\partial \xi} & \frac{\partial y}{\partial \xi} & \frac{\partial t}{\partial \xi} \\ \frac{\partial x}{\partial \eta} & \frac{\partial y}{\partial \eta} & \frac{\partial t}{\partial \eta} \end{bmatrix} = \sum_{i=1}^{n} \begin{bmatrix} N_i & N_i & N_i \\ \frac{\partial N_i}{\partial \xi} & \frac{\partial N_i}{\partial \xi} & \frac{\partial N_i}{\partial \xi} \\ \frac{\partial N_i}{\partial \eta} & \frac{\partial N_i}{\partial \eta} & \frac{\partial N_i}{\partial \eta} \end{bmatrix} \begin{bmatrix} x_i & 0 & 0 \\ 0 & y_i & 0 \\ 0 & 0 & t_i \end{bmatrix} \qquad (3.41)$$

where as before the i nodal values are summed over the nodes on the periphery and midside nodes are present the nodal coordinates become the departures from linearity.

3.3.6 *Strain-displacement relations*

It is now possible to derive the relationship between the flexural strains and the discrete nodal displacements. The transformation relationship, eqn. 3.40 , can be regarded as the standard two-dimensional transformation with a variable thickness correction. Thus the flexural strain components, eqn. 3.5, can be written in the form

$$\begin{bmatrix} \frac{\partial^2 u}{\partial x \partial z} & \frac{\partial^2 v}{\partial x \partial z} \\ \frac{\partial^2 u}{\partial y \partial z} & \frac{\partial^2 v}{\partial y \partial z} \end{bmatrix}_{3D} = \frac{\partial}{\partial z} \left\{ \begin{bmatrix} \frac{\partial u}{\partial x} & \frac{\partial v}{\partial x} \\ \frac{\partial u}{\partial y} & \frac{\partial v}{\partial y} \end{bmatrix} - \frac{z}{t} \begin{Bmatrix} \frac{\partial t}{\partial x} \\ \frac{\partial t}{\partial y} \end{Bmatrix} \begin{bmatrix} \frac{\partial u}{\partial z} , & \frac{\partial v}{\partial z} \end{bmatrix} \right\}_{2D} \qquad \ldots (3.42)$$

where all the derivatives to the right involve only the two-dimensional transformation. Since the displacement field will be constrained to have approximately zero shear strains, the second derivatives in z can be dealt with by noting that $\frac{\partial u}{\partial z} \simeq -\frac{\partial w}{\partial x}$ and $\frac{\partial v}{\partial z} \simeq -\frac{\partial w}{\partial y}$. Eqn. 3.42 now becomes

$$\begin{bmatrix} \frac{\partial^2 u}{\partial x \partial z} & \frac{\partial^2 v}{\partial x \partial z} \\ \frac{\partial^2 u}{\partial y \partial z} & \frac{\partial^2 v}{\partial y \partial z} \end{bmatrix} = \left\{ \begin{bmatrix} \frac{\partial^2 u}{\partial x \partial z} & \frac{\partial^2 v}{\partial x \partial z} \\ \frac{\partial^2 u}{\partial y \partial z} & \frac{\partial^2 v}{\partial y \partial z} \end{bmatrix} + \frac{1}{t} \left\{ \begin{matrix} \frac{\partial t}{\partial x} \\ \frac{\partial t}{\partial y} \end{matrix} \right\} \begin{bmatrix} \frac{\partial w}{\partial x} , & \frac{\partial w}{\partial y} \end{bmatrix} \right\} \tag{3.43}$$

The plate flexure strain-displacement relationship can now be written from eqns. 3.15, 3.22, 3.40 and 3.43 as

$$\varepsilon_f = \left\{ \begin{matrix} \frac{\partial^2 u}{\partial x \partial z} \\ \frac{\partial^2 v}{\partial y \partial z} \\ \frac{\partial^2 u}{\partial y \partial z} + \frac{\partial^2 v}{\partial x \partial z} \end{matrix} \right\} = \sum_{i=1}^{n} \left[\begin{array}{c|c|c} \frac{1}{t}\frac{\partial t}{\partial x}\frac{\partial N_i}{\partial x} & 0 & \frac{t_i}{t}\frac{\partial N_i}{\partial x} \\ \hline \frac{1}{t}\frac{\partial t}{\partial y}\frac{\partial N_i}{\partial y} & -\frac{t_i}{t}\frac{\partial N_i}{\partial y} & 0 \\ \hline \frac{1}{t}\frac{\partial t}{\partial y}\frac{\partial N_i}{\partial x} + \frac{1}{t}\frac{\partial t}{\partial x}\frac{\partial N_i}{\partial y} & -\frac{t_i}{t}\frac{\partial N_i}{\partial x} & \frac{t_i}{t}\frac{\partial N_i}{\partial y} \end{array} \right] \left\{ \begin{matrix} w \\ \theta_x \\ \theta_y \end{matrix} \right\}. \tag{3.44}$$

where the summation is taken over all nodes n and derivatives are found from the standard two-dimensional relations. In matrix from eqn. 3.44 becomes

$$\varepsilon_f = \begin{bmatrix} B'_1, & \ldots & B'_i, & \ldots & B'_n \end{bmatrix} \begin{Bmatrix} \delta_1 \\ \vdots \\ \delta_i \\ \vdots \\ \delta_x \end{Bmatrix} \tag{3.45}$$

or $$\varepsilon_f = B\delta^e \tag{3.46}$$

where B_i is the submatrix relating the flexural strains at any point ξ,η to the displacement components of node i.

3.3.7 *Shape function array*

It is now possible to relate all the displacements and derivatives at any point ξ,η within the element to the discrete nodal displacements. Using eqns 3.22 and 3.44 gives

$$\begin{Bmatrix} w \\ \frac{\partial u}{\partial z} \\ \frac{\partial v}{\partial z} \\ \frac{\partial w}{\partial x} \\ \frac{\partial w}{\partial y} \\ \frac{\partial^2 u}{\partial x \partial z} \\ \frac{\partial^2 v}{\partial y \partial z} \\ \frac{\partial^2 u}{\partial y \partial z} + \frac{\partial^2 v}{\partial x \partial z} \end{Bmatrix} = \sum_{i=1}^{n} \begin{bmatrix} N_i & 0 & 0 \\ 0 & 0 & \frac{1}{t} N_i t_i \\ 0 & -\frac{1}{t} N_i t_i & 0 \\ \frac{\partial N_i}{\partial x} & 0 & 0 \\ \frac{\partial N_i}{\partial y} & 0 & 0 \\ \frac{1}{t}\frac{\partial t}{\partial x}\frac{\partial N_i}{\partial x} & 0 & \frac{t_i}{t}\frac{\partial N_i}{\partial x} \\ \frac{1}{t}\frac{\partial t}{\partial y}\frac{\partial N_i}{\partial y} & -\frac{t_i}{t}\frac{\partial N_i}{\partial y} & 0 \\ \frac{1}{t}\frac{\partial t}{\partial y}\frac{\partial N_i}{\partial x} + \frac{1}{t}\frac{\partial t}{\partial x}\frac{\partial N_i}{\partial y} & -\frac{t_i}{t}\frac{\partial N_i}{\partial x} & \frac{t_i}{t}\frac{\partial N_i}{\partial y} \end{bmatrix} \begin{Bmatrix} w \\ \theta_x \\ \theta_y \end{Bmatrix} \tag{3.37}$$

or more concisely

$$\delta^* \quad = \quad w\delta^e \qquad (3.48)$$

The use of a shape function array is numerically convenient since on extracting the appropriate rows any element matrix can easily be formed. However the shape function array has yet to be constrained to preclude shear strains.

3.3.8 *Kinematic constraints*

The unconstrained nodal variables for the triangular and quadrilateral elements, Fig. 3.3 are now reduced to the constrained nodal configurations, Fig. 3.1, by the application of sets of independent shear constraints. The 20 unconstrained variables for ISOFLEX 6 and ISOFLEX 3 triangles require 8 and 11 constraints respectively, and the 27 unconstrained variables for the ISOFLEX 8 and ISOFLEX 4 quadrilaterals require 11 and 15 constraints respectively. If these constraints were enforced so that the shear strains were exactly zero throughout an element domain then the Kirchhoff requirement for thin plates would be satisfied exactly. However, the constraints adopted here are enforced so that the shear strains are zero at discrete points within an element domain, but since an element gains only a small quantity of shear strain energy the Kirchhoff requirement is effectively satisfied. Furthermore, the unconstrained variables and applied kinematic constraints are such that the elements pass the patch test for arbitrary triangular and quadrilateral element geometry.

(i) The midside translation and rotation - 2 constraints along each edge

It can be verified that a planar beam element can be formulated in a similar manner to the technique proposed in this chapter by specifying unconstrained nodal variables at three nodes as $(w, \frac{\partial u}{\partial z})$ i = 1,3 with quadratic variations of $w = f(x^2)$ and $\frac{\partial u}{\partial z} = f(x^2)$. If the two variables at the central node are eliminated by constraining the shears to be zero at the two Gauss points, and the integration for the element stiffness is carried out using the two point Gauss rule, then the resulting element stiffness matrix is identical to that given by the standard formulation based on a variation of $w = f(x^3)$ with explicit integration.

For the ISOFLEX elements the transverse tangential shear strain γ_t is constrained to zero at the two Gauss points on each edge of the element. If each edge is imagined to be a narrow beam then these constraint positions are ideal in accordance with the optimum constraint positions for the corresponding beam element. Furthermore. boundary constraints have the advantage of being identical for two adjacent elements even though the computation is repeated. The direction of the tangent at each Gauss point for curvilinear or straight element boundaries is given by the covarient base vectors $\vec{J}_\xi$ or $\vec{J}_\eta$, eqn. 3.36.

(ii) The two rotations at the centre - 2 constraints

The work done during a rigid body displacement of an element is zero requiring the shear forces in the x and y directions to be zero. These shear forces can be found by integrating the shear stresses over the element area and since stresses are proportional to strains this reduces to the following integrations

$$\int \gamma_{xz} \, dA = 0 \qquad (3.49)$$

$$\int \gamma_{yz} \, dA = 0 \qquad (3.50)$$

These integrations are computed numerically.

(iii) The central lateral deflection - 1 constraint

From vertical equilibrium

$$\int \nabla\gamma \, dA = \int \left(\frac{\partial \gamma_{xz}}{\partial x} + \frac{\partial \gamma_{yz}}{\partial y} \right) dA = 0 \qquad (3.51)$$

and Green's theorem can be used to give a transformed version which avoids second derivatives[I5] as

$$\int \gamma_n \, dS = 0 \qquad (3.52)$$

where γ is the normal shear strain and dS is around the periphery. This integral is computed using the two point Gauss rule along each edge of the element. This constraint applies to the quadrilateral elements only since the addition of a central lateral displacement variable to the triangular elements did not affect their performance. For the quadrilateral element to pass the patch test it is an inescapable requirement that it should respond with w as a quadratic in x and y[I4-6]. A quadrilateral element has $x = f(1,\xi,\eta,\xi\eta)$ and on expanding $w = x^2$, the term $\xi^2\eta^2$ appears. This term is provided here by the central variable for w which uses the bubble function $(1 - \xi^2)(1 - \eta^2)$.

(iv) Mid-side rotation - 1 constraint on each edge

For the lower order elements the tangential rotations are enforced to be linear along each edge of the element simply by excluding the midside tangential rotation $\Delta\theta_t$, the departure from linearity, from the element computations.

Extracting the appropriate rows from the shape function array, eqn. 3.47 , transforming the edge shears and integrating the shears over the area and around the periphery gives for the quadrilaterals, for example,

$$\left\{\begin{bmatrix} \gamma_{t1} \\ \vdots \\ \gamma_{t8(6)} \\ \int \gamma_{xz} dA \\ \int \gamma_{yz} dA \\ \int \gamma_n dS \end{bmatrix}\right\} \left\{\begin{bmatrix} 0 \\ \vdots \\ 0 \end{bmatrix}\right\} \begin{array}{cc} \left[M_A \right. & \left. \vdots \; M_B \right] \\ 11x16 & 11x11 \\ (8x12) & (8x8) \end{array} \left\{\begin{bmatrix} \delta_A \\ \hline \delta_B \end{bmatrix}\right\} \qquad (3.53)$$

where δ_A are the variables for the required nodal configuration and δ_B are the unwanted variables, and the array sizes in brackets refer to the triangles. After transforming the columns of M for the tangential and normal rotations at the midsides the variables δ_A and δ_B are

$$\{\delta_A \mid \delta_B\}^T = \{(W, \theta_x, \theta_y)_i, \ldots, \Delta\theta_{tj}, \ldots, \mid (\Delta W, \Delta\theta_n)_j, \ldots, \Delta\theta_{xk}, \Delta\theta_{yk}, \Delta W_k\} \tag{3.54}$$

where i refers to corner nodes, j refers to midside nodes and k refers to the central node.

From eqn. 3.53 the unwanted variables can be expressed in terms of the wanted variables as

$$\delta_B = - M_B^{-1} M_A \delta_A \tag{3.55}$$

Rearranging the columns of the unconstrained shape function array, eqn. 3.47 , to coincide with the wanted and unwanted nodal variables, and introducing the above expression gives

$$\{\delta^*\} = [W_A - W_B M_B^{-1} M_A] \{\delta_A\} \tag{3.56}$$

or

$$\delta^* = W_C \delta^e \tag{3.57}$$

where $W_C = W_A - W_B M_B^{-1} M_A$ and is the constrained shape function array which gives the displacements and strain variables at any point ξ,η within the element in terms of required element variables δ^e.

The inversion of the matrix M_B followed by a matrix multiplication for the product $M_B^{-1}\ M_A$ can be avoided and solved collectively by a scheme suggested by Faddeeva[F2]. The product is equivalent to the solution of n systems of a special form

$$\begin{bmatrix} M_B & -M_A \\ -I & O \end{bmatrix} \tag{3.58}$$

where I is the square n by n unit matrix which is the same size as M_B. By annulling all the rows in the lower left corner, and by the addition of suitable linear combinations of the first n rows, the product $M_B^{-1}\ M_A$ is obtained in the lower right corner. This can be accomplished by the ordinary forward elimination of the Gauss process.

3.3.9 *Numerically integrated stiffness matrix*

Introducing the standard expression

$$dxdy = |J|\ d\xi d\eta \tag{3.59}$$

and noting that B is a function of ξ,η, eqn. 3.20 can be rewritten in the form

$$K^e = \int_{-1}^{+1}\int_{-1}^{+1} B^T D\, B\ |J|\ d\xi d\eta \tag{3.60}$$

or in submatrix form

$$K^e_{ij} = \int_{-1}^{+1}\int_{-1}^{+1} B_i^T D\, B_j\ |J|\ d\xi d\eta \tag{3.61}$$

where K^e_{ij} is a typical submatrix linking nodes i and j. When evaluating the triple product $B_i^T D \; B_j$ advantage should be taken of the sparsity of B and D thus saving many unnecessary matrix manipulations.

The integration of the stiffness coefficients is carried out numerically, and eqn. 3.61 is replaced by a weighted summation of the values at certain points in the element

$$K^e = \sum_{i=1}^{n} W_p \left[f(\xi_p, \eta_p)\right] \tag{3.62}$$

where $\left[f(\xi_p,\eta_p)\right] = B^T DB|J|$ is evaluated at the appropriate sampling points ξ_p, η_p and W_p is the corresponding weight coefficient at this point.

3.3.10 *Nodal and distributed loading*

As with other finite element displacement models, the force-displacement relationship takes the form

$$F^e = K^e \, \delta^e + \bar{F}^e \tag{3.63}$$

where $\bar{F}^e$ represents a set of unique nodal forces required to maintain equilibrium at $\delta^e = 0$. Those forces may be associated with external surface tractions, body forces and initial strains. In the present context we will consider only the following constituents:

$$\bar{F}^e = \bar{F}^e_1 + \bar{F}^e_2 \tag{3.64}$$

where $\bar{F}^e_1$, $\bar{F}^e_2$ are the consistent nodal forces associated with concentrated nodal loads and distributed pressures respectively.

The vector $\bar{F}^e$ will consist of three force components for corner nodes and one for a midside node. Thus for example

$$\bar{F}^e = \begin{Bmatrix} \bar{F}^e_1 \\ \vdots \\ \bar{F}^e_i \\ \vdots \\ \bar{F}_n \end{Bmatrix} \quad \text{with } \bar{F}_i = \begin{Bmatrix} P_{xi} \\ M_{xi} \\ M_{yi} \end{Bmatrix} \quad \text{for corner nodes} \qquad \text{or } \bar{F}_i = \{\Delta M_{xi}\} \quad \text{for midside nodes} \tag{3.65}$$

where ΔM_x is associated with the departure from linearity of the tangential rotation $\Delta\theta_T$, but since this has no physical significance it will, in general, be neglected.

The consistent nodal forces $\bar{F}^e_2$ due to a distributed pressure q over the area of an element can be determined simply as

$$\bar{F}^e = - \int_A W^T q \; dA \tag{3.66}$$

where dA is the infinitesimal surface area dxdy, and W here refers to the first row of the shape function array for the lateral deflection. The integration is carried out numerically and concurrently with the stiffness integration. In general q will vary over the surface of an element and must therefore be interpolated from the values specified at the nodes as

$$q = \sum_{i=1}^{n} N_i \, q_i \tag{3.67}$$

where N_i here refer to the standard shape functions for an element with n nodes as opposed to the hierarchical shape functions mentioned previously.

3.4 REDUCED NUMERICAL INTEGRATION AND SPURIOUS MECHANISMS

The reduced numerical integration rules adopted here permit an economical evaluation of the element integrals, and the resulting stiffness matrix gives an improved structural response over the correct order of integration†. The reduced numerical integration employed here is the three-point rule for the triangles and the four-point rule for the quadrilaterals[Z1] (i.e. 2 x 2 Gauss points). However, to prevent spurious mechanisms the stiffness of the higher order quadrilateral is integrated by a five-point rule suggested by Irons[I6] as

$$\int_{-1}^{1}\int_{-1}^{1} f(\xi,\eta)\,d\xi d\eta = a\,f(0,0) + \sum_{1}^{4} b f(\pm B,\pm B) \tag{3.68}$$

where $b = (1 - \frac{1}{4}a)$ and $B = (3b)^{-\frac{1}{2}}$, and with $a = 0.2$ becomes

$$\int_{-1}^{1}\int_{-1}^{1} f(\xi,\eta)\,d\xi d\eta = 0.2f(0,0) + 0.95 \sum_{1}^{4} (\pm 0.59234888, \pm 0.59234888) \tag{3.69}$$

Ideally the stiffness matrix for an element should have a rank of (the number of nodal variables) - (the number of rigid body notions available)[I4]. The ISOFLEX plate flexure elements therefore require a rank of

---

†For Gaussian integration in one dimension n points gives exact values for the integral of a polynomial of degree 2n-1.

$$9 - 3 = 6 \quad \text{for ISOFLEX 3}$$

$$12 - 3 = 9 \quad \text{for ISOFLEX 6}$$

$$12 - 3 = 9 \quad \text{for ISOFLEX 4}$$

$$16 - 3 = 13 \quad \text{for ISOFLEX 8}$$

Since each integration point can contribute at most 3 (the rank of the modulus matrix) the integration rules mentioned previously should provide adequate rank thus avoiding spurious mechanisms.

3.5 STRESS SMOOTHING

Since reduced numerical integration has been adopted for the evaluation of the element integrals it is natural to expect these integration points to be the most appropriate stations for sampling the stresses. These points have the added attraction of enabling the element stress matrices to be evaluated concurrently with the stiffness matrix thus avoiding further entries to the shape function subroutine and increasing the computational efficiency. For the higher order quadrilateral, for numerical convenience, the stresses are sampled at the four corner points of the five-point rule.

Although the integration points give the most accurate stresses, nodal values may be more convenient. These nodal values are obtained by a linear and bilinear extrapolation of the values at the integration points, and is equivalent to a least squares best fit of the nodal values, *vide* Appendix 2.

The three integration points for the triangles, or the four integration points for the quadrilateral are used to construct a fictitious triangular or quadrilateral element subdomain. Since the stresses are assumed to vary linearly or bilinearly, the smoothed stresses both inside and outside of the fictitious element subdomain are given as

$$\tilde{\sigma} = \sum_{i=1}^{n} N_i \sigma_i \tag{3.70}$$

where $\tilde{\sigma}$ is the smoothed stress at, for example a node of the element, N_i are the linear or bilinear shape functions, and σ_i are the stress values at the n vertices of the fictitious element.

3.6 NUMERICAL RESULTS

Various numerical examples were selected to establish the validity and generality of the proposed formulation.

3.6.1 *Patch tests*

All the elements of the ISOFLEX family pass the patch test with rectangular, parallelograms and arbitrary triangular and quadrilateral geometry, Figs 3.4 to 3.6. A mixed mesh consisting of all the elements of the family, Fig.3.7, also passes this test. In this case, at the element interfaces between the lower and higher order elements, the departure from linearity of the midside rotation was constrained to zero to ensure at least C^0 continuity.

The ISOFLEX 8 element passes a super patch test of a complete cubic displacement perturbation (linear flexural strains) with quadrilateral geometry and 2 x 2 Gauss quadrature.

Although the numerical integration rules adopted are of sufficient order to prevent an individual element mechanism, a collective mechanism may have occurred. To guard against this possibility the patch tests of Figs 3.4 to 3.6 were repeated in a different form. Only sufficient boundary constraints to prevent rigid body motions, namely the translations and rotations at node number 1, were prescribed, together with the forces (reactions) already computed from the previous tests. If there was any danger of a singular assembled matrix then this procedure would encourage it to occur. Since all the elements gave constant stresses to an accuracy of six significant places for these exacting tests, it is reasonable to assume that a collective mechanism is unlikely to occur for other element shapes.

3.6.2 *Square plate convergence studies*

These convergence studies were carried out for the simple case of a thin isotropic square plate of side length ℓ, Poisson's ratio $\nu = 0.3$ and flexural rigidity D. The boundary conditions were taken as simply supported or clamped around the entire periphery, and the load cases considered were a central concentrated load or a uniformly distributed load. Taking advantage of the double symmetry, only one quarter of the plate was analysed with meshes varying as 1 x 1, 2 x 2, 4 x 4 and 8 x 8 elements. The finite element results for deflections, averaged nodal moments, reactions and external potential energy† are given in Tables 3.1 to 3.10 and are plotted against the total number of variables for one quarter of the plate before enforcing geometric boundary conditions in Figs 3.11 to 3.22. In all cases the results converge to the exact analytical solutions given by Timoshenko[T3] and the convergence is rapid compared with the other finite element results.[A4,A6,C2,R2] The distribution of moment within the elements along the centre line of the plate is given for 2 x 2 and 4 x 4 meshes in Tables 3.11 to 3.18. and plotted in Figs 3.23 to 3.38. In all cases these results compare

---

† A measure of element performance is the change in external potential energy π given by

$$\pi = \sum_{n} \{p\}^T \{w\}$$

where p is the load and w the displacement at each node, and the product is summed over the whole plate.

well with the analytical solutions given by Timoshenko and a 16 x 16 finite difference solution.[D1] For the triangles the smoothed nodal moments within the elements adjacent to the centre line of the plate are more accurate than the averaged nodal moments. For all of the elements, it can be seen that the moment values at the Gauss points on the element boundary, which are easily obtained from the smoothed nodal moments, given very good accuracy.

The prediction of moments in the vicinity of a point load is a severe test for finite element solutions, since the values tend to infinity, but even here the results shown are in excellent agreement with the exact analytical solutions.

The convergence of a simply supported square plate with a central point load is compared for various finite element formulations. The central deflection is plotted against the total number of variables for one quarter of the plate in Fig. 3.39. It can be seen that the convergence characteristics of the ISOFLEX elements are satisfactory.

3.6.3 *Clamped disc*

To demonstrate the accuracy of the curvilinear members of the ISOFLEX family when used to idealize a structure with curved boundaries, a clamped disc under concentrated and uniform loading was analysed. Taking advantage of the axi-symmetry one quarter of the plate was idealized with a coarse mesh of three curved ISOFLEX 8 quadrilaterals, or six curved ISOFLEX 6 triangles. The deflection and moment profiles are shown in Figs 3.30 to 3.41 and, considering the coarseness of mesh, are in good agreement with the exact theoretical values.

3.6.4 *Tapered beam*

To demonstrate the ability of the formulation to deal with variable thickness structures, a simple cantilever beam with a tapering thickness was analysed using eight ISOFLEX 4 elements, Fig. 3.8. The theoretical answer for deflection is 6,725 (using Simpsons rule with five stations along the length of the beam to integrate the virtual work equation) compared with the finite element solution of 6,663. The former value would become smaller with more integration stations.

3.6.5 *Skew rhombic plate with two edges simply supported*

A comparitive study was made on a skew rhombic plate of side ℓ, uniform thickness t, an angle of skew of 60°, and Poisson's ratio of 0.31, subjected to a uniformly distributed load, Fig. 3.9. The central deflection and flexural moment for the ISOFLEX elements were compared with a finite difference solution and the $ARI^{A4,A6,R1}$ triangle. Table 3.19 summarises the results. The smoothed nodal moments slightly overestimate the central value of the moment M_x, so it could be expected that the moments at the integration points would given even greater accuracy.

3.6.6. *Acute skew rhombic plate with all edges simply supported*

To establish the response of strongly distorted quadrilateral ISOFLEX elements, a comparative study was made of a thin acute skew rhombic plate with simply supported edges around the entire periphery, Fig. 3.10. The acute angle of skew was 30°, the side length was ℓ, and Poisson's ratio ν was taken as 0.3. Under a uniformly distributed load q, the flexural moments are infinite in the obtuse corner for Kirchhoff's theory, and no exact solution exists. This example is regarded as the most difficult of all thin plate flexural problems. Morley[M7] uses a series expansion with coefficients determined by the least squares method and these results are precise. The plate is idealised with mesh divisions of 2 x 2, 4 x 4, 8 x 8 and 16 x 16 elements for both the ISOFLEX 4 (with 27, 75, 243 and 867 unknowns) and the ISOFLEX 8 (with 39, 115, 387 and 1411 unknowns), with the quadrilateral elements specialised to rhomboids. For comparison, the results obtained by Sander[W6] using the quadrilateral element derived by de Veubeke[V1] are used. The vertical displacement w and two principal bending moments M'_x and M'_y in the centre of the plate are given in Table 3.20, and plotted against the total number of equations including geometric boundary constraints, Figs 3.42 to 3.43. The results for the ISOFLEX quadrilaterals are good for both displacements and averaged nodal moments (the moments at the integration points would give even greater accuracy). On the other hand the influence of the singularity on the results of the Veubeke's displacement model is such that even with a system of more than 1,000 equations the errors are significant. Fig. 3.44 shows how the elements are able to represent the singularity. The distribution of the principle moments M'_x, M'_y is plotted for the ISOFLEX 4 model (16 x 16 mesh, 867 unknowns), the ISOFLEX 8 model (16 x 16 mesh, 1,411 unknowns) and the de Veubeke quadrilateral (14 x 14 mesh, 1,095 unknowns). The results of the ISOFLEX elements are good, whereas the results for the Veubeke quadrilateral are such that it could not be used to predict the M'_y moments; even the sign is wrong. It should be noted that Wolf[W6], who has also analysed the same plate with a hybrid model based on a quadratic expansion for the moments, and cubic displacements and linear normal rotations along the element boundary, achieved a similar accuracy to the ISOFLEX results. However, this was only made possible by enforcing stress boundary conditions of zero normal moment within the elements around the boundary of the plate. If this constraint, which is inconvenient to implement, was not enforced, this element also produced poor results.

3.7 CONCLUSIONS

(i) A formulation for a general family of thin plate flexure elements has been developed. The elements may be used in triangular or quadrilateral form and are capable of representing plates with tapering thickness and curved boundaries.

(ii) The simple nodal configurations require a minimum of data preparation and allow the standard grillage beam element to be incorporated into an idealization.

(iii) The criteria for convergence is satisfied and there are no limitations such as low rank and spurious mechanisms.

(iv) The results of the numerical examples establish the validity of the formulation for an extensive range of thin plate problems, and the results are good even for coarse mesh idealizations.

(v) The ISOFLEX elements are a unified formulation which can be easily implemented by a single compact shape function subroutine, and are computationally efficient.

CHAPTER 4

EXTENSIONAL-FLEXURAL ELEMENTS FOR THE ANALYSIS OF CELLULAR STRUCTURES

4.1 INTRODUCTION

The analysis of cellular structures by the finite element method requires specialised element formulations if results of an accuracy suitable for design purposes are to be achieved with economy. Cellular structures such as certain offshore production platforms and modern elevated highway bridges, are essentially an assemblage of spatial plates subjected to flexural pertabations, and can therefore be idealized by planar extensional-flexural finite elements. The nodal configuration of such elements should be chosen for user convenience, and there are obvious advantages if the elements are capable of accurately representing the beam action of the webs with only a single element over the depth and a small number of elements along the length of the structure. Since for cellular structures the evaluation of the element stiffness matrices is usually the most expensive computational step, it is important that the element formulation is computationally efficient.

Extensional-flexural elements with three translations and three rotations as variables at the vertices are commonly used for the analysis of cellular structures. Elements with this simple nodal configuration have the advantage of being readily incorporated into finite element systems which accept only elements with a constant number of variables at each node, and transformations from the local to the global coordinate system are straightforward. These elements can also be used in conjunction with the standard space beam element for the analysis of, for example, a steel box girder bridge section with eccentric stiffness or cross-bracing. Such extensional-flexural elements require an extensional element formulation with two translations and an in-plane rotation at the vertices. Extensional elements with this simple nodal configuration are proposed in this chapter.

If a single quadrilateral extensional element with two translations and a rotation at each of the vertices is used to idealise a beam, beam action cannot be reproduced accurately. The reason for this inadequacy is that the nodal variables for such an element are only sufficient to define a linear variation of longitudinal displacement along the length of the beam instead of the quadratic variation required by beam theory.[T3] A higher order element with the required longitudinal displacement variation could be created by the introduction of a midside node on the longitudinal edges at which a tangential displacement variable is specified. This additional variable would have the minor disadvantage of producing an element with different numbers of nodal variables, but this is preferable to the use of higher order derivatives which require special treatment for abrupt changes of plate thicknesses or properties. Furthermore, if the departure from linearity of the midside tangential displacement is used instead of the absolute value, then such an element can still be used in conjunction with a standard beam element, simply by constraining this variable to be zero in the presence of a beam. A higher order element with beam performance could reduce the overall cost of an analysis since fewer elements would be required along the length of a structure. A midside node can also be used to define element boundaries that are curved in-plane, and this gives an improved geometric definition for many structures. Higher order elements with such an additional midside node are also proposed in this chapter.

Early attempts to create elements suitable for the analysis of cellular structures employed standard extensional elements with only the two translations u and v as nodal variables. When these elements were combined with flexural elements, difficulties were encountered in the transformation of the resulting elements from the local to the global axes, and an expensive fine mesh division was required for satisfactory results. To overcome these problems several authors developed extensional elements with an additional in-plane rotation θ_z as a nodal variable. Abu-Gazaleh[A2] developed a rectangular element with the in-plane rotation $\theta_z = \frac{1}{2} \left(\frac{\partial v}{\partial x} - \frac{\partial u}{\partial y} \right)$ at each node and this element was extended to a quadrilateral shape by William.[W4] The use of this nodal rotation invited small angular discontinuities between the element edges at a node and the element does not pass the patch test,[I7,I10,S8] for convergence even for a rectangular shape. Macleod[M5] developed a rectangular element with the nodal rotation θ_z taken alternatively as $\frac{\partial v}{\partial x}$ and $-\frac{\partial u}{\partial y}$ around the element, but these variables are not suitable for cellular structures because the web and flange elements would separate in the presence of shear. Lim et al[L3] and Sisodiya et al[S5] simultaneously developed a quadrilateral element with the nodal rotation θ_z taken as $\frac{\partial v}{\partial x}$. This element had a biased displacement field and could approximate the web beam action with a relatively coarse mesh, but an expensive numerical integration rule was required for the evaluation of the element stiffness matrix. Moffatt[M2] and Fam and Turkstra[F6] have recently developed elements with u,v, $\frac{\partial v}{\partial x}$ and ε_x as nodal variables. These elements possess an accurate beam response but they cannot accommodate a discontinuity in the longitudinal strain for abrupt changes of plate thicknesses or properties. An expensive numerical integration rule was also required here for the evaluation of the element stiffness matrices, and the nodal variables chosen would require a special beam element. Irons[I4-6] has developed a doubly curved shell element, but for cellular structures the additional computational expense associated with the double curvature would be unwarranted since in general cellular structures are an assemblage of flat or almost flat plates. The question arises therefore as to whether accurate and economical extensional elements can be formulated with the simple nodal configuration of three variables at the vertices and an additional midside variable for higher order elements.

In this chapter a formulation is given for a family of extensional elements which, when combined with the flexural elements of the previous chapter, are particularly efficient for the analysis of cellular structures. These elements hereafter referred to as the ISOBEAM family, form the beginning of a second generation of isoparametric extensional elements. The proposed formulation employs a biased displacement field, a reduced numerical integration rule[Z2], and includes incompatible displacement modes[W3] for additional performance. The ISOBEAM elements may have tapering thickness and boundaries that are curved in-plane and have the simplest nodal configurations, Fig. 4.1, which allow the standard space beam element to be incorporated into an idealisation. The triangular extensional elements are degenerated quadrilaterals. The elements fulfil the requirements for convergence for rectangular, parallelogram and trapezoidal element shapes, and no limitations such as low rank and spurious mechanisms have been noted. The formulation given includes anisotropic plate properties and can take account of stacked eccentric plates. The performance of the ISOBEAM elements is demonstrated by convergence studies and comparisons with classical solutions and experimental results. It is shown that only a few high aspect elements are required along the length of a structure and a single element over the depth of the web, to provide accurate results even in the vicinity of a support or wheel load. The ISOBEAM elements are a unified formulation which can be easily implemented from a single compact shape function subroutine, and they are also computationally efficient.

In parallel with the development of the new element family there is a need for information on the problem of the idealisation of a structure. The mesh divisions required for an idealisation will be indicated in this chapter by reference to convergence studies and the analysis of several cellular structures, and the results are compared with theoretical and experimental values.

4.2 REQUIREMENTS FOR ELEMENTS FOR THE ANALYSIS OF CELLULAR STRUCTURES

The requirements for finite elements suitable for the analysis of cellular structures may be summarised as follows:

(i) The elements should be capable of being used in triangular and quadrilateral form and should be capable of representing tapering thickness and boundaries curved in-plane when necessary.

(ii) The nodal configuration should be simple and permit the standard space frame element to be incorporated into an idealisation. Second or higher order derivatives should be avoided and low order elements should have a constant number of variables at each node.

(iii) As a mesh of arbitrary shaped elements is refined, convergence to the correct solution should be ensured. With certain provisos the existence of fine-mesh convergence for an element can be established by the patch test.[I7,I10]

(iv) The equations produced should not be ill-conditioned and fail for certain element geometries.

(v) The coarse mesh performance should be such that if an idealisation is in error the results are not unreasonable.

(vi) Since for cellular structures the evaluation of the element stiffness matrices is usually the most expensive computational step, it is important that the element formulation is computationally efficient.

(vii) Ideally the element family should be coded into a single compact shape function subroutine. This would ensure easy implementation and also save a substantial area of fast core storage.

(viii) The extensional element displacement and stress fields should be biased to take account of the higher order variations of displacements and stresses in the longitudinal direction of a cellular structure relative to the transverse direction.

(ix) The stress components should be available at the nodes.

4.3 THEORY FOR CONSTRAINED EXTENSIONAL ELEMENTS

The theory given in the subsequent section introduces a new approach for the formulation of extensional elements. The variation of a displacement and its derivative within the element are specified independently by suitable shape functions. These independent variations are then constrained to be compatible at discrete points within the element domain. The element formulations proposed here have a good performance and require only a low order numerical integration rule for the evaluation of the element stiffness matrix.

4.3.1 *Unconstrained displacement fields*

The unconstrained nodal configuration and coordinate systems are shown in Fig. 4.2. The discrete nodal displacements for the ith node are chosen as the global translations u and v and the local in-plane rotation $\theta_z = \frac{\partial v}{\partial x_\xi}$ which refers to the rotation of a line η = constant at each node.

By employing suitable shape functions $\bar{N}_i$ the global displacement field and the in-plane rotation derivative can be written independently as

$$\delta = \sum_{i=1}^{n} \bar{N}_i \, \delta_i \tag{4.1}$$

or in expanded form is

$$\begin{Bmatrix} u \\ v \\ \dfrac{\partial v}{\partial x_\xi} \end{Bmatrix} = \sum_{i=1}^{n} \begin{bmatrix} N_i & 0 & 0 \\ 0 & N_i & 0 \\ 0 & 0 & N_i \end{bmatrix} \begin{Bmatrix} u \\ v \\ \dfrac{\partial v}{\partial x_\xi} \end{Bmatrix}_i \tag{4.2}$$

where n is the total number of nodes. For midside nodes the discrete nodal displacements become

$$\begin{Bmatrix} u \\ v \\ \dfrac{\partial v}{\partial x_\xi} \end{Bmatrix}_i \rightleftarrows \begin{Bmatrix} \Delta u \\ \Delta v \\ \Delta\dfrac{\partial v}{\partial x_\xi} \end{Bmatrix}_i \tag{4.3}$$

where the symbol Δ refers to the departure from linearity of the value with respect to the values at the corner nodes. This departure from linearity is defined as

$$\Delta\delta_i = \delta_i - \frac{1}{2}(\delta_\ell + \delta_m) \tag{4.4}$$

where ℓ and m refer to the two corner nodes.

4.3.2 *Hierarchical shape functions*

The hierarchical shape functions used here take account of the variables specified as the departure from linearity. The hierarchical shape functions are defined in natural coordinates as

$$N_i = \frac{1}{4}(1 + \xi_o)(1 + \eta_o) \qquad \text{for } i = 1,4$$
$$N_i = \frac{1}{2}(1 - \xi^2)(1 + \eta_o) \qquad \text{for } i = 5,6 \qquad (4.5)$$

where $\xi_o = \xi\xi_i$ and $\eta_o = \eta\eta_i$

4.3.3 *Additional incompatible displacement modes*

In general the addition of incompatible displacement modes violates interelement compatibility. However since the magnitudes of the modes are selected by requiring that the total strain energy of the element is a minimum, guaranteed convergence could be expected for some element geometries. Accordingly, for an improved element performance the following incompatible modes were included in the quadrilateral element formulations. The incompatible modes added to the displacement field of eqn. 4.2 are

$$u = \sum_i N_i^I \alpha_i$$
$$v = \sum_j N_j^I \beta_j \qquad (4.6)$$

where i = 1,2 and j = 1 for the four node quadrilateral

and i = 1 and j = 1 for the six node quadrilateral

and the displacement amplitudes α_i and β_j are additional nodeless variables in the global directions. The incompatible shape functions N^I are defined as

$$\begin{aligned} N_1^I &= (1 - \eta^2) \\ N_2^I &= (1 - \xi^2) \end{aligned} \tag{4.7}$$

These incompatible displacement nodes are shown in Fig.4.3.

4.3.4 *Hierarchical mapping and the Jacobian matrix*

It is now necessary to establish the relationship between the Cartesian and natural curvilinear coordinate systems. The x and y coordinates and thickness t at the point ξ,η within the element can be written in a special form as

$$\begin{Bmatrix} x \\ y \\ t \end{Bmatrix} = \sum_{i=1}^{n} N_i \begin{Bmatrix} x \\ y \\ t \end{Bmatrix}_i \tag{4.8}$$

where the hierarchical shape functions N_i at each node are in terms of the natural ξ,η coordinates and the summation is taken over n nodes sufficient to define the element geometry. When midside nodes are included the nodal coordinates $\{x,y,t\}_i^T$ become the departures from linearity $\{\Delta x, \Delta y, \Delta t\}_i^T$ which are defined simply as

$$\begin{Bmatrix} \Delta x \\ \Delta y \\ \Delta t \end{Bmatrix}_i = \begin{Bmatrix} x \\ y \\ t \end{Bmatrix}_i - \frac{1}{2} \begin{Bmatrix} x \\ y \\ t \end{Bmatrix}_\ell - \frac{1}{2} \begin{Bmatrix} x \\ y \\ t \end{Bmatrix}_m \tag{4.9}$$

where i is now a midside node and ℓ and m are the adjacent corner nodes.

Since the shape functions are in terms of the natural ξ, η coordinates it is necessary to establish a relationship to calculate the Cartesian derivatives for the components of the strain matrix. From the chain rule in two dimensions

$$\begin{Bmatrix} \frac{\partial}{\partial \xi} \\ \frac{\partial}{\partial \eta} \end{Bmatrix} = \begin{bmatrix} \frac{\partial x}{\partial \xi} & \frac{\partial y}{\partial \xi} \\ \frac{\partial x}{\partial \eta} & \frac{\partial y}{\partial \eta} \end{bmatrix} \begin{Bmatrix} \frac{\partial}{\partial x} \\ \frac{\partial}{\partial y} \end{Bmatrix} = [J] \begin{Bmatrix} \frac{\partial}{\partial x} \\ \frac{\partial}{\partial y} \end{Bmatrix} \tag{4.10}$$

where J is defined as the Jacobian matrix.

Inverting the Jacobian matrix in eqn. 4.10 gives the required transformation relationship as

$$\begin{Bmatrix} \frac{\partial}{\partial x} \\ \frac{\partial}{\partial y} \end{Bmatrix} = \frac{1}{\det [J]} \begin{bmatrix} \frac{\partial y}{\partial \eta} & -\frac{\partial y}{\partial \xi} \\ -\frac{\partial x}{\partial \eta} & \frac{\partial x}{\partial \xi} \end{bmatrix} \begin{Bmatrix} \frac{\partial}{\partial \xi} \\ \frac{\partial}{\partial \eta} \end{Bmatrix} = \begin{bmatrix} \frac{\partial \xi}{\partial y} & \frac{\partial \eta}{\partial x} \\ \frac{\partial \xi}{\partial y} & \frac{\partial \eta}{\partial y} \end{bmatrix} \begin{Bmatrix} \frac{\partial}{\partial \xi} \\ \frac{\partial}{\partial \eta} \end{Bmatrix} \tag{4.11}$$

For numerical convenience the coordinates and the components of the Jacobian matrix at any point ξ,η within the element can be computed collectively from eqn. 4.8 as

$$\begin{bmatrix} x & y & t \\ \frac{\partial x}{\partial \xi} & \frac{\partial y}{\partial \xi} & \frac{\partial t}{\partial \xi} \\ \frac{\partial x}{\partial \eta} & \frac{\partial y}{\partial \eta} & \frac{\partial t}{\partial \eta} \end{bmatrix} = \sum_{i=1}^{x} \begin{bmatrix} N_i & N_i & N_i \\ \frac{\partial N_i}{\partial \xi} & \frac{\partial N_i}{\partial \xi} & \frac{\partial N_i}{\partial \xi} \\ \frac{\partial N_i}{\partial \eta} & \frac{\partial N_i}{\partial \eta} & \frac{\partial N_i}{\partial \eta} \end{bmatrix} \begin{bmatrix} x_i & 0 & 0 \\ 0 & y_i & 0 \\ 0 & 0 & t_i \end{bmatrix} \tag{4.12}$$

where as before the i nodal values are summed over the nodes defining the element geometry and when midside nodes are present the nodal coordinates become the departures from linearity.

For incompatible modes the Jacobian is calculated at the ξ,η origin so that the elements will pass the patch test for shapes, including rectangles, parallelograms and trapeziums.[T6]

4.3.5 *Kinematic constraints*

The unconstrained nodal variables and the incompatible displacement variables when present, are now reduced to the constrained extensional nodal configurations, Fig. 4.1 by the application of appropriate sets of independent constraints.

(i) The midside normal displacement and in-plane rotation - 4 constraints

The constraints for these variables are enforced in a discrete fashion so that the displacement field and in-plane rotation derivative which are specified independently, eqn. 4.2, become effectively linked. From the first two lines of eqn. 4.2 the in-plane rotation can be obtained by differentiation and must be expressed in the local axes in the line η = constant. This local axes is defined by the vectors $\hat{J}_\xi$ and $\hat{j}$ (see previous chapter) and so

$$\begin{Bmatrix} \dfrac{\partial}{\partial \xi} \\ \\ \dfrac{\partial}{\partial \eta} \end{Bmatrix} = \begin{bmatrix} \vec{J}_\xi \cdot \hat{J}_\xi & \vec{J}_\xi \cdot \hat{j}_\xi \\ \\ \vec{J}_\eta \cdot \hat{J}_\xi & \vec{J}_\eta \cdot \hat{j}_\xi \end{bmatrix} \begin{Bmatrix} \dfrac{\partial}{\partial x_\xi} \\ \\ \dfrac{\partial}{\partial y_\xi} \end{Bmatrix}_i \qquad (4.13)$$

where $\hat{J}$ are the covariant and $\hat{j}$ the contravariant unit base vectors. On solving eqn. 4.13 the local derivative $\dfrac{\partial N_i}{\partial x_\xi}$ is found and hence the in-plane rotation derivative $\dfrac{\partial v}{\partial x_\xi}$ can be obtained as

$$\frac{\partial v}{\partial x_\xi} = \sum_{i=1}^{x} \frac{\partial N_i}{\partial x_\xi} \vec{U}_i \cdot \hat{j} \qquad (4.14)$$

where $\vec{U}_i$ is the vector of displacements at node i.

The in-plane rotation derivative found above and the in-plane rotation derivative specified in eqn. 4.2 are now constrained to be identical at the Gauss points along the top and bottom edges of the element

$$\frac{\partial v}{\partial x_\xi} - \frac{\partial v}{\partial x_\xi} = 0 \qquad (4.15)$$

Expanding eqn. 4.15 from eqns 4.2 and 4.14 for each side Gauss point gives

$$\begin{Bmatrix} \left(\dfrac{\partial v}{\partial x_\xi} - \dfrac{\partial V}{\partial x_\xi} \right)_1 \\ \cdot \\ \cdot \\ \cdot \end{Bmatrix} = \begin{Bmatrix} 0 \\ \cdot \\ \cdot \\ \cdot \end{Bmatrix} = \begin{bmatrix} \underset{4\text{x}14}{M_A} & \vdots & \underset{4\text{x}4}{M_B} \end{bmatrix} \begin{bmatrix} \delta_A \\ \hline \delta_B \end{bmatrix} \qquad (4.16)$$

where δ_A are the variables for the required nodal configuration and δ_B are the variables to be discarded. The columns of M are transformed for the tangential and normal displacements at the midside nodes, the displacement vector is

$$\{\delta_A \mid \delta_B\}^T = \{ (u,\, v,\, \frac{\partial v}{\partial x_\xi})_i \; . \; . \; . \; \Delta U'_j \; . \mid (\Delta v, \Delta \frac{\partial v}{\partial x_\xi})_j \; . \} \tag{4.17}$$

where i refers to the corner nodes and j to the midside nodes.

Rearranging eqn. 4.16 gives an expression for the variables to be discarded as

$$\delta_B = - M_B^{-1} M_A \delta_A \tag{4.18}$$

If W is the shape function array, which is constructed from the values and derivatives of the u and v variations, eqn. 4.2, then introducing expression 4.18 gives

$$\{\delta^*\} = [W_A - W_B M_B^{-1} M_A] \{\delta_A\} \tag{4.19}$$

or $$\delta^* = W_c \delta^e \tag{4.20}$$

where δ^* is a vector of displacements and derivatives at any point ξ,η within the element, W_c is the constrained shape function array and δ^e are the required element variables.

(ii) The incompatible displacement amplitudes - 2 or 3 constraints

When incompatible displacement modes are required the constraints imposed are that the external forces associated with the nodeless displacement amplitudes should be zero. The new shape function array, eqn. 4.20 is expanded to include the two or three columns corresponding to the incompatible displacement modes. The force displacement relationship requires the computation of the rows of the stiffness matrix which correspond to the incompatible displacement amplitudes

$$\left\{\begin{matrix} P_1 \\ \cdot \\ \cdot \end{matrix}\right\} = \left\{\begin{matrix} 0 \\ \cdot \\ \cdot \end{matrix}\right\} = \Big[\underset{3\times12}{K_A} \;\Big|\; \underset{3\times3}{K_\alpha} \Big] \left\{\begin{matrix} \delta_A \\ \hline \delta_\alpha \end{matrix}\right\} \qquad (4.21)$$

and hence

$$\delta_\alpha = - K_\alpha^{-1} \; K_A \; \delta_A \qquad (4.22)$$

The new shape function array is now given from eqn. 4.20 and 4.22 as

$$\{\delta^*\} = \left[W_c - W_\alpha \; K_\alpha^{-1} \; K_A \right] \{\delta_A\} \qquad (4.23)$$

or

$$\delta^* = W_d \; \delta^e \qquad (4.24)$$

where the components of δ^* are

$$\delta^* = \{u, \frac{\partial u}{\partial x}, \frac{\partial u}{\partial y}, v, \frac{\partial v}{\partial x}, \frac{\partial v}{\partial y}\}^T \qquad (4.25)$$

and W_d is a 6 x 12 or 6 x 14 shape function array, the size of which depends on the element chosen.

The inversion of the matrices M_B and K_α are avoided by the collective scheme mentioned in the previous chapter.

4.3.6 *Degenerate triangles*

The ISOBEAM triangles are formed from the quadrilateral elements by specifying two nodes at one end of the quadrilateral to be coincident, and combining the variables at that node. However to ensure the compatibility of variables at this degenerate node the in-plane rotation $\frac{\partial v}{\partial x}$ was employed as opposed to $\frac{\partial v}{\partial x_\xi}$. The degenerate end of the quadrilateral was chosen to be adjacent to the longest sides of the triangle to preserve the beam action, and this can be carried out automatically in the shape function subroutine. The use of degenerate triangles is acceptable providing values of ξ and η, for which the shape function array may be required, lie within the element domain. Additional incompatible modes are not acceptable in this case. These triangular members of the ISOBEAM family are proposed but as yet have not been investigated numerically.

4.3.7 *Strain-displacement relation*

The strain components in two-dimensions can now be related to the discrete nodal displacements by extracting the appropriate rows from the shape function array. The two-dimensional strain components are defined as

$$\varepsilon = \begin{Bmatrix} \varepsilon_x \\ \varepsilon_y \\ \varepsilon_{xy} \end{Bmatrix} = \begin{Bmatrix} \frac{\partial u}{\partial x} \\ \frac{\partial v}{\partial y} \\ \frac{\partial u}{\partial y} + \frac{\partial v}{\partial x} \end{Bmatrix} \tag{4.26}$$

and in terms of the nodal displacements

$$\varepsilon = B\,\delta^{e} \tag{4.27}$$

where B is the strain matrix which is formed from the shape function array.

4.3.8 *Stress-strain relation*

The stress components σ in two-dimensions are related to the strain components ε by the familiar equation

$$\sigma = D\,\varepsilon \tag{4.28}$$

where D is the extensional modulus matrix. This modulus matrix can be written as

$$D = \begin{bmatrix} d_x & d_1 & 0 \\ d_1 & d_y & 0 \\ 0 & 0 & d_{xy} \end{bmatrix} \tag{4.29}$$

where for an isotropic material

$$dx = dy = \frac{E}{1-\nu^2}$$

$$d_1 = \frac{\nu E}{1-\nu^2} \tag{4.30}$$

$$d_{xy} = \frac{E}{2(1+\nu)}$$

in which E is the elastic modulus and ν is Poisson's ratio. For an orthotropic material in which the principal directions of orthotropy coincide with the X and Y axes the modulus matrix is given by

$$\begin{aligned} d_x &= \frac{E_x}{1-\nu_{xy}\,\nu_{yx}} \\ d_y &= \frac{E_y}{1-\nu_{xy}\,\nu_{yx}} \\ d_1 &= \frac{\nu_{xy}\,E_y}{1-\nu_{xy}\,\nu_{yx}} \\ d_{xy} &= G \end{aligned} \tag{4.31}$$

where E_x and E_y are the elastic moduli and ν_{xy} and ν_{yx} are Poisson's ratios with respect to the x and y axes, and G is the shear modulus.

The stress components can be related to the discrete nodal displacements by combining eqns 4.27 and 4.28

$$\sigma = D\ B\ \delta^e \tag{4.32}$$

and advantage should be taken of the sparse nature of D to avoid any unnecessary multiplications during the evaluation of this matrix product.

4.3.9 *Numerically integrated stiffness matrix*

The element stiffness matrix is defined as[Z1]

$$K^e = \int B^T D B \, dv \tag{4.33}$$

Introducing the standard expression

$$dv = t|J| \, d\xi \, d\eta \tag{4.34}$$

and noting that B is a function of ξ,η, eqn.4.33 can be rewritten in the form

$$K^e = \int_{-1}^{+1}\int_{-1}^{+1} B^T D B \, t|J| \, d\xi \, d\eta$$

or in submatrix form

$$K^e_{ij} = \int_{-1}^{+1}\int_{-1}^{+1} B_i^T D B_j \, t|J| \, d\xi \, \partial\eta \tag{4.36}$$

where K_{ij} is a typical submatrix linking nodes i and j. When evaluating the triple product $B_i^T D B_j$ advantage should be taken of the sparsity of D thus avoiding many unnecessary matrix manipulations.

The integration of the stiffness coefficients is carried out numerically, and eqn.4.36 is replaced by a weighted summation of the values at certain points in the element

$$K^e = \sum_{p=1}^{n} W_p \left[f(\xi_p, \eta_p) \right] \tag{4.37}$$

where $\left[f(\xi_p,\eta_p) \right] \equiv B^T D B t|J|$ is calculated at the appropriate sampling points ξ_p, η_p and W_p is the corresponding weight coefficient at this point.

4.4 REDUCED NUMERICAL INTEGRATION AND SPURIOUS MECHANISMS

The reduced numerical integration rule adopted here permits an economical evaluation of the element stiffness matrices. The four point Gauss rule is used for all elements of the ISOBEAM family.

The stiffness matrix should have a rank of (the number of nodal variables) - (the number of rigid body motions available)[14]. The ISOBEAM elements therefore require a rank of

9	-	3	=	6	for	ISOBEAM	3
11	-	3	=	8	"	"	5
12	-	3	=	9	"	"	4
14	-	3	=	11	"	"	6

Since each integration point can contribute at most 3 (the rank of the modulus matrix) the four point integration rule could provide adequate rank thus avoiding spurious mechanisms.

4.5 STRESS SMOOTHING

Since reduced numerical integration has been adopted for the evaluation of the element stiffness matrices, it is natural to expect the integration points to be the most appropriate stations to sample the stresses. These stations enable the stress and strain matrices to be evaluated concurrently with the stiffness matrix thus reducing the number of entries to the shape function subroutine and increasing the computational efficiency.

The stress values at the integration points are the most accurate[B5], but nodal values may be more convenient for the interpretation of results. The nodal values are obtained by a bi-linear extrapolation of the integration point values and is equivalent to a least squares best fit of the nodal values, *vide* Appendix 2. The integration points are used to construct a fictitious quadrilateral element subdomain and the smoothed stresses both inside and outside of the subdomain are given as

$$\tilde{\sigma} = \sum_{i=1}^{4} N_i \, \sigma_i \qquad (4.38)$$

where $\tilde{\sigma}$ is a smoothed stress at, for example, a node of the element, N_i are the bi-linear shape functions, and σ_i are the stress values at the four vertices of the fictitious quadrilateral element.

4.6 EXTENSIONAL-FLEXURAL ELEMENTS

The extensional elements described in this chapter and the flexural elements of the previous chapter are now combined to form thin flat extensional-flexural elements in space. Since both the extensional and flexural element formulations take account of curved boundaries the resulting ISOBEAM shell elements may also have boundaries that are curved in-plane. The element orientation in space is taken as the least squares best fit of the corner nodes. The element stiffness matrices are evaluated and combined in the local coordinate axes, where the local x direction is defined by the first two element nodes and the local y direction lies in the element plane. When the global element nodes are not coplanar the orientation of the local element axes can be taken as the least squares best fit plane. The relationship between local nodal variables δ' and global variables δ is given as

$$\delta' = T\delta \tag{4.39}$$

where T is the super diagonal transformation matrix

$$T = \begin{bmatrix} T_1 & 0 & 0 & 0 \\ 0 & T_2 & 0 & 0 \\ 0 & 0 & T_3 & 0 \\ 0 & 0 & 0 & T_4 \end{bmatrix} \tag{4.40}$$

The matrix T_i is a 6 x 6 transformation matrix of direction cosines where i is for each corner node. By the rules of orthogonal transformation the global stiffness matrix K is obtained from the local stiffness matrix K' as

$$K = T^T K' T \tag{4.41}$$

When evaluating this triple produce advantage should be taken of both the sparsity of T and K' thus avoiding many unnecessary matrix manipulations.

4.7 STACKED PLATES

For a stack of extensional-flexural elements each with an eccentricity of e from a nodal plane, the relationship between the local element variables δ' and the global variables δ is given at each node by

$$\delta' = T_e \, \delta \tag{4.42}$$

where T_e is the transformation matrix for eccentricity defined by

$$T_e = \begin{bmatrix} 1 & 0 & 0 & 0 & e & 0 \\ 0 & 1 & 0 & -e & 0 & 0 \\ 0 & 0 & 1 & 0 & 0 & 0 \\ 0 & 0 & 0 & 1 & 0 & 0 \\ 0 & 0 & 0 & 0 & 1 & 0 \\ 0 & 0 & 0 & 0 & 0 & 1 \end{bmatrix} \tag{4.43}$$

where e is the eccentricity and is measured from the plane of the plate to the reference plane. This transformation is valid for small eccentricities.

4.8 NUMERICAL RESULTS

Various numerical examples were selected to establish the validity and generality of the proposed formulation. The performance of the degenerate triangular elements was not investigated numerically.

4.8.1 *Patch tests*

Both quadrilateral elements of the ISOBEAM family pass the patch test with rectangular, parallelogram and trapezoidal element geometry, Fig. 4.4.

4.8.2 *Straight cantilever beam*

The in-plane performance of the ISOBEAM 4 and ISOBEAM 6 elements was tested by analysing a cantilever beam, Fig. 4.5. The beam was idealized with one mesh division over the depth and from 1 to 4 elements along the length and the results are given in Table 4.2 and compared the engineers theory of bending ETB including shear deformation. It should be emphasized that for ISOBEAM 4 the longitudinal stress is approximately constant over the length of the element and for improved results an extrapolation procedure could be used for the values at the support. However, for ISOBEAM 6 in which the stresses vary linearly along the length of the element, the values can be obtained directly. The shear stress values were obtained from the average of the four corner node values for both element types and this result is satisfactory. For the ISOBEAM 6 element the values for deflection w, longitudinal stress σ_x, transverse stress σ_y and shear stress σ_{xy} are satisfactory for a single element idealization with an element aspect ratio of 8 to 1.

4.8.3 *Curved cantilever beam*

The performance of the ISOBEAM 4 and ISOBEAM 6 elements when used to idealize a curved structure was tested by analysing a curved slender cantilever beam, Fig. 4.6. The beam was idealized with one mesh division over the depth and from 2 to 8 elements along the length and the results are given in Table 4.2 and compared with the engineers theory of bending ETB, excluding shear deformations.

The penalty for using the straight sided ISOBEAM 4 element for a curved structure is not significant for the deflection values, and the stress values would be improved if an extrapolation procedure were employed. For the ISOBEAM 6 element the results for the vertical deflection w and the longitudinal stress σ_x, are satisfactory for a two element idealization with an element aspect ratio of 13.35 to 1.

4.8.4 *Straight single cell box girder*

The first three dimensional structure to be considered was a straight single cell box girder of uniform thickness, Fig. 4.7. This girder was analysed for fixed end conditions with diaphragms assumed to have infinite stiffness in-plane to prevent distortion and infinite stiffness out-of-plane to prevent warping. The loading was a concentrated load on one web at midspan. For the analysis this load was separated into flexural and distortional components so that the results could be compared with those obtained using the elementary theory of bending ETB, and beam on elastic foundations analogy BEF[B6] respectively.

The girder was idealized with both ISOBEAM 4 and ISOBEAM 6 elements with one mesh division over the width and depth, and from 2 to 16 mesh divisions over the length of the girder, Fig. 4.8. The values at the midspan for the deflection w_F and the longitudinal stress σ_F caused by the flexural component of load, and the distortional warping stress σ_{DW} and transverse distortional flexural stress σ_{DF} caused by the distortional component of the load obtained using the various mesh divisions, are given in Table 4.3. It can be seen that the finite element results converge to the same value with ISOBEAM 6 giving the highest rate of convergence. It should be noted that the ETB and BEF results do not agree exactly with the converged finite element results because these techniques involve additional simplifying assumptions not made in the finite element analyses.

It should be emphasized that for ISOBEAM 4 the longitudinal extensional strain is approximately constant over the length of the element and for improved results an extrapolation procedure could be used for σ_F and σ_{DW} values directly under the load. However, for ISOBEAM 6 in which the strains vary linearly along the length of the element, the peak values can be obtained directly. The difference in computer cost between the two elements for this structure was negligible.

4.8.5 *Straight three cell box girder bridge model*

A straight three cell bridge model, Fig. 4.9, was analysed with ISOBEAM 4 and ISOBEAM 6 elements. This model is a 1/60 scale representation of an approach span to the lower Yarra Bridge, Melbourne and was constructed in perspex[M2]. Details of the model and instrumentation are given in Fig. 4.10.

The model was loaded eccentrically with a point load applied to a cantilever at midspan, Fig. 4.9.

Taking advantage of symmetry only one-half of the model was analysed using the idealization shown in Fig. 4.11 for both element types. In both cases the diaphragm was represented by ISOBEAM 4 elements and the support stiffnesses were transformed to the nodes at the outer webs on the assumption that the diaphragm was infinitely rigid in its own plane.

The experimental results of the displacements and strains are given in Figs 4.12 to 4.14. These results compare favourably with the finite element results, Figs 4.13 to 4.15. The strain results for both elements are similar and it should be noted in particular that the formulations accommodate a linear variation of transverse extensional strain over the depth of the webs, Fig. 4.15(c). This strain variation would not be present if the formulation had not included incompatible displacement modes. Finally it should be noted that good results have been obtained for a structure which includes an abrupt change in thickness of the inner webs.

4.8.6 *Straight multicell bridge model*

Experiments have been conducted at the Transport and Road Research Laboratory on a six-cell perspex model[D2]. The model was simply supported at both ends and subjected to a central point load applied to the top flange. For the finite element analysis a coarse mesh idealization of one-quarter of the model was chosen, Fig. 4.16. It should be noted that for an accurate analysis in the vicinity of the stress concentration a localized fine mesh would be required.

It can be seen that the experimental values and the finite element results, Fig. 4.17 are in general in good agreement for deflections, longitudinal extensional strains and transverse flexural strains. Although no experimental results were available directly under the applied load it could be expected that high peak values would be present due to the exceptionally thin walls and small contact area of the applied load. However, in a concrete bridge the cell walls would be thicker and the load would be applied over a less concentrated area (a train of wheel loads for example). In this case, for design purposes, a coarse mesh analysis should be adequate, but a static equilibrium check of longitudinal stresses should always be performed.

4.8.7 *Curved single cell box girder bridge model*

Further experimental verification of the proposed finite element formulations was provided by reference to experimental results obtained from a curved single cell model[L3] shown in Fig. 4.18. The model was idealized with a coarse mesh of 4 by 2 by 1 for both the ISOBEAM 4 and ISOBEAM 6 elements , Fig. 4.19.

The experimental results are given in Fig. 4.18 for a point load of 100 lbf placed over the outer web at the midspan. The finite element results for both elements agree well with the experimental values, Figs 4.20 to 4.21. It should be noted that it was necessary to use an extrapolation procedure to obtain the results shown for ISOBEAM 4 whereas the results for ISOBEAM 6 were obtained directly.

4.9 CONCLUSIONS

(i) A formulation for a family of triangular and quadrilateral extensional-flexural elements has been proposed. The formulation has been developed for triangular and quadrilateral elements that are efficient in representing the special geometric properties and structural behaviour of cellular structures. The geometric properties of the elements take account of boundaries curved in-plane and tapering thickness.

(ii) The simple nodal configurations require a minimum of data preparation and allow the standard space beam element to be incorporated into an idealization.

(iii) The criteria for convergence for the quadrilateral elements is satisfied for rectangular, parallelogramic and trapezoidal element geometry and can therefore be used for the analysis of right, skewed and trapezoidal cellular structures. Numerical studies have not been conducted for the proposed formulation for the triangular elements.

(iv) Theoretical and experimental results for several cellular bridge structures were used as a basis for determining the accuracy of the proposed quadrilateral elements. Reliable results were obtained for displacements and extensional-flexural stresses with as few as one mesh division over the depth and four to six mesh divisions over the length of a structure. In particular it should be noted that these elements provide an accurate estimation of the extensional transverse and shear stresses in addition to the longitudinal stresses in the webs.

(v) A comparison of results between the ISOBEAM 4 and ISOBEAM 6 elements indicate that for a similar computer time they are equally efficient. The higher order element, ISOBEAM 6, has the advantage of accommodating curved boundaries, requires fewer elements and data input, and the stress components are available directly without an extrapolation procedure.

(vi) The ISOBEAM elements are a unified formulation which can be easily implemented by a single compact shape function subroutine, and are computationally efficient.

GENERAL CONCLUSIONS

5.1 SUMMARY OF WORK

The work described in this thesis has involved the development of the following:

(i) The LUSAS general finite element computer system for the analysis of a wide range of static linear structures.

(ii) The ISOFLEX family of elements which are particularly efficient in representing the structural response of thin plates in flexure.

(iii) The ISOBEAM family of elements which are particularly efficient in representing the structural response of cellular structures subjected to flexural and torsional perturbations.

5.2 CONCLUDING REMARKS

A general finite element computer system, LUSAS, has been developed and the application of this system to various structural problems has been described. These problems represent a wide range of static linear structures having various geometries, boundary conditions and loading conditions. In each case the finite element results compare well with the theoretical and experimental results, thus establishing the overall validity of the computer system and emphasizing the versatility of the finite element method. The LUSAS computer system could therefore be utilized for parametric studies of many static linear structures for the formulation of design rules.

By virtue of its modularity, flexibility and efficiency, the LUSAS computer system forms a sound basis for the continued development of a general analysis system within the Civil Engineering Department of Imperial College. Possible developments are, for example, incremental techniques for the dynamic response of structures including material and geometric non-linearities. In addition, singular finite elements could be developed and incorporated for the analysis of crack propogation as found in fatigue problems. The computer system has also been organised so that a multilevel substructure facility could be quickly and easily introduced for the analysis of large structures with similar superelements or bifurcations. The addition of these facilities would enable the finite element method to be applied to many problems encountered in, for example, the field of OFFSHORE ENGINEERING.

In recent years many finite element formulations have appeared in the literature, but to date these have not included formulations for a family of thin plate flexure elements or a family of extensional-flexural elements. These element families which incorporate many useful features may prove advantageous to engineers who nowadays have to decide not whether a problem can be solved but which elements should be used. The accuracy, efficiency and easy implementation of the proposed element families are persuasive features.

The field of application of the present element formulations is wide. Since both element families converge to the correct solution with very coarse meshes, and since they are computationally efficient, they could be effective for the study of non-linear extensional-flexural plate problems, including geometric and material non-linearities. A special purpose computing system could be assembled and developed from the LUSAS modules for this purpose.

Although the proposed element formulations are justified by the patch test, the theoretical basis is obscurred by the application of kinematic constraints and the use of inexact numerical integration. If the true theoretical basis could be established a more systematic approach to the development of these incompatible elements would be advantageous to future research. Perhaps the concept of substitute shape functions[Z4] would apply here.

REFERENCES

A1 Argyris, J.H. Energy theorems and structural analysis, Aircraft Engineering, 1954-55.

A2 Abu-Gazaleh, B.N. Analysis of plate-type prismatic structures. Ph.D. Univ. of California, Berkeley, 1965.

A3 Ahmad, S. et al. Analysis of thick and thin shell structures by curved finite elements. Int. J. Numer. Meth. Eng., 1970, 2, 419-451.

A4 Allman, D.J. Triangular finite elements for plate bending with constant and linearly varying bending moments. IUTAM Colloquium on high-speed computing of elastic structures, Univ. of Liege, Belgium, 1970.

A5 Adini, A. and Clough, R.W. Analysis of plate bending by the finite element method and Report to Nat. Sci. Found/ USA, G.7337, 1961.

A6 Allman, D.J. A simple cubic displacement element for plate bending. Int. J. Numer. Meth. Eng., 1976, 10, 263-281.

A7 ASKA reference manual, Univ. of Stuttgart, ISD-report No. 73, 1971.

B1 Bazeley, G.P. et al. Triangular elements in plate bending - conforming and non-conforming solutions. Proc. Conf. Matrix Methods Struct. Mech. WPAFB, Ohio, Oct. 1965.

B2 Baldwin, J.T., Razzaque, A. and Irons, B. Shape function subroutine for an isoparametric thin plate element, Int. J. Num. Meth. in Eng., Vol. 7, 431-440, 1973.

B3 Bettees, P. The finite element method for plates in flexure. M.Sc. thesis, Imperial College, 1968.

B4 Bates, D. Curved, super-parametric finite elements in the analysis of thick and thin plates and slabs. M.Sc. thesis, Imperial College, 1972.

B5 Barlow, J. Optimal stress locations in finite element models. Int. J. Num. Meth. in Eng., Vol. 10, 243-251, 1976.

B6 Billington, C.J. The theoretical and experimental elastic behaviour of box girder bridges, Ph.D. thesis, Imperial College, 1974.

B7 Basu, A.K. and Dawson, J.M. Orthotropic sandwich plates. Proc. Instn. Civ. Engrs, 1970, suppl. 87-115.

B8 Brebbia, C.A. and Connor, J.J. Fundamentals of finite element techniques, Butterworths, 1973.

C1 Clough, R.W. The finite element in plane stress analysis, ASCE Conf. Pittsburgh, Sept. 1960.

C2 Clough, R.W. and Felippa, C.A. A refined quadrilateral element for analysis of plate bending, Proc. 2nd Conf. Matrix Methods in Struct. Mech. WPAFB 1968.

C3 Cook, R.D. and Samaan, G.L. Observations regarding assumed-stress hybrid plate elements, Int. J. Num. Meth. Eng., Vol. 8, No. 3, 1974.

C4 Clough, R.W. and Tocher, J.L. Finite element stiffness matrices for analysis of plates in bending. Proc. Conf. Matrix Methods Struct. Mech. WPAFB, Ohio, Oct. 1965.

C5 Cowper, G.R. Gaussian quadrature formulas for triangles. Int. J. for Num. Meth. Eng. 7 (1973) 405-408.

C6 Cook, R.D. More on reduced integration and isoparametric elements. Int. J. Num. Meth. Eng. (8), 141-148, 1972.

C7 Cheung, Y.K. Folded plate structures by the finite strip method. J. Struct. Div. Proc. ASCE, Vol. 95, 1969, pp. 2963-79.

C8 Clough, R.W. and Penzien, J. Dynamics of structures. McGraw-Hill, New York, 1975.

C9 Corum, J.M. et al. Theoretical and experimental stress analysis of ORNL thin-shell cylinder to cylinder model 1, USAEC Rpt. ORNL-4553, Oak Ridge National Laboratory.

D1 Djahani, P. Elastic-plastic analysis of discretely stiffened plates. Ph.D. thesis to be submitted to the University of London, 1977.

D2 Das, P.C. and Crisfield, M.A. Multicell bridge decks - model tests and theoretical analysis. Report LR 493, Transport and Road Research Laboratory, Crowthorne, 1972.

D3 Dean, J.A. The collapse behaviour of steel plating subject to complex loading. Ph.D. thesis, Imperial College, 1975.

E1 Elias, Z.M. Duality in finite element methods, Proc. ASCE, Journal of the Eng. Mech. Div., Vol. 94, No. EM-4, Aug. 1968, pp. 931-946.

F1 Fenves, J. et al. Numerical and computer methods in structural mechanics. Academic Press, 1973.

F2 Fuchs, G., Roy, J.R., Schrem, E. Hypermatrix solution of large sets of symmetric positive-definite linear equations. Computer Methods in Applied Mechanics and Engineering 1, 1972.

F3 Faddeeva, V.N. Computational methods of linear algebra. Dover Publications.

F4 Fried, I. Shear in C^o and C^1 bending finite elements. Int. J. Solids Struct., Vol. 9, 449-460, 1973.

F5 Fried, I. and Yang, S.K. Triangular, nine-degrees-of-freedom, C^o plate bending element of quadratic accuracy. Quart. appl. math., Oct. 1973.

F6 Fam, A. and Turkstra, C. A finite element scheme for box bridge analysis. Computers and Structures, Vol. 5, 179-186, 1975.

G1 Gallagher, R.H. Large-scale computer programs for structural analysis, from general purpose finite element computer programs. Edited by Marcal, P.V. New York, ASME 1970.

G2 Genysis reference manual, The Genesys Centre, Loughborough, Sept. 1972.

G3 Greste, O. Finite element analysis of tubular K joints. Univ. Calif. Rpt. UCSESM 70-11, 1970.

H1 Hinton, E., Razzaque, A., Zienkiewicz, O.C. and Davies, J.D. A simple finite element solution for plates of homogeneous, sandwich and cellular construction. Proc. Instn. Civ. Engrs. Part 2, March 1975.

H2 Hinton, E., Scott, F.C. and Ricketts, R.E. Local least squares stress smoothing for parabolic isoparametric elements. Int. J. for Num. Meth. Eng. 9 (1974) 235-256.

H3 Herrman, L.R. A bending analysis for plates, Proc. conf. on matrix methods in structural mechanics, WPAFB, Ohio, 1965.

I1 Irons, B.M. A frontal solution program for finite element analysis. Int. J. Num. Meth. Eng., Vol. 2 (1970), 5-32.

I2 Irons, B.M. and Kan, D.K.Y. Equation solving algorithms for the finite-element method, O.N.R. Symp. on Numerical and Computer Methods in Structural Mechanics, Univ. of Illinois (1971).

I3 Irons, B.M. and Razzaque, A. A further modification to Ahmad's shell element. Int. J. Num. Meth. Eng., Vol. 5 (1973) 588-589.

I4 Irons, B.M. The semiloof shell element. Lecture notes, International Research Seminar on the Theory and Application of Finite Elements, July 1973, Calgary University, Canada.

I5 Irons, B.M. Un nouvel element de coques generales semiloof. Methods de Calcul Scientific et Technique, Colloques IRIA, Rocquencourt, Paris 1973.

I6 Irons, B.M. The semiloof shell element. Internal report, Univ. of Calgary, 1973.

I7 Irons, B. and Razzaque, A. Experience with the patch test, from the mathematical foundations of the finite element method with applications to partial differential equations, Academic Press, 1972.

I8 Irons, B.M. and Draper, K.J. Inadequacy of node connections in a stiffness solution for plate bending, JAIAA, 3, 5, May 1965.

I9 Irons, B.M. and Razzaque, A. Shape function formulations for elements other than displacement models. Conference on variational methods in engineering, Southampton University, 1972.

I10 Irons, B.M. The patch test, Internal report, Univ. of Calgary, 1973.

I11 Irons, B.M. Numerical integration applied to finite element methods. Conf. use of digital computers in structural engineering, Newcastle University, 1966.

J1 Javadi, F. The analysis and design of structural joints for off-shore platforms. Ph.D. thesis to be submitted, Imperial College.

K1 Key, S.W. and Bersinger, Z.E. The analysis of thin shells with transverse shear strains by the finite element method. Proc. Conf. Matrix Meth. Struct. Mech. WPAFB, Ohio, 1965.

L1 Lyons, L.P.R. Elastic analysis of pierced shear walls, CIRIA report 145, 1970.

L2 Lim, T.K. Elastic analysis of bridge structures by the finite element method. Ph.D. thesis, Univ. of London, 1971.

L3 Lim, T.K. et al. Finite element analysis of curved box girder bridges. Proc. Int. Conf. Bridge Design and Construction, Edit. Rockey, K.C.,Crosby Lockwood, 1971.

L4 Lim, T.K. and Moffatt, K.R. Finite element analysis of curved slab bridges with special references to local stresses. Proc. Int. Conf. Bridge Design and Construction, Edit. Rockey, K.C., Crosby Lockwood, 1971.

L5 Lim, T.K. and Moffatt, K.R. Internal communication, Imperial College.

L6 Lyons, L.P.R., Cassell, A.C. and Hobbs, R. Structural analysis by finite element elements. Internal report, Imperial College, 1973.

L7 Lightfoot, E. and Sawko, F. Grid frameworks resolved by generalised slope deflection. Engineering, London, Vol. 87, 1959, pp. 18-20.

L8 Lyons, L.P.R. The LUSAS computer code. Internal volume, Imperial College, January 1977.

M1 Melosh, R.J. and Bamford, R.M. Efficient solution of load-deflection equations. J. of Structural Div., A.S.C.E. 95, ST4, Proc. Paper 6510 (1969) 661-676.

M2 Moffatt, K.R. Finite element analysis of box girder bridges. Ph.D. thesis, University of London, 1974.

M3 Meyer, C. Solution of linear equations - State-of-the-art, J. of Struct. Div. A.S.C.E., July, 1973.

M4 Meyer, C. Special problems related to linear equation solvers, J. of Struct. Div. A.S.C.E., April 1975.

M5 Macleod, I.A. New rectangular finite element for shear wall analysis. Proc. A.S.C.E. 1969, 95, ST3, 399-409.

M6 Melosh, R.J. A flat triangular shell element stiffness matrix, Proc. Conf. Matrix Meth. Struct. Mech., WPAFB Ohio, 1965.

M7 Morley, L.S.D. Skew plates and structures, Pergamon, 1963.

M8 Melosh, R.J. Basis for derivation of matrices for the direct stiffness method. A.I.A.A. Journal, Vol. 1, 1963, pp. 1631-1637.

M9 Morley, L.S.D. The triangular equilibrium element in the solution of plate bending problems. Aero. Quarterly, May 1968, pp.149-169.

M10 Morley, L.S.D. A triangular equilibrium element with linearly varying bending moments for plate bending problems. Journal of the Royal Aero. Soc., Vol. 71, 1967, p.715

M11 Martin, H.C. and Carey, G.F. Introduction to finite element analysis. McGraw-Hill, 1973.

N1 Noor, A.K. and Fulton, R.E. Impact of CDC STAR-100 computer on finite element systems. J. of Structural Div. ASCE, April 1975.

O1 Oden, J.F. Finite elements of non-linear continua, McGraw-Hill, New York, 1972.

O2 Owens, G. Ultimate load behaviour of composite box girder bridges. Ph.D. thesis to be submitted to Imperial College.

P1 Popov, E.P. and Sharifi, P. A refined curved element for thin shells of revolution. Intern. J. Num. Meth. Eng. 3 (1971), 495-508.

P2 Przemieniecki, J.S. Theory of matrix structural analysis. McGraw-Hill, 1968.

P3 Pawsey, S. and Clough R.W. Improved numerical integration of thick shell finite elements. Int. J. Num. Meth. Eng. Vol. 3, 1971.

P4 Pian, T.H.H. Derivation of element stiffness matrices by assumed stress distributions. AIAA J., 2, 1333-1336, 1964.

P5 Pian, T.H.H. Hybrid models, Conf. on Num. and Comp. Meth. In Struct. Mech. Urbana, Illinois, 1971.

P6 Pian, T.H.H. and Tong, P. Basis of finite element methods for solid continua. Int. J. Num. Meth. Eng. Vol. 1, No. 1, Jan. 1969.

P7 Pian, T.H.H. Derivation of element stiffness matrices. AIAA J., Vol. 2, No. 3, March 1969.

P8 Plantema, F.J. Sandwich construction, Wiley, 1966.

R1 Razzaque, A. Program for triangular bending elements with derivative smoothing. Int. J. Num. Meth. Eng. 6 (1973) 333-343.

R2 Razzaque, A. Finite element analysis of plates and shells. Ph.D., Univ. of Wales, Swansea, 1973.

S1 Schrem, E. Computer implementation of the finite element procedure, ONR Symp. on Numerical and Computer Methods in Structural Mechanics, Univ. of Illinois (1971).

S2 Scordelis, A.C. Analysis of continuous box girder bridges. Depart. No. SESM-67-25 at Univ. of California, Berkeley.

S3 Sisodiya, R.G. Finite element analysis of bridges. Ph.D. thesis, Univ. of Calgary, Canada, 1971.

S4 Scordelis, A.C. Analytical solutions for box girder bridges. Developments in bridge design and construction. Edit. Rockey, K.C. Crosby,Lockwood Publishers, 1971.

S5 Sisodiya, R.G. et al. New finite elements with application to box girder bridges. Proc. Instn. Civ. Engrs, suppl. (XVII), 1972, pp.207-225.

S6 Severn, R. and Taylor, P. The finite element method for flexure of slabs when stress distributions are assumed. Proc. Instn. Civ. Engrs. 1966, 34, pp. 153-170.

S7 Stricklin, J.A. et al. A rapidly converging triangular plate element. J. AIAA, Vol. 7, 1969.

S8 Strang, G. and Fix, G.J. An analysis of the finite element method, Prentice-Hall, 1973.

S9 Scordelis, A.C. Analysis of simply supported box girder bridges. Report No. SESM-66-17, Dept. of Civ. Eng., Univ. of Calif. Berkeley, 1966.

T1 Too, J.J.M. Two dimensional plate shell and finite prism isoparametric elements and thin applications. Ph.D. thesis, University of Wales, Swansea, 1971.

T2 Torbe, I. and Church, K. A general quadrilateral plate element, Int. J. Num. Meth. Eng. Vol. 9, 855-868, 1975.

T3 Timoshenko, S.P. and Woinowskey-Krieger, S. Theory of plates and shells. McGraw-Hill.

T4 Turner, M.J., Clough, R.W., Martin, H.C. and Topp, L.J. Stiffness and deflection analysis of complex structures. J. Aero. Sci. 23, 1956, pp.805-823.

T5 Tong, P. New displacement hybrid finite element model for solid continua. Int. J. for Num. Meth. in Eng., Vol. 2, 1970, pp.73-83.

T6 Taylor, R.L., Beresford, P.J. and Wilson, E.L. A non-conforming element for stress analysis. Int. J. Num. Meth. Eng. Vol. 10, 6, 1976, 1211-1219.

U1 Utku, S. Stiffness matrix for the triangular elements of non-zero Gaussian curvature. J. AIAA, Vol. 5, 1659-1667, 1967.

V1 de Veubeke, B.F. A conforming quadrilateral element for plate bending. Int. J. of Solids Struct., Jan. 1968.

V2. de Veubeke, B.F. and Sander, G. An equilibrium model for plate bending, Int. J. Solids Struct., 1968.

V3 de Veubeke, B.F. Upper and lower bounds in matrix structural analysis. Pergamon Press, Oxford, 1969.

V4 Vlasov, V.Z. Thin-walled elastic beams, Israel Program for Scientific Translations, 1961.

W1 Wilson, E.L., Bathe, K.J. and Doherty, W.P. Direct solution of large systems of linear equations. Computers and Structures, Vol. 4, 1974.

W2 Westlake, J.R. Numerical matrix inversion and solution of linear equations. Wiley.

W3 Wilson, E.L., Taylor, R.L., Doherty, W.P. and Ghaboussi, J. Incompatible displacement models, in Numerical and Computer Methods in Structural Mechanics, Academic Press, 1973.

W4 William, K.J. Finite element analysis of cellular structures. Ph.D. Univ. of California, Berkeley, 1969.

W5 Wempner, G.A., Oden, J.T. and Kross, D.K. Finite element analysis of thin shells. J. Eng. Mech. Div. ASCE 94, 1273-1294, 1968.

W6 Wolf, J.P. Generalised stress models for finite element analysis, Ph.D. thesis, Institut fur Banstatik, Zurich, 1974.

W7 Ward, J.K. The El Atazar Dam. Ph.D. thesis, University of London, 1975.

Y1 Yamamoto, R. and Isshiki, H. Variational principles and dualistic scheme for intersection problems in elasticity. Journal for the Faculty of Eng., Univ. of Tokyo, Vol. XXX, No. 1, 1969.

Z1 Zienkiewicz, O.C. The finite element method in engineering science, London, McGraw-Hill, 1971.

Z2 Zienkiewicz, O.C., Taylor, R.L. and Too, J.M. Reduced integration technique in general analysis of plates and shells. Int. J. Num. Meth. Eng., 1971, 3, 275-290.

Z3 Zienkiewicz, O.C. and Phillips, D.V. An automatic mesh generation scheme for plane and curved surfaces by isoparametric coordinates, Int. J. Num. Meth. Eng., Vol. 3,4, 1971, 519-528.

Z4 Zienkiewicz, O.C. Recent developments, trends and application of finite element methods. Keynote address, Int. Conf. on Finite Element Meth. in Eng., Adelaide, December 1976.

Appendix I

TRM3

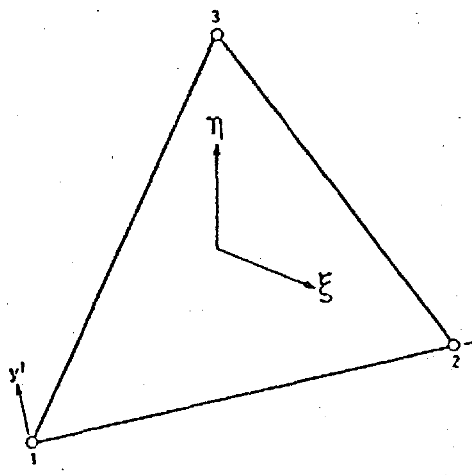

TRIANGULAR PLANE MEMBRANE ELEMENT

Number of nodes	3
Degrees of freedom	u,v at each node
Displacement field	linear
References	C1 , Z1
STRESS OUTPUT	
Standard	$\sigma_x, \sigma_y, \tau_{xy}, \sigma_{max}, \sigma_{min}, \theta$ at centroid
Option	$N_x, N_y, N_{xy}, N_{max}, N_{min}, \theta$ at centroid
DATA INPUT	
STRUCTURE	plane stress/strain
OPTION	local stresses
NODE COORDINATES	x, y at each node
PLATE PROPERTIES	E_x, E_y, G, ν, θ, t orthotropic
RIGIDITIES	$C_x, C_y, C_{xy}, C1, \theta$ orthotropic
CL	P_x, P_y at any node
CBF	X,Y for element

TRMI3

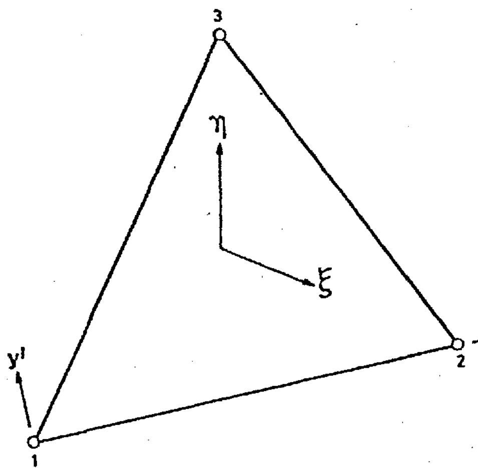

TRIANGULAR PLANE MEMBRANE ELEMENT

Number of nodes	3
Degrees of freedom	u,v at each node + α, β at centre
Displacement field	linear + higher order incompatible modes
References	Z1 and authors developments
STRESS OUTPUT	
Standard	$\sigma_x, \sigma_y, \tau_{xy}, \sigma_{max}, \sigma_{min}, \theta$ at centroid
Option	$N_x, N_y, N_{xy}, N_{max}, N_{min}, \theta$ at entroid
DATA INPUT	
STRUCTURE	plane stress/strain
OPTION	local stresses
NODE COORDINATES	x,y at each node
PLATE PROPERTIES	E_x, E_y, G, ν, θ, t orthotropic
RIGIDITIES	$C_x, C_y, C_{xy}, C_1, \theta$ orthotropic
CL	P_x, P_y at any node
CBF	X,Y for element

TRM6

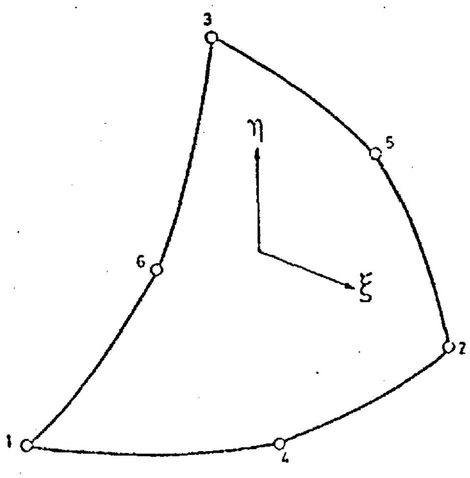

TRIANGULAR PLANE MEMBRANE ELEMENT

Number of nodes	6
Degrees of freedom	u,v at each node
Displacement field	quadratic
References	Z1
STRESS OUTPUT	
Standard	$\sigma_x, \sigma_y, \sigma_{xy}, \sigma_{max}, \sigma_{min}, \theta$ at each node
DATA INPUT	
STRUCTURE	plane stress/strain
OPTION	local stresses
NODE COORDINATES	x,y at each node
PLATE PROPERTIES	E_x, E_y, G, ν, θ, t orthotropic
RIGIDITIES	$C_x, C_y, C_{xy}, C_1, \theta$ orthotropic
CL	P_x, P_y at any node
CBF	X,Y for element

Elements available for analysing
plane stress and plane strain problems

TRM10

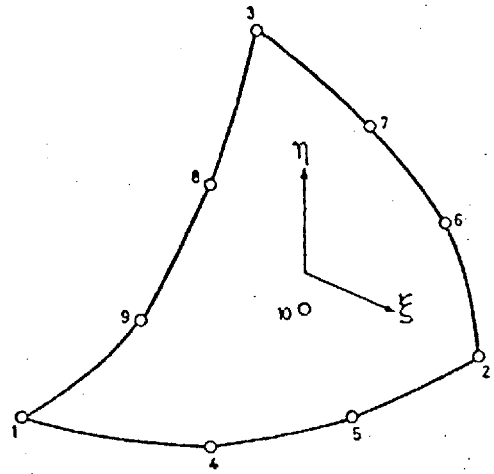

TRIANGULAR PLANE MEMBRANE ELEMENT

Number of Nodes	10
Degrees of freedom	u,v at each node
Displacement field	cubic
References	Z1

STRESS OUTPUT

Standard	$\sigma_x, \sigma_y, \tau_{xy}, \sigma_{max}, \sigma_{min}, \theta$ at each node

DATA INPUT

STRUCTURE	plane stress/strain
OPTION	local stresses
NODE COORDINATES	x,y at each node
PLATE PROPERTIES	E_x, E_y, G, ν, θ, t orthotropic
RIGIDITIES	$C_x, C_y, C_{xy}, C_1, \theta$ orthotropic
CL	P_x, P_y at each node
CBF	X,Y for element

QDM4

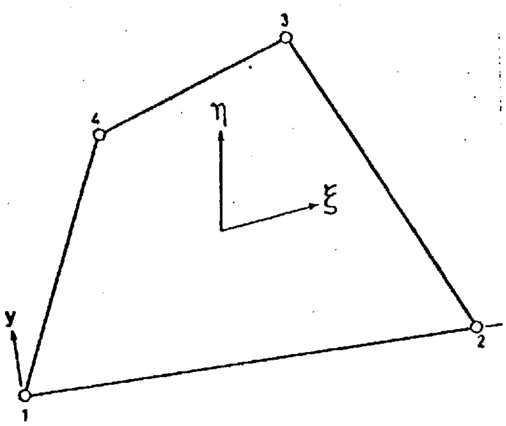

QUADRILATERAL PLANE MEMBRANE ELEMENT

Number of nodes	4
Degrees of freedom	u,v at each node
Displacement field	linear + selected higher terms
References	Z1

STRESS OUTPUT

Standard	$\sigma_x, \sigma_y, \tau_{xy}, \sigma_{max}, \sigma_{min}, \theta$ at each node
Option	$N_x, N_y, N_{xy}, N_{max}, N_{min}, \theta$ at each node

DATA INPUT

STRUCTURE	plane stress/strain
OPTION	local stresses
NODE COORDINATES	x,y at each node
PLATE PROPERTIES	E_x, E_y, G, ν, θ, t orthotropic
RIGIDITIES	$C_x, C_y, C_{xy}, C_1, \theta$ orthotropic
CL	P_x, P_y at any node
CBF	X,Y for element

QDMI4

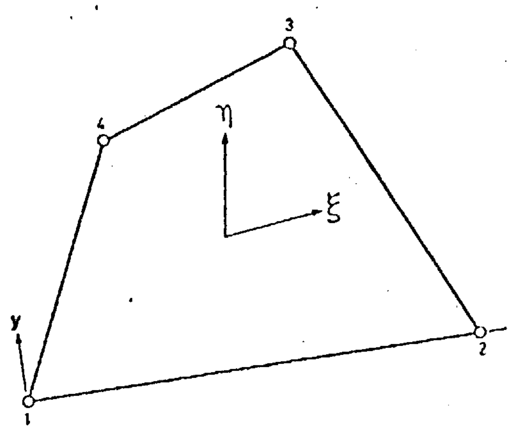

QUADRILATERAL PLANE MEMBRANE ELEMENT

Number of Nodes	4
Degrees of freedom	u,v at each node + , which are eliminated
Displacement field	linear + higher order + incompatible modes
References	W3

STRESS OUTPUT

Standard	$\sigma_x, \sigma_y, \tau_{xy}, \sigma_{max}, \sigma_{min}, \theta$ at each node
Option	$N_x, N_y, N_{xy}, N_{max}, N_{min}, \theta$ at each node

DATA INPUT

STRUCTURE	plane stress/strain
OPTION	local stresses
NODE COORDINATES	x,y at each node
PLATE PROPERTIES	E_x, E_y, G, ν, θ, t orthotropic
RIGIDITIES	$C_x, C_y, C_{xy}, C_1, \theta$ orthotropic
CL	P_x, P_y at any node
CBF	X,Y for element

Elements available for analysing plane stress and plane strain problems

QDM8

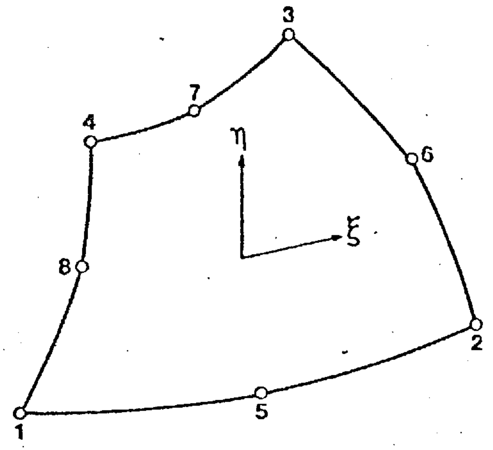

QUADRILATERAL PLANE MEMBRANE ELEMENT

Number of nodes	8
Degrees of freedom	u,v at each node
Displacement field	quadratic + selected higher order terms
References	Z1
STRESS OUTPUT	
Standard	$\sigma_x, \sigma_y, \tau_{xy}, \sigma_{max}, \sigma_{min}, \theta$ at each node
DATA INPUT	
STRUCTURE	plane stress/strain
OPTION	local stresses
NODE COORDINATES	x,y at each node
PLATE PROPERTIES	$\sigma_x, \sigma_y, G, \nu, \theta$, t orthotropic
RIGIDITIES	$C_x, C_y, C_{xy}, C_1, \theta$ orthotropic
CL	P_x, P_y at any node
CBF	X,Y for element

QDM12

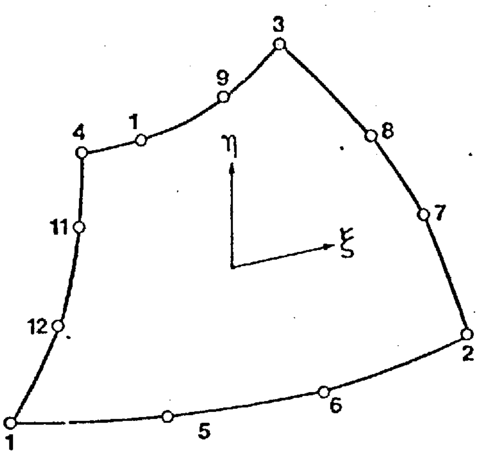

QUADRILATERAL PLANE MEMBRANE ELEMENT

Number of Nodes	12
Degrees of freedom	u,v at each node
Displacement field	cubic + selected higher order terms
References	Z1
STRESS OUTPUT	
Standard	$\sigma_x, \sigma_y, \sigma_{xy}, \sigma_{max}, \sigma_{min}, \theta$ at each node
DATA INPUT	
STRUCTURE	plane stress/strain
OPTION	local stresses
NODE COORDINATES	x,y at each node
PLATE PROPERTIES	E_x, E_y, G, ν, θ, t orthotropic
RIGIDITIES	$C_x, C_y, C_{xy}, C_1, \theta$ orthotropic
CL	P_x, P_y at any node
CBF	X,Y for element

JOINT2.

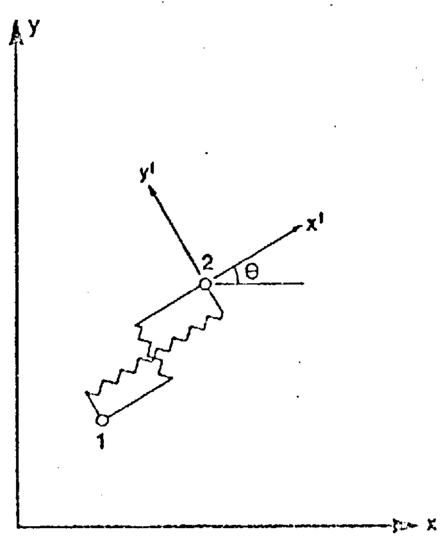

JOINT ELEMENT

Number of nodes	2
Degrees of freedom	u,v at each node
Displacement field	-
References	authors developments
Notes	connects two nodes, which may be coincident by orthogonal set of springs
STRESS OUTPUT	
Standard	F_x, F_y at each node
DATA INPUT	
STRUCTURE	plane stress/strain
OPTION	as required
NODE COORDINATES	x,y at each node
JOINT RIGIDITIES	K_x, K_y, θ
CL	P_x, P_y at any node

Elements available for analysing plane stress and plane strain problems

BAR2

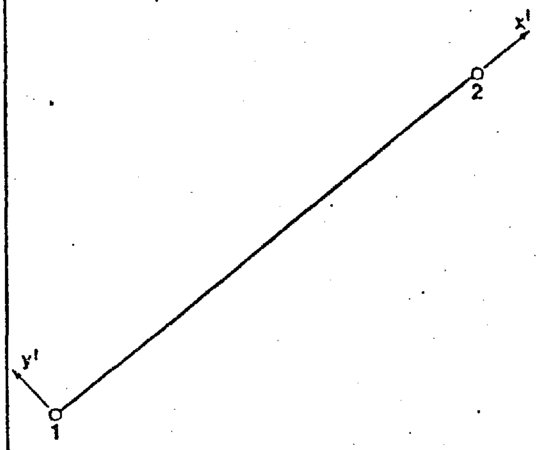

STRAIGHT PLANE TRUSS ELEMENT

Number of nodes	2
Degrees of freedom	u,v at each node
Displacement field	linear
References	P2
STRESS OUTPUT	
Standard	F_x' axial force
DATA INPUT	
STRUCTURE	plane truss/stress/strain
OPTION	as required
NODE COORDINATES	x,y at each node
BEAM RIGIDITIES	EA
CL	P_x, P_y at any node

BEAM2

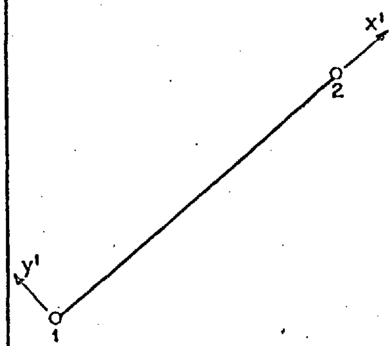

STRAIGHT PLANE FRAME BEAM ELEMENT

Number of nodes	2
Degrees of freedom	u,v,θ at each node
Displacement field	cubic
References	P2
STRESS OUTPUT	
Standard	F_x', F_y', M_z' forces and moments at each node
DATA INPUT	
STRUCTURE	plane frame/stress
ELEMENT NODES	element and node numbers and R and F end conditions
NODE COORDINATES	x,y at each node
BEAM RIGIDITIES	EA, EI, GA
CL	P_x, P_y, M_z at any node
UDL	W_x, W_y load/unit projected length

GRID2

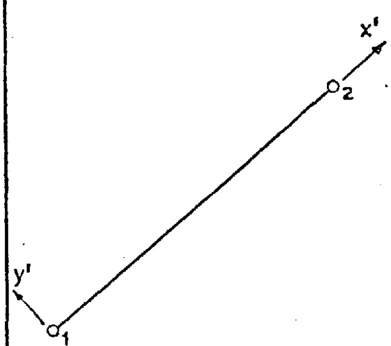

STRAIGHT GRILLAGE ELEMENT

Number of nodes	2
Degrees of freedom	w, θ_x, θ_y
Displacement field	cubic
References	P2
STRESS INPUT	
Standard	S_z', M_x', M_y'
DATA INPUT	
STRUCTURE	grillage/plate bending
NODE COORDINATES	x,y at each node
BEAM RIGIDITIES	EI,GJ,GA
CL	P_z, M_x, M_y at any node
UDL	W_z, load/unit length

Elements available for analysing plane truss plane frame and grillage problems

TRSM3

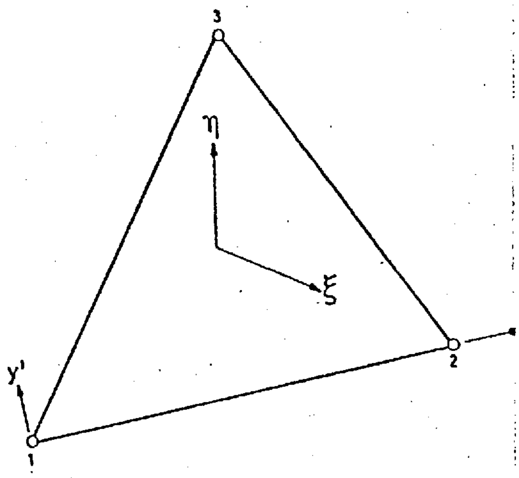

TRIANGULAR SPACE MEMBRANE ELEMENT

Number of nodes	3
Degrees of freedom	u,v,w at each node
Displacement field	linear
References	C1 and authors developments
STRESS OUTPUT	
Standard	$\sigma'_x, \sigma'_y, \tau'_{xy}, \sigma_{max}, \sigma_{min}, \theta$ at centroid
Option	$N'_x, N'_y, N'_{xy}, N_{max}, N_{min}, \theta$ at centroid
DATA INPUT	
STRUCTURE	space membrane
OPTION	local stresses
NODE COORDINATES	x,y,z at each node
PLATE PROPERTIES	E_x, E_y, G, ν, θ, t orthotropic
CL	P_x, P_y, P_z at any node
CBF	X,Y,Z for element

TRSMI3

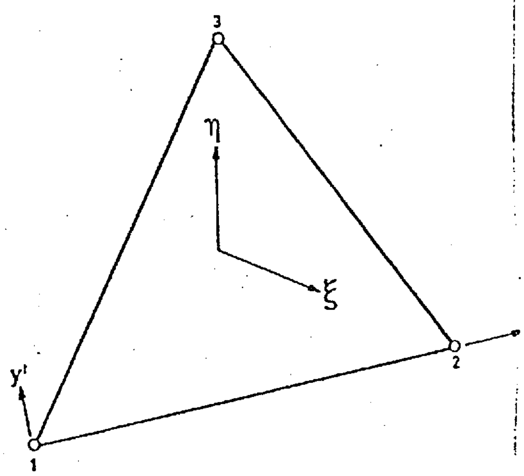

TRIANGULAR SPACE MEMBRANE ELEMENT

Number of nodes	3
Degrees of freedom	u,v,w at each node + α,β which are eliminated
Displacement field	linear + higher order incompatible modes
References	Z1 and authors developments
STRESS OUTPUT	
Standard	$\sigma'_x, \sigma'_y, \tau'_{xy}, \sigma_{max}, \sigma_{min}, \theta$ at centroid
Option	$N'_x, N'_y, N'_{xy}, N_{max}, N_{min}, \theta$ at centroid
DATA INPUT	
STRUCTURE	space membrane
OPTION	local stresses
NODE COORDINATES	x,y,z at each node
PLATE PROPERTIES	E_x, E_y, G, ν, θ, t orthotropic
CL	P_x, P_y, P_z at any node
CBF	X,Y,Z for element

QDSM4

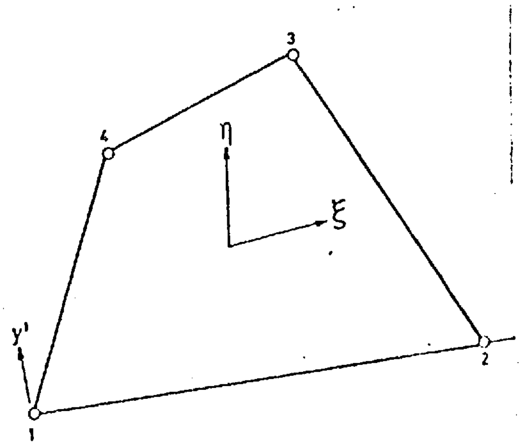

QUADRILATERAL SPACE MEMBRANE ELEMENT

Number of nodes	4
Degrees of freedom	u,v,w at each node
Displacement field	linear
References	Z1
STRESS OUTPUT	
Standard	$\sigma'_x, \sigma'_y, \tau'_{xy}, \sigma_{max}, \sigma_{min}, \theta$ at centroid
Option	$N'_x, N'_y, N'_{xy}, N_{max}, N_{min}, \theta$ at centroid
DATA INPUT	
STRUCTURE	space membrane
OPTION	local stresses
NODE COORDINATES	x,y,z at each node
PLATE PROPERTIES	E_x, E_y, G, ν, θ, t orthotropic
CL	P_x, P_y, P_z at any node
CBF	X,Y,Z for element

Elements available for analysing space membrane problems

QDSMI4

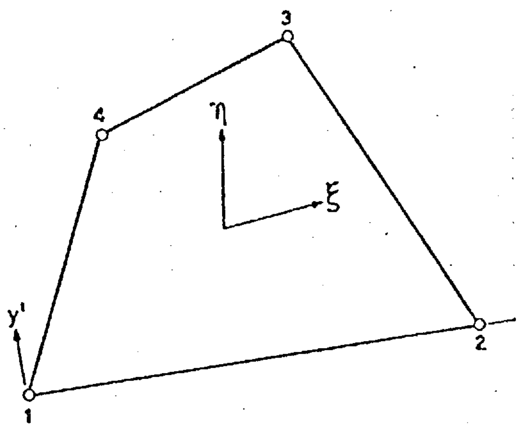

QUADRILATERAL SPACE MEMBRANE ELEMENT

Number of nodes	4
Degrees of freedom	u,v,w at each node and α,β which are eliminated
Displacement field	linear + higher order incompatible modes
References	W3
STRESS OUTPUT	
Standard	σ'_x, σ'_y, τ'_{xy}, σ_{max}, σ_{min}, θ at centroid
Option	N'_x, N'_y, N'_{xy}, N_{max}, N_{min}, θ at centroid
DATA INPUT	
STRUCTURE	space membrane
OPTION	local stresses
NODE COORDINATES	x,y,z at each node
PLATE PROPERTIES	E_x,E_y,G,ν,θ, t orthotropic
CL	P_x,P_y,P_z at any node
CBF	X,Y,Z for element

BARS2

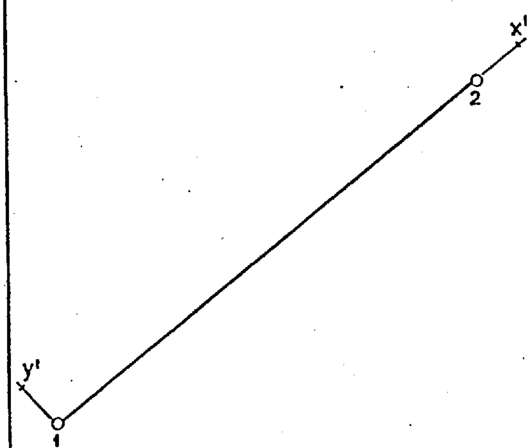

STRAIGHT SPACE TRUSS ELEMENT

Number of nodes	2
Degrees of freedom	u,v,w at each node
Displacement field	linear
References	P2
STRESS OUTPUT	
Standard	F'_x axial force
DATA INPUT	
STRUCTURE	space truss/membrane
OPTION	as required
NODE COORDINATES	x,y,z at each node
BEAM RIGIDITIES	EA
CL	P_x,P_y,P_z at any node

Elements available for analysing space membrane problems

TRB3

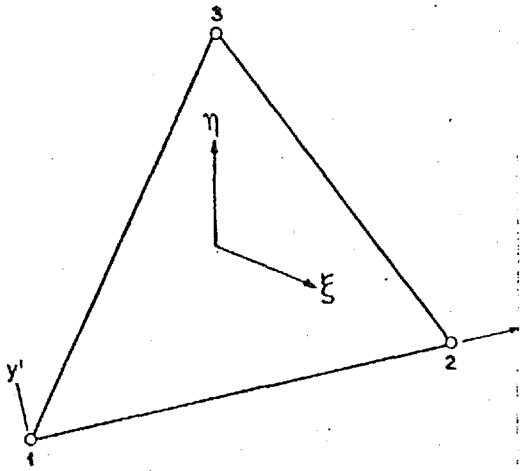

TRIANGULAR PLATE BENDING ELEMENT

Number of nodes	3,
Degrees of freedom	w, θ_x, θ_y at each node
Displacement field	cubic with derivative smoothing
References	this thesis
STRESS OUTPUT	
Standard	$\sigma_x, \sigma_y, \tau_{xy}, \sigma_{max}, \sigma_{min}$, θ at each node
Option	M_y, M_x, M_{xy}, M_{max}, M_{min}, θ at each node
DATA INPUT	
STRUCTURE	plate bending
OPTION	local stresses
NODE COORDINATES	x,y at each node
PLATE PROPERTIES	E_x, E_y, G, ν, θ, t orthotropic
RIGIDITIES	D_x, D_y, D_{xy}, D_1, θ orthotropic
CL	P_z, M_x, M_y at any node
UDL	W_z

QDB4

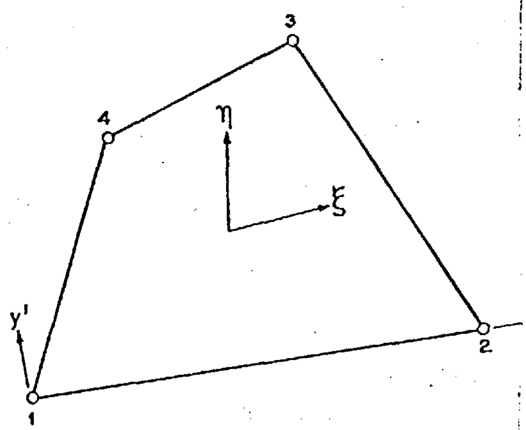

QUADRILATERAL PLATE BENDING ELEMENT

Number of nodes	4
Degrees of freedom	w, θ_x, θ_y at each node
Displacement field	cubic + higher order terms
References	this thesis
STRESS OUTPUT	
Standard	$\sigma_x, \sigma_y, \sigma_{xy}, \sigma_{max}, \sigma_{min}$, θ at each node
Option	$M_y, M_x, M_{xy}, M_{max}, M_{min}$, θ at each node
DATA INPUT	
STRUCTURE	plate bending
OPTION	local stresses
NODE COORDINATES	x,y at each node
PLATE PROPERTIES	E_x, E_y, G, ν, θ, t orthotropic
RIGIDITIES	$D_x, D_y, D_{xy}, D_1, \theta$ orthotropic
CL	P_z, M_x, M_y at any node
CBF	Wz

JOINT2

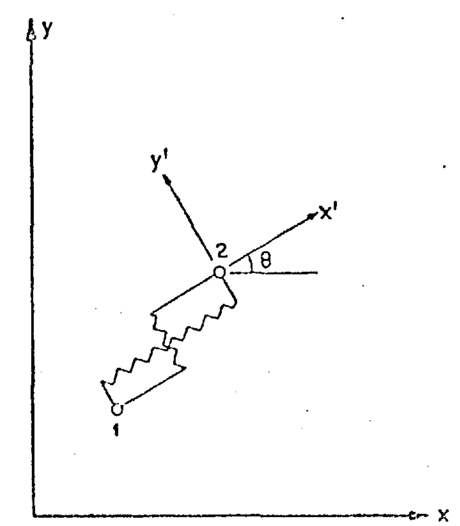

JOINT ELEMENT

Number of nodes	2
Degrees of freedom	w, θ_x, θ_y at each node
Displacement field	-
References	authors developments
Notes	connects two nodes, which may be coincident, by orthogonal set of springs
STRESS OUTPUT	
Standard	F_z, M_x, M_y
DATA INPUT	
STRUCTURE	plate bending/grillage
OPTION	as required
NODE COORDINATES	x,y at each node
JOINT PROPERTIES	K'_z , $K\theta'_x$, $K\theta'_y$, θ
CL	P_z, M_x, M_y at any node

Elements available for analysing thin plate flexure problems

QDSB 4 / QDSB I4

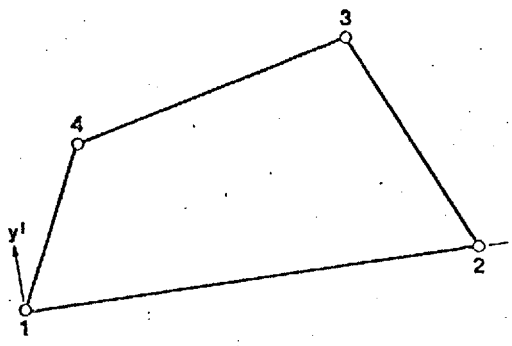

QUADRILATERAL FACET SHELL ELEMENT

Number of nodes	3
Degrees of freedom	$u, v, w, \theta_x, \theta_y, \theta_z$ at each node
Displacement field	linear + higher order incompatible modes
References	this thesis
Notes	a biased element with beam performance for cellular structures

STRESS OUTPUT

Standard	$\sigma'_x, \sigma'_y, \sigma'_{xy}$ for extensional/flexural stresses
Option	N'_x, N'_y, N_{xy} for extensional/flexural stresses

DATA INPUT

STRUCTURE	shell
OPTION	local stresses
NODE COORDINATES	x,y,z at each node
PLATE PROPERTIES	$E_x, E_y, G, \nu, \theta, t_m, t_b$ orthotropic
CL	$P_x, P_y, P_z, M_x, M_y, M_z$ at any node
CBF	X,Y,Z for element

QDSB 6 / QDSB I6

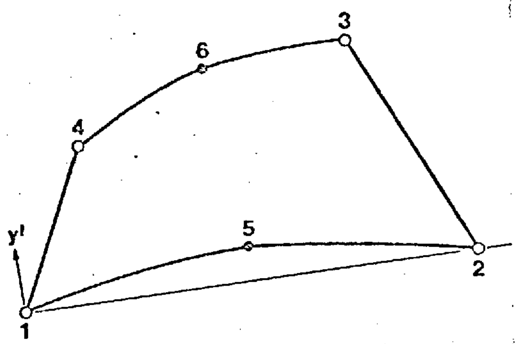

QUADRILATERAL FACET SHELL ELEMENT

Number of nodes	6
Degrees of freedom	$u, v, w, \theta_x, \theta_y, \theta_z$ at corners, u' midside
Displacement field	linear + higher order incompatible modes
References	this thesis
Notes	a biased element with beam performance for cellular structures

STRESS OUTPUT

Standard	$\sigma'_x, \sigma'_y, \sigma'_{xy}$ for extensional/flexural stresses
Option	N'_x, N'_y, N'_{xy} for extensional/flexural stresses

DATA INPUT

STRUCTURE	shell
OPTION	local stresses
NODE COORDINATES	x,y,z at each node
PLATE PROPERTIES	$E_x, E_y, G, \nu, \theta, t_m, t_b$ orthotropic
CL	$P_x, P_y, P_z, M_x, M_y, M_z$ at any node
CBF	X,Y,Z for element

BMS2

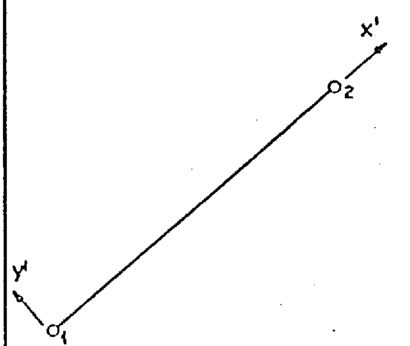

SPACE FRAME ELEMENT

Number of nodes	2 + 1 for definition of local xy plane
Degrees of freedom	$u, v, w, \theta_x, \theta_y, \theta_z$ at first two nodes
Displacement field	cubic
References	P2
Notes	eccentricity included for ribbed plates

STRESS OUTPUT

Standard	$F'_x, S'_y, S'_z, M'_x, M'_y, M'_z$

DATA INPUT

STRUCTURE	space frame/shell
OPTION	local stresses
NODE COORDINATES	x,y,z at each node
BEAM RIGIDITIES	$EA, EI_y, EI_z, GJ_x, GA_y, GA_z$,
CL	$P_x, P_y, P_z, M_x, M_y, M_z$ at each node

Elements available for analysing shell and space frame structures

QDTS8

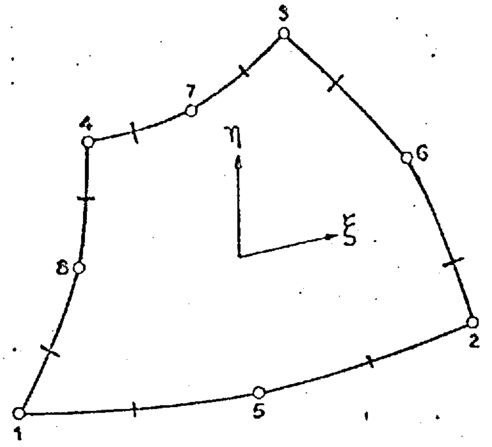

QUADRILATERAL THIN SHELL ELEMENT

Number of nodes	8
Degrees of freedom	u,v,w at corners, u,v,w,θ_1,θ_2 at sides
Displacement field	effectively cubic
References	I4-I6

STRESS OUTPUT

Standard	σ'_x, σ'_y, σ'_{xy} for extensional/flexural stresses

DATA INPUT

STRUCTURE	thin shell
NODE COORDINATES	x,y,z at each node
PLATE PROPERTIES	E_x,E_y,G,ν,θ,t
CL	P_x,P_y,P_z/M_1,M_2 at nodes
BFP	P at any node

Elements available for analysing three-dimensional thin curved shell problems

PEN12

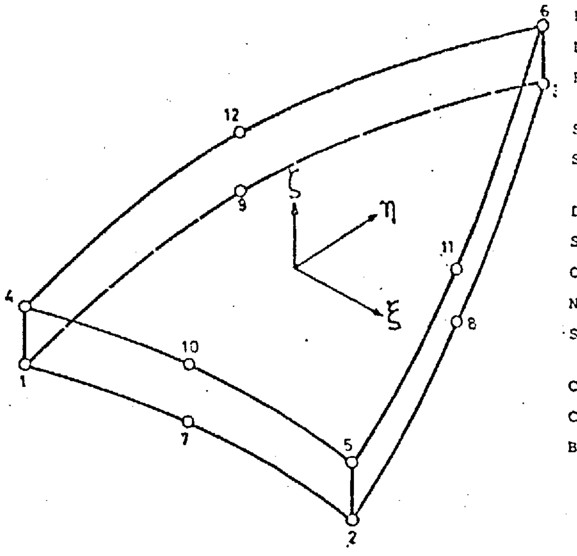

PENTAHEDRONAL ELEMENT WITH CURVED EDGES

Number of nodes	12
Degrees of freedom	u,v,w at each node
Displacement field	linear + quadratic
References	Z1
STRESS OUTPUT	
Standard	$\sigma_x, \sigma_y, \sigma_z, \tau_{xy}, \tau_{yz}, \tau_{zx}$ at each node
DATA INPUT	
STRUCTURE	solid
OPTION	as required
NODE COORDINATES	x,y,z at each node
SOLID PROPERTIES	E,ν isotropic
CL	P_x, P_y, P_z at any node
CBF	X,Y,Z for element
BFP	p, Δt at any node

HEX16

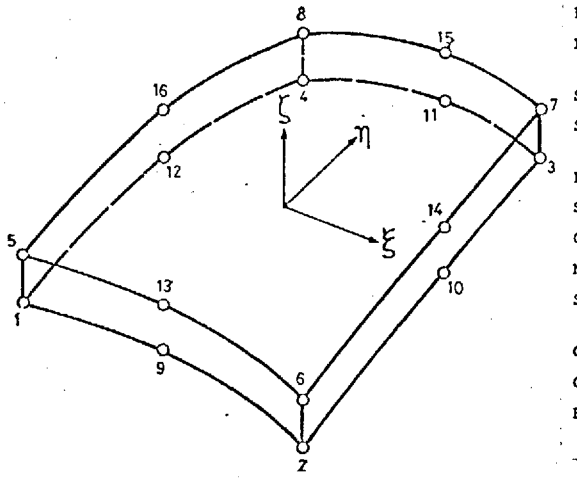

HEXAHEDRONAL ELEMENT WITH CURVED EDGES

Number of nodes	16
Degrees of freedom	u,v,w at each node
Displacement field	linear + quadratic + higher order
References	Z1
STRESS OUTPUT	
Standard	$\sigma_x, \sigma_y, \sigma_z, \tau_{xy}, \tau_{yz}, \tau_{zx}$ at each node
DATA INPUT	
STRUCTURE	solid
OPTION	as required
NODE COORDINATES	x,y,z at each node
SOLID PROPERTIES	E,ν isotropic
CL	P_x, P_y, P_z at any node
CBF	X,Y,Z for element
BFP	P, Δt at any node

JOINT2

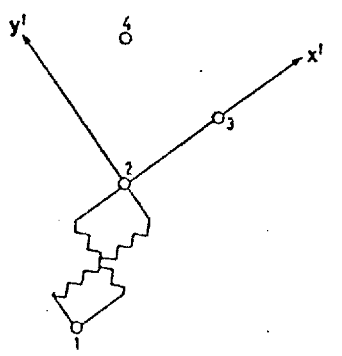

JOINT ELEMENT

Number of nodes	2 + 2 to define local x,y,z spring directions
Degrees of freedom	u,v,w at each node
Displacement field	-
References	this thesis
Notes	connects two nodes, which may be coincident by an orthogonal set of springs. Nodes 3 and 4 must be restrained if not part of the structure
STRESS OUTPUT	
Standard	F'_x , F'_y , F'_z at each node
DATA INPUT	
STRUCTURE	solid
OPTION	as required
NODE COORDINATES	x,y,z at each node
JOINT RIGIDITIES	K'_x , K'_y , K'_z stiffnesses
CL	P_x, P_y, P_z at any node

Elements available for analysing three-dimensional thick shell problems

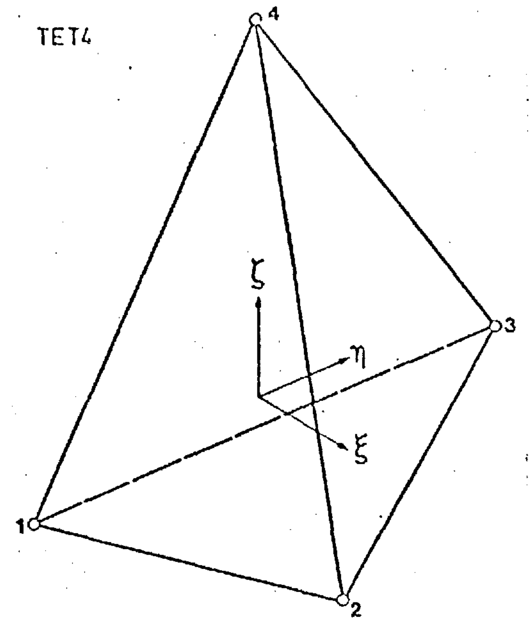

TETRAHEDRONAL ELEMENT WITH STRAIGHT EDGES

Number of nodes	4,
Degrees of freedom	u,v,w at each node
Displacement field	linear
References	Z1
STRESS OUTPUT	
Standard	$\sigma_x, \sigma_y, \sigma_z, \tau_{xy}, \tau_{yz}, \tau_{zx}$ at each node
DATA INPUT	
STRUCTURE	solid
OPTION	as required
NODE COORDINATES	x,y,z at each node
SOLID PROPERTIES	E,ν isotropic
CL	P_x, P_y, P_z at any node
CBF	X,Y,Z for element
BFP	P, Δt at any node

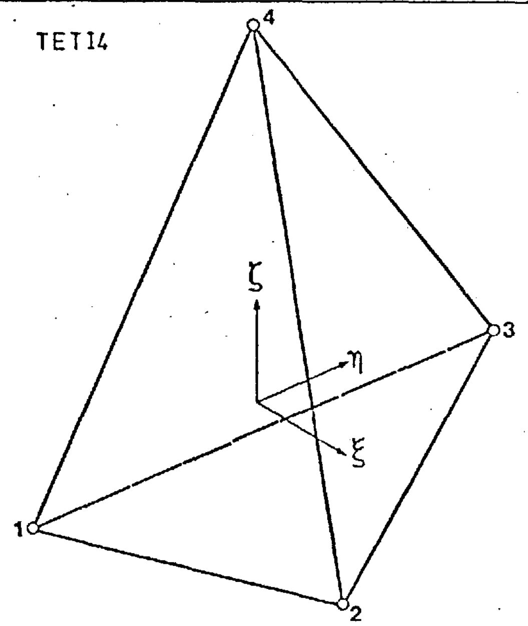

TETRAHEDRONAL ELEMENT WITH STRAIGHT EDGES

Number of nodes	4
Degrees of freedom	u,v,w at each node + α,β,γ, which are eliminated
Displacement field	linear + higher order incompatible modes
References	Z1 and authors developments
STRESS OUTPUT	
Standard	$\sigma_x, \sigma_y, \sigma_z, \tau_{xy}, \tau_{yz}, \tau_{zx}$ at each node
DATA INPUT	
STRUCTURE	solid
OPTION	as required
NODE COORDINATES	x,y,z at each node
SOLID PROPERTIES	E,ν isotropic
CL	P_x, P_y, P_z at any node
CBF	X,Y,Z for element
BFP	P, Δt at any node

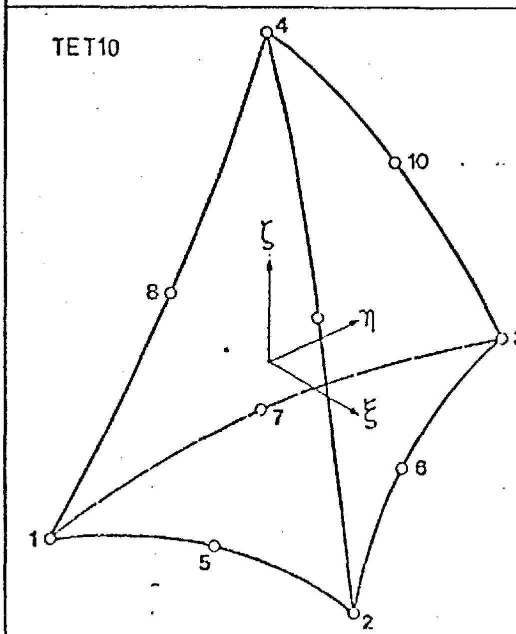

TETRAHEDRONAL ELEMENT WITH CURVED EDGES

Number of nodes	10
Degrees of freedom	u,v,w at each node
Displacement field	quadratic
References	Z1
STRESS OUTPUT	
Standard	$\sigma_x, \sigma_y, \sigma_z, \tau_{xy}, \tau_{yz}, \tau_{zx}$ at each node
DATA INPUT	
STRUCTURE	solid
OPTION	as required
NODE COORDINATES	x,y,z at each node
SOLID PROPERTIES	E,ν isotropic
CL	P_x, P_y, P_z at any node
CBF	X,Y,Z for element
BFP	P, Δt at any node

Elements available for analysing three-dimensional solid problems

PEN6

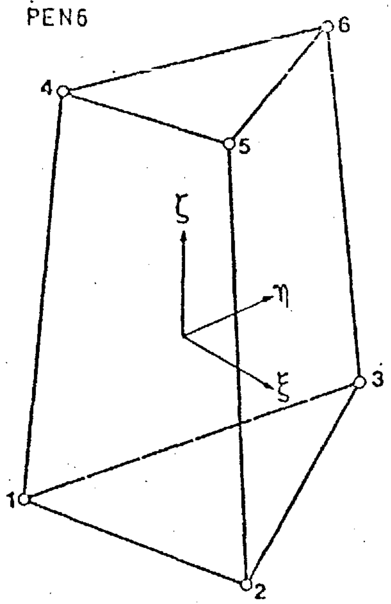

PENTRAHEDRAL ELEMENT WITH STRAIGHT EDGES

Number of nodes	6
Degrees of freedom	u,v,w at each node
Displacement field	linear + selected higher order terms
References	21
STRESS OUTPUT	
Standard	$\sigma_x,\sigma_y,\sigma_z,\tau_{xy},\tau_{yz},\tau_{zx}$ at each node
DATA INPUT	
STRUCTURE	solid
OPTION	as required
NODE COORDINATES	x,y,z at each node
SOLID PROPERTIES	E,ν isotropic
CL	P_x,P_y,P_z at any node
CBF	X,Y,Z for element
BFP	P, Δt at any node

PENI6

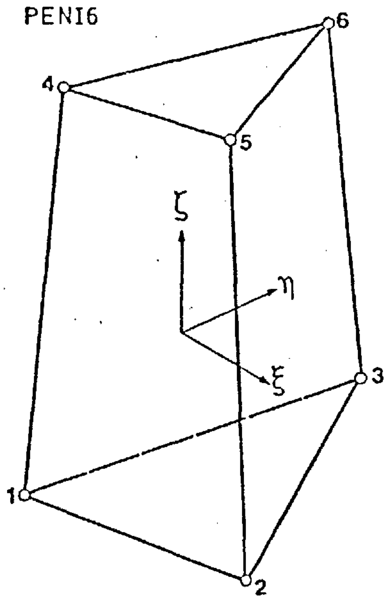

PENTRAHEDRAL ELEMENT WITH STRAIGHT EDGES

Number of nodes	6
Degrees of freedom	u,v,w at each node + α,β,γ which are eliminated
Displacement field	linear + higher order + incompatible modes
References	21 and authors developments
STRESS OUTPUT	
Standard	$\sigma_x,\sigma_y,\sigma_z,\tau_{xy},\tau_{yz},\tau_{zx}$ at each node
DATA INPUT	
STRUCTURE	solid
OPTION	as required
NODE COORDINATES	x,y,z at each node
SOLID PROPERTIES	E,ν isotropic
CL	P_x,P_y,P_z at any node
CBF	X,Y,Z for element
BFP	P, Δt at any node

PEN15

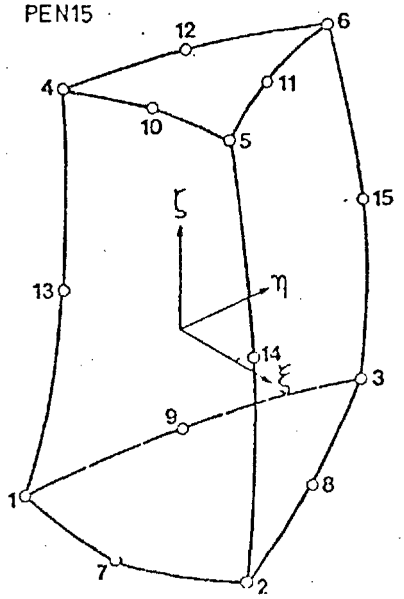

PENTRAHEDRAL ELEMENT WITH CURVED EDGES

Number of nodes	15
Degrees of freedom	u,v,w at each node
Displacement field	quadratic + selected higher order terms
References	21
STRESS OUTPUT	
Standard	$\sigma_x,\sigma_y,\sigma_z,\tau_{xy},\tau_{yz},\tau_{zx}$ at each node
DATA INPUT	
STRUCTURE	solid
OPTION	as required
NODE COORDINATES	x,y,z at each node
SOLID PROPERTIES	E,ν isotropic
CL	P_x,P_y,P_z at any node
CBF	X,Y,Z for element
BFP	P, Δt at any node

Elements available for analysing three-dimensional solid problems

HEX8

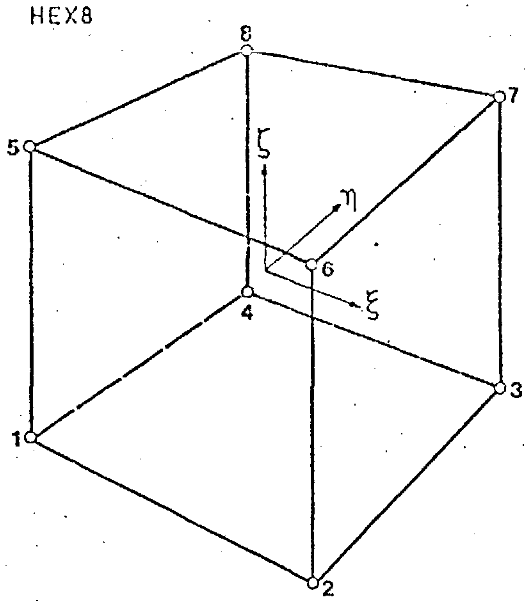

HEXAHEDRONAL ELEMENT WITH STRAIGHT EDGES

Number of nodes	8
Degrees of freedom	u,v,w at each node
Displacement field	linear + selected higher order terms
References	Z1
STRESS OUTPUT	
Standard	$\sigma_x, \sigma_y, \sigma_z, \tau_{xy}, \tau_{yz}, \tau_{zx}$ at each node
DATA INPUT	
STRUCTURE	solid
OPTION	as required
NODE COORDINATES	x,y,z at each node
SOLID PROPERTIES	E,ν isotropic
CL	P_x, P_y, P_z at any node
CBF	X,Y,Z for element
BFP	P, Δt at any node

HEXI8

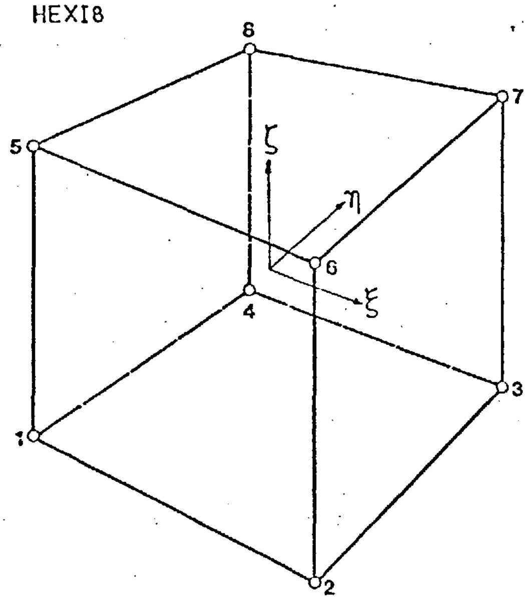

HEXAHEDRONAL ELEMENT WITH STRAIGHT EDGES

Number of nodes	8
Degrees of freedom	u,v,w at each node + α,β,γ which are eliminated
Displacement field	linear + higher order + incompatible modes
STRESS OUTPUT	
Standard	$\sigma_x, \sigma_y, \sigma_z, \tau_{xy}, \tau_{yz}, \tau_{zx}$ at each node
DATA INPUT	
STRUCTURE	solid
OPTION	as required
NODE COORDINATES	x,y,z at each node
SOLID PROPERTIES	E,ν isotropic
CL	P_x, P_y, P_z at any node
CBF	X,Y,Z for element
BFP	P, Δt

HEX20

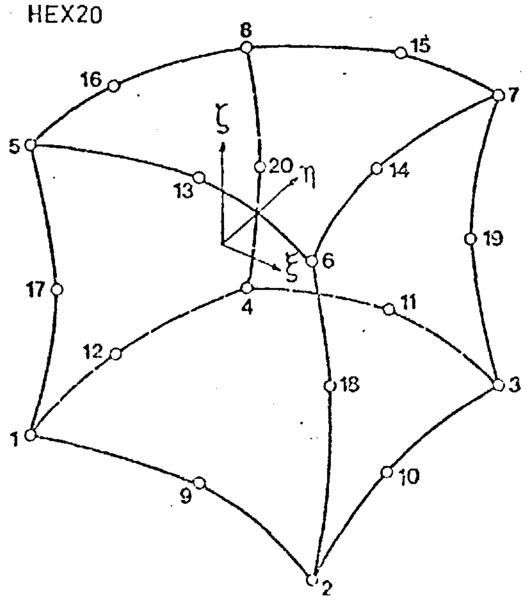

HEXAHEDRONAL ELEMENT WITH CURVED EDGES

Number of nodes	20
Degrees of freedom	u,v,w at each node
Displacement field	quadratic + selected higher order terms
References	Z1
Notes	extrapolated stresses
STRESS OUTPUT	
Standard	$\sigma_x, \sigma_y, \sigma_z, \tau_{xz}, \tau_{yz}, \tau_{zx}$ at each node
DATA INPUT	
STRUCTURE	solid
OPTION	as required
NODE COORDINATES	x,y,z at each node
SOLID PROPERTIES	E,ν isotropic
CL	P_x, P_y, P_z at any node
CBF	X,Y,Z for element
BFP	P,Δt at any node

Elements available for analysing three-dimensional solid problems

TAX3

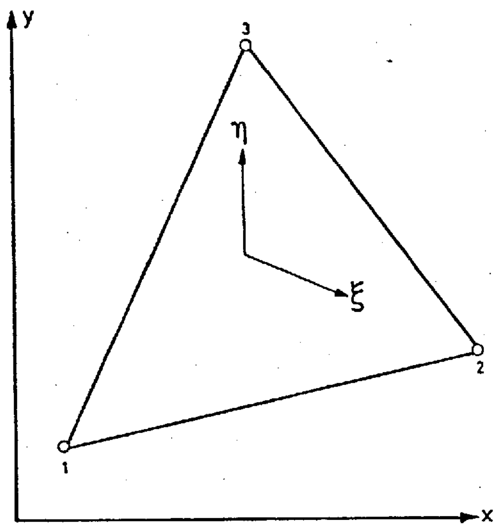

TRIANGULAR AXI-SYMMETRIC ELEMENT

Number of nodes	3.
Degrees of freedom	u,v at each node
Displacement field	linear
References	Z1

STRESS OUTPUT

Standard	$\sigma_x, \sigma_y, \sigma_z, \sigma_{xy}$ at centroid

DATA INPUT

STRUCTURE	axi-symmetric solid
NODE COORDINATES	x,y at each node
MATERIAL PROPERTIES	E,ν for element
CL	P_x, P_y at any node for 1 radian
CBF	X,Y for element

TAX6

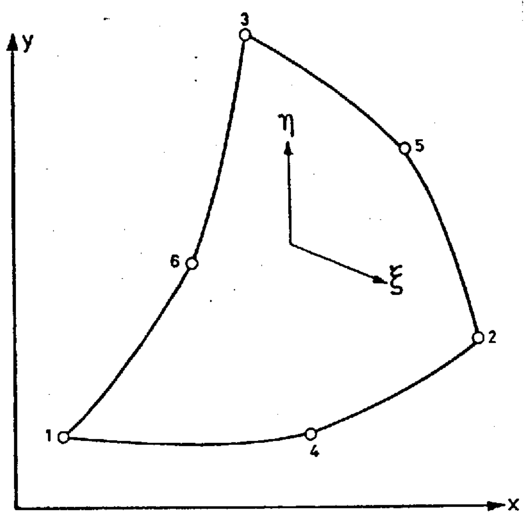

TRIANGULAR AXI-SYMMETRIC ELEMENT

Number of nodes	6
Degrees of freedom	u,v at each node
Displacement field	quadratic
References	Z1

STRESS OUTPUT

Standard	$\sigma_x, \sigma_y, \sigma_z, \sigma_{xy}$ at nodes

DATA INPUT

STRUCTURE	axi-symmetric solid
NODE COORDINATES	x,y at each node
MATERIAL PROPERTIES	E,ν for element
CL	P_x, P_y at any node for 1 radian
CBF	X,Y for element

QAX4

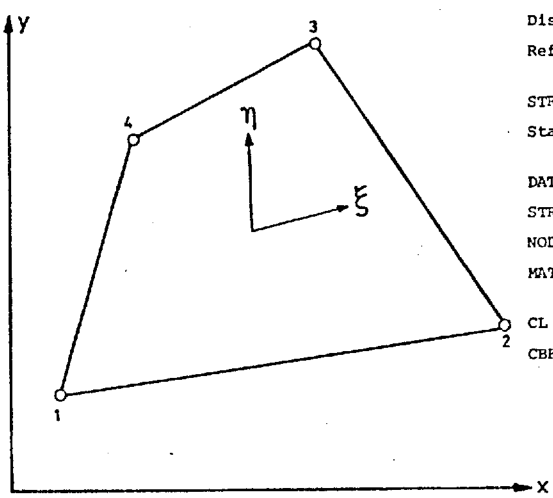

QUADRILATERAL AXI-SYMMETRIC ELEMENT

Number of nodes	4
Degrees of freedom	u,v at each node
Displacement field	linear + higher order
References	Z1

STRESS OUTPUT

Standard	$\sigma_x, \sigma_y, \sigma_z, \sigma_{xy}$ at nodes

DATA INPUT

STRUCTURE	axi-symmetric solid
NODE COORDINATES	x,y at each node
MATERIAL PROPERTIES	E,ν for element
CL	P_x, P_y at any node for 1 radian
CBF	X,Y for element

Elements available for analysing axi – symmetric solid problems

QAX8

QUADRILATERAL AXI-SYMMETRIC ELEMENT

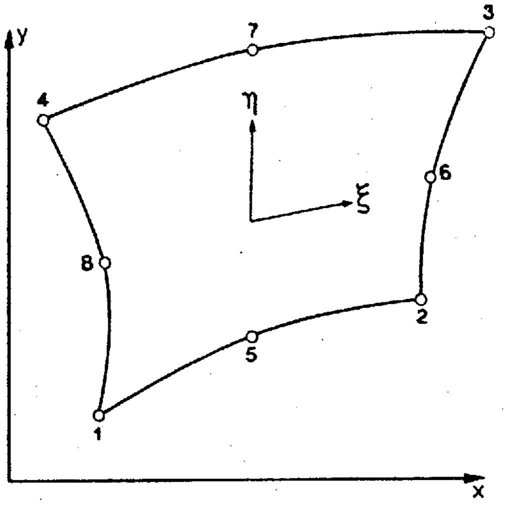

Number of nodes	8
Degrees of freedom	u,v at each node
Displacement field	quadratic + higher order
References	21

STRESS OUTPUT

Standard	$\sigma_x, \sigma_y, \sigma_z, \sigma_{xy}$ at nodes

DATA INPUT

STRUCTURE	axi-symmetric solid
NODE COORDINATES	x,y at each node
MATERIAL PROPERTIES	E,ν for element
CL	P_x, P_y at any node for 1 radian
CBF	X,Y for element

Elements available for analysing three dimensional solid problems

APPENDIX 2

A2.1 GENERAL PROCEDURE FOR SMOOTHED NODAL STRESS VALUES

It has been demonstrated by Barlow[B5] that optimal points for calculating accurate stresses exist within finite element domains, and that these points often coincide with numerical integration points. Although whenever possible the stresses should be sampled at these optimal points, this is not always compatible with the output schemes of finite element computer systems, and is often not convenient for the interpretation of results when nodal values may be preferred.

Nodal stress values can be obtained by extrapolation of the stress values at the integration points. The procedure described here gives smoothed nodal values that are the least squares best fit of the unsmoothed nodal values, and these give consistently superior results.[H1,H2] Also the proposed procedure is easy to implement, and can be applied to all finite element models with optimal stress locations at points other than the nodes.

Consider the parabolic distribution of a typical stress $\sigma(\xi)$ for a one dimensional element[H2], Fig. A2.1. The straight line $\tilde{\sigma}(\xi)$ represents the smoothed stresses and is defined uniquely by the values of the stress at the two Gauss points $(\pm \frac{1}{\sqrt{3}})$. On changing the scale of the coordinate axis by putting $\zeta' = \zeta\sqrt{3}$, points 1 and 2 now have coordinates $\zeta' = \pm 1$. The smoothed stress $\tilde{\sigma}(\zeta')$ can now be calculated quite simply at any position ζ' along the element from the linear interpolation formula

$$\tilde{\sigma} = \sum_{j=1}^{2} N_j \tilde{\sigma}_j \tag{A2.1}$$

where the shape functions are

$$N_j = \frac{1}{2}(1 + \zeta' \zeta'_j) \text{ with } \zeta'_j = \pm 1$$

For the smoothed stresses at the extremities of the element coordinates of $\zeta' = \pm\sqrt{3}$ were inserted.

This extrapolation procedure can be visualised by imagining the stress sampling points to be the nodes j of a new fictitious element where the smoothed stress values $\tilde{\sigma}_j$ are known. Then, by the use of appropriate shape functions, usually an order of one less than the original element shape functions, the smoothed stresses $\tilde{\sigma}$ can be calculated inside or outside of the fictitious element domain, for instance at the nodes i of the original element.

For a parabolic quadrilateral element with eight nodes, there are four optimal stress sampling points, located at the 2 x 2 Gauss points, Fig. A2.2. A fictitious quadrilateral element can be constructed with four nodes j which are coincident with the optimal stress points. If the stresses are assumed to vary bi-linearly, for any point inside or outside of this fictitious element domain, the smoothed stresses are given as

$$\tilde{\sigma} = \sum_{j=1}^{4} N_j \, \tilde{\sigma}_j \tag{A2.2}$$

with

$$N_j = \frac{1}{4}(1 + \zeta' \, \zeta_j') \, (1 + \eta' \, \eta_j') \tag{A2.3}$$

For the smoothed stress values at node 1 of the parent element, for example, the natural coordinates are $\zeta' = -\sqrt{3}$ and $\eta' = -\sqrt{3}$, and for node 5 $\zeta' = 0$ and $\eta' = -\sqrt{3}$, and so on.

Clearly, this stress smoothing procedure can be easily extended to apply to one, two and three dimensional elements where optimal stresses are available at points other than the nodes.

Model	Variational Principle	Assumed Inside Each Element	Along inter-element boundary	Unknowns in Final Equations	References
Compatible	Minimum Potential Energy	Continuous displacements	Displacement compatibility	Nodal displacements	Melosh[M8]
Equilibrium	Minimum Complementary Energy	Continuous and equilibrating stresses	Equilibrium boundary tractions	(i) Stress parameters (ii) Generalised nodal displacements	Elias[E1] Morley[M9,M10] Veubeke[V3]
Hybrid I	Modified Complementary Energy	Continuous and equilibrating stresses	Assumed compatible displacements	Nodal displacements	Pian[P7]
Hybrid II	Modified Potential Energy	Continuous displacements	Assumed equilibrating boundary tractions	Displacement parameters and boundary forces	Yamameto[Y1]
Hybrid III	Modified Potential Energy	Continuous displacements	Assumed boundary tractions for each elements and assumed boundary displacements	Nodal displacements	Tong[T5]
Mixed	Reissner's Principle	Continuous stresses and displacements	Different combinations of boundary displacements and tractions	Different combination of boundary displacements and tractions	Herrman[H3]

Table 1.1 Classification of finite element methods[P6]

Type of code for innermost reduction loop, and tape reading action		Standard Fortran,& BACKSPACE-READ-BACKSPACE	Machine code, & random access disc	Percentage saving
Central processing time (secs)	Forward elimination	164	122	27
	Backsubstitution	19	11	40
	Total for problem	287	236	18
Total problem cost (central processing time + I/O)		59.3	44.7	25

Table 2.1 Comparison of computing costs for the solution of a problem with and without the machine code and random access facilities.

	Mesh in a symmetric quarter Total number of unknowns		1 x 1 12	2 x 2 27	4 x 4 75	8 x 8 243	Theory
CONCENTRATED CENTRAL LOAD	Central deflection w x $10^{-5}.Pl^2/D$ ≈ energy π (element/theory)	Mesh A	1,043 (0.899)	1,105 (0.953)	1,145 (0.987)	1,156 (0.997)	1,160
		Mesh B	1,007 (0.868)	1,132 (0.976)	1,151 (0.992)	1,157 (0.997)	
	Corner reaction x 10^{-4} P (element/theory)	Mesh A	114 (0.094)	1,092 (0.896)	1,160 (0.952)	1,201 (0.985)	1,219
		Mesh B	875 (0.718)	1,173 (0.962)	1,222 (1.002)	1,221 (1.002)	
UNIFORMLY DISTRIBUTED LOAD	Energy π x $10^{-6}.ql^6/D$ (element/thoery)	Mesh A	1,056 (0.620)	1,532 (0.900)	1,661 (0.976)	1,692 (0.994)	1,702
		Mesh B	908 (0.533)	1,504 (0.884)	1,654 (0.972)	1,690 (0.993)	
	Central deflection w x $10^{-6}.ql^4/D$ (element/theory)	Mesh A	4,225 (1.040)	4,062 (1.000)	4,062 (1.000)	4,062 (1.000)	4,062
		Mesh B	3,632 (0.894)	4,063 (1.000)	4,069 (1.002)	4,064 (1.000)	
	Central bending moment* M_x x $10^{-5}.ql^2$ (element/theory)	Mesh A	6,761 (1.411)	5,074 (1.059)	4,819 (1.006)	4,786 (0.999)	4,790
		Mesh B	5,444 (1.137)	5,211 (1.088)	4,935 (1.030)	4,835 (1.009)	
	Corner twisting moment* M_{xy} x $10^{-5}ql^2$ (element/theory)	Mesh A	3,379 (1.040)	3,428 (1.055)	3,325 (1.023)	3,276 (1.008)	3,250
		Mesh B	1,822 (0.561)	2,750 (0.846)	3,086 (0.950)	3,198 (0.984)	

(* Nodal average of values extrapolated from integration points)

Table 3.1 Simply supported square plate under central concentrated load and uniformly distributed load. ISOFLEX 3 resul

	Mesh in a symmetric quarter Total number of unknowns		1 x 1 12	2 x 2 27	4 x 4 75	8 x 8 243	Theory
CONCENTRATED CENTRAL LOAD	Central deflection w x $10^{-6}pl^2/D$ ≈ energy π (element/theory)	Mesh A	3,154 (0.563)	5,190 (0.927)	5,492 (0.981)	5,579 (0.996)	5,600
		Mesh B	2,262 (0.404)	4,908 (0.876)	5,428 (0.969)	5,561 (0.993)	
	Edge bending moment* M_y x$10^{-4}P$ (element/theory)	Mesh A	1,126 (0.896)	1,275 (1.014)	1,257 (1.000)	1,257 (1.000)	1,257
		Mesh B	475 (0.378)	963 (0.766)	1,110) (0.883)	1,173 (0.933)	
UNIFORMLY DISTRIBUTED LOAD	Energy π x $10^{-7}ql^4/D$ (element/theory)	Mesh A	2,629	3,710	3,857	3,886	-
		Mesh B	943	3,151	3,698	3,843	
	Central deflection w x $10^{-6}ql^4/D$ (element/theory)	Mesh A	1,051 (0.834)	1,279 (1.015)	1,267 (1.006)	1,267 (1.006)	1,260
		Mesh B	377 (0.299)	1,108 (0.879)	1,231 (0.977)	1,257 (0.998)	
	Central bending moment* M_x x$10^{-5}ql^2$ (element/theory)	Mesh A	3,075 (1.331)	2,929 (1.268)	2,402 (1.040)	2,313 (1.001)	2,310
		Mesh B	2,059 (0.891)	2,402 (1.040)	2,357 (1.020)	2,311 (1.000)	
	Edge bending moment* M_y x$10^{-5}ql^2$ (element/theory)	Mesh A	3,754 (0.732)	4,893 (0.954)	5,078 (0.990)	5,117 (0.997)	5,130
		Mesh B	792 (0.154)	3,417 (0.666)	4,181 (0.815)	4,626 (0.902)	

(* Nodal average of values extrapolated from integration points).

Table 3.2 Clamped square plate under central concentrated load and uniformly distributed load. ISOFLEX 3 results

Mesh in a symmetric quarter Total number of unknowns			1 x 1 17	2 x 2 43	4 x 4 131	8 x 8 451	Theory
CONCENTRATED CENTRAL LOAD	Central deflection w	Mesh	1,056	1,143	1,161	1,163	
	x 10^{-5}.pl^2/D	A	(0.910)	(0.985)	(1.001)	(1.003)	1,160
	≃ energy π	Mesh	1,060	1,155	1,167	1,166	
	(element/theory)	B	(0.914)	(0.996)	(1.006)	(1.005)	
	Corner reaction	Mesh	441	782	750	873	
	x $10^{-4}P$	A	(0.362)	(0.642)	(0.615)	(0.716)	1,219
	(element/theory)	Mesh	703	608	934	1,092	
		B	(0.577)	(0.499)	(0.766)	(0.896)	
UNIFORMLY DISTRIBUTED LOAD	Energy π	Mesh	1,056	1,543	1,672	1,700	
	x 10^{-6}.ql^6/D	A	(0.620)	(0.907)	(0.982)	(0.999)	1,702
	(element/theory)	Mesh	1,017	1,547	1,671	1,699	
		B	(0.598)	(0.909)	(0.982)	(0.998)	
	Central deflection w	Mesh	4,225	4,127	4,097	4,080	
	x 10^{-6}.ql^4/D	A	(1.040)	(1.016)	(1.009)	(1.004)	4,062
	(element/theory)	Mesh	4,068	4,126	4,098	4,081	
		B	(1.001)	(1.016)	(1.009)	(1.005)	
	Central bending*	Mesh	6,762	5,410	4,965	4,836	
	moment M_x x10^{-5}.ql^2	A	(1.412)	(1.129)	(1.037)	(1.010)	4,790
	(element/theory)	Mesh	5,438	4,948	4,833	4,800	
		B	(1.135)	(1.033)	(1.009)	(1.002)	
	Corner twisting*	Mesh	3,378	3,353	3,158	3,131	
	moment M_{xy} x$10^{-5}ql^2$	A	(1.039)	(1.032)	(0.972)	(0.963)	3,250
	(element/theory)	Mesh	3,716	3,814	3,620	3,446	
		B	(1.153)	(1.174)	(1.114)	(1.060)	

(* Nodal average of values extrapolated from integration points)

Table 3.3 Simply supported square plate under central concentrated load and uniformly distributed load. ISOFLEX 6 results

			1 x 1	2 x 2	4 x 4	8 x 8	Theory
	Mesh in a symmetric quarter / Total number of unknowns		17	43	131	451	
CONCENTRATED CENTRAL LOAD	Central Deflection w $\times 10^{-6} PL^2/D$ = energy π (element/theory)	Mesh A	3,154 (0.563)	5,323 (0.951)	5,590 (0.998)	5,631 (1.006)	5,600
		Mesh B	3,164 (0.565)	5,399 (0.964)	5,640 (1.007)	5,657 (1.010)	
	Edge bending moment $M_y^* \times 10^{-4}.P$ (element/theory)	Mesh A	1,126 (0.896)	1,263 (1.005)	1,238 (0.985)	1,244 (0.990)	1,257
		Mesh B	695 (0.553)	1,173 (0.933)	1,242 (0.988)	1,265 (1.006)	
UNIFORMLY DISTRIBUTED LOAD	Energy π $\times 10^{-7}.ql^4/D$ (element/theory)	Mesh A	2,629	3,854	3,937	3,925	-
		Mesh B	1,307	3,659	3,917	3,926	
	Central deflection w $\times 10^{-6}.ql^4/D$ (element/theory)	Mesh A	1,051 (0.834)	1,277 (1.013)	1,280 (1.016)	1,275 (1.012)	1,260
		Mesh B	527 (0.418)	1,233 (0.979)	1,279 (1.015)	1,276 (1.013)	
	Central bending moment M_x^* $\times 10^{-5}.\ ql^2$ (element/theory)	Mesh A	3,076 (1.332)	2,712 (1.174)	2,425 (1.050)	2,333 (1.010)	2,310
		Mesh B	2,312 (1.001)	2,425 (1.050)	2,332 (1.010)	2,301 (0.996)	
	Edge bending moment $M_y^* \times 10^{-5} ql^2$ (element/theory)	Mesh A	3,754 (0.732)	4,786 (0.933)	5,021 (0.979)	5,063 (0.987)	5,130
		Mesh B	1,258 (0.245)	4,105 (0.800)	4,939 (0.963)	5,130 (1.000)	

(* Nodal average of values extrapolated from integration points).

Table 3.4 Clamped square plate under central concentrated load and uniformly distributed load. ISOFLEX 6 results

	Mesh in a symmetric quarter Total number of unknowns	1 x 1 12	2 x 2 27	4 x 4 75	8 x 8 243	Theory
CONCENTRATED CENTRAL LOAD	Central deflection w x $10^{-5}.Pl^2/D$ = energy π (element/theory)	1,069 (0.922)	1,146 (0.988)	1,157 (0.997)	1,159 (0.999)	1,160
	Corner reaction x 10^{-4} P (element/theory)	618 (0.507)	913 (0.749)	1,124 (0.922)	1,195 (0.980)	1,219
UNIFORMLY DISTRIBUTED LOAD	Energy π x $10^{-6}.ql^6/D$ (element/theory)	977 (0.574)	1,516 (0.891)	1,657 (0.974)	1,689 (0.992)	1,702
	Central deflection w x $10^{-6}.ql^4/D$ (element/theory)	3,906 (0.962)	4,051 (0.997)	4,061 (1.000)	4,062 (1.000)	4,062
	Central bending moment* M_x x $10^{-5}.ql^2$ (element/theory)	6,093 (1.272)	5,124 (1.069)	4,873 (1.017)	4,809 (1.004)	4,790
	Corner twisting moment* M_{xy} x $10^{-5}.ql^2$ (element/theory)	3,281 (1.009)	3,423 (1.053)	3,333 (1.025)	3,279 (1.009)	3,250

(* Nodal average of values extrapolated from integration points)

Table 3.5 Simply supported square plate under central concentrated load and uniformly distributed load. ISOFLEX 4 results

	Mesh in a symmetric quarter Total number of unknowns	1 x 1 12	2 x 2 27	4 x 4 75	8 x 8 243	Theory
CONCENTRATED CENTRAL LOAD	Central deflection w $\times 10^{-6} . Pl^2/D$ $\approx$ energy π (element/theory)	6,250 (1.116)	5,440 (0.971)	5,573 (0.995)	5,603 (1.000)	5,600
	Edge bending moment* $M_y \times 10^{-4} . P$ (element/theory)	1,500 (1.193)	1,277 (1.016)	1,259 (1.002)	1,256 (0.999)	1,257
UNIFORMLY DISTRIBUTED LOAD	Energy π $\times 10^{-7} . ql^4/D$ (element/theory)	3,906	3,837	3,874	3,887	-
	Central deflection w $\times 10^{-6} . ql^4/D$ (element/theory)	1,562 (1.239)	1,245 (0.988)	1,261 (1.000)	1,264 (1.003)	1,260
	Central bending moment* $M_x \times 10^{-5} . ql^2$ (element/theory)	4,875 (2.110)	2,509 (1.086)	2,368 (1.025)	2,311 (1.000)	2,310
	Edge bending moment* $M_y \times 10^{-5} . ql^2$ (element/theory)	3,750 (0.730)	4,738 (0.923)	5,007 (0.976)	5,097 (0.994)	5,130

(* Nodal average of values extrapolated from integration points)

Table 3.6 Clamped square plate under central concentrated load and uniformly distributed load. ISOFLEX 4 results

	Mesh in a symmetric quarter Total number of unknowns	1 x 1 16	2 x 2 39	4 x 4 115	8 x 8 387	Theory
CONCENTRATED CENTRAL LOAD	Central deflection w $\times 10^{-5}.Pl^2/D$ ≈ energy π (element/theory)	1,188 (1.024)	1,162 (1.002)	1,160 (1.000)	1,160 (1.000)	1,160
	Corner reaction $\times 10^{-4}.P$ (element/theory)	130 (0.107)	967 (0.793)	1,160 (0.952)	1,204 (0.988)	1,219
UNIFORMLY DISTRIBUTED LOAD	Energy π $\times 10^{-6}.\ ql^6/D$ (element/theory)	1,055 (0.620)	1,525 (0.896)	1,657 (0.974)	1,702 (1.000)	1.702
	Central deflection w $\times 10^{-6}.\ ql^4/D$ (element/theory)	4,219 (1.039)	4,070 (1.002)	4,063 (1.000)	4,062 (1.000)	4,062
	Central bending moment* $M_x \times 10^{-5}.ql^2$ (element/theory)	6,771 (1.414)	5,164 (1.078)	4,876 (1.018)	4,810 (1.004)	4,790
	Corner twisting moment* $M_{xy} \times 10^{-5}.ql^2$ (element/theory)	3,938 (1.212)	3,470 (1.068)	3,336 (1.026)	3,280 (1.009)	3,250

(* Nodal average of values extrapolated from integration points)

Table 3.7 Simply supported square plate under central concentrated load and uniformly distributed load. ISOFLEX 8 results with four point numerical integration.

	Mesh in a symmetric quarter Total number of unknowns	1 x 1 16	2 x 2 39	4 x 4 115	8 x 8 387	Theory
CONCENTRATED CENTRAL LOAD	Central deflection w $\times 10^{-6} Pl^2/D$ ≈ energy π (element/theory)	6,250 (1.116)	5,688 (1.016)	5,617 (1.003)	5,612 (1.002)	5,600
	Edge bending moment $\overset{*}{M_y} \times 10^{-4}P$ (element/theory)	1,500 (1.193)	1,322 (1,052)	1,261 (1.003)	1,256 (0.999)	1,257
UNIFORMLY DISTRIBUTED LOAD	Energy π $\times 10^{-7}. ql^4/D$ (element/theory)	3,906	3,961	3,896	3,892	-
	Central deflection w $\times 10^{-6}.ql^4/D$ (element/theory)	1,563 (1.240)	1,298 (1.030)	1,267 (1.006)	1,265 (1.004)	1,260
	Central bending moment $\overset{*}{M_x} \times 10^{-5}.ql^2$ (element/theory)	3,875 (2.110)	2,747 (1.189)	2,383 (1.032)	2,312 (1.001)	2,310
	Edge bending moment $\overset{*}{M_y} \times 10^{-5}.ql^2$ (element/theory)	3,750 (0.731)	4,893 (0.954)	5,012 (0.977)	5,095 (0.993)	5,130

(* Nodal average of values extrapolated from integrating points)

Table 3. 8 Clamped square plate under central concentrated load and uniformly distributed load. ISOFLEX 8 results four point numerical interpretation

	Mesh in a symmetric quarter Total number of unknowns	1 x 1 16	2 x 2 39	4 x 4 115	8 x 8 387	Theory
CONCENTRATED CENTRAL LOAD	Central deflection w $\times 10^{-5}.Pl^2/D$ $\simeq$ energy π (element/theory)	1,171 (1.009)	1,158 (0.998)	1,160 (1.000)	1,161 (1.001)	1,160
	Corner reaction $\times 10^{-4}$ P (element/theory)	833 (0.683)	903 (0.741)	1,097 (0.900)	1,146 (0.940)	1,219
UNIFORMLY DISTRIBUTED LOAD	Energy π $\times 10^{-6}.ql^6/D$ (element/theory)	1.050 (0.617)	1.524 (0.815)	1.658 (0.974)	1,692 (0.994)	1,702
	Central deflection w $\times 10^{-6}.ql^4/D$ (element/theory)	4,201 (1.034)	4,067 (1.001)	4,064 (1.000)	4,065 (1.001)	4,062
	Central bending moment* $M_x \times 10^{-5}.ql^2$ (element/theory)	6,670 (1.392)	5,133 (1.072)	4,870 (1.017)	4,811 (1.004)	4,790
	Corner twisting moment* $M_{xy} \times 10^{-5}.ql^2$ (element/theory)	3,882 (1.194)	3,455 (1,063)	3,329 (1.024)	3,276 (1.008)	3,250

(* Nodal average of values extrapolated from integration points)

Table 3.9 Simply supported square plate under central concentrate load and uniformly distributed load. ISOFLEX 8 results with five point numerical integration

Load	Mesh in a symmetric quarter Total number of unknowns	1 x 1 16	2 x 2 39	4 x 4 115	8 x 8 387	Theory
CONCENTRATED CENTRAL LOAD	Central deflection w x $10^{-6}Pl^2/D$ $\simeq$ energy π (element/theory)	6,154 (1.098)	5,640 (1.007)	5,608 (1.001)	5,614 (1.002)	5,600
	Edge bending moment $\overset{*}{M}_y$ x 10^{-4} P (element/theory)	1,447 (1.151)	1,299 (1.033)	1,255 (9.984)	1,255 (9.984)	1,257
UNIFORMLY DISTRIBUTED LOAD	Energy π x $10^{-7}.ql^4/D$ (element/theory)	3,847	3,931	3,892	3,871	-
	Central deflection w x $10^{-6}.ql^4/D$ (element/theory)	1,539 (1.221)	1,287 (1.021)	1,266 (1.004)	1,266 (1.004)	1,260
	Central bending moment $\overset{*}{M}_x$ x $10^{-5}.ql^2$ (element/theory)	4,801 (2.078)	2,708 (1.172)	2,375 (1.028)	2,312 (1.000)	2,310
	Edge bending moment $\overset{*}{M}_y$ x $10^{-5}.ql^2$ (element/theory)	3,693 (0.770)	4,831 (0.942)	4,993 (0.973)	5,092 (0.993)	5,130

(* Nodal average of values extrapolated from integrating points)

Table 3.10 Clamped square plate under central concentrated load and uniformly distributed load. ISOFLEX 8 results with five point numerical integration.

Element model		Deflection $w \times 10^{-5}\ pl^2/D$ along centre line at x/l			
		0.125	0.25	0.375	0.5
ISOFLEX 3	Mesh A	367	713	1,004	1,145
	Mesh B	367	715	1,008	1,151
ISOFLEX 6	Mesh A	370	719	1,014	1,161
	Mesh B	370	720	1,017	1,167
ISOFLEX 4		367	714	1,005	1,157
ISOFLEX 8 Five point integration		367	714	1,006	1,160
Theory[T3]		367	714	1,007	1,160
16 x 16 FD[D1]		367	715	1,009	1,167

Table 3.11 Deflections along centre line of simply supported square plate under concentrated central load. 4 x 4 mesh (one quarter plate)

Element model		Deflection $w \times 10^{-6} ql^4/D$ along centre line of x/l			
		0.125	0.25	0.375	0.5
ISOFLEX 3	Mesh A	1,627	2,943	3,779	4,062
	Mesh B	1,618	2,935	3,778	4,069
ISOFLEX 6	Mesh A	1,638	2,964	3,809	4,096
	Mesh B	1,638	2,964	3,809	4,098
ISOFLEX 4		1,622	2,937	3,775	4,062
ISOFLEX 8 Five point integration		1,624	2,940	3,778	4,064
Theory T3 16 x 16 FD D1		1,623	2,938	3,776	4,062

Table. 3.12 Deflections along centre line of simply supported square plate under uniformly distributed load. 4 x 4 mesh (one quarter plate)

Element model		Deflection w x $10^{-6}pl^2/D$ along centre line of x/l			
		0.125	0.25	0.375	0.5
ISOFLEX 3	Mesh A	762	2,465	4,398	5,492
	Mesh B	728	2,406	4,325	5,423
ISOFLEX 6	Mesh A	780	2,498	4,452	5,590
	Mesh B	773	2,498	4,466	5,639
ISOFLEX 4		771	2,465	4,372	5,573
ISOFLEX 8 Five point integration		771	2,468	4,393	5,608
Theory T3		-	-	-	5,600

Table 3.13 Deflections along centre line of clamped square plate under concentrated central load. 4 x 4 mesh (one quarter plate)

Element model		Deflection $w \times 10^{-6} ql^4/D$ along centre line at x/l			
		0.125	0.25	0.375	0.5
ISOFLEX 3	Mesh A	272	757	1,131	1,267
	Mesh B	255	726	1,096	1,231
ISOFLEX 6	Mesh A	283	768	1,144	1,280
	Mesh B	278	765	1,141	1,278
ISOFLEX 4		277	755	1,126	1,261
ISOFLEX 8 Five point integration		279	759	1,131	1,266
Theory T3		-	-	-	1,260

Table 3.14 Deflections along centre line of clamped square plate under uniformly distributed load. 4 x 4 mesh (one quarter plate).

Element models		Moments M_x x 10^{-4}p along centre line at location x/l, these nodal values refer to smoothed distribution in elements							
		Element 1		Element 2		Element 3		Element 4	
		0	0.125	0.125	0.25	0.25	0.375	0.375	0.500
ISOFLEX 3	Mesh A	-17	-270	-146	-581	-473	-1,211	-1,071	-3,203
	Mesh B	-80	-315	-235	-600	-619	-1,062	-1,200	-3,385
ISOFLEX 6	Mesh A	-27	-234	-268	-572	-595	-1,221	-1,204	-3,341
	Mesh B	51	-218	-155	-561	-477	-1,211	-1,302	-3,499
ISOFLEX 4		-8	-231	-249	-566	-601	-1,247	- 785	-3,701
ISOFLEX 8 Five point integration		4	-245	-226	-601	-514	-1,321	- 746	3,736
Theory T3		0	-	-	-	-	1,221	-1,221	-
16 x 16 FD[D1]		0	-245	-245	-593	-593	-1,251	-1,251	-4,619

Table 3.15 Distribution of moments in elements along centre line of simply supported square plate under concentrated central load. 4 x 4 mesh (one quarter plate)

Element models		Moments $M_x \times 10^{-5} ql^2$ along centre line at locations x/l, these nodal values refer to smoothed distribution in elements							
		Elements 1		Elements 2		Elements 3		Elements 4	
		0	0.125	0.125	0.25	0.25	0.375	0.375	0.500
ISOFLEX 3	Mesh A	-32	-2,761	-2,407	-4,111	-3,798	-4,752	-4,535	-4,839
	Mesh B	-16	-2,726	-2,542	-4,103	-3,981	-4,714	-4,707	-4,935
ISOFLEX 6	Mesh A	-238	-2,924	-2,707	-4,456	-4,071	-5,059	-4,715	-5,089
	Mesh B	-345	-2,487	-2,833	-3,909	-4,205	-4,622	-4,853	-4,832
ISOFLEX 4		-122	-2,808	-2,595	-3,992	-3,986	-4,671	-4,669	-4,873
ISOFLEX 8 Five point integration		-176	-2,563	-2,636	-3,961	-4,009	-4,655	-4,870	-4,678
Theory [T3]		0	-	-	-	-	-	-	-4,790
16 x 16 FD[D1]		0	-2,486	-2,486	-3,887	-3,887	-4,579	-4,579	-4,785

Table 3.16 Distribution of moments along centre line of simply supported square plate under uniform load. 4 x 4 mesh (one quarter plate)

Element models		Moments $M_x \times 10^{-4} p$ along centre line at location x/l, these nodal values refer to smoothed distribution in elements							
		Element 1		Element 2		Element 3		Element 4	
		0	0.125	0.125	0.25	0.25	0.375	0.375	0.500
ISOFLEX 3	Mesh A	1,257	523	517	11	+92	-675	-539	-2,682
	Mesh B	1,208	514	547	14	-21	-510	-649	-2,834
ISOFLEX 6	Mesh A	1,238	633	523	78	+11	-652	-654	-2,797
	Mesh B	1,407	527	615	28	+119	-665	-751	-2,961
ISOFLEX 4		1,260	498	514	30	-8	-701	-240	-3,162
ISOFLEX 8 Five point integration		1,255	493	543	18	+82	-779	-200	3,199
Theory [T3] 16 x 16 FD[D1]		1,257	-	-	-	-	-	-	

Table 3.17 Distribution of moments in elements along centre line of clamped square plate under concentrated central load. 4 x 4 mesh (one quarter plate)

Element models		Moments $M_x \times 10^{-5} ql^2$ along centre line at locations x/l, these nodal values refer to smoothed distribution in elements							
		Element 1		Element 2		Element 3		Element 4	
		0	0.125	0.125	0.25	0.25	0.375	0.375	0.500
ISOFLEX 3	Mesh A	5,078	906	717	-1,318	-1,135	-2,225	-2,042	-2,415
	Mesh B	4,753	1,047	998	-1,198	-1,172	-2,119	-2,129	-2,357
ISOFLEX 6	Mesh A	5,021	1,178	960	-1,210	-1,182	-2,277	-2,120	-2,538
	Mesh B	5,623	885	770	-1,146	-1,378	-2,072	-2,272	-2,332
ISOFLEX 4		5,008	804	877	-1,195	-1,199	-2,118	-2,120	-2,368
ISOFLEX 8		4,993	825	880	-1,218	-1,198	-2,126	-2,118	-2,375
Theory [T3] 16 x 16 FD[D1]		5,130	-	-	-	-	-	-	-2,310

Table 3.18 Distribution of moments in elements along centre line of clamped square plate under unform load. 4 x 4 mesh (one quarter plate)

Mesh over whole plate		2 x 2	4 x 4	16 x 16 Finite difference
Central deflection w $\times 10^{-6}ql^2/D$ (element/ finite difference)	ARI	7,230 (0.910)	7,718 (0.971)	7,945
	ISOFLEX 3	7,323 (0.922)	7,786 (0.980)	
	ISOFLEX 6	8,293 (1.044)	8,089 (1.018)	
	ISOFLEX 4	7,730 (0.973)	7,925 (0.997)	
	ISOFLEX 8 Five point integration	7,944 (1.000)	7,936 (0.999)	
Central moment* M_x $\times 10^{-5}ql^2$ (element/ finite difference)	ARI	7,602 (0.793)	9,172 (0.957)	9,589
	ISOFLEX 3	10,151 (1.059)	9,813 (1.023)	
	ISOFLEX 6	11,113 (1.159)	9,973 (1.0400	
	ISOFLEX 4	10,308 (1.075)	10,191 (1.063)	
	ISOFLEX 8 Five point integration	11,626 (1,212)	10,090 (1.052)	

(* Nodal average of values extrapolated from integration points)

Table 3.19 Skew rhombic plate, two edges simply supported, values of deflection and moments at centre for various elements.

Mesh over whole plate		2 x 2	4 x 4	8 x 8	16x16	Theory
Central deflection w $\times 10^{-7} ql^4/D$ (element/theory)	ISOFLEX 4	5,635 (1.381)	4,670 (1,145)	4,279 (1,049)	4,207 (1.031)	4,080
	ISOFLEX 8 Five point integration	6,825 (1,673)	4,917 (1.205)	4,371 (1.071)	4,242 (1.040)	
Central principal moment* M'_{max} $\times 10^{-5} ql^2$ (element/theory)	ISOFLEX 4	2,231 (1.168)	2,583 (1.352)	1,932 (1.012)	1,949 (1.020)	1,910
	ISOFLEX 8 Five point integration	3,687 (1.930)	2,249 (1.177)	1,979 (1.036)	1,954 (1.023)	
Central principal moment* M'_{min} $\times 10^{-5} ql^2$ (element/theory)	ISOFLEX 4	1,477 (1,368)	1,672 (1,548)	1,142 (1.057)	1,148 (1.063)	1,080
	ISOFLEX 8 Five point integration	1,952 (1.807)	1,689 (1.564)	1,306 (1,209)	1,166 (1.080)	

(* Nodal average of values extrapolated from integration points)

Table 3.20 Acute skew rhombic plate, all edges simply supported, values of deflection and principal moments at centre for various elements.

Description of values		Number of elements along length	Finite element analysis: ISOBEAM 4 value (element/theory)		Finite element analysis: ISOBEAM 6 value (element/theory)		Engineer beam theory ETB
LOAD CASE 1	Vertical deflection w at free end	1 2 4	-192.0 -192.0 -192.0	(1.000)	-192.0 -192.0 -192.0	(1.000)	192.0
	Longitudual stress σ_x at A	1 2 4	-3.000 -3.000 -3.000	(1.000)	-3.000 -3.000 -3.000	(1.000)	-3.0
	Longitudual stress σ_x at B	1 2 4	-3.000 -3.000 -3.000	(1.000)	-3.000 -3.000 -3.000	(1.000)	-3.0
	Transverse stress σ_y at B	1 2 4	0.0 0.0 0.0	(1.000)	0.0 0.0 0.0	(1.000)	0.0
	Shear stress σ_{xy} at C	1 2 4	0.0 0.0 0.0	(1.000)	0.0 0.0 0.0	(1.000)	0.0
LOAD CASE 2	Vertical deflection at free end	1 2 4	1560.3 1940.9 2036.6	(0.753) (0.937) (0.983)	-2052.0 -2063.8 -2067.3	(0.991) (0.997) (0.998)	2071.0
	Longitudual stress σ_x at A	1 2 4	-24.00 -36.00 -42.00	(0.500) (0.750) (0.875)	-48.00 -48.00 -48.00	(1.000)	-48.0
	Longitudual stress σ_x at B	1 2 4	-24.00 -24.00 -24.00	(1.000)	-24.00 -24.00 -24.00	(1.000)	-24.0
	Transverse stress σ_y at B	1 2 4	-0.063 +0.125 0.070	-	-0.063 +0.125 +0.070	-	0.0
	Shear stress σ_{xy} at C	1 2 4	-1.000 -1.000 -1.000	(1.000)	-1.000 -1.000 -1.000	(1.000)	-1.0 averag

Table 4.1 Straight cantilever beam results

Description of values		Number of elements along length	Finite element analysis		Beam theory
			ISOBEAM 4 value (element/ theory)	ISOBEAM 6 value (element/ theory)	
Load Case 1	Vertical deflection w at free end	2 4 8	-1823.5 (1.052) -1756.3 (1.013) -1739.6 (1.003)	-1728.0 (0.997) -1733.0 (0.999) -1734.0 (1.000)	1,734
	Longitudual stress $\sigma_{x'}$ at A	2 4 8	-3.173 (1.058) -3.040 (1.013) -3.010 (1.003)	-2.844 (0.948) -2.962 (0.987) -2.990 (0.997)	-3.000
Load Case 2	Vertical deflection w at free end	2 4 8	-43,869 (0.947) -45,730 (0.988) -46,182 (0.997)	-45,653 (0.986) -46,261 (0.999) -46,326 (1.001)	-46,300
	Longitudual stress $\sigma_{x'}$ at A	2 4 8	-123.3 (1.197) -100.4 (0.975) -102.4 (0.994)	-101.8 (0.988) -102.8 (0.998) -103.0 (1.000)	-103.0

Table 4.2 Curved cantilever beam results

MESH	$\frac{W_F^{FE} - W_F^{ETB}}{W_F^{ETB}} \times 100$ *		$\frac{\sigma_F^{FE} - \sigma_F^{ETB}}{\sigma_F^{ETB}} \times 100$		$\frac{\sigma_{DW}^{FE} - \sigma_{DW}^{BEF}}{\sigma_F^{ETB}} \times 100$		$\frac{\sigma_{DF}^{FE} - \sigma_{DF}^{BEF}}{\sigma_F^{ETB}} \times 100$	
	ISOBEAM 4	ISOBEAM 6	ISOBEAM 4	ISOBEAM 6	ISOBEAM 4	ISOBEAM 6	ISOBEAM 4	ISOBEAM 6
2 x 1 x 1	- 87.0	- 3.0	- 100.0	+0.6	- 46.1	- 41.1	- 48.2	- 27.3
4 x 1 x 1	- 21.9	- 1.0	- 50.1	+0.8	- 43.2	- 20.0	- 22.5	+ 1.8
8 x 1 x 1	- 5.8	- 0.5	- 25.2	+0.4	- 33.2	- 9.8	- 1.5	+ 7.2
16x 1 x 1	- 1.8	- 0.5	- 12.8	-0.5	- 22.1	- 5.0	+ 4.4	+ 7.1

* Note: $W_F^{ETB} = \frac{Wl^3}{192EI} + \frac{Wl}{4AG}$ where A is area of web

Table 4.3 Straight single cell box fixed ends. Effect of mesh size on displacements and stresses at midspan for flexural and distortional components of eccentric point load at mid-span

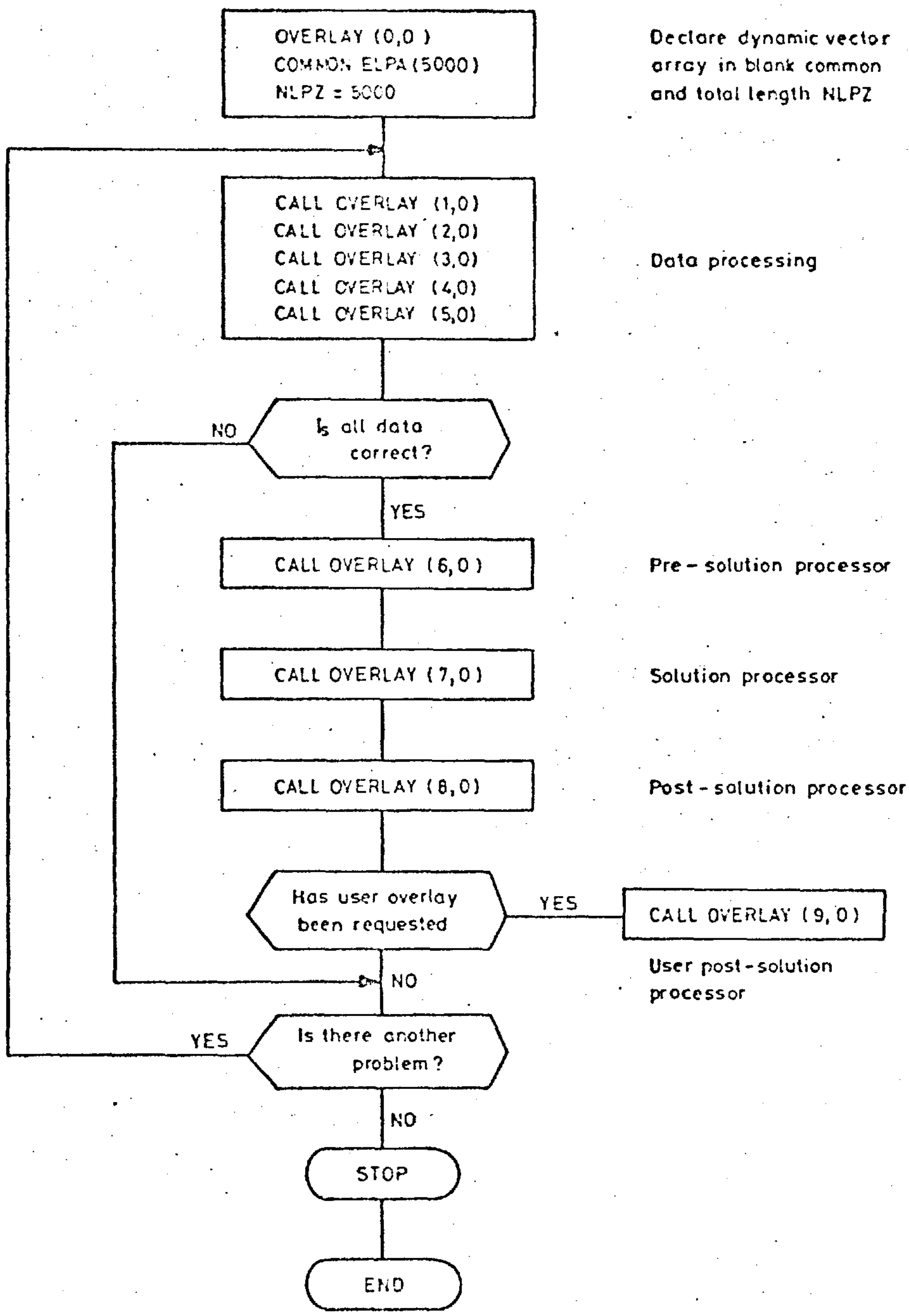

Fig 2·1 Flow diagram of main program overlay of the LUSAS computer system

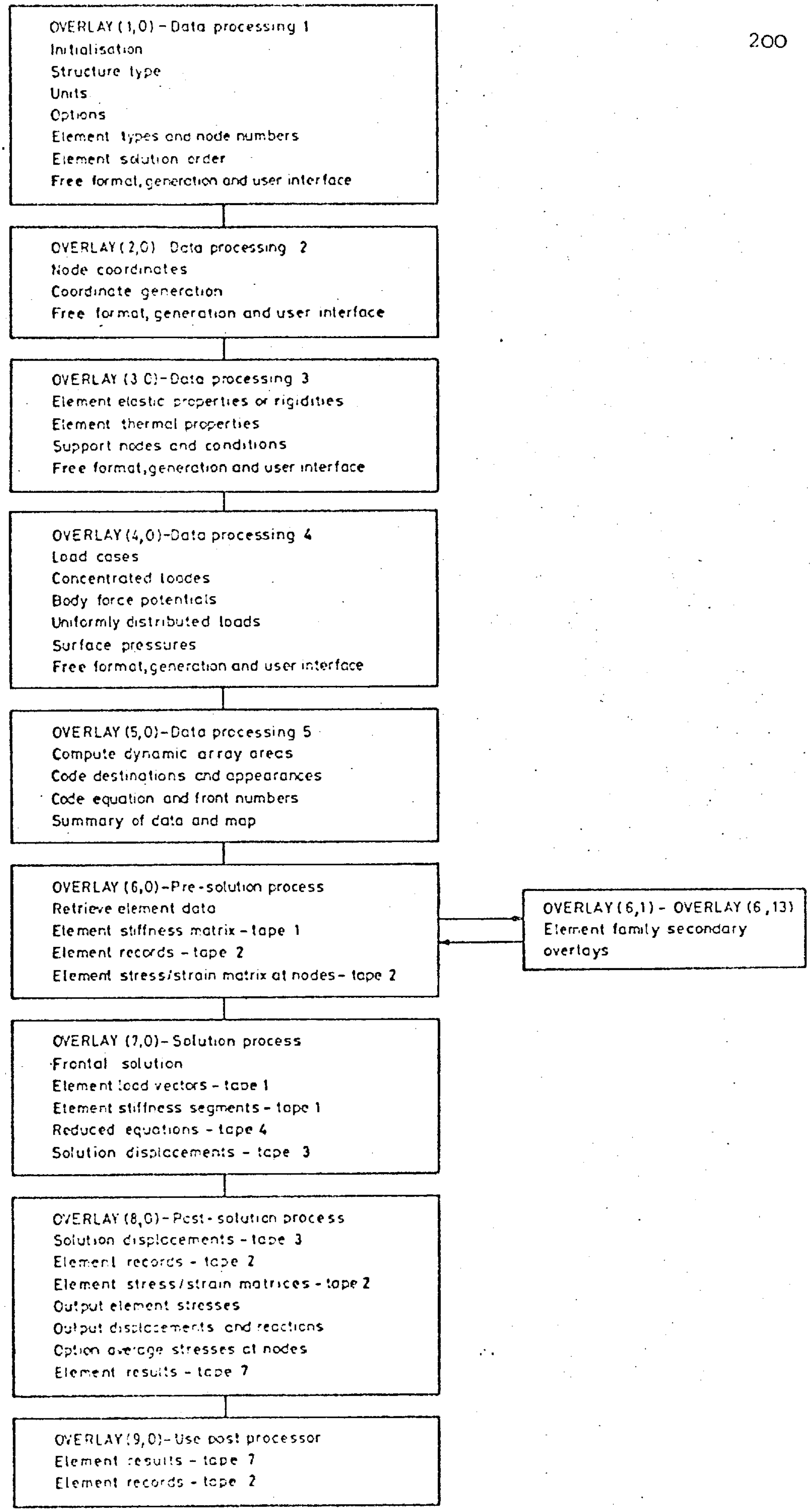

Fig 2·2 Primary and secondary overlay structure of the LUSAS computer system

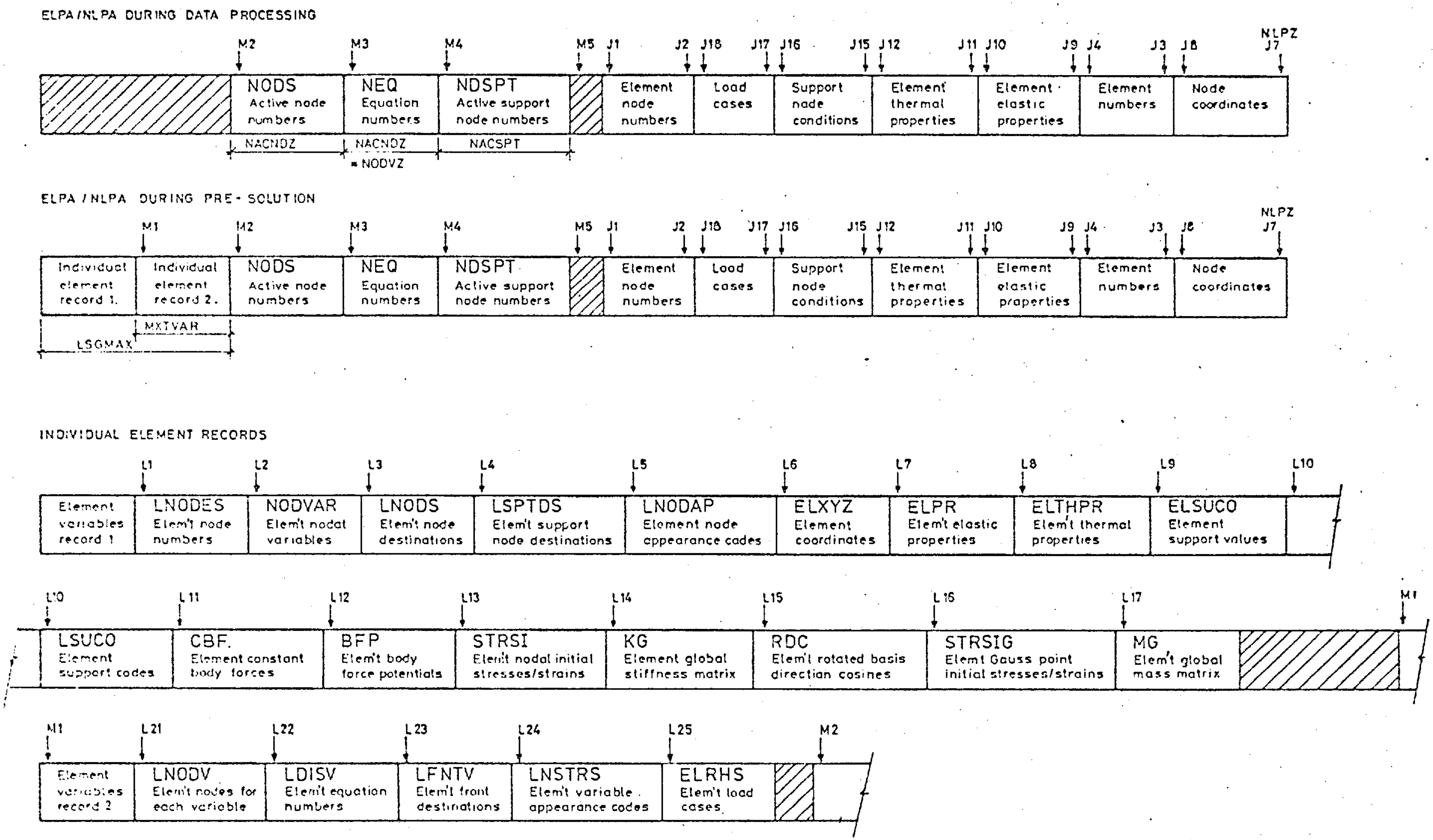

Fig 2·3 Dynamic vector array during data processing and pre-solution

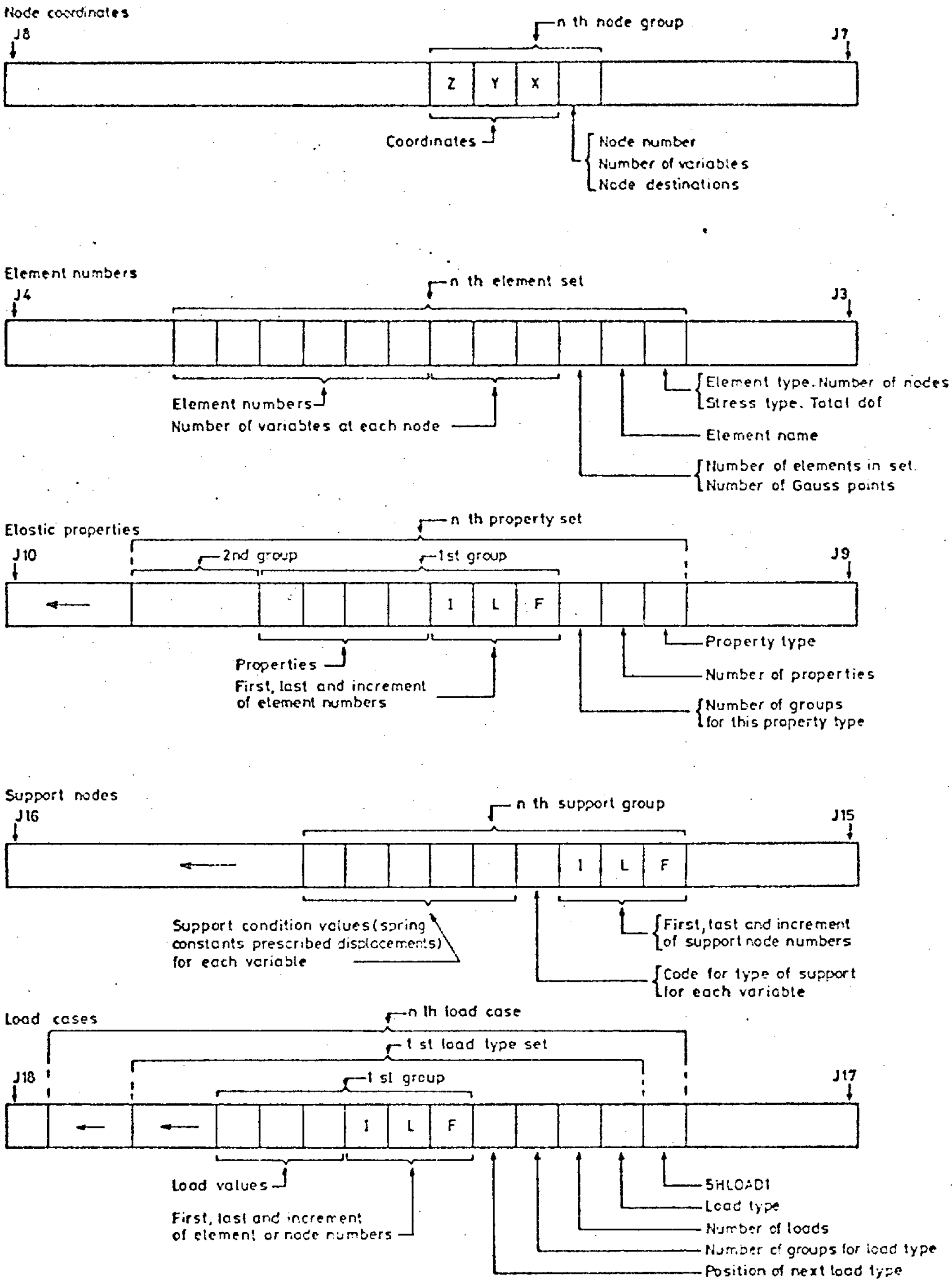

Fig 2·4 Data structure for arrays during data processing

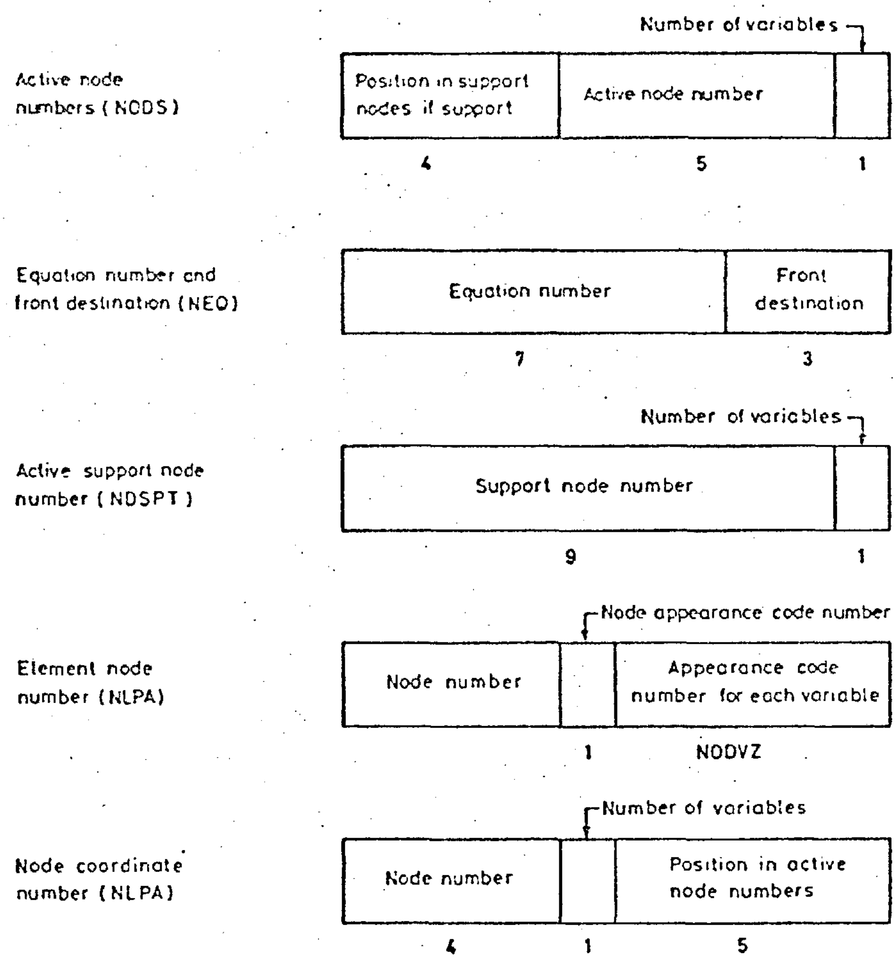

Node and variable appearance code numbers

Inactive	= 0
Intermediate appearance	= 1
Last appearance	= 2
First and last appearance	= 3
First of several appearances	= 4

Fig 2·5 Computer word structure for various arrays after integer compaction at end of data processing

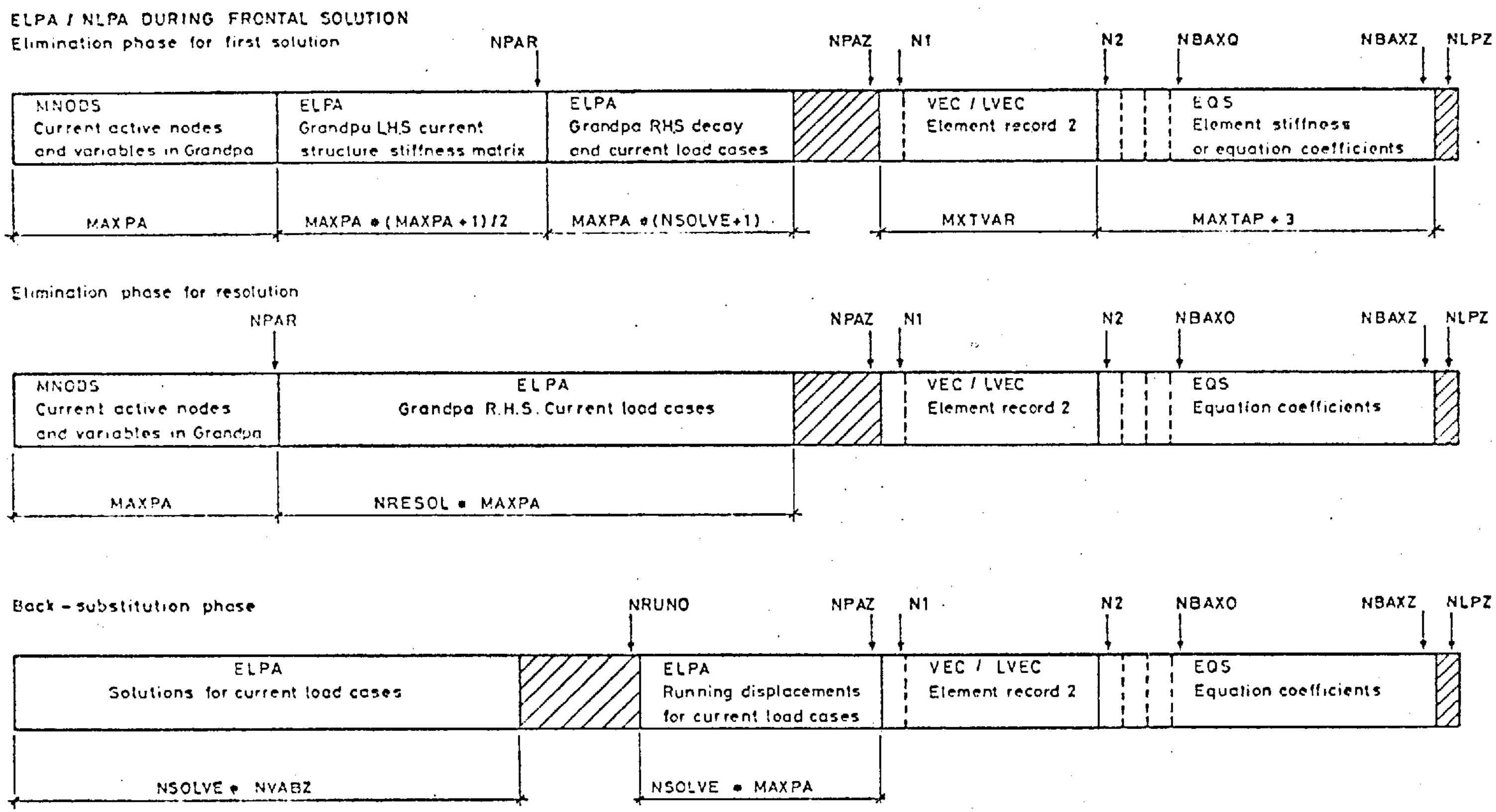

Fig 2·6 Dynamic vector array during frontal solution

NLPA / ELPA DURING POST-SOLUTION PROCESS FOR RESULTS

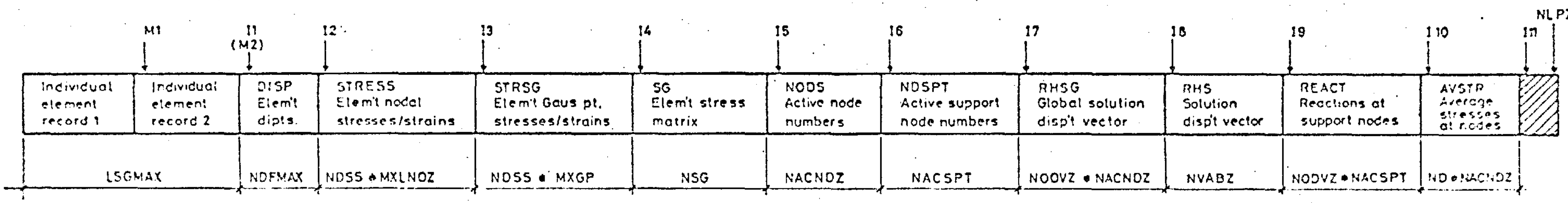

VARIABLE NAMES

LSGMAX	=	maximum length of combined individual element records
MXTVAR	=	maximum length of element record 2
NACNDZ	=	total number of active nodes (nodes with variables)
NODVZ	=	maximum number of variables at a node
NACSPT	=	total number of active support nodes
MAXPA	=	maximum number of variables that appear in the solution front
NSOLVE	=	number of load cases to be processed during first solution phase
NRESOL	=	number of load cases that can be processed during resolution or back substitution phase
MAXTAP	=	maximum size of buffered element stiffness records or equation coefficients
NVABZ	=	total number of equations for problem
NDFMAX	=	maximum number of variables for an element
NDSS	=	total number of stresses and strains at a point
MXLNDZ	=	maximum number of element nodes
MXGP	=	maximum number of Gauss points for an element
NSG	=	maximum size of element stress matrix
ND	=	maximum number of stresses at a point

Fig 2·7 Dynamic vector array during post-solution process for results

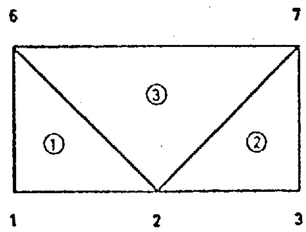

Element number	Element variables	Element destination vector	Position of variables in current overall stiffness matrix
1	1 2 6	1 2 3	1* 2 6
2	2 3 7	2 1 4	3* 2 6 7
3	2 7 6	2 4 3	2* 6* 7*

* Element contributions complete, variable eliminated

Fig 2·8 Simple example of housekeeping in the frontal solution procedure

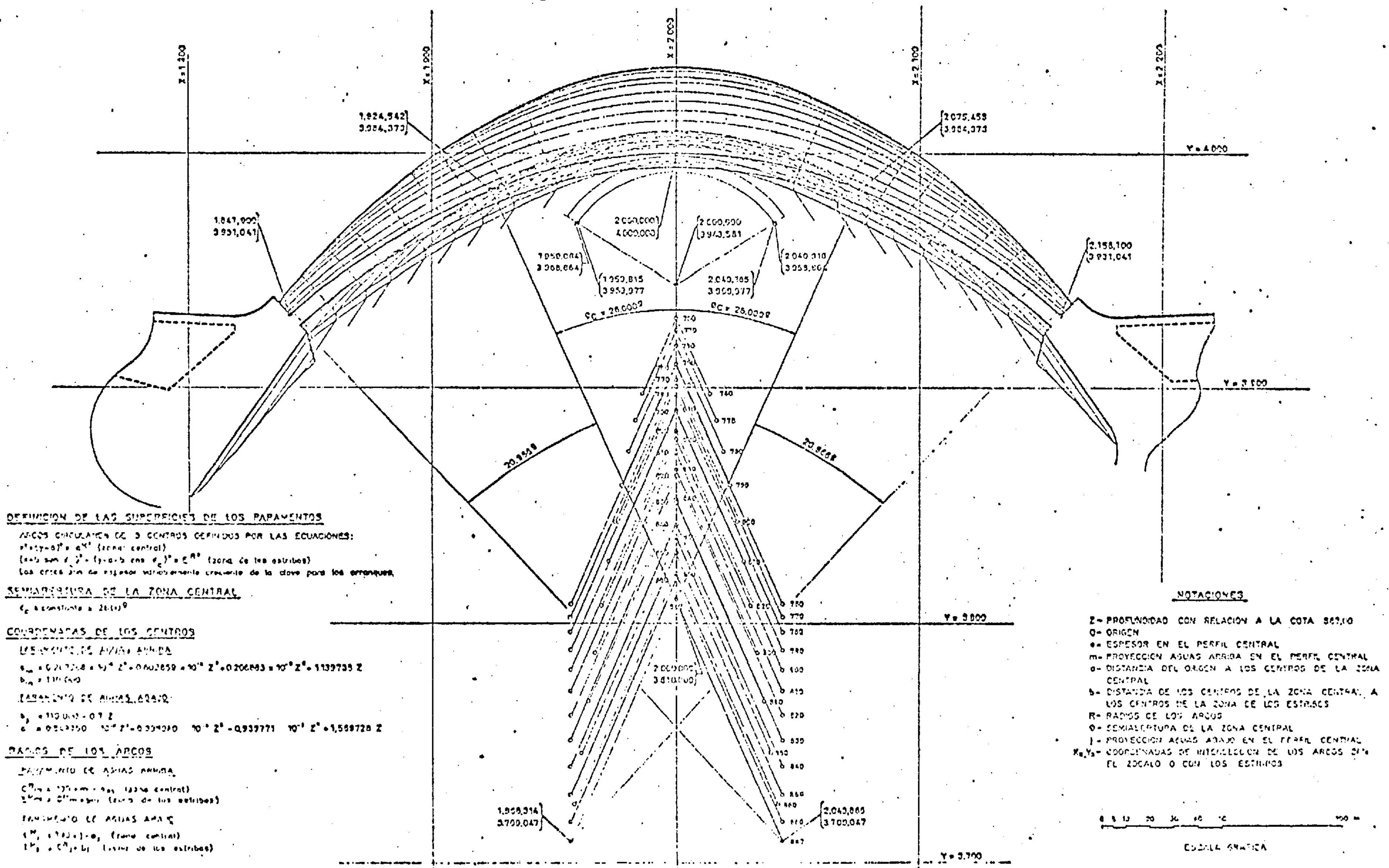
X = 1.800
X = 1.900
X = 2.000
X = 2.100
X = 2.200
Y = 4.000
Y = 3.900
Y = 3.800
Y = 3.700
1.924,542
3.984,373
2.075,458
3.984,373
1.847,900
3.931,041
2.158,100
3.931,041
2.000,000
4.000,000
2.000,000
3.943,581
2.040,185
3.950,077
20,9558
20,9558
2.000,000
3.810,000
1.956,914
3.700,047
2.043,086
3.700,047
DEFINICION DE LAS SUPERFICIES DE LOS PARAMENTOS
ARCOS CIRCULARES DE 3 CENTROS DEFINIDOS POR LAS ECUACIONES:
(zona central)
(zona de los estribos)
Los arcos son de espesor variablemente creciente de la clave para los arranques.
SEMIABERTURA DE LA ZONA CENTRAL
COORDENADAS DE LOS CENTROS
PARAMENTO DE AGUAS ARRIBA
PARAMENTO DE AGUAS ABAJO
RADIOS DE LOS ARCOS
PARAMENTO DE AGUAS ARRIBA
(zona central)
(zona de los estribos)
PARAMENTO DE AGUAS ABAJO
(zona central)
(zona de los estribos)
NOTACIONES
Z = PROFUNDIDAD CON RELACION A LA COTA
O = ORIGEN
e = ESPESOR EN EL PERFIL CENTRAL
m = PROYECCION AGUAS ARRIBA EN EL PERFIL CENTRAL
a = DISTANCIA DEL ORIGEN A LOS CENTROS DE LA ZONA CENTRAL
b = DISTANCIA DE LOS CENTROS DE LA ZONA CENTRAL A LOS CENTROS DE LA ZONA DE LOS ESTRIBOS
R = RADIOS DE LOS ARCOS
j = PROYECCION AGUAS ABAJO EN EL PERFIL CENTRAL
EL ZOCALO O CON LOS ESTRIBOS
ESCALA GRAFICA

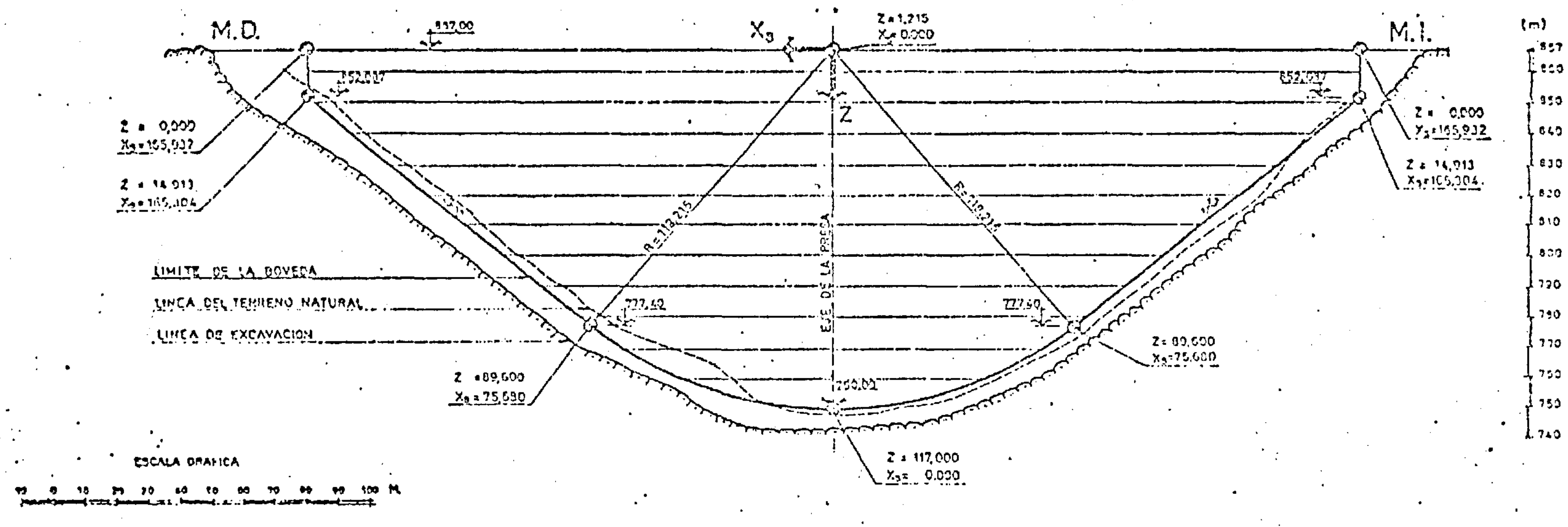

DEFINICION DE LAS FORMAS DEL PERFIL CENTRAL

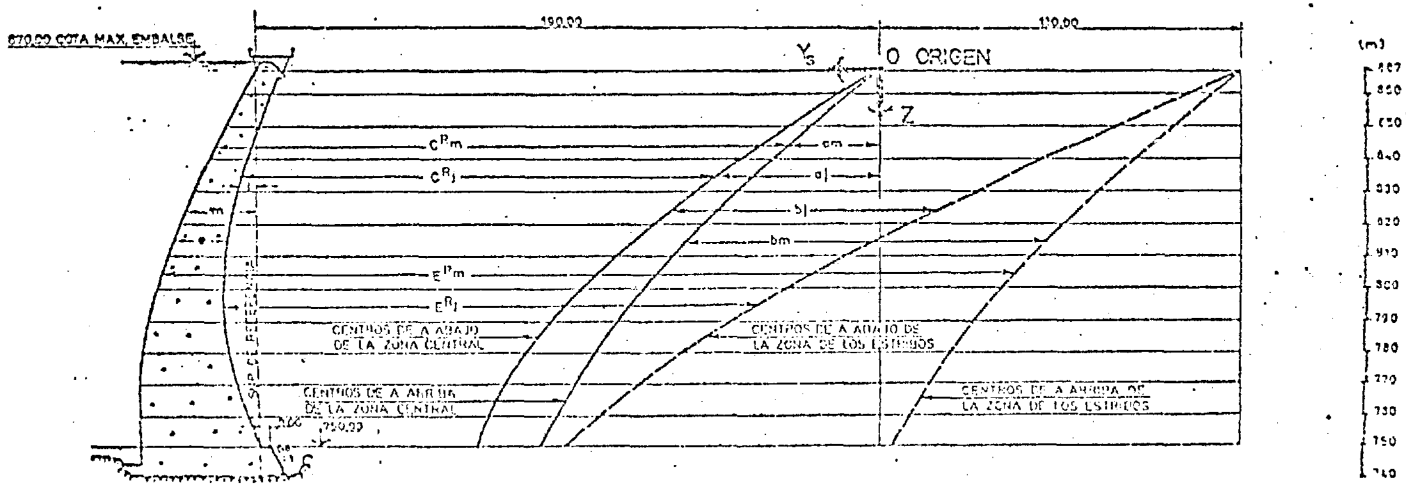

Fig.2·10 Downstream elevation and central profile of the dam

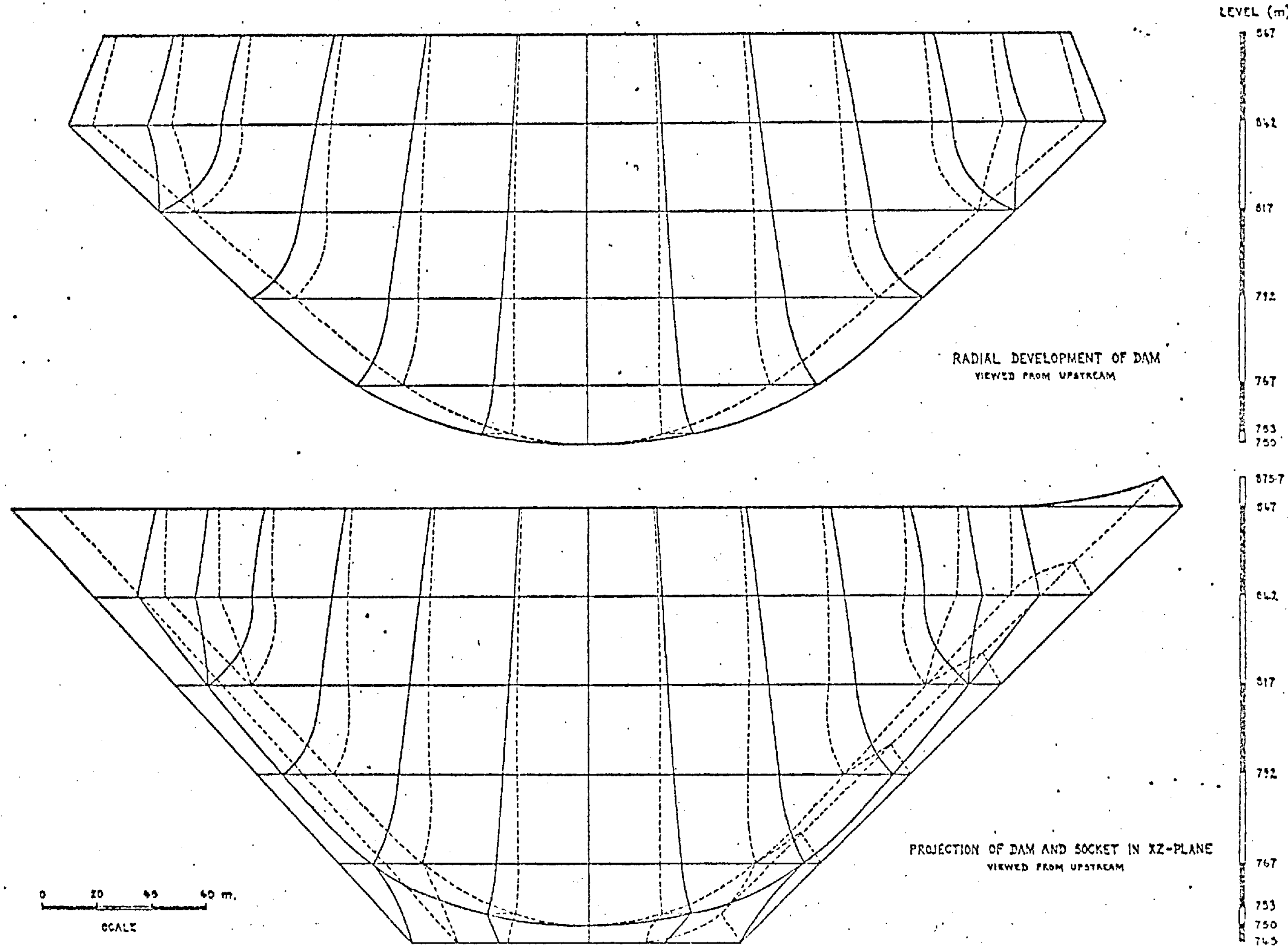

Fig. 2·11 Three-dimensional idealisation of the dam and socket.

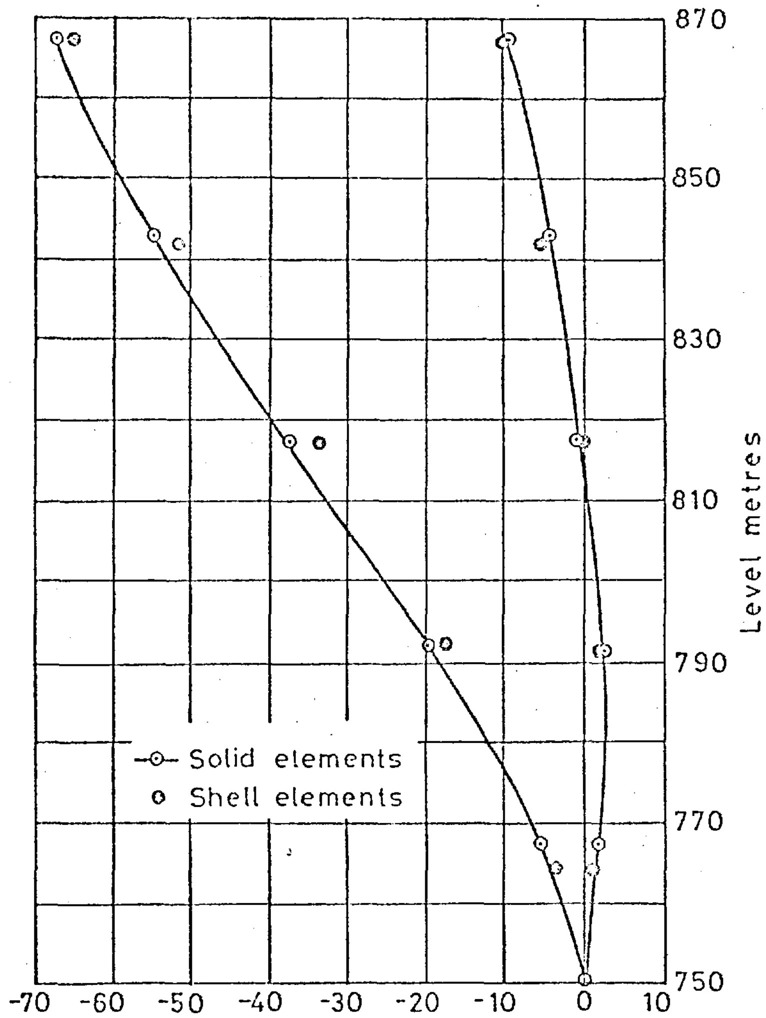

(a) Vertical and horizontal displacements on centre line

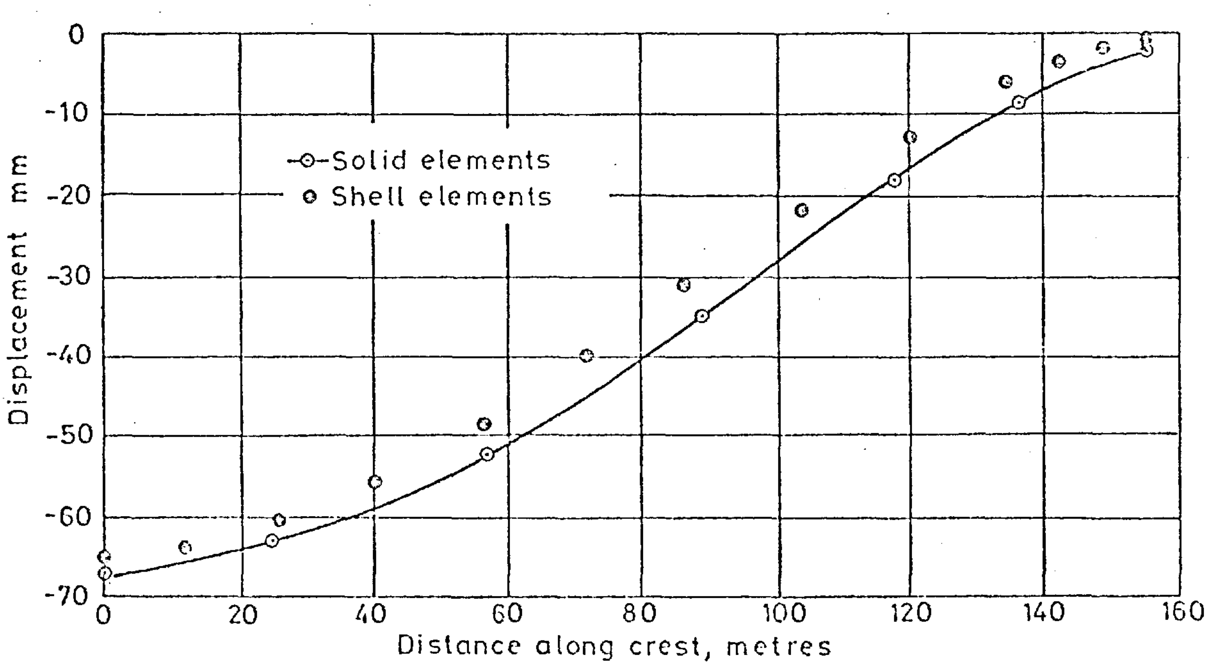

(b) Horizontal displacements along crest

Fig 2.12 El Altazar Dam, displacements

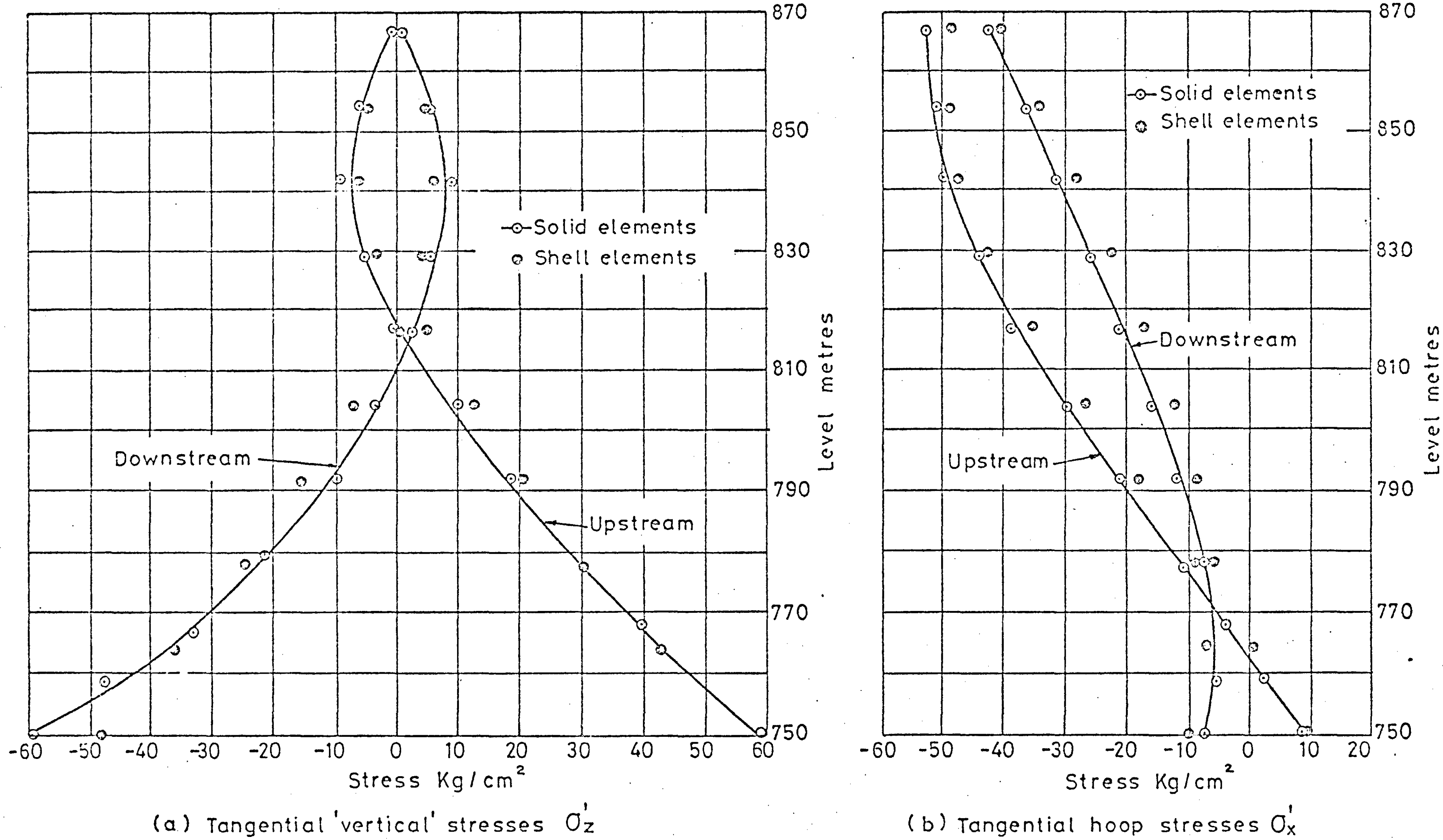

Fig. 2·13 El Altazar Dam, surface stresses at central section

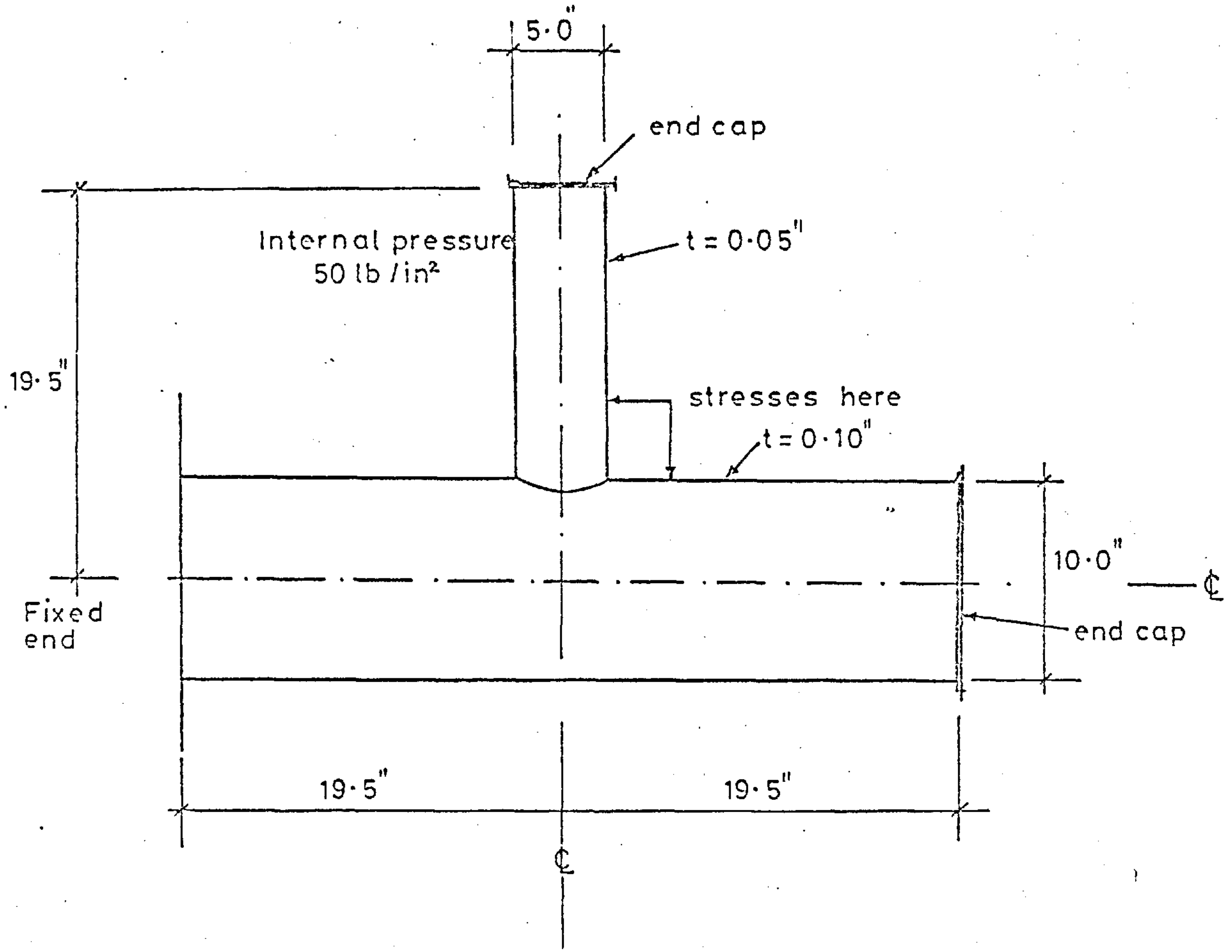

Fig 2·14 Thin intersecting cylindrical shell problem

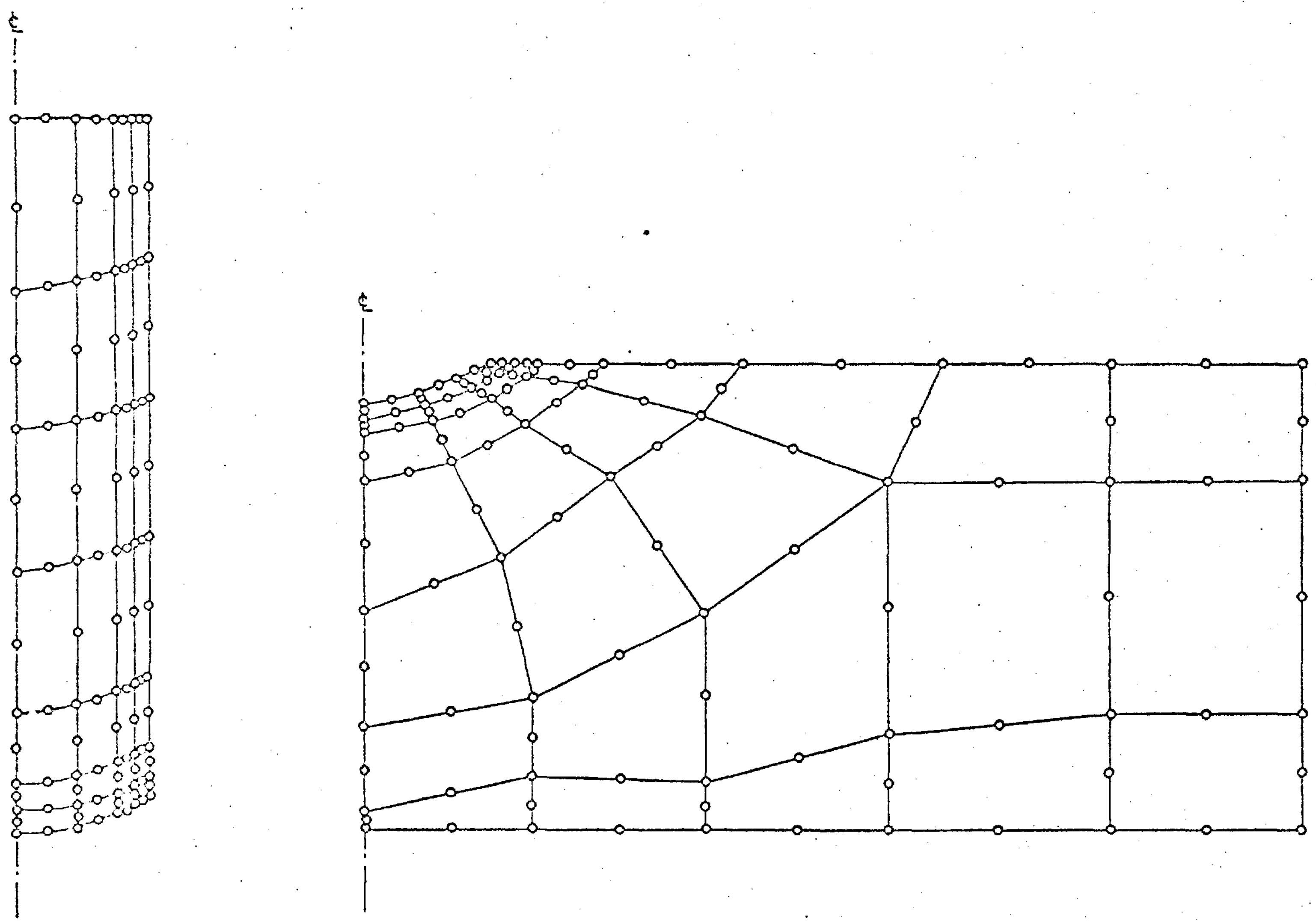

Fig.2·15 Thin intersecting cylindrical shell idealization

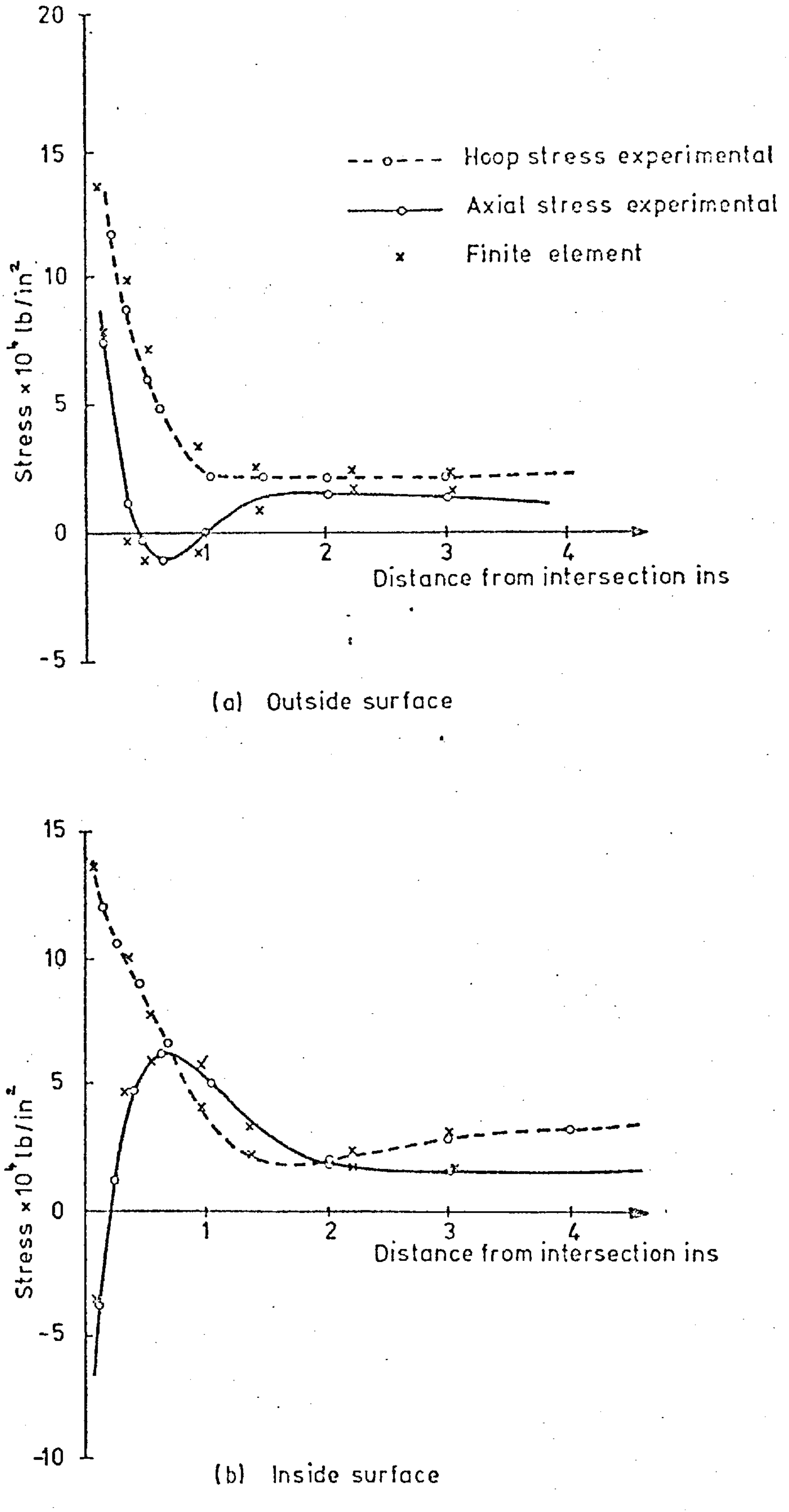

Fig 2·16 Stresses on inside and outside surface of main cylinder

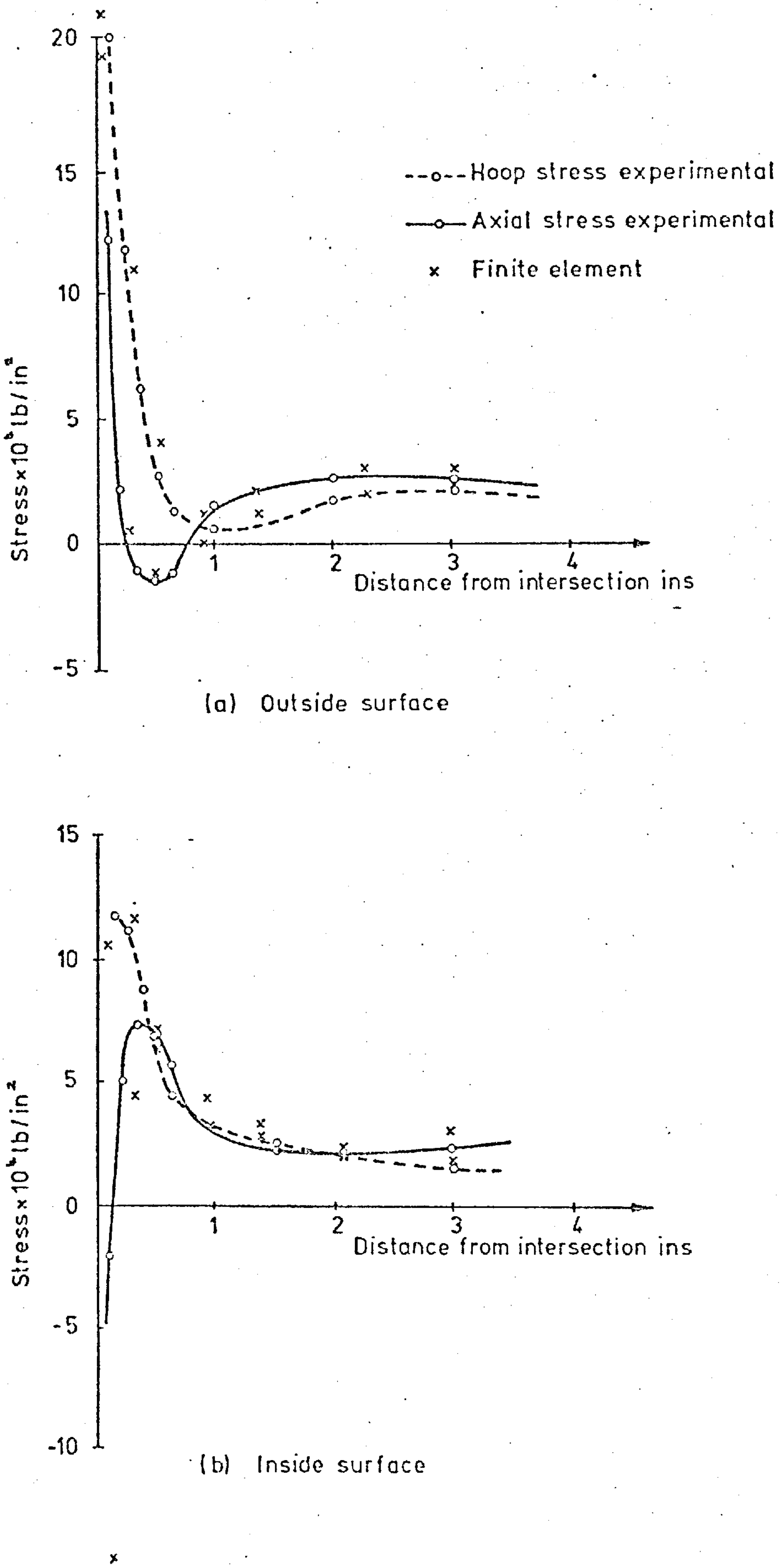

Fig 2·17 Stresses on inside and outside surface of branch cylinder

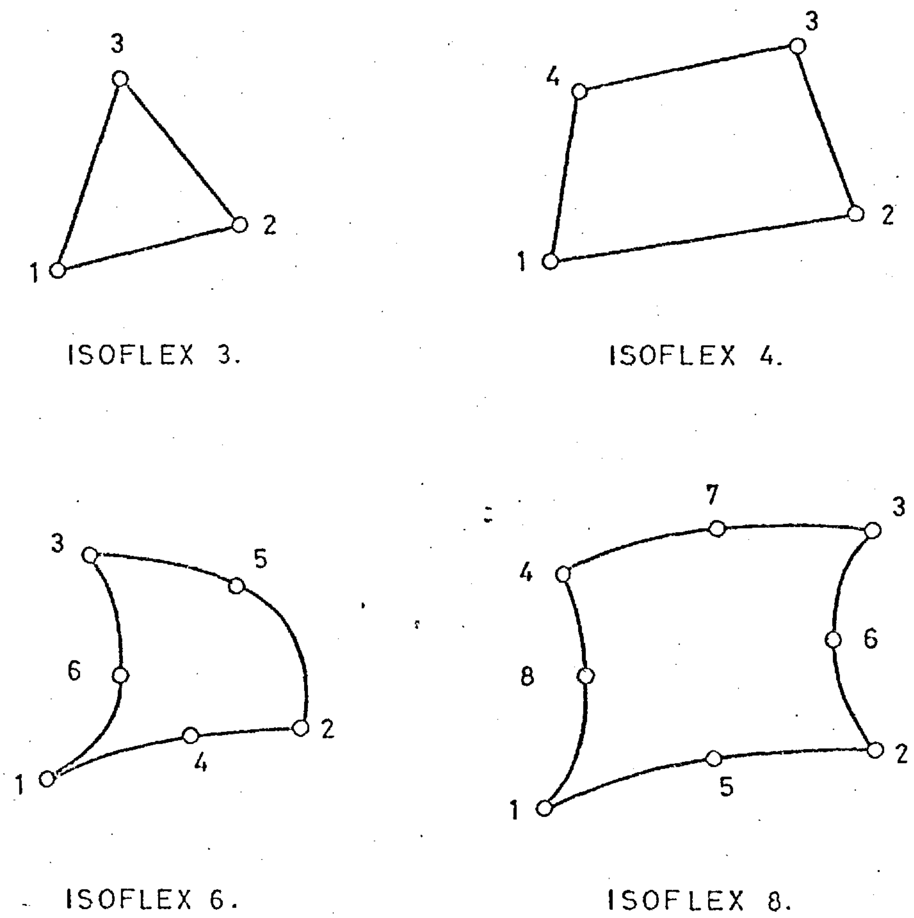

Nodal variables $\delta_i = \begin{Bmatrix} w \\ \theta x \\ \theta y \end{Bmatrix}_i = \begin{Bmatrix} w \\ \dfrac{\partial w}{\partial y} \\ -\dfrac{\partial w}{\partial x} \end{Bmatrix}_i$ for corner nodes

$\delta_i = \{\Delta\theta_T\}_i$ for midside nodes

Fig 3·1 The ISOFLEX family and nodal configurations

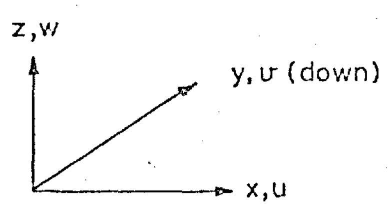

(i) Right-handed cartesian co-ordinates

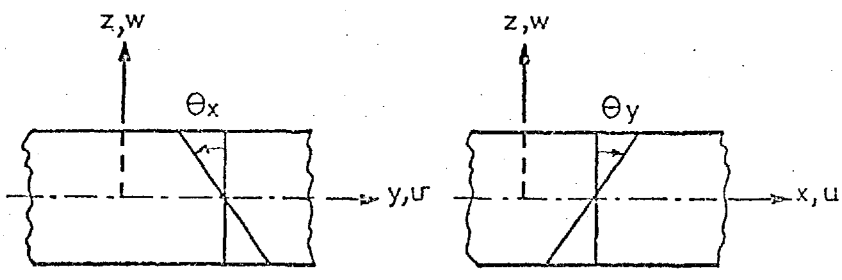

(ii) Positive θx and θy (right-hand-screw rule)

Fig 3·2 Global co-ordinate system and sign convention

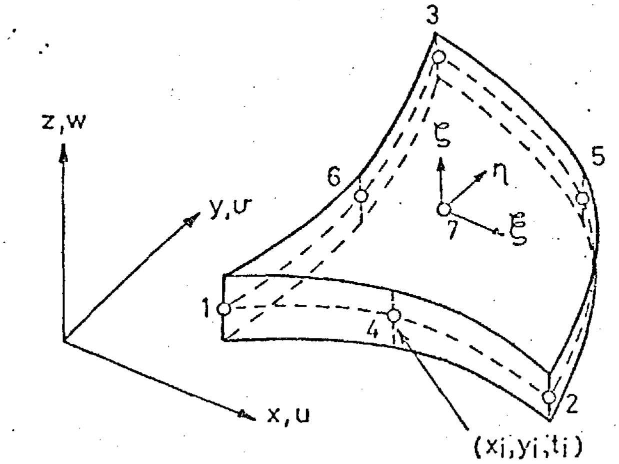

(a) TRIANGLE

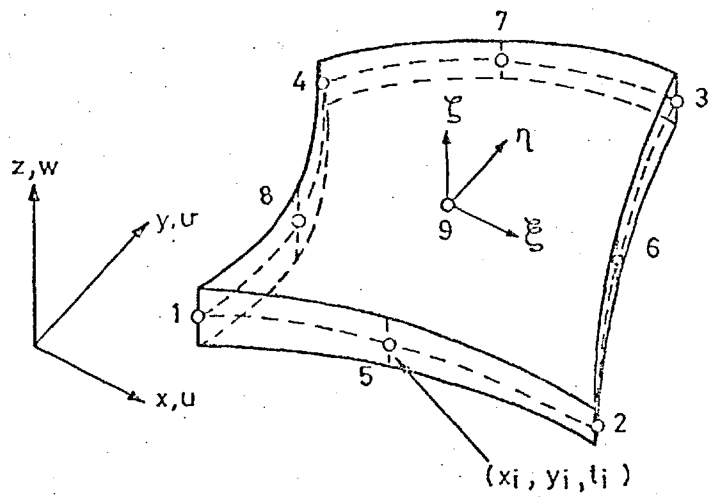

(b) QUADRILATERAL

Nodal variables $\quad \delta_i = \begin{Bmatrix} w \\ \theta_x \\ \theta_y \end{Bmatrix}_i$ for corner nodes

$\delta_i = \begin{Bmatrix} \Delta w \\ \Delta\theta_x \\ \Delta\theta_y \end{Bmatrix}_i$ for midside nodes and central node of quadrilateral

$\delta_i = \begin{Bmatrix} \Delta\theta_x \\ \Delta\theta_y \end{Bmatrix}$ for central node of triangle

Fig 3·3 Unconstrained element nodal configurations and co-ordinate systems

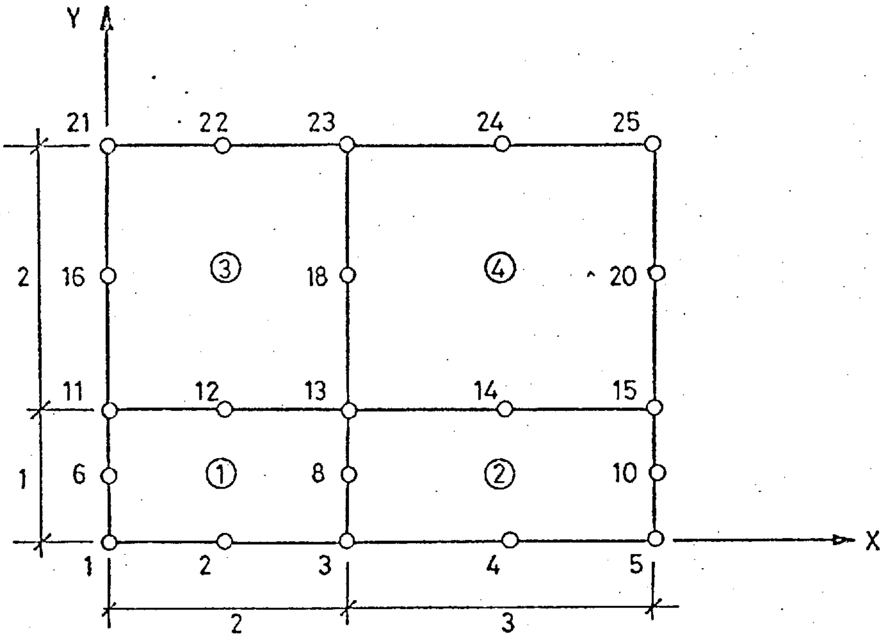

Fig 3·4 Rectangular patch test

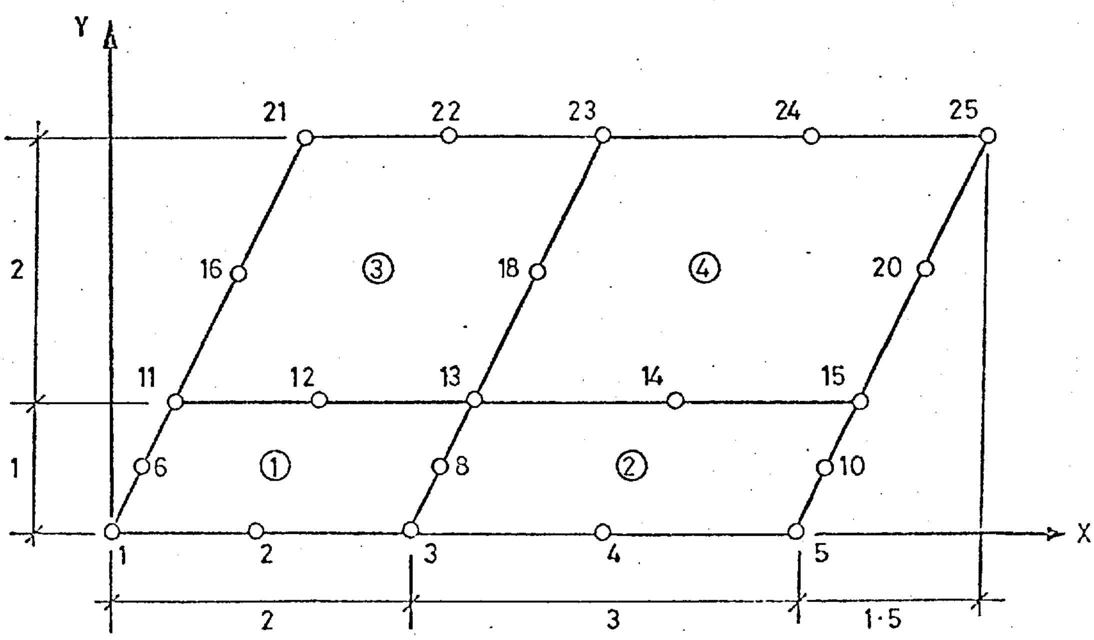

Fig 3·5 Parallelogram patch test

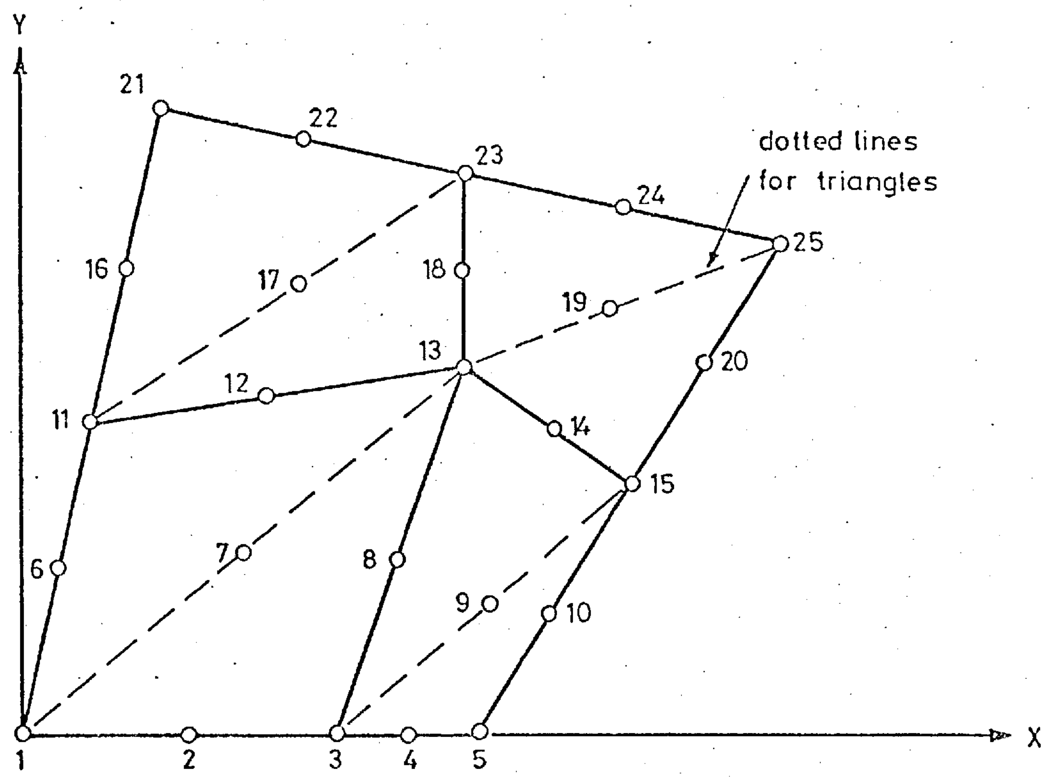

Assumed displacement field:

$$w = 1 + 2x + 3y + 4x^2 + 5xy + 6y^2$$
$$\therefore w = 151 \cdot 0 \quad \text{at node 15}$$

Constant strain state:

$$\frac{\partial^2 w}{\partial x^2} = 8, \quad \frac{\partial^2 w}{\partial y^2} = 12, \quad \frac{\partial^2 w}{\partial x \partial y} = 5$$

Constant moment state:

$$\left\{\begin{bmatrix} Mx \\ My \\ Mxy \end{bmatrix}\right\} = \left\{\begin{bmatrix} 1 & 0\cdot 3 & 0 \\ 0\cdot 3 & 1 & 0 \\ 0 & 0 & 0\cdot 35 \end{bmatrix}\right\} \left\{\begin{bmatrix} -8 \\ -12 \\ -10 \end{bmatrix}\right\} = \left\{\begin{bmatrix} -11\cdot 6 \\ -14\cdot 4 \\ -3\cdot 5 \end{bmatrix}\right\}$$

Finite element results:

$$w = 151\cdot 0 \quad \text{at node 13} \qquad \left\{\begin{array}{l} Mx = -11\cdot 6 \\ My = -14\cdot 4 \\ Mxy = -3\cdot 5 \end{array}\right\} \text{at all nodes}$$

Fig. 3·6 Quadrilateral patch test

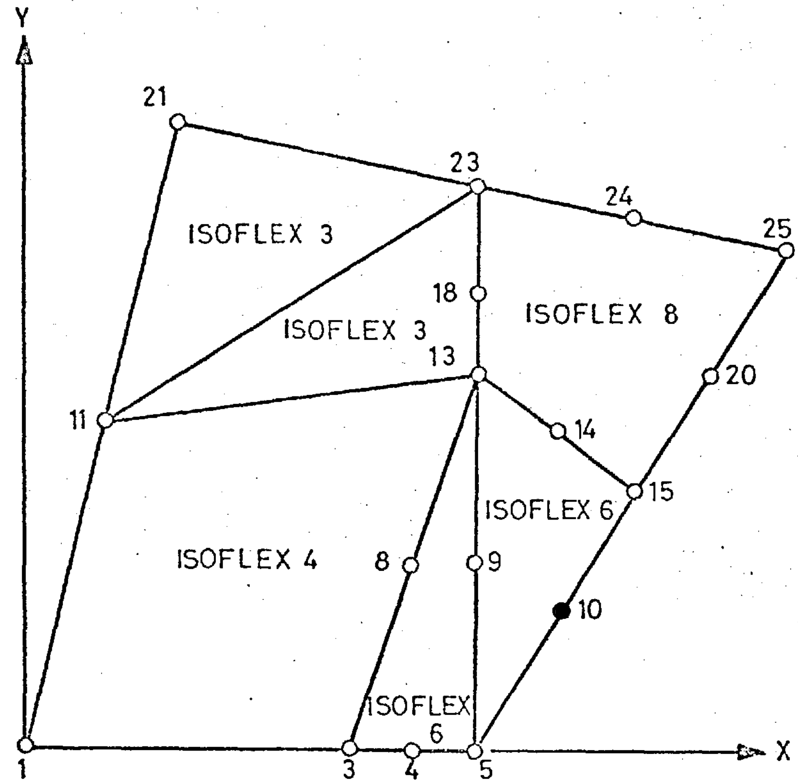

Fig 3·7 Mixed patch Test

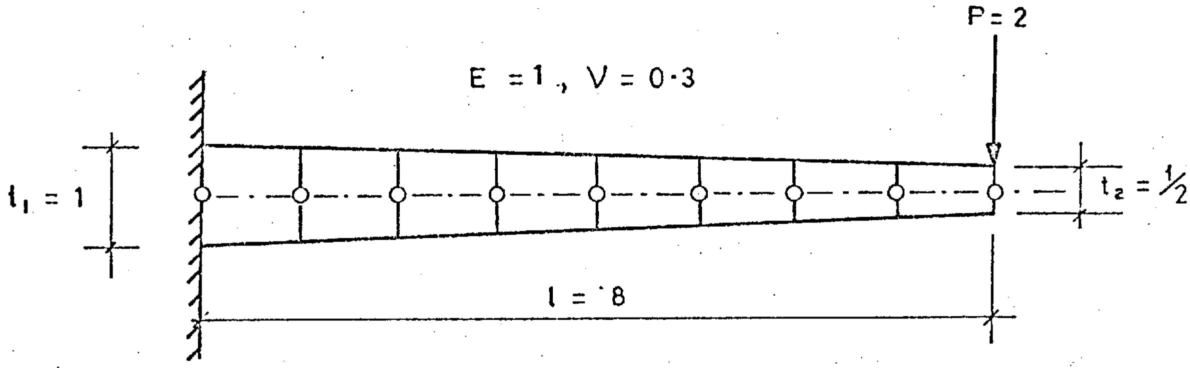

Fig 3·8 Tapered beam example for variable thickness

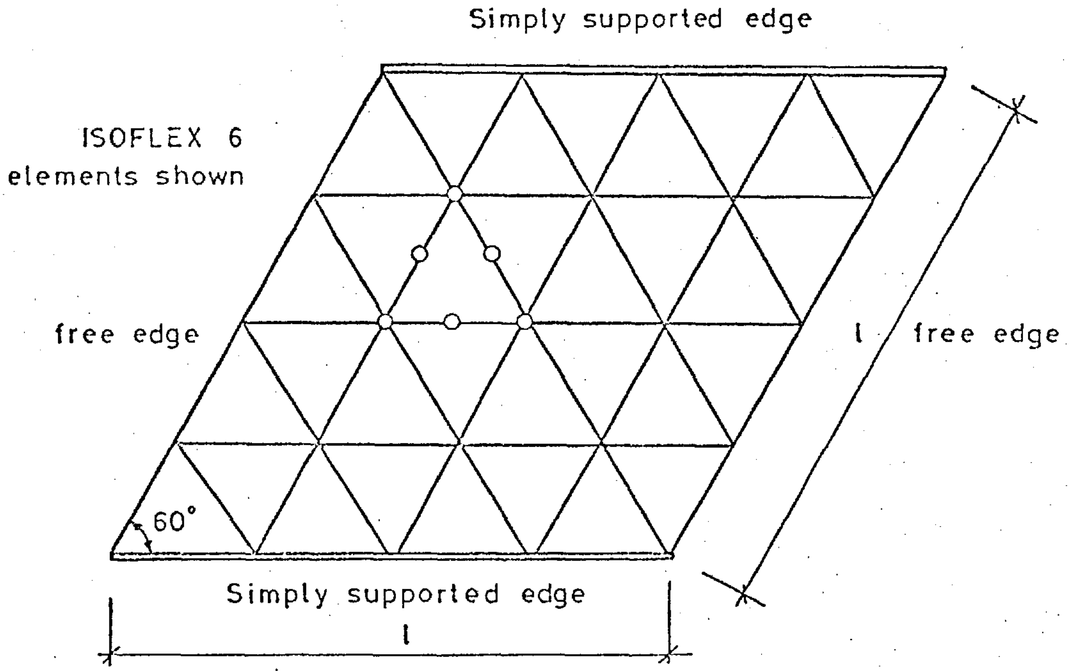

Fig 3·9 Skew rhombic plate with 4×4 mesh shown. Two edges simply supported

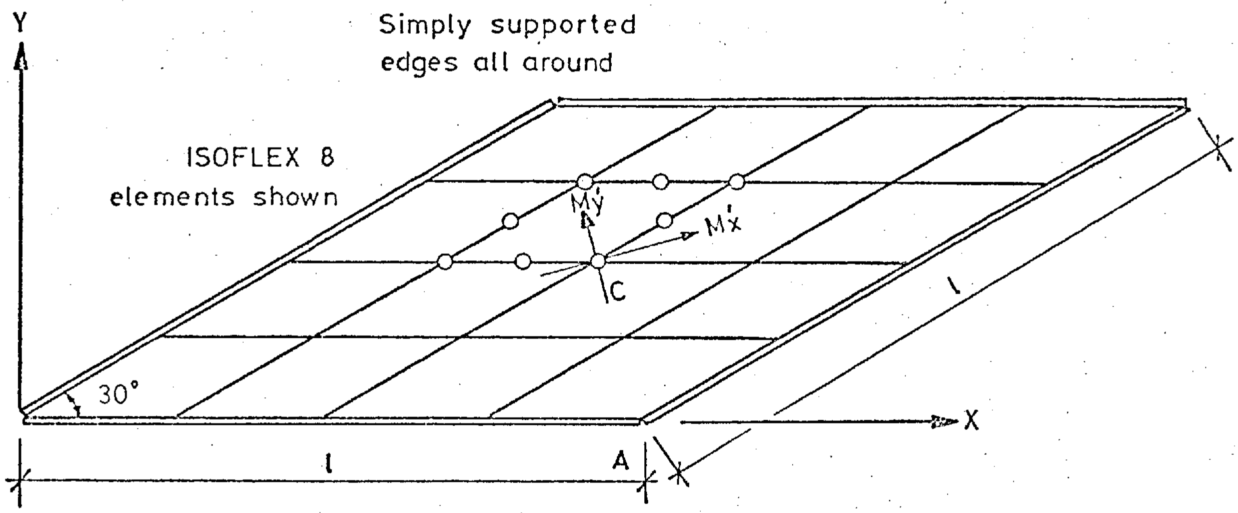

Fig 3·10 Acute skew rhombic plate with 4×4 mesh shown. All edges simply supported.

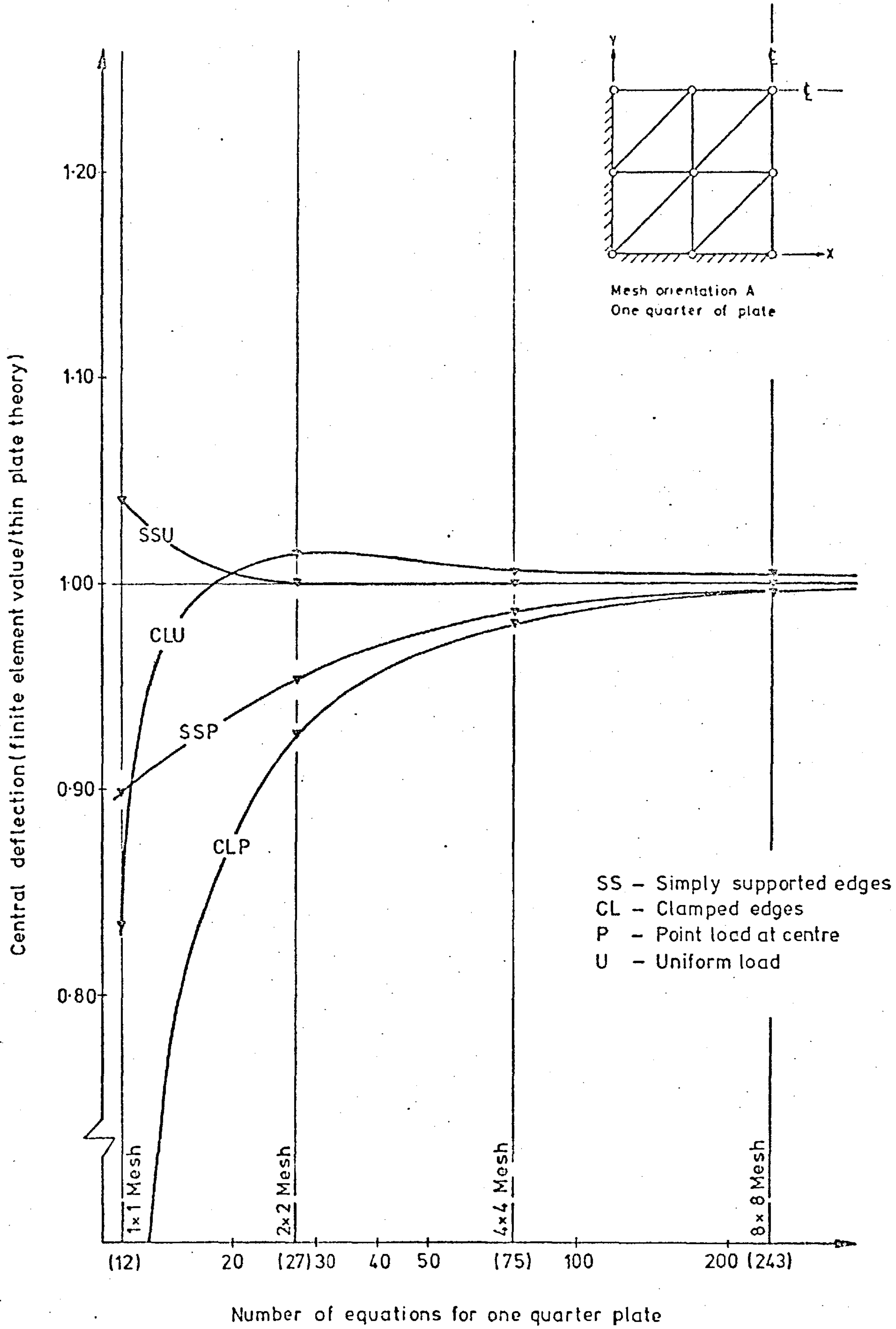

Fig 3·11 Convergence of deflections for a square plate. ISOFLEX 3. Mesh A.

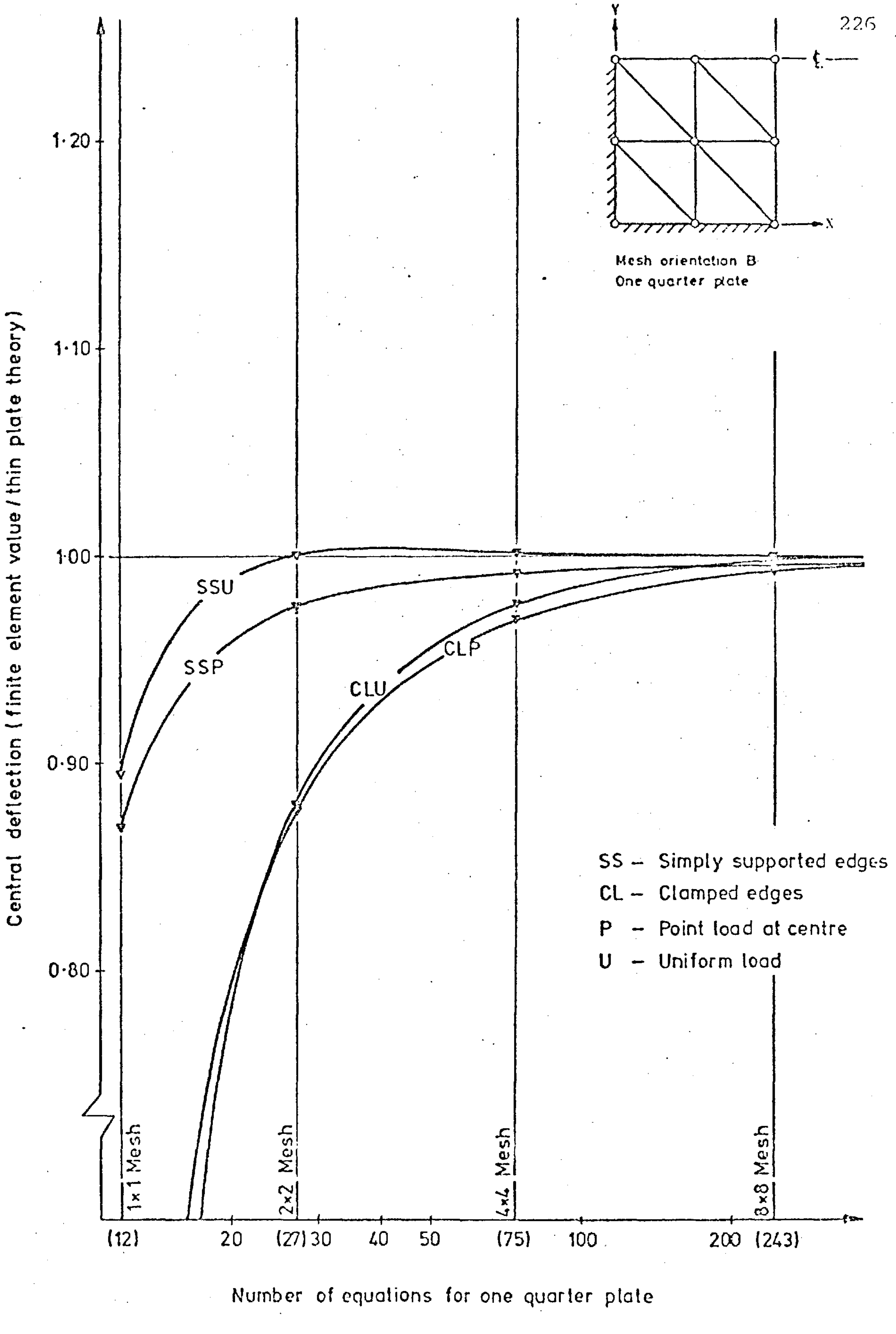

Fig 3·12 Convergence of deflections for a square plate. ISOFLEX 3. Mesh B

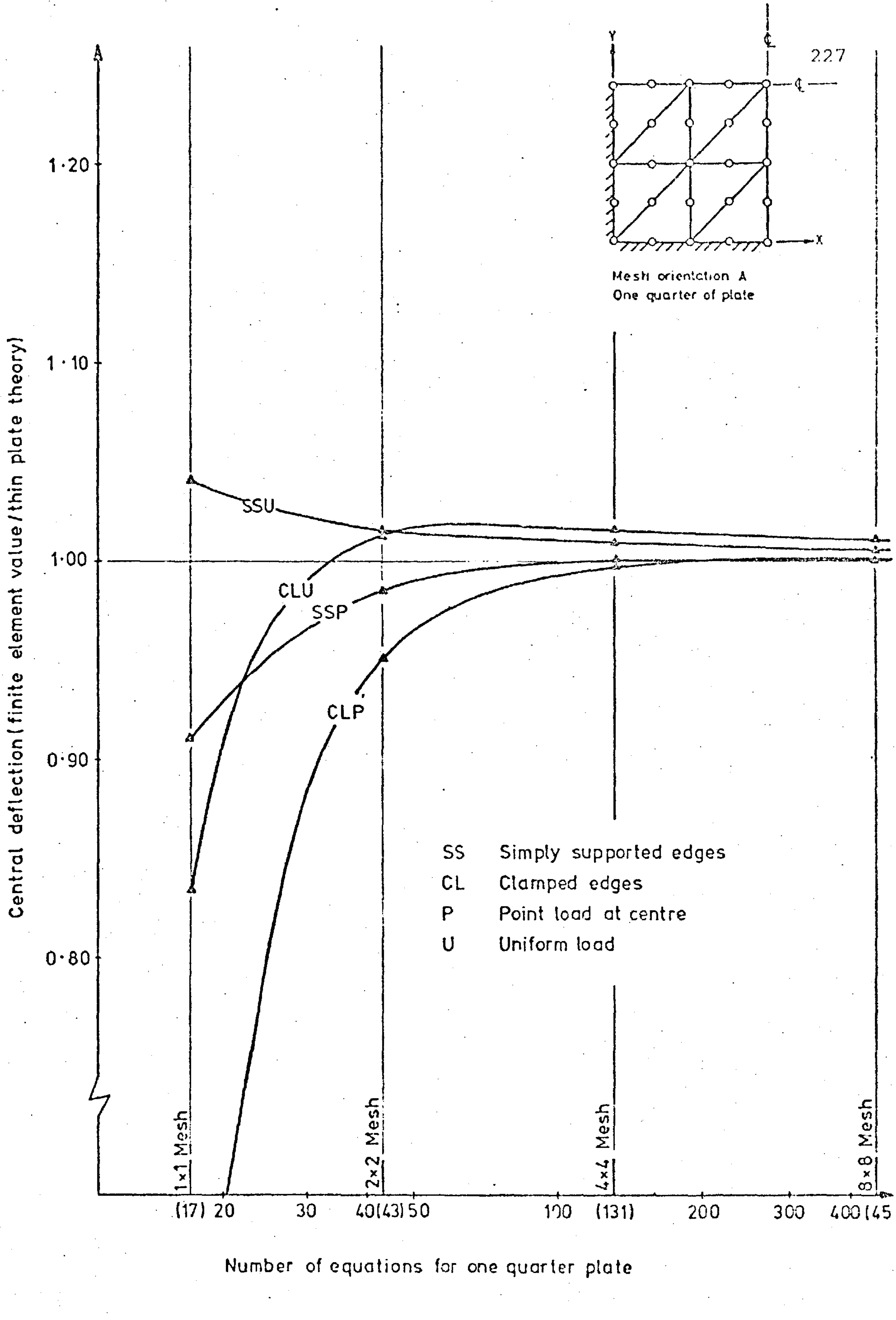

Fig 3·13 Convergence of deflections for a square plate. ISOFLEX 6. Mesh A.

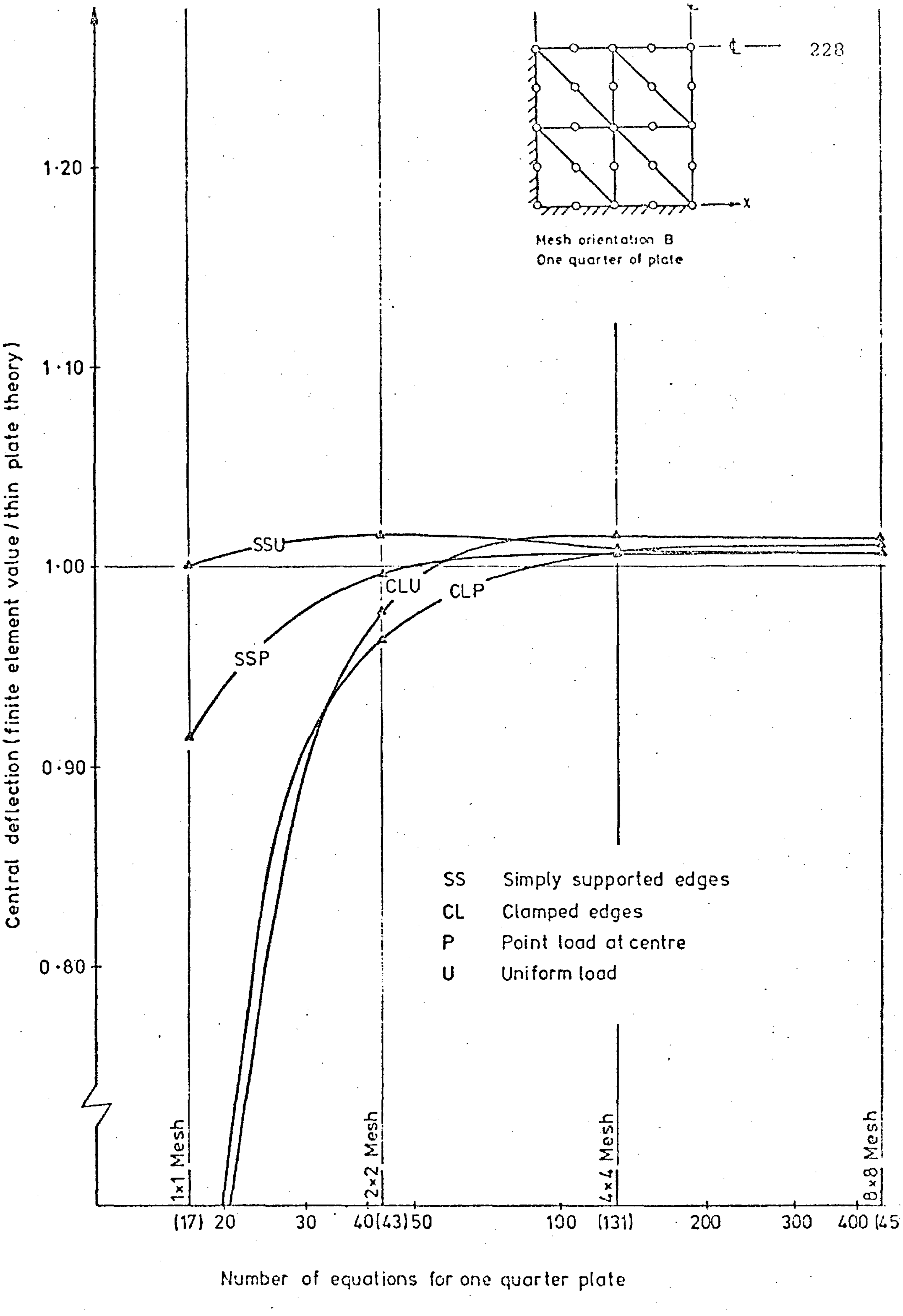

Fig 3·14 Convergence of deflections for a square plate. ISOFLEX 6. Mesh B.

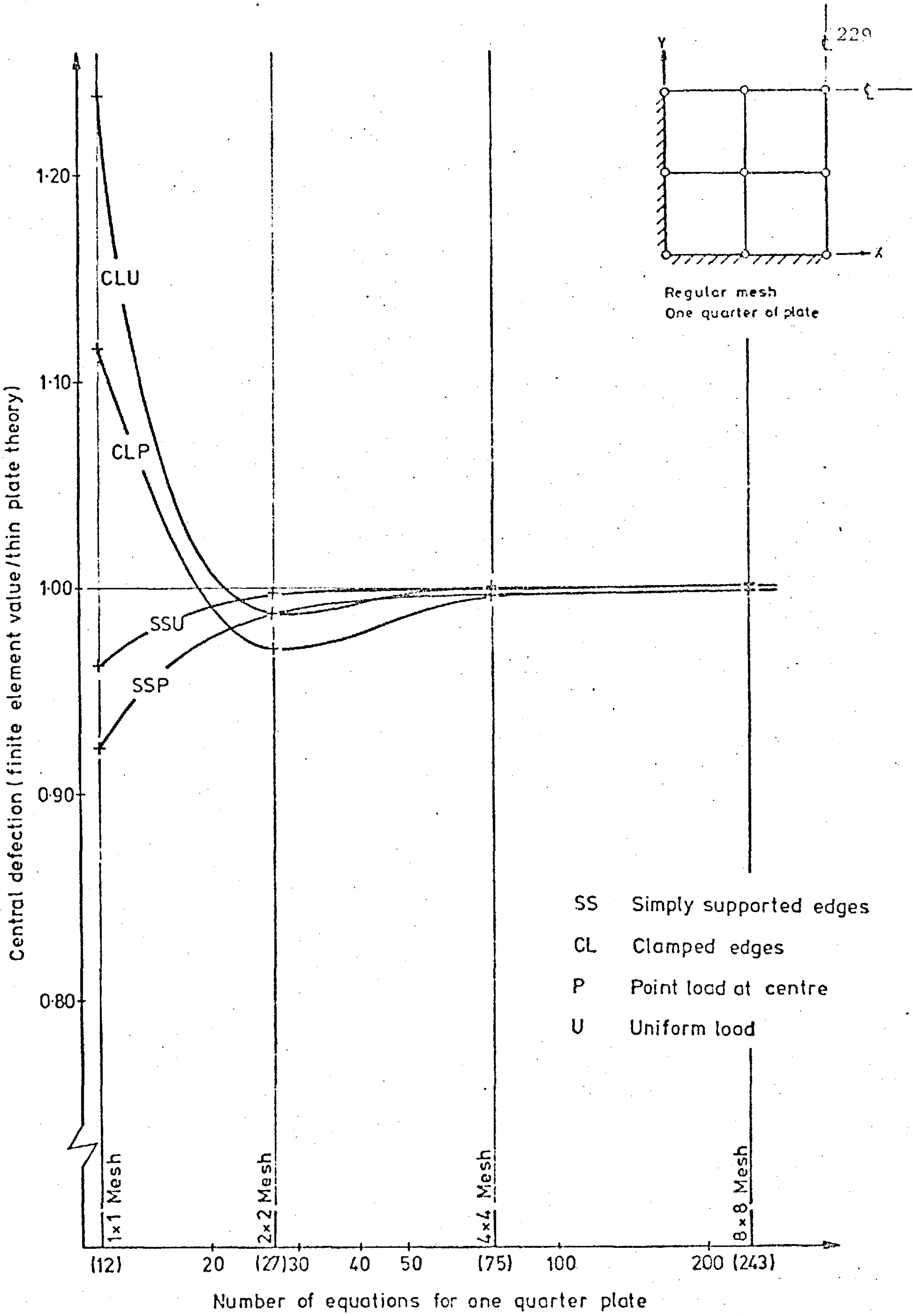

Fig 3·15 Convergence of deflections for a square plate. ISOFLEX 4.

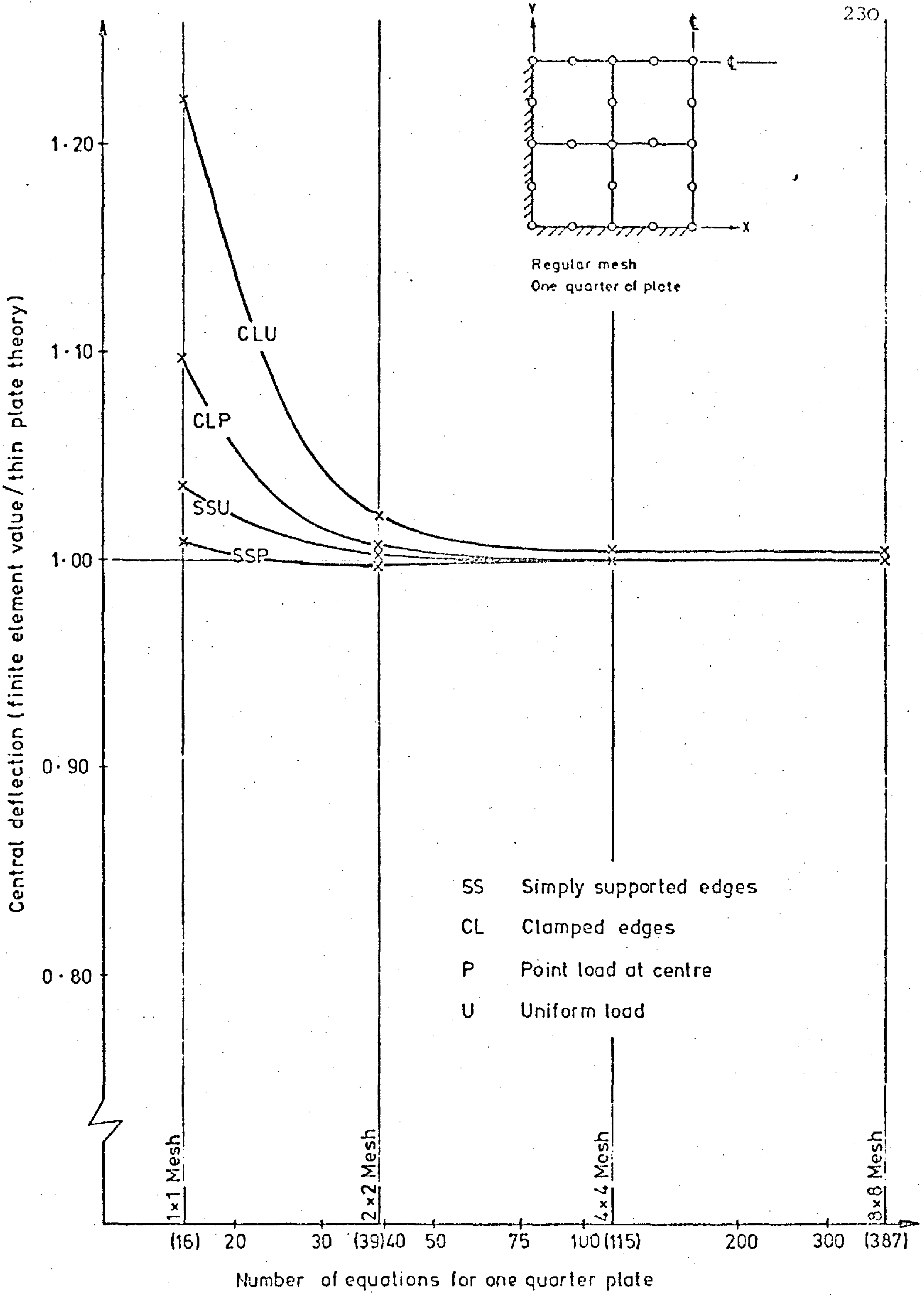

Fig 3·16 Convergence of deflections for a square plate. ISOFLEX 8, five point intergration.

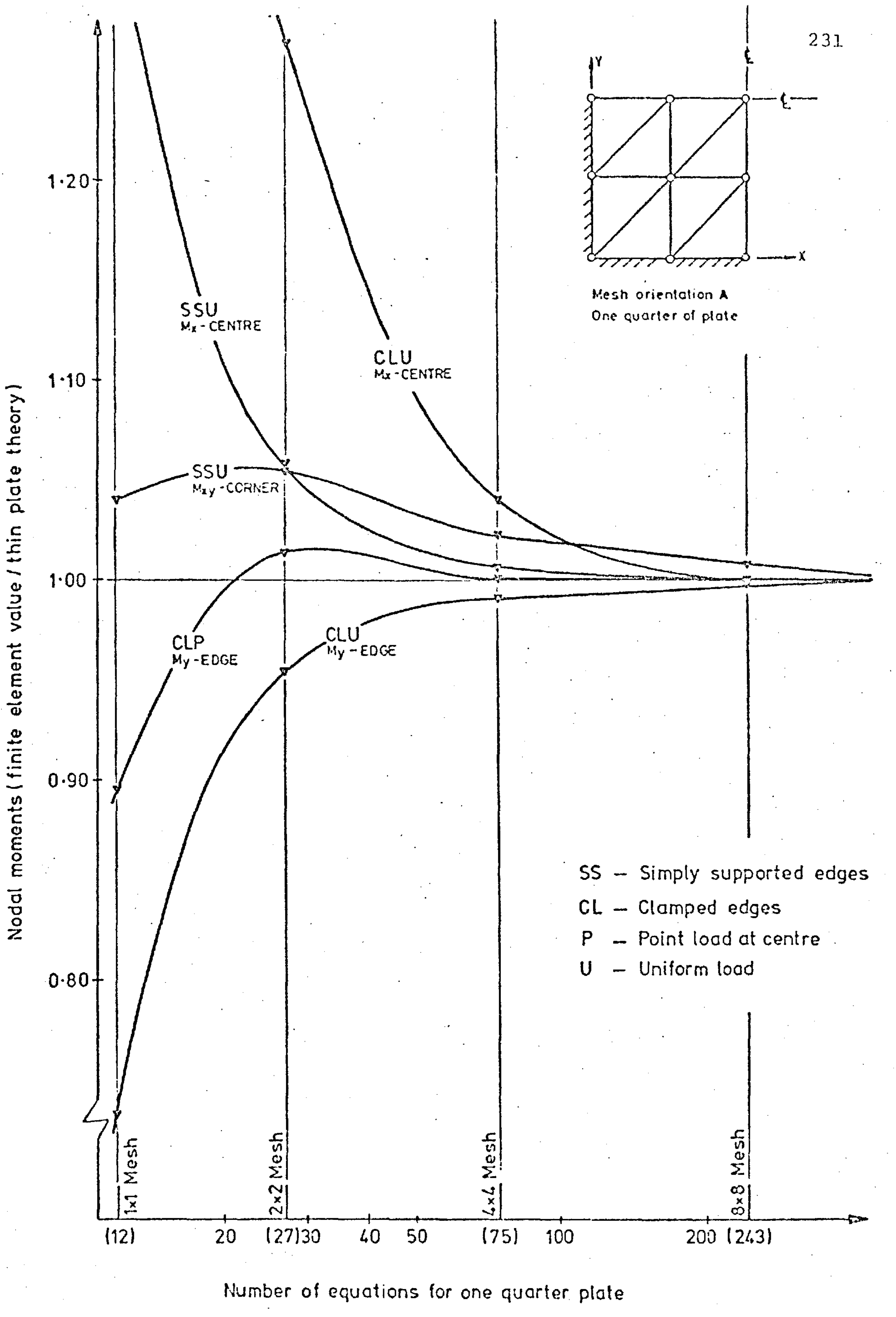

Fig. 3·17 Convergence of averaged nodal moment for a square plate. ISOFLEX 3. Mesh A

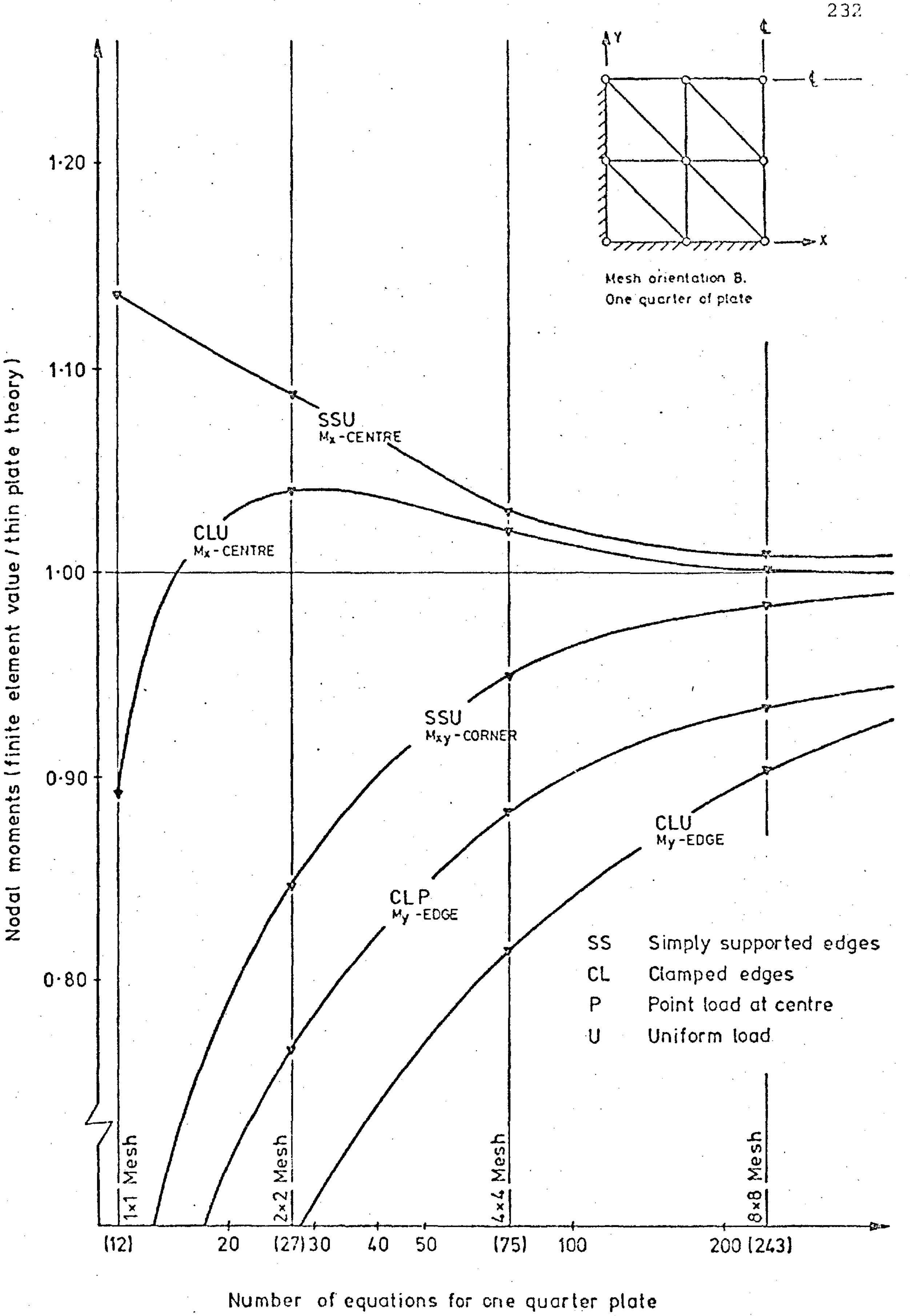

Fig 3·18 Convergence of averaged nodal moments for a square plate. ISOFLEX 3. Mesh B.

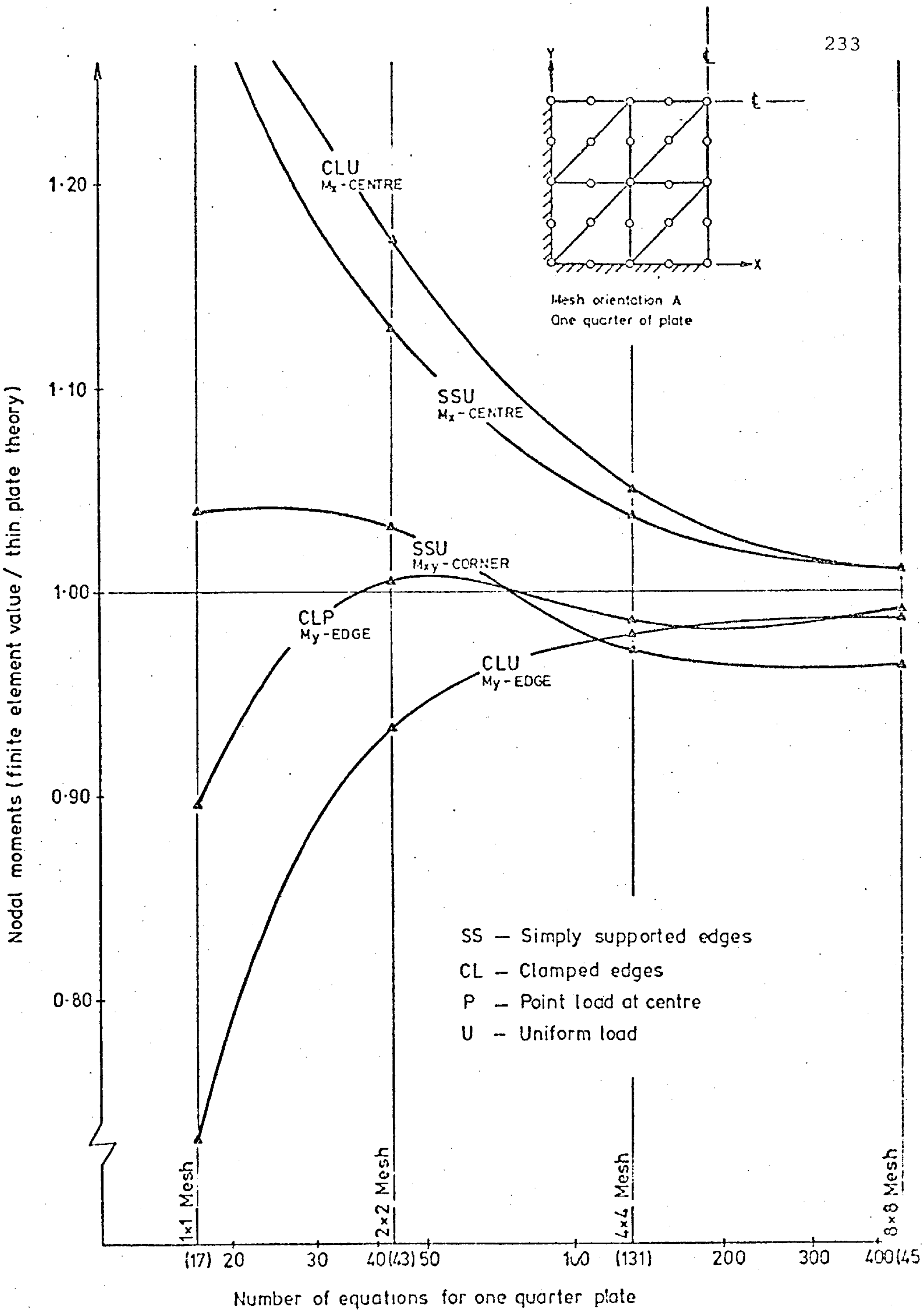

Fig 3·19 Convergence of averaged nodal moments for a square plate. ISOFLEX 6. Mesh A.

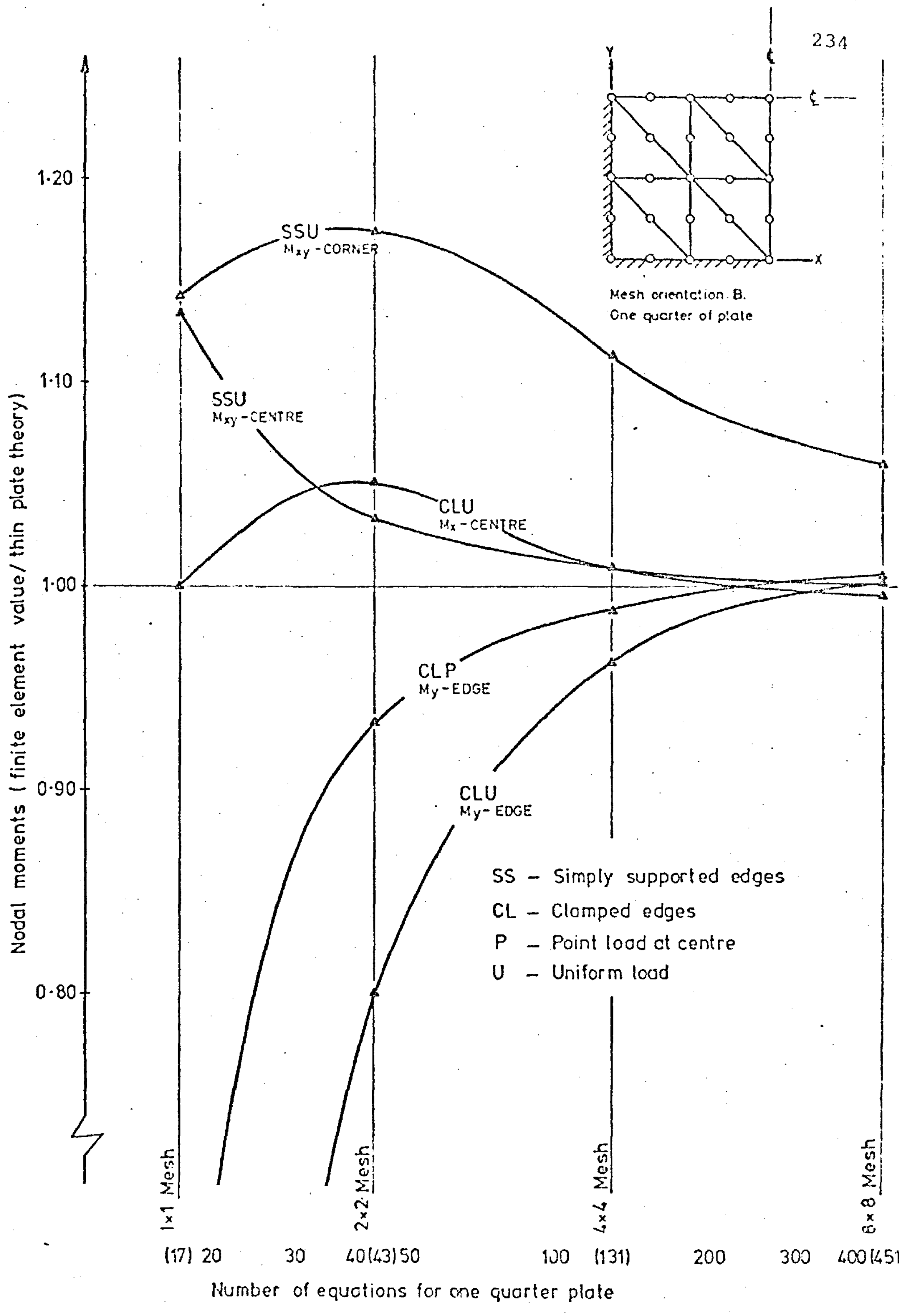

Fig 3·20 Convergence of averaged nodal moments for a square plate. ISOFLEX 6. Mesh B.

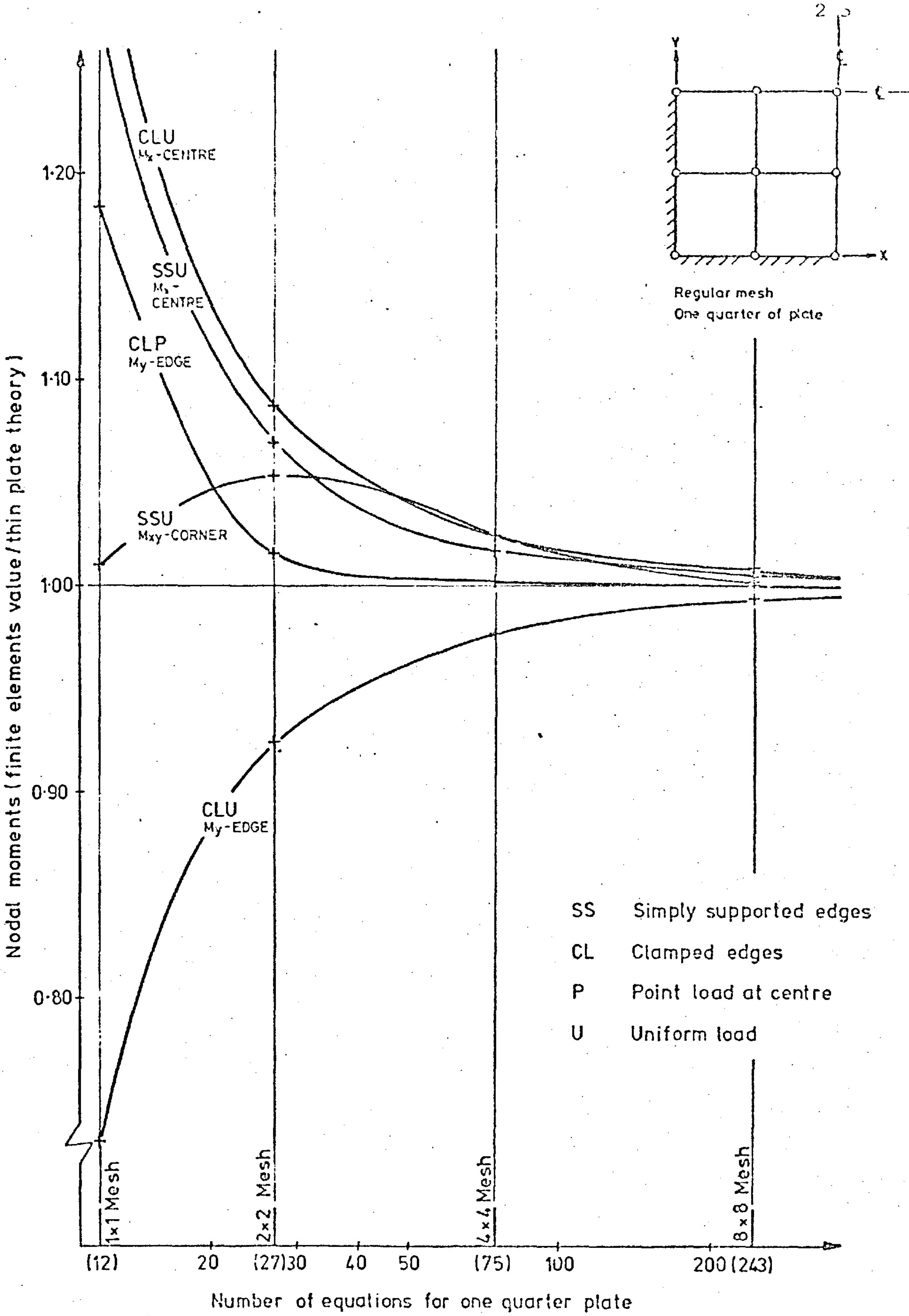

Fig 3·21 Convergence of averaged nodal moments for a square plate. ISOFLEX 4.

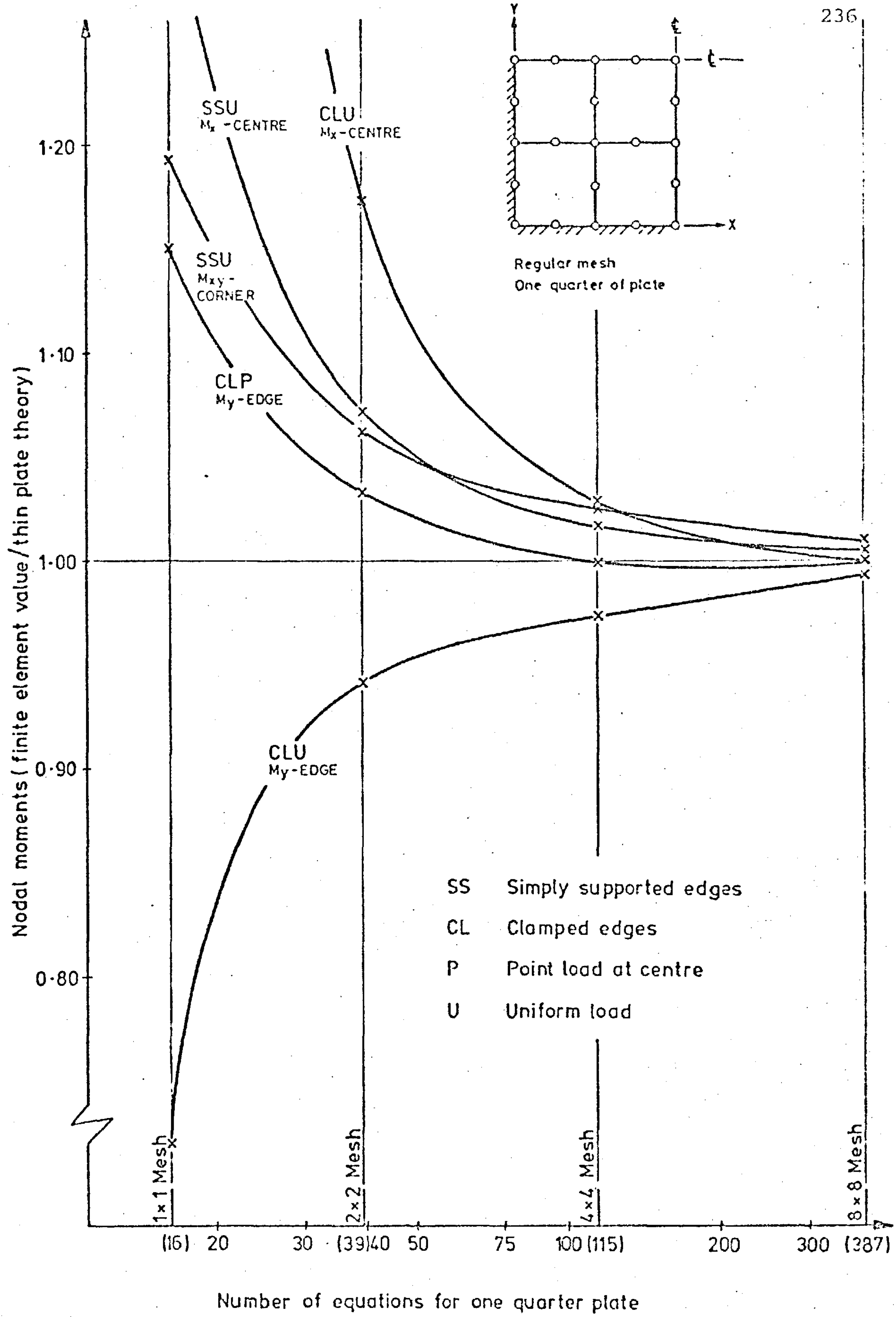

Fig 3·22 Convergence of averaged nodal moments for a square plate. ISOFLEX 8, five point integration

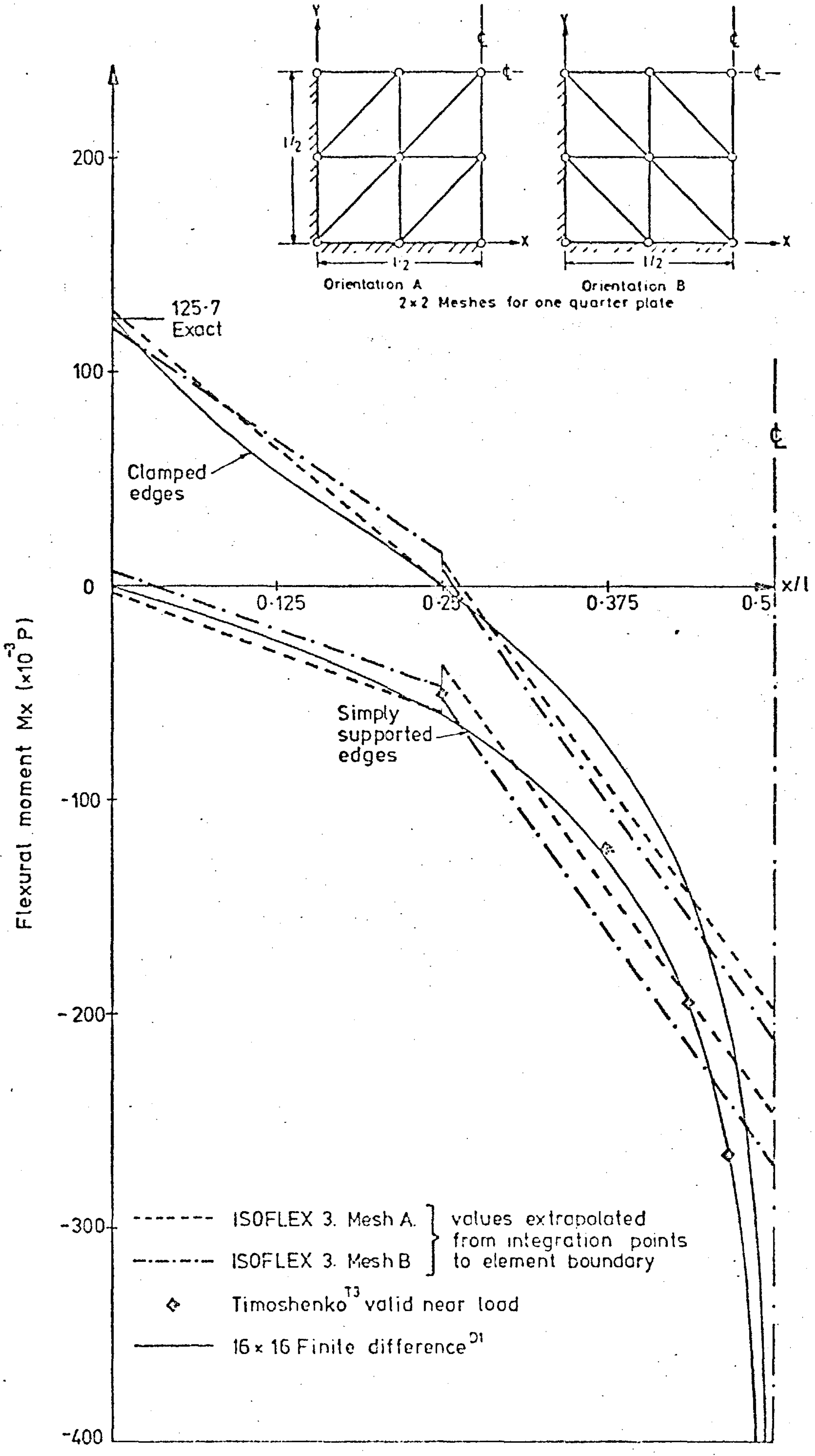

Fig 3·23
Distribution of Mx moments along centre line of square plates under central point load
2×2 Mesh ISOFLEX 3

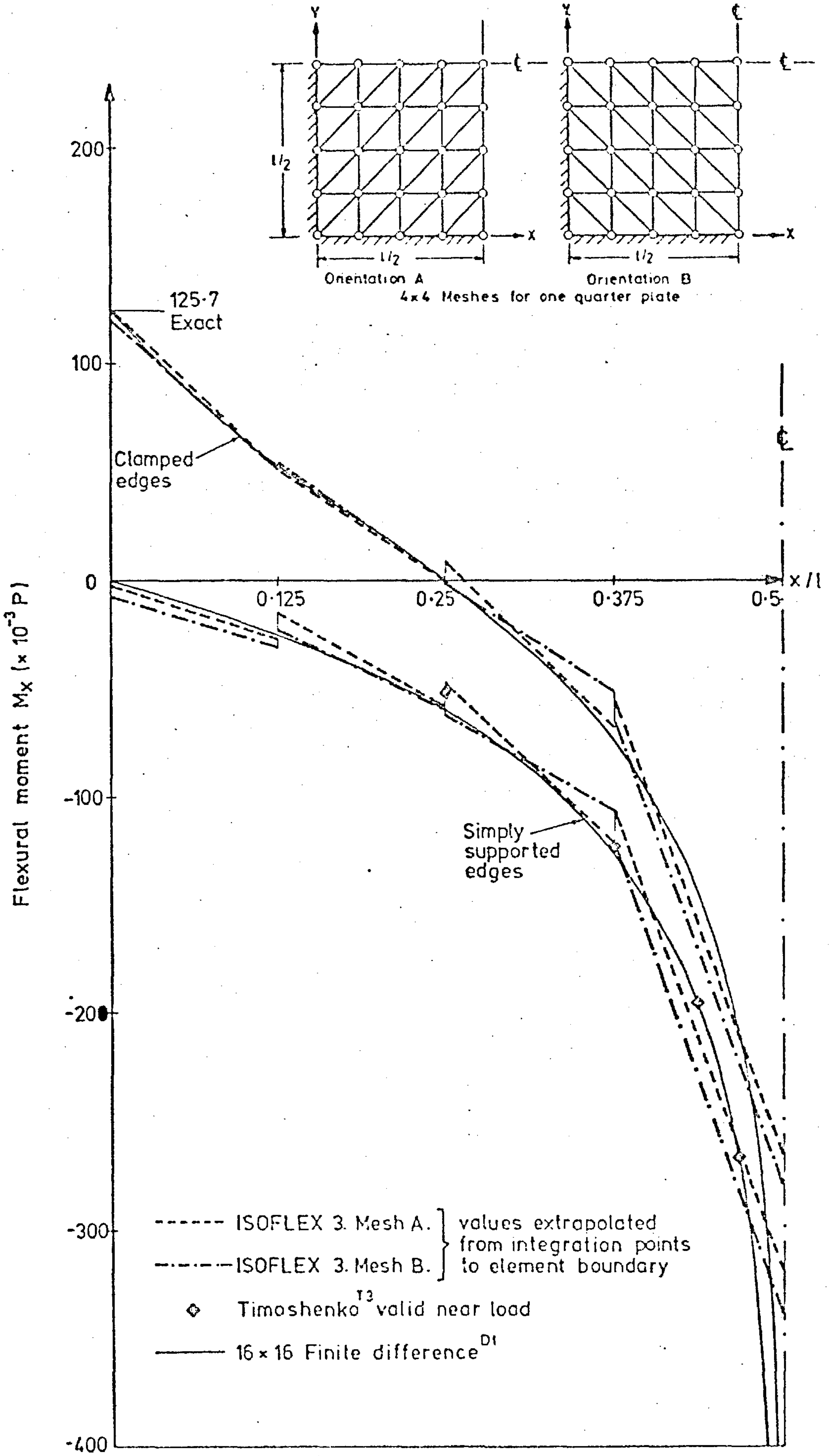

Fig 3·24
Distribution of Mx moments along centre line of square plates under central point load. 4x4 Mesh ISOFLEX 3.

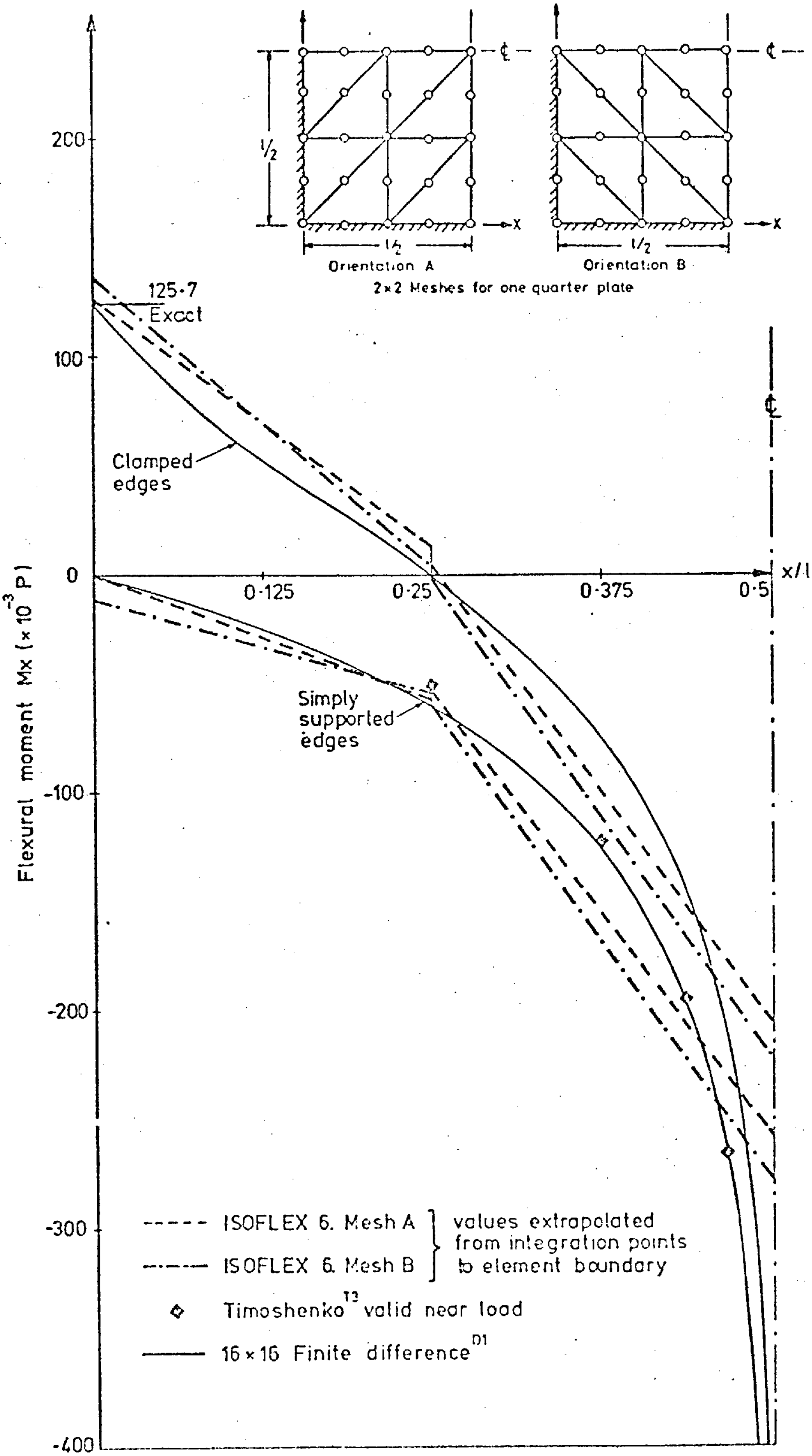

Fig 3·25
Distribution of Mx moments along centre line of square plates under central point load. 2×2 Mesh ISOFLEX 6.

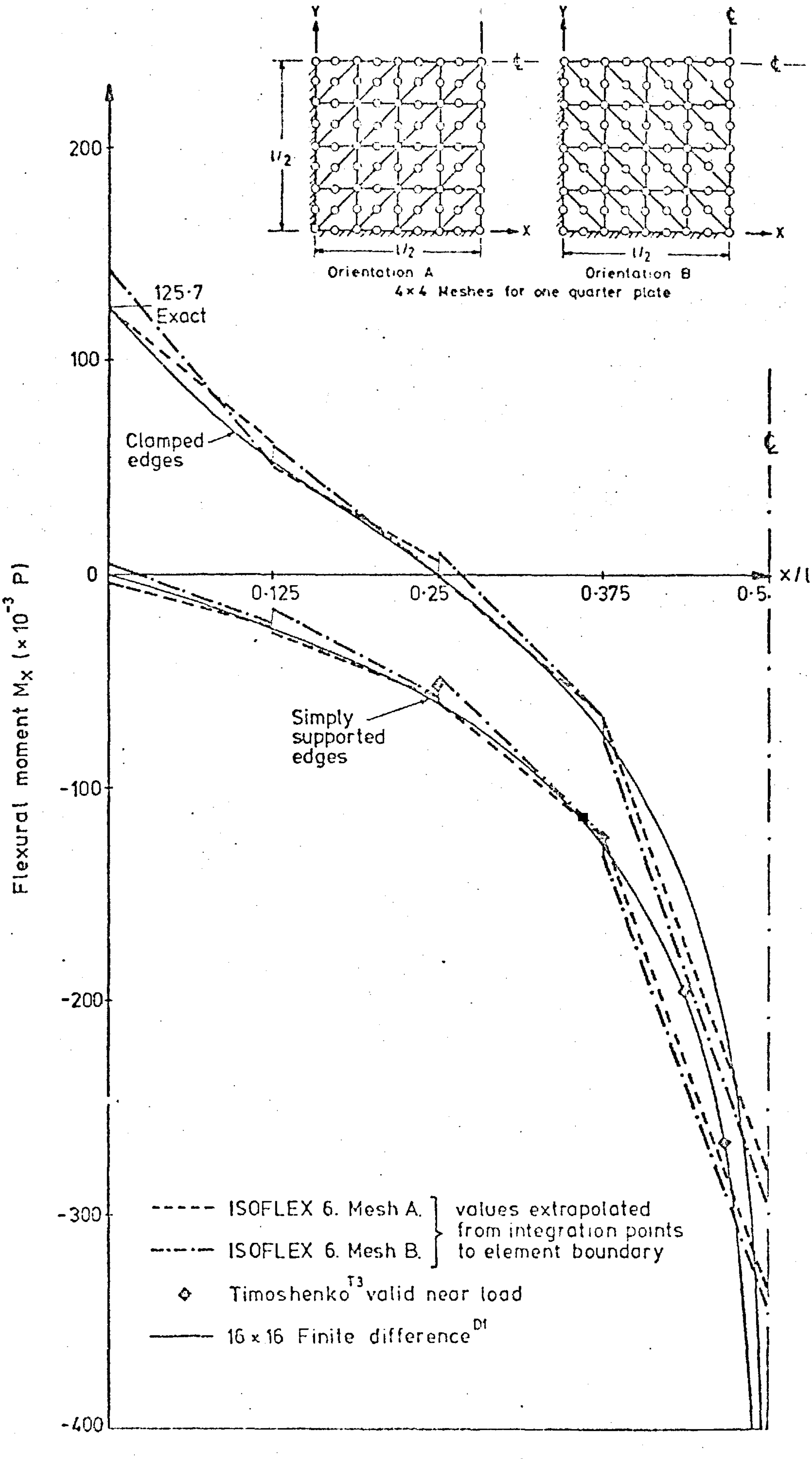

Fig 3·26

Distribution of Mx moments along centre line of square plates under central point load. 4×4 Mesh ISOFLEX 6.

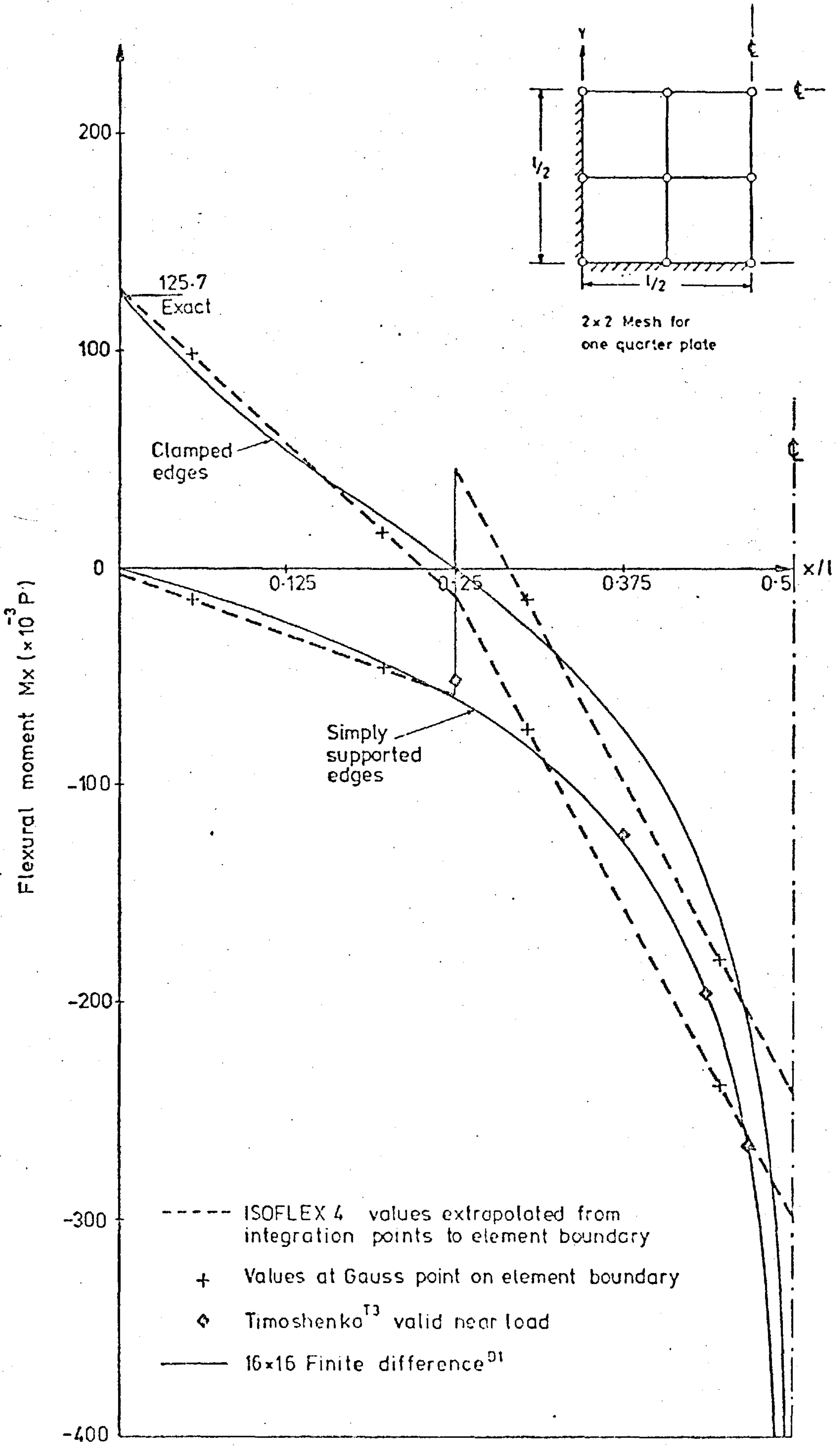

Fig 3·27
Distribution of Mx moments along centre line of square plates under central point load.
2×2 Mesh ISOFLEX 4

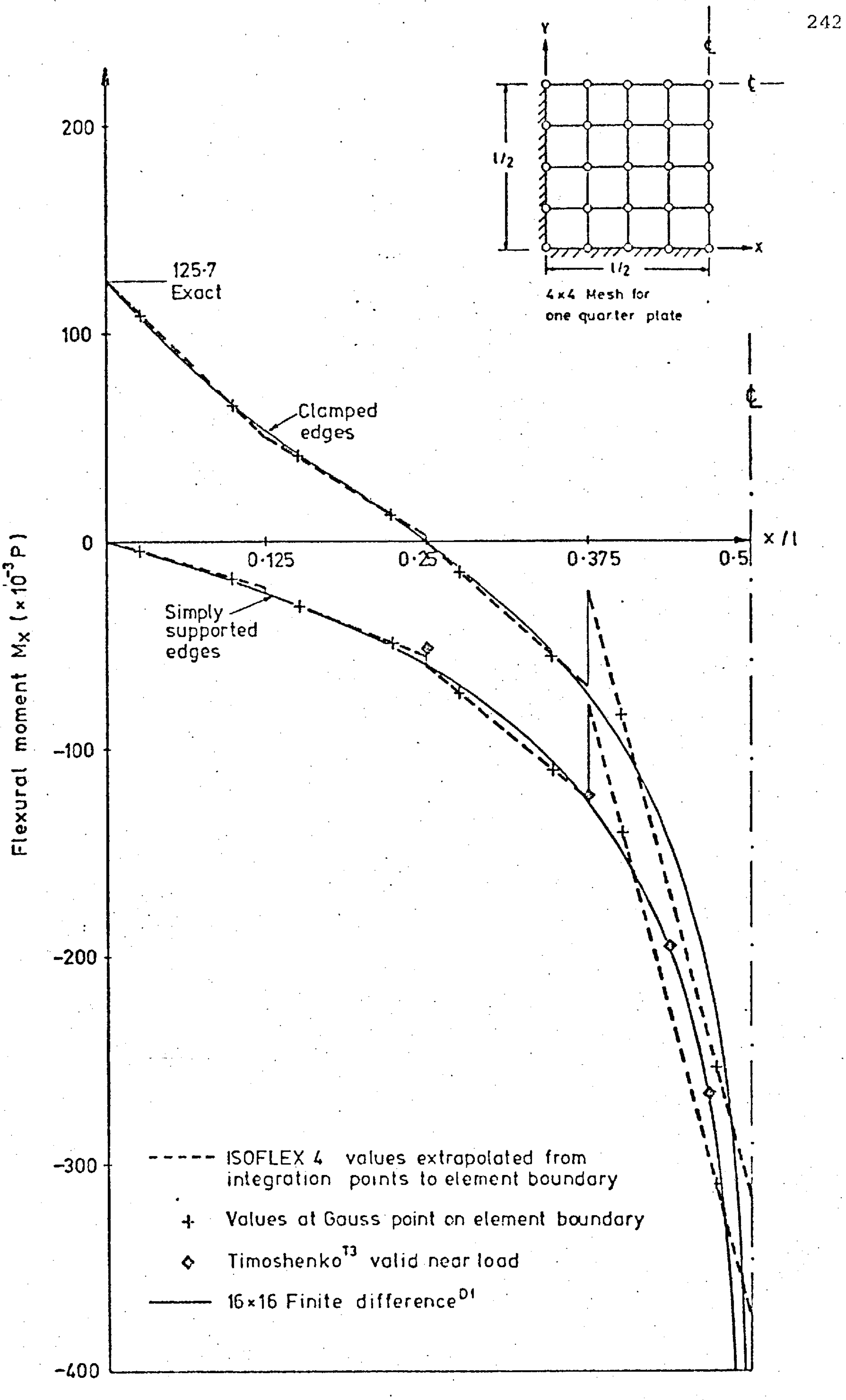

Fig 3·28
Distribution of Mx moments along centre line of square plates under central point load. 4×4 Mesh ISOFLEX 4.

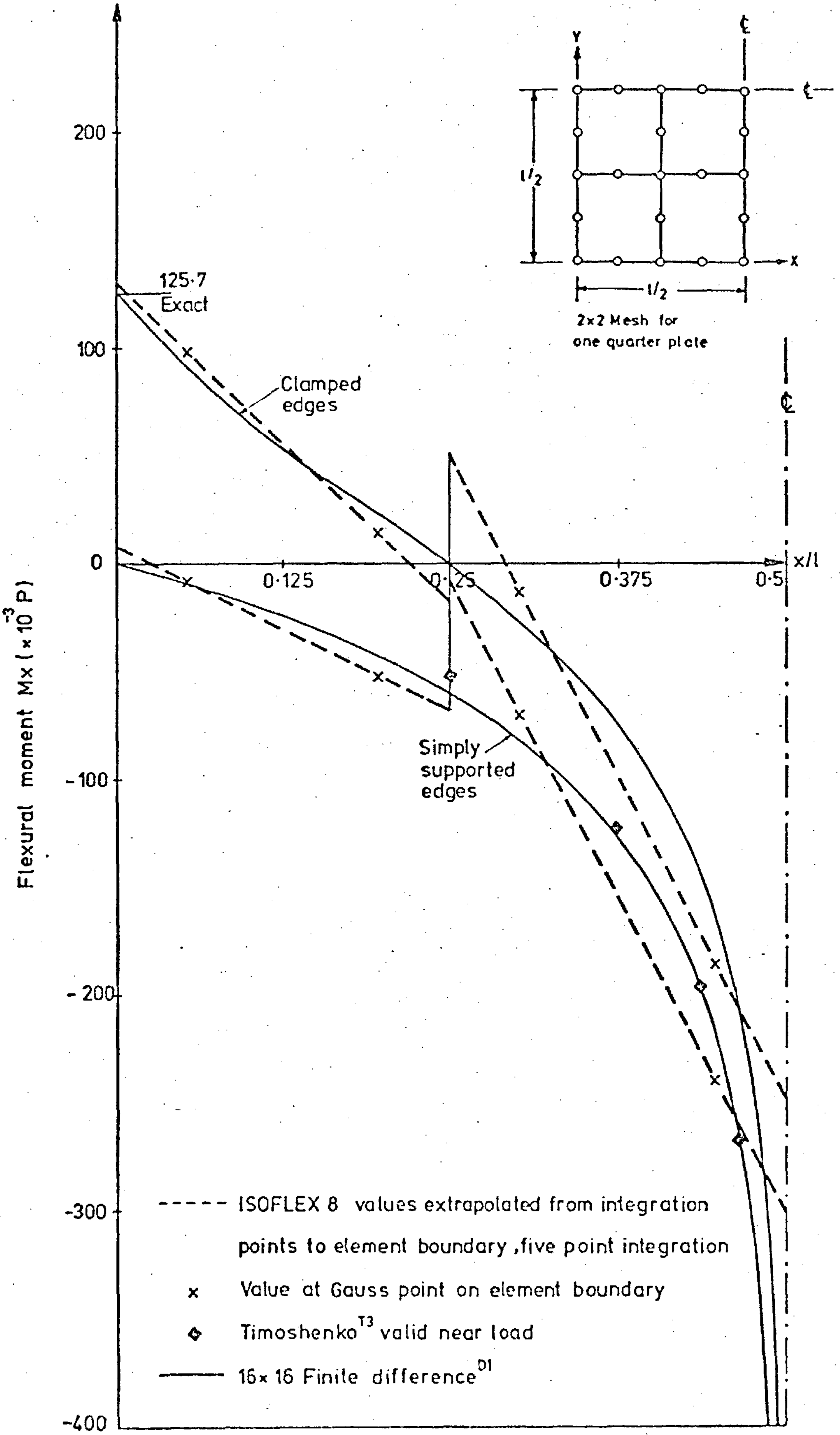

Fig 3·29
Distribution of Mx moments along centre line of square plates under central point load 2x2 Mesh ISOFLEX 8

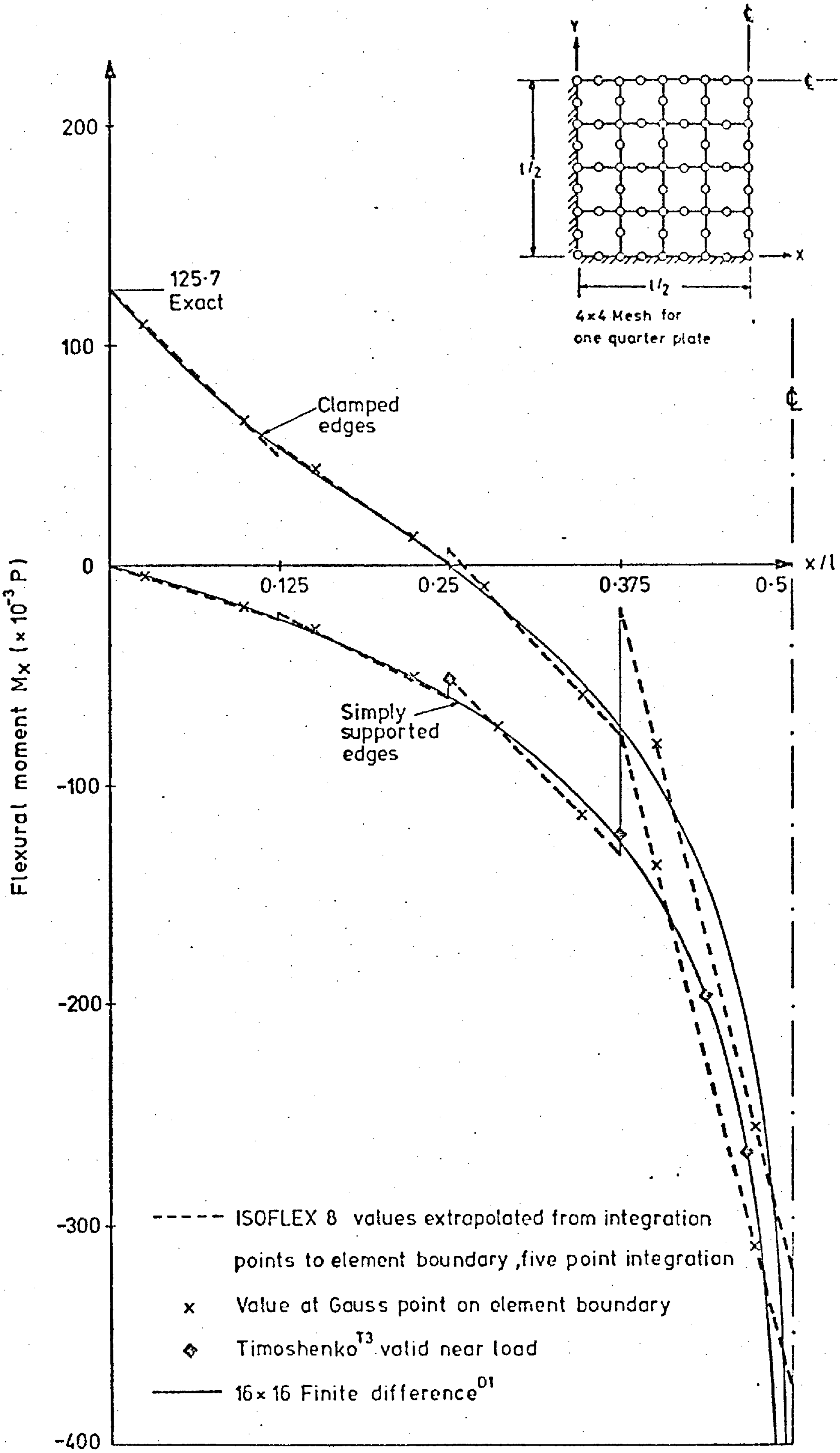

Fig 3·30
Distribution of Mx moments along centre line of square plates under central point load. 4x4 Mesh ISOFLEX 8.

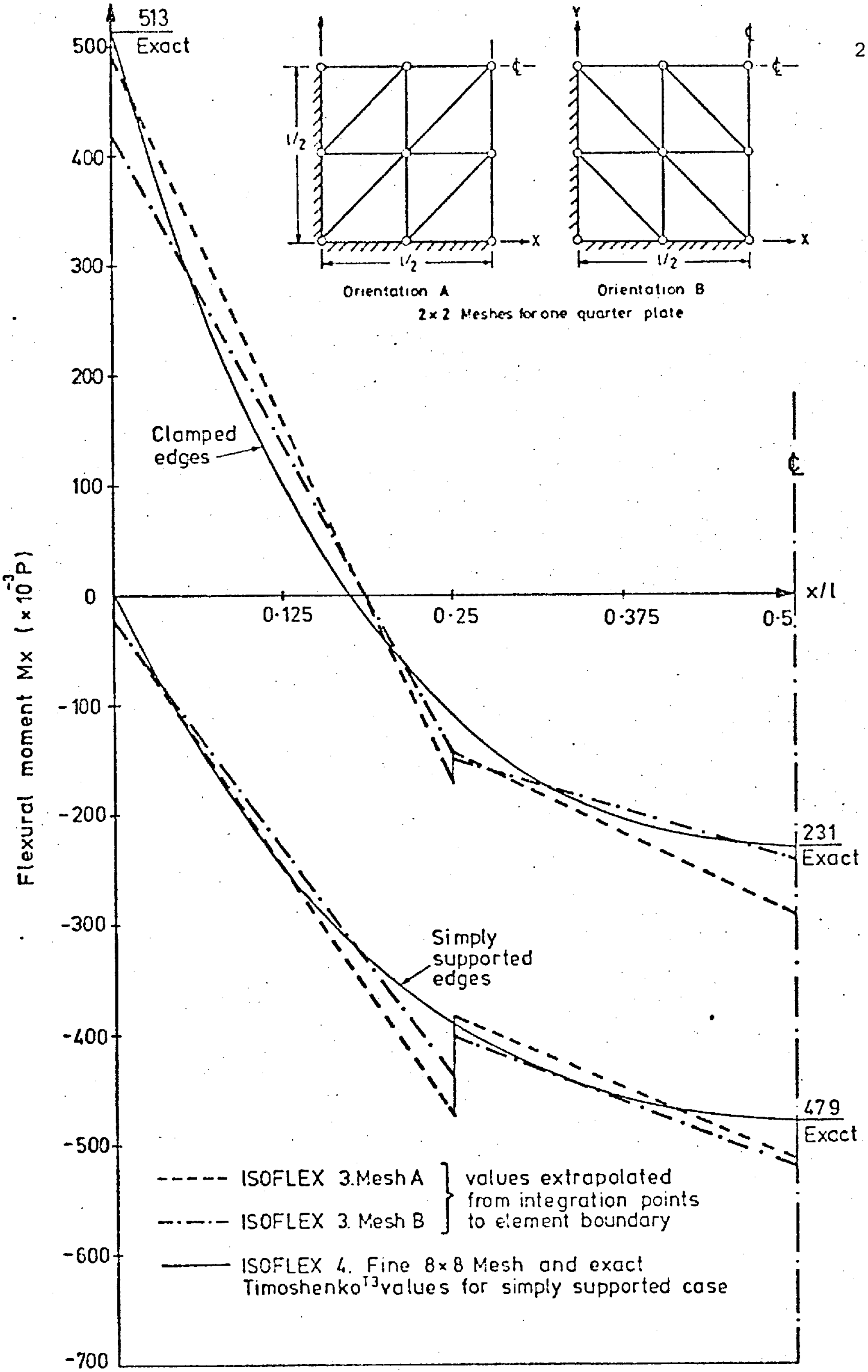

Fig 3·31
Distribution of Mx moments along centre line of square plates under uniform load 2×2 Mesh ISOFLEX 3.

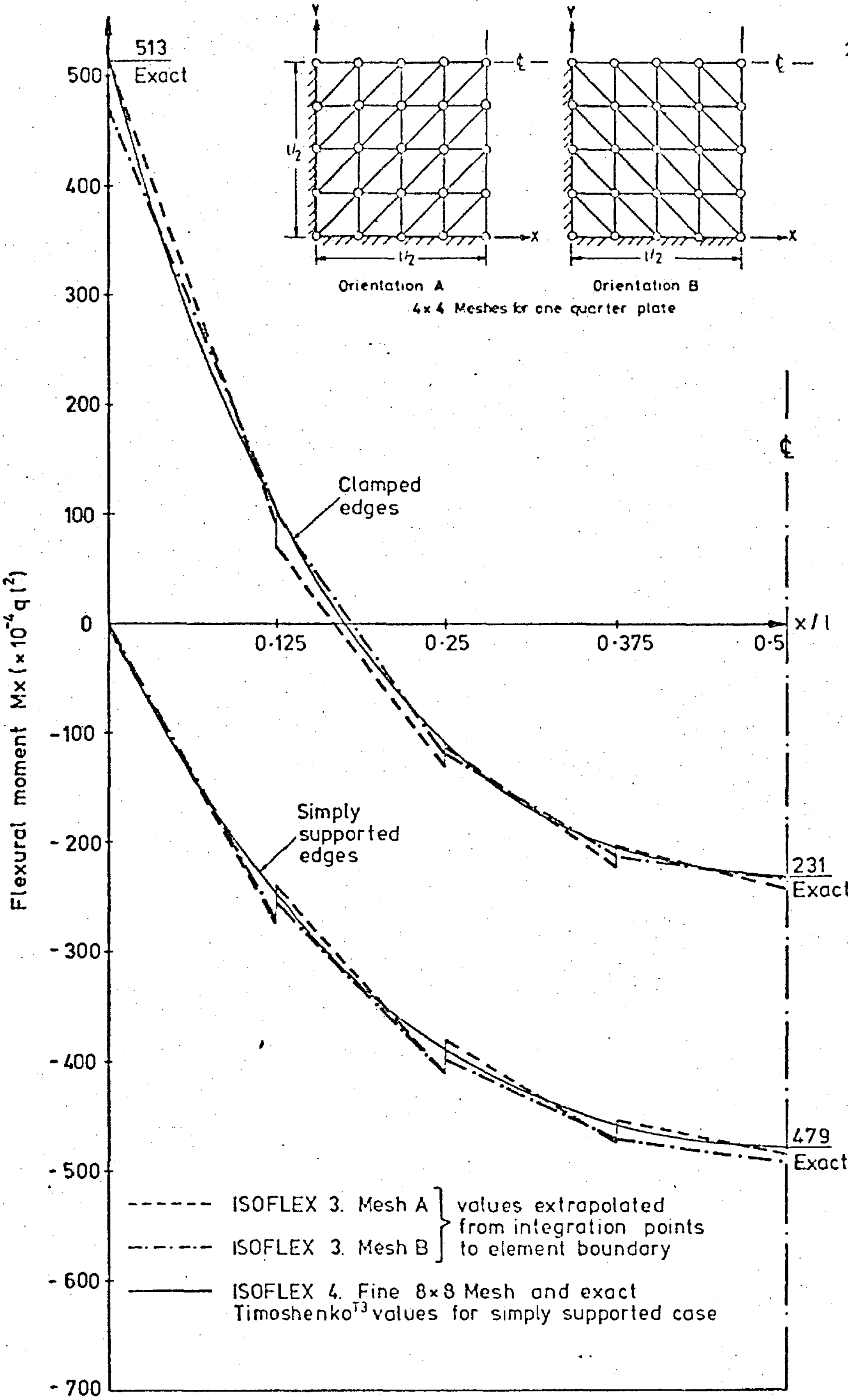

Fig 3·32
Distribution of Mx moments along centre line of square plates under uniform load 4x4 Mesh ISOFLEX 3.

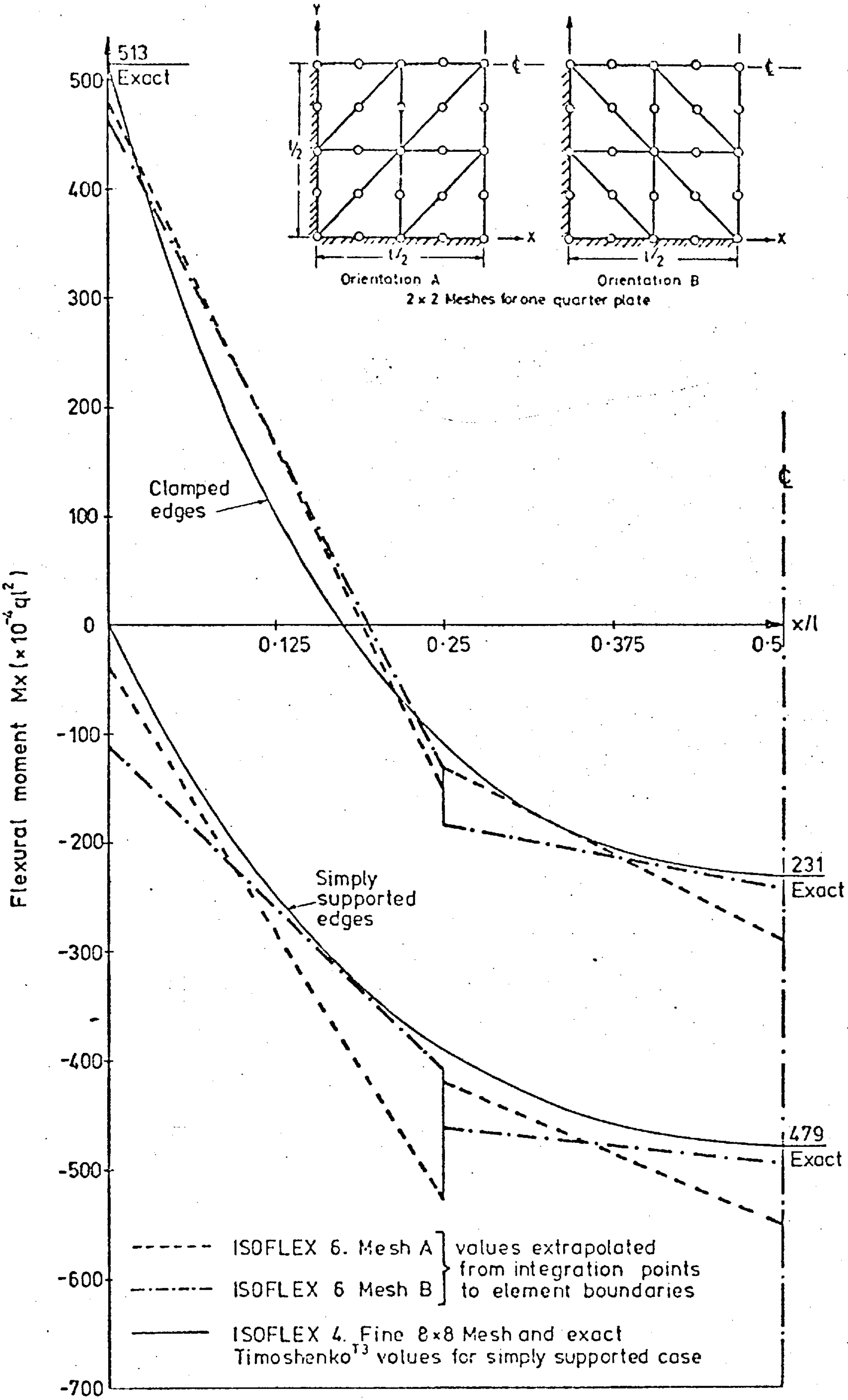

Fig 3·33
Distribution of Mx moments along centre line of square plates under uniform load 2×2 Mesh ISOFLEX 6.

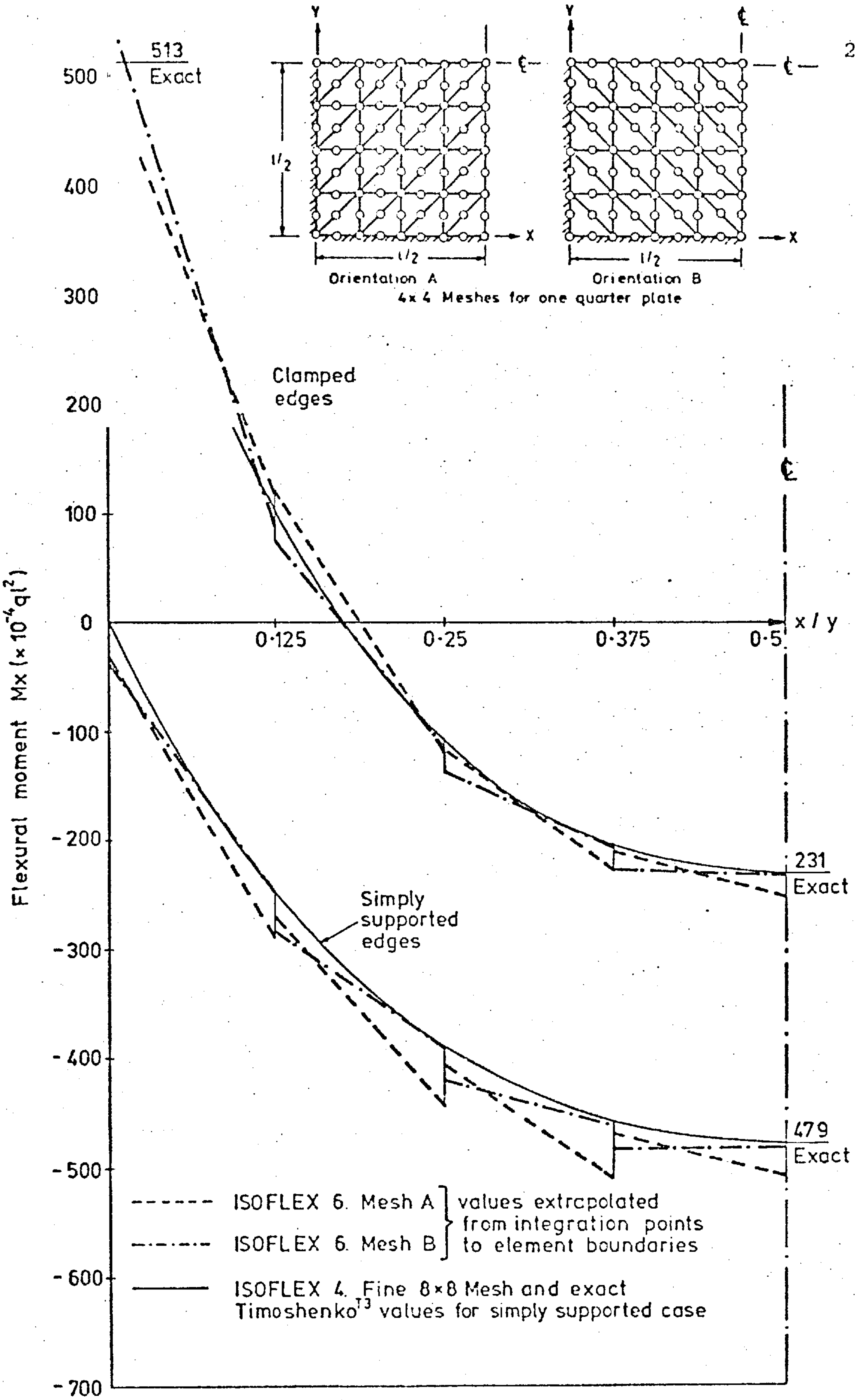

Fig 3·34
Distribution of Mx moments along centre line of square plates under uniform load
4 x 4 Mesh ISOFLEX 6.

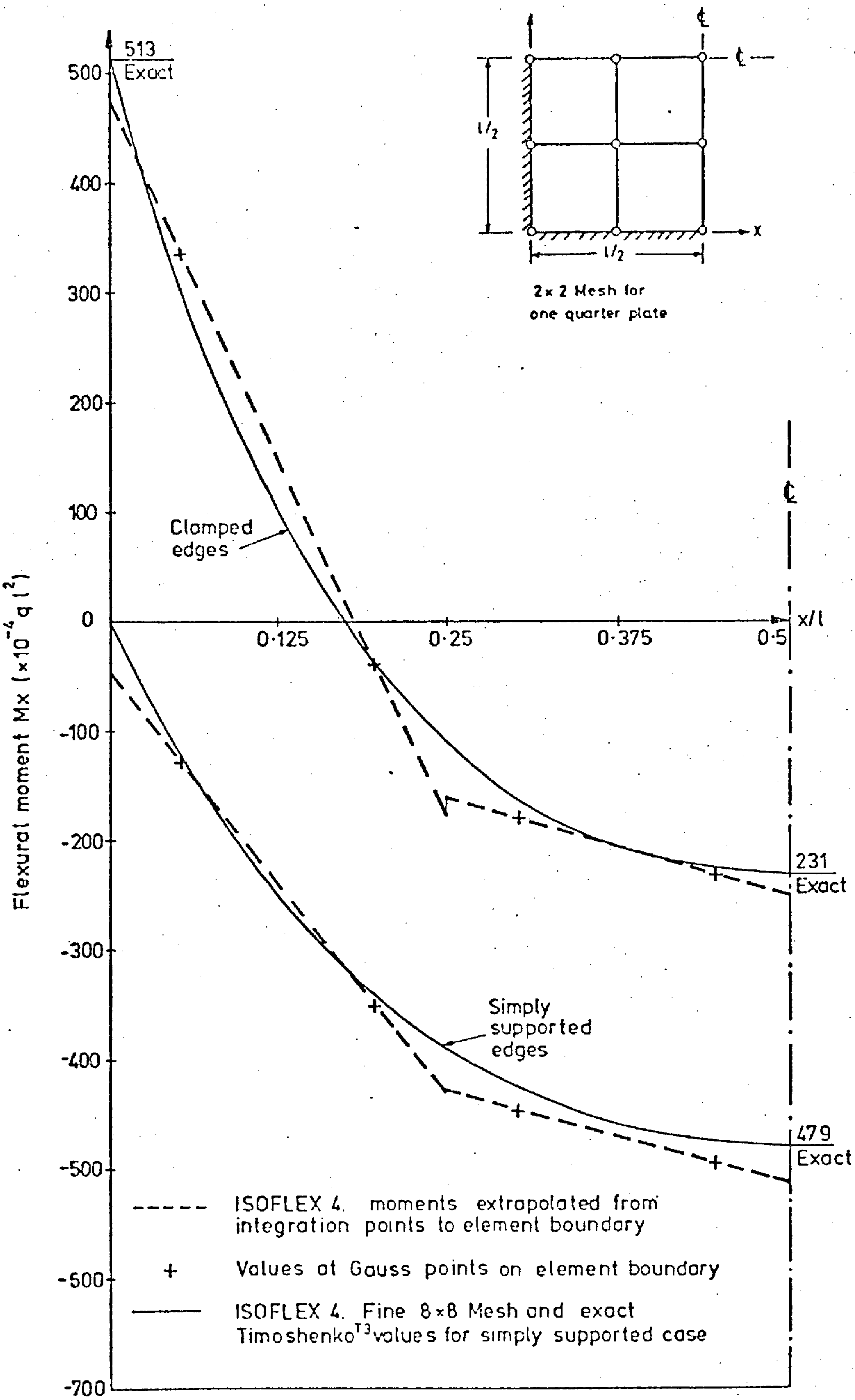

Fig 3·35
Distribution of Mx moments along centre line of square plates under uniform load 2× 2 Mesh ISOFLEX 4.

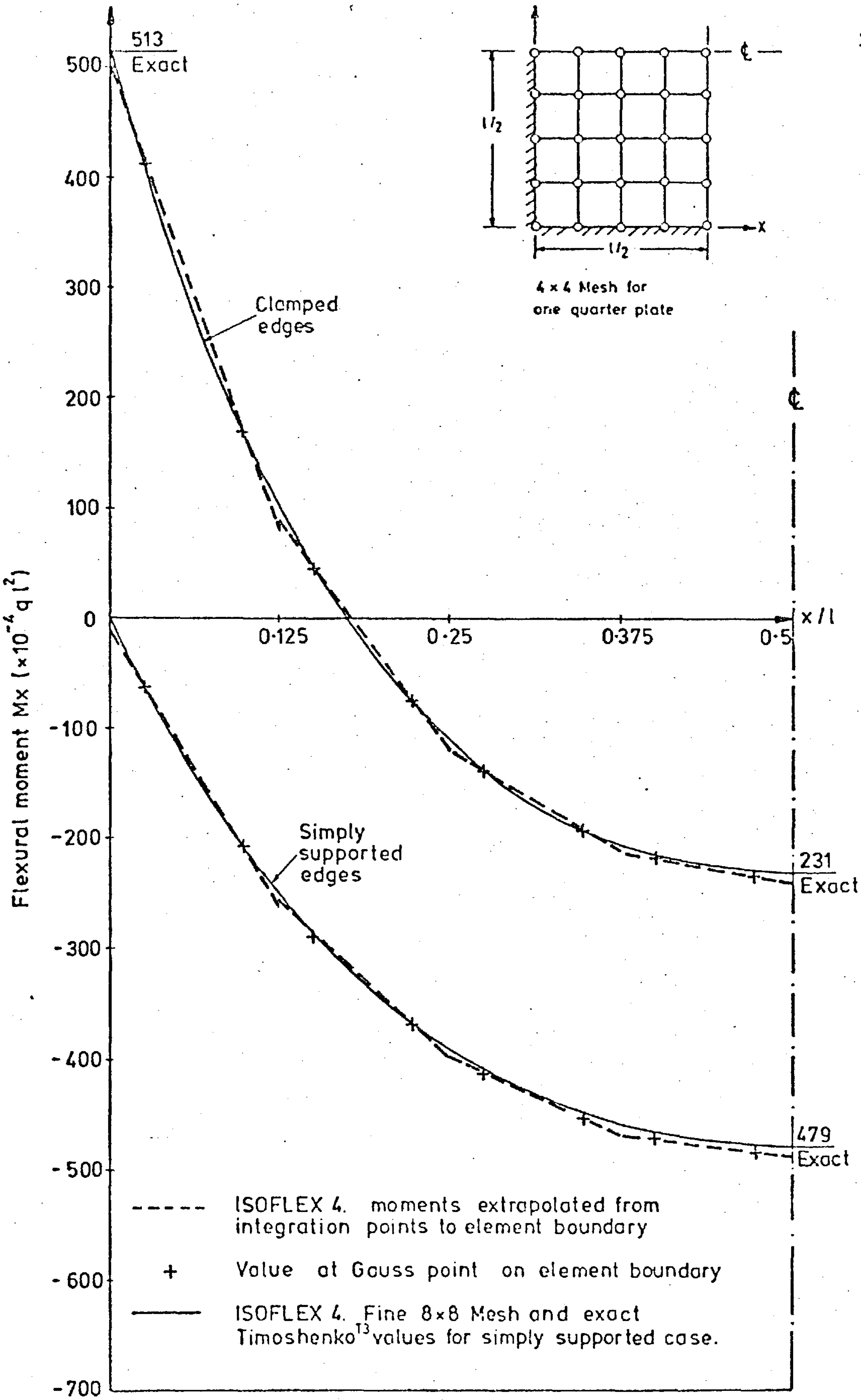

Fig 3·36
Distribution of Mx moments along centre line of square plates under uniform load 4 x 4 Mesh ISOFLEX 4.

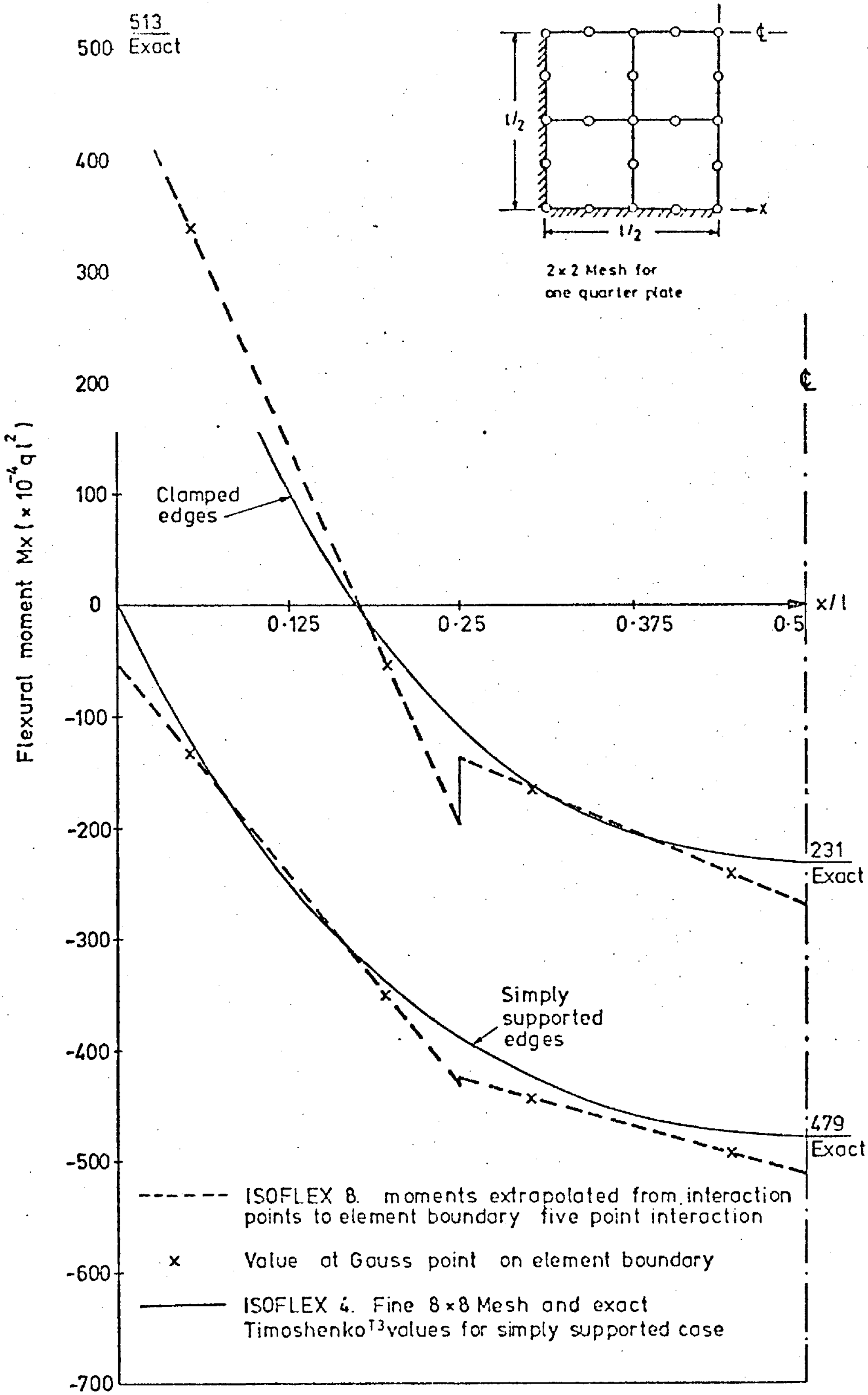

Fig 3·37
Distribution of Mx moments along centre line of square plates under uniform load 2 x 2 Mesh ISOFLEX 8.

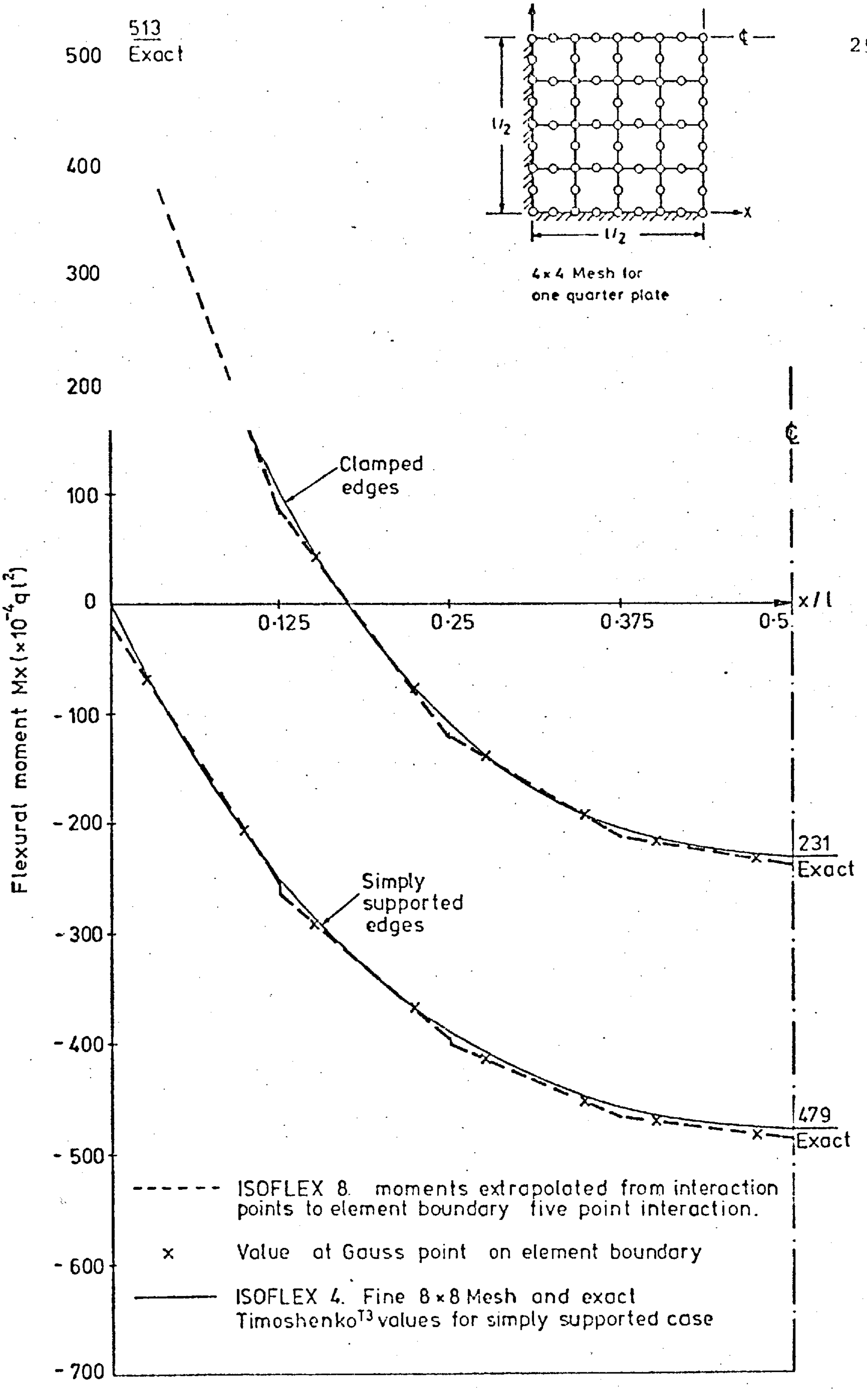

Fig 3·38
Distribution of Mx moments along centre line of square plates under uniform load 4 x 4 Mesh ISOFLEX 8.

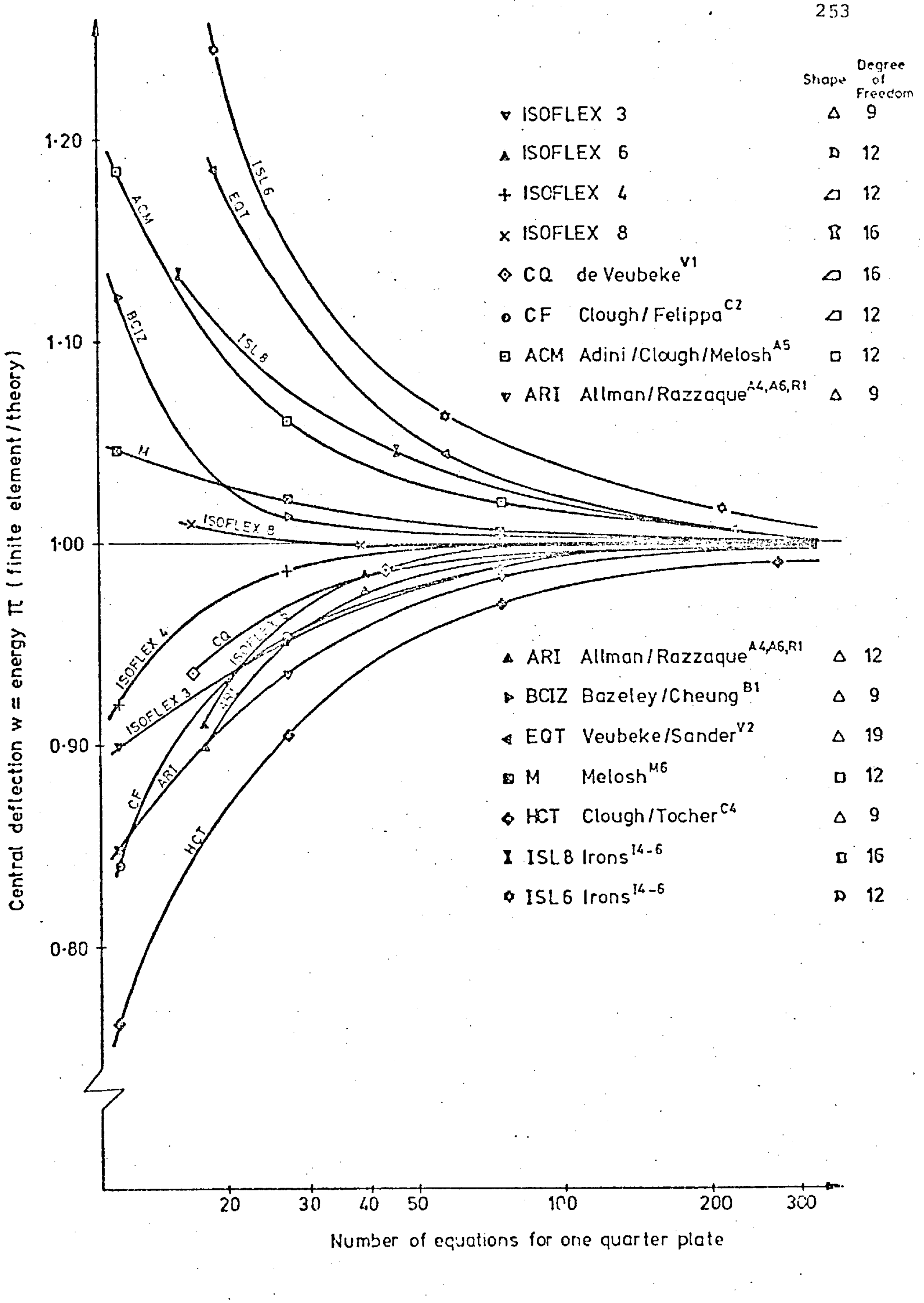

Fig 3·39
Convergence of various elements for a simply supported square plate under a concentrated central load

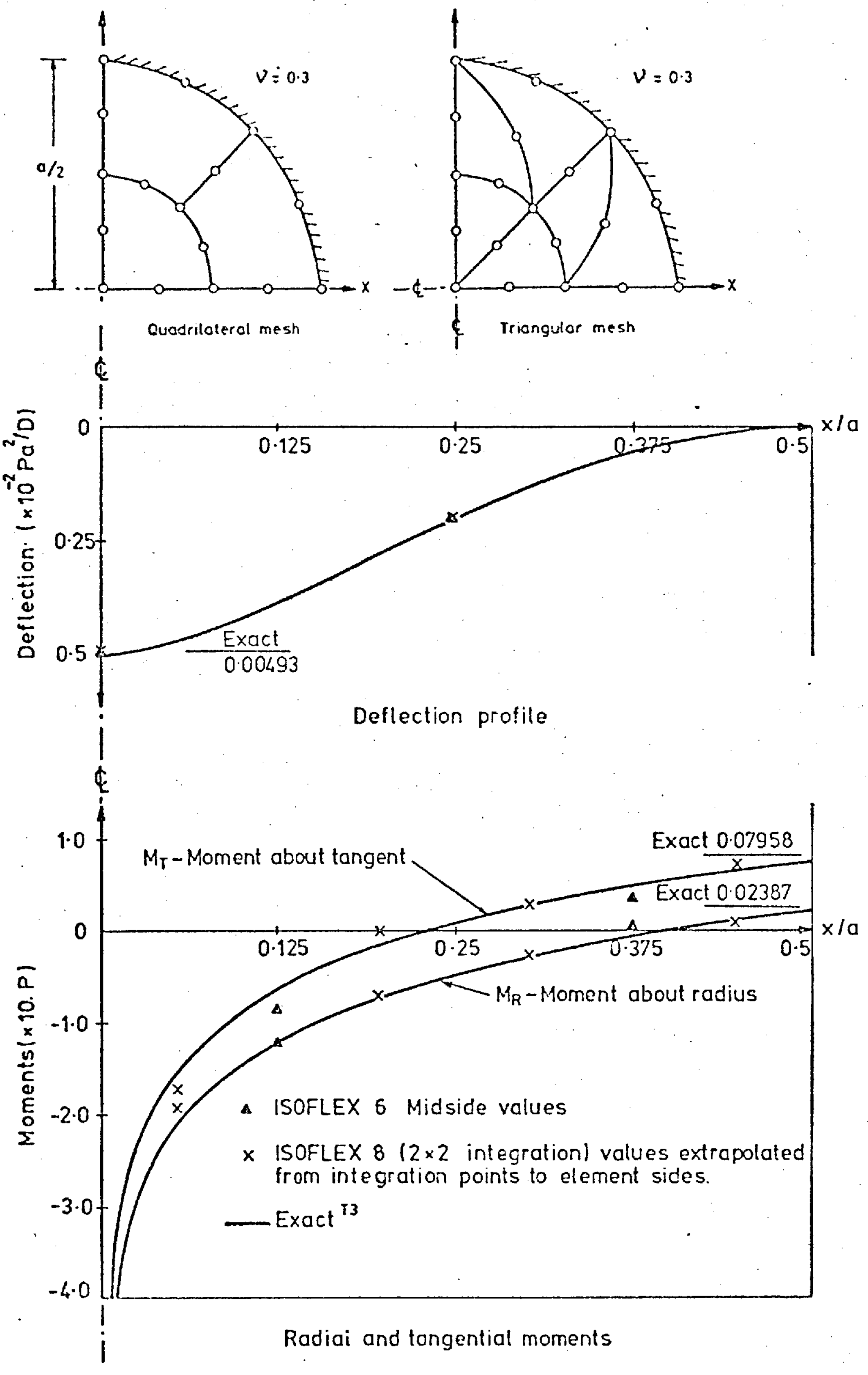

Fig 3·40 Clamped disc under concentrated central load

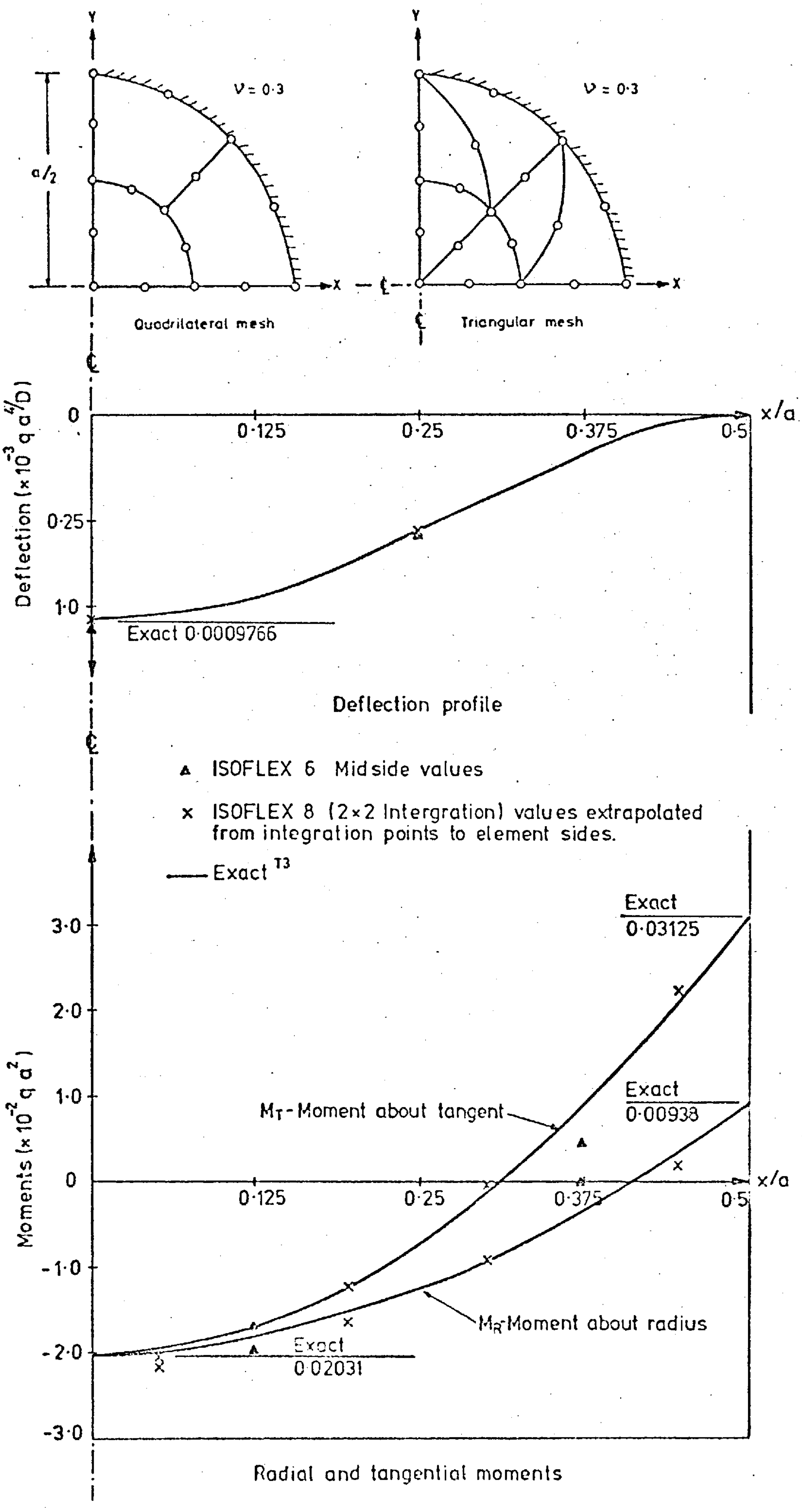

Fig 3·41 Clamped disc under uniform load

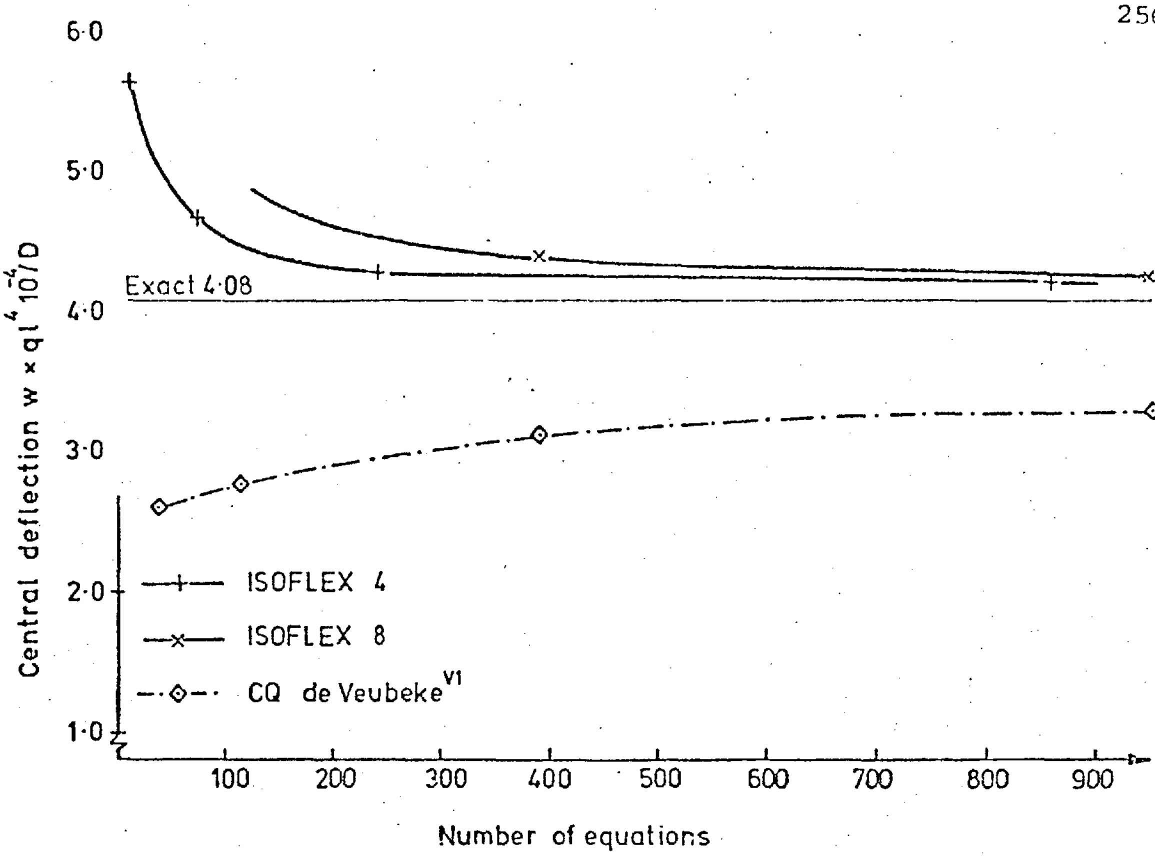

Fig 3·42 Convergence of central deflection for acute skew rhombic plate under uniform load.

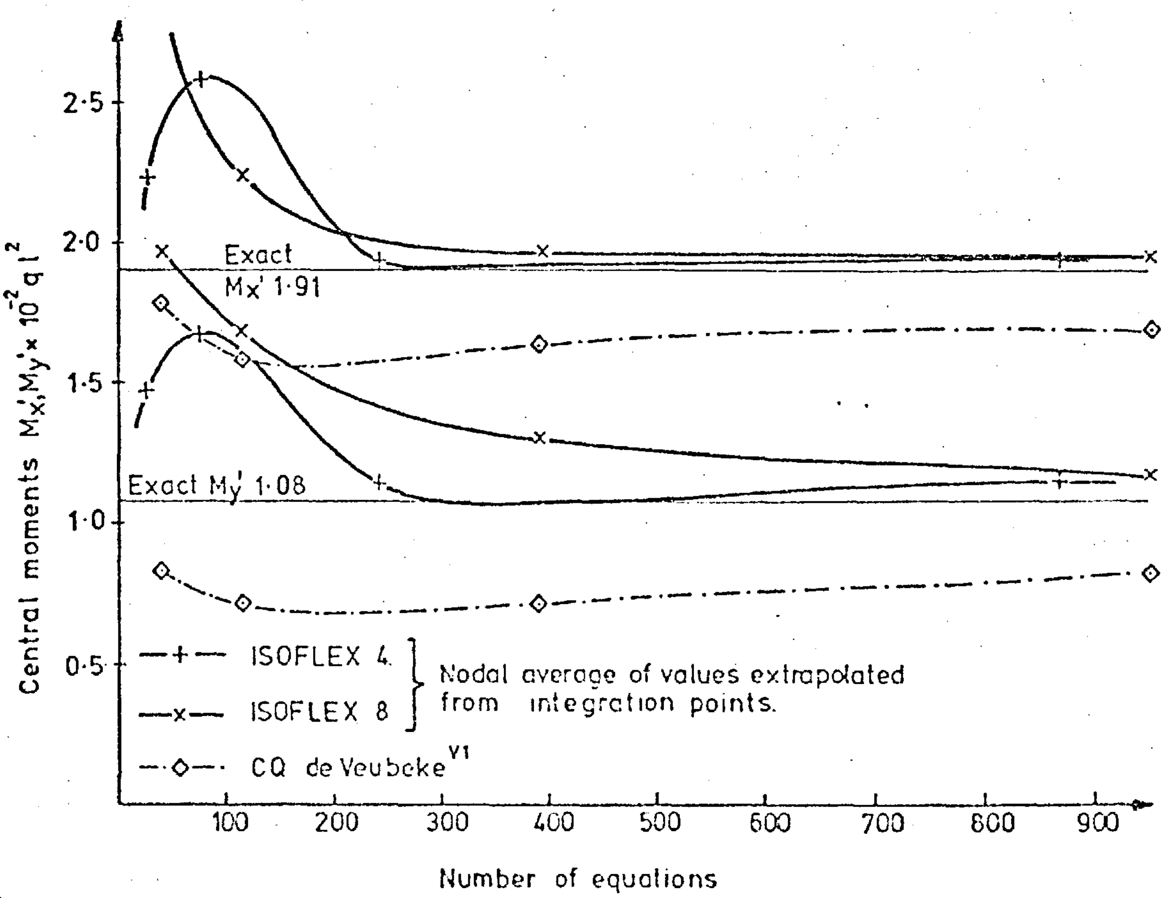

Fig 3·43 Convergence of principal moments for acute skew rhombic plate under uniform load

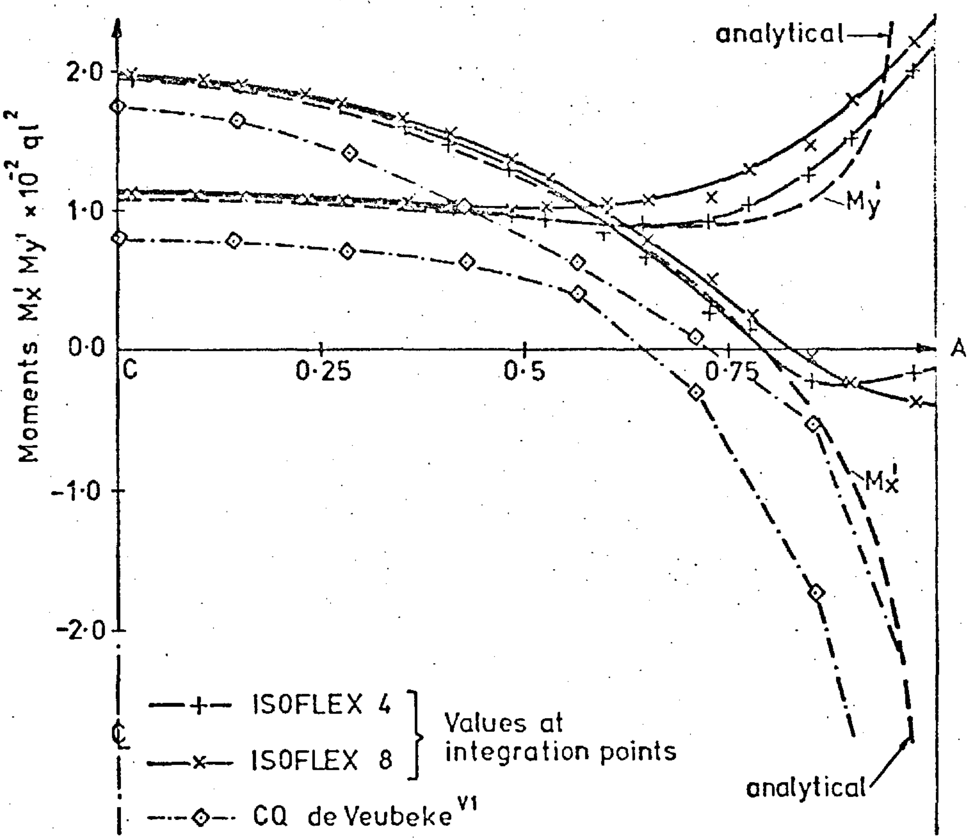

Fig 3·44 Principal moments M_x' M_y' from centre to obtuse corner of acute skew rhombic plate. 16×16 Mesh

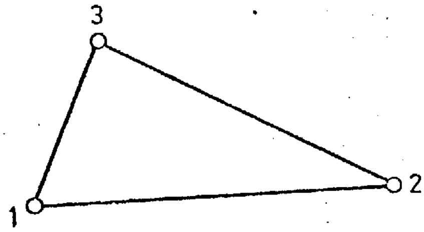

ISOBEAM 3.

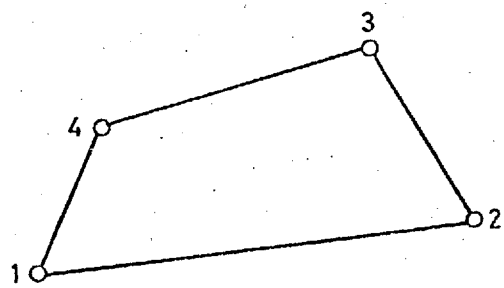

ISOBEAM 4.

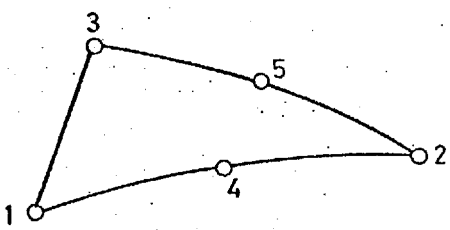

ISOBEAM 5.

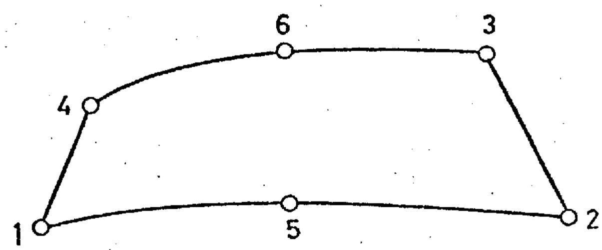

ISOBEAM 6.

Nodal variables $\quad \delta_i = \left\{ \begin{matrix} u \\ u \\ w \\ \theta_x \\ \theta_y \\ \theta_z \end{matrix} \right\}_i = \left\{ \begin{matrix} v \\ v \\ w \\ \frac{\partial w}{\partial y} \\ \frac{\partial w}{\partial x} \\ \frac{\partial v}{\partial x_\xi} \end{matrix} \right\}_i$ for corner nodes of extensional-flexural elements †

$\delta_i = \left\{ \begin{matrix} u \\ v \\ \frac{\partial v}{\partial x_\xi} \end{matrix} \right\}_i$ for corner nodes of extensional elements†

$\delta_i = \left\{ \Delta u' \right\}_i$ for midside nodes along edge direction

† Note $\frac{\partial v}{\partial x_\xi}$ becomes $\frac{\partial v}{\partial x}$ for the triangles.

Fig 4·1 The ISOBEAM family and nodal configurations

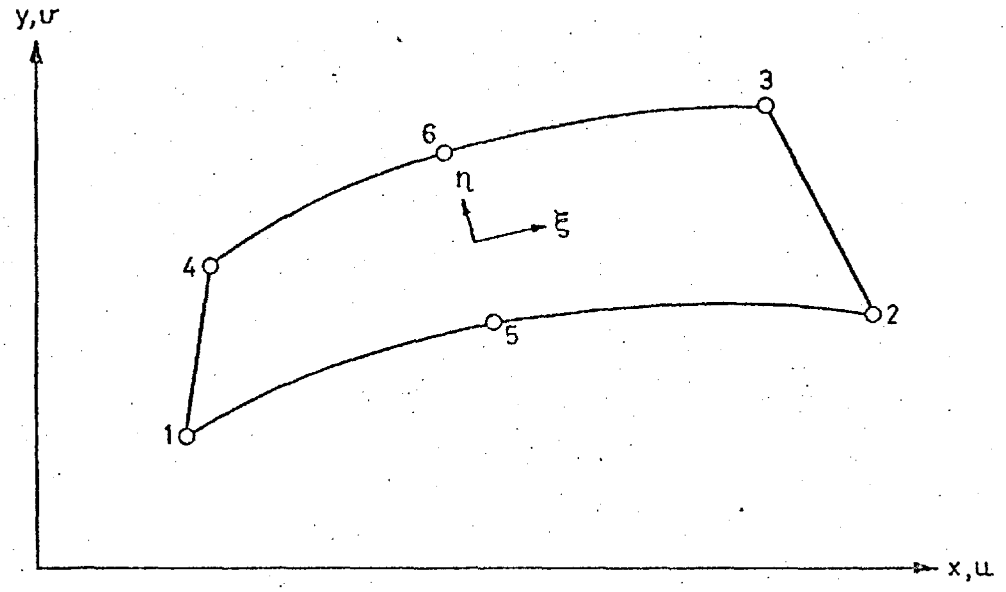

Nodal variables $\delta_i = \begin{Bmatrix} u \\ v \\ \dfrac{\Delta \partial v}{\partial x_\xi} \end{Bmatrix}_i$ for corner nodes

$\delta_i = \begin{Bmatrix} \Delta u \\ \Delta v \\ \dfrac{\Delta \partial v}{\Delta \partial x_\xi} \end{Bmatrix}$ for midside nodes

Fig 4·2 Unconstrained element nodal configuration and coordinate systems

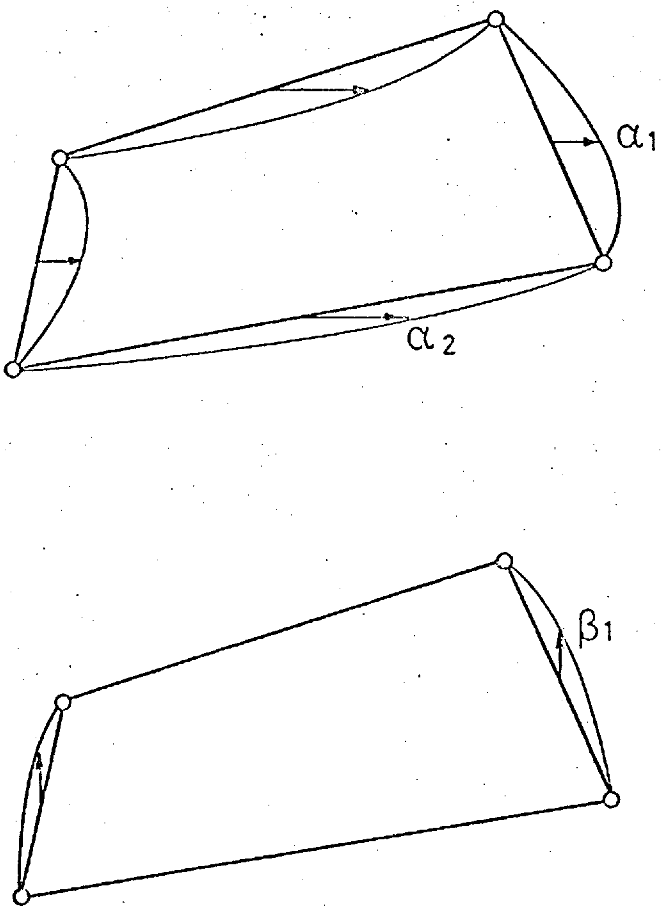

Fig 4.3 Incompatible displacement modes

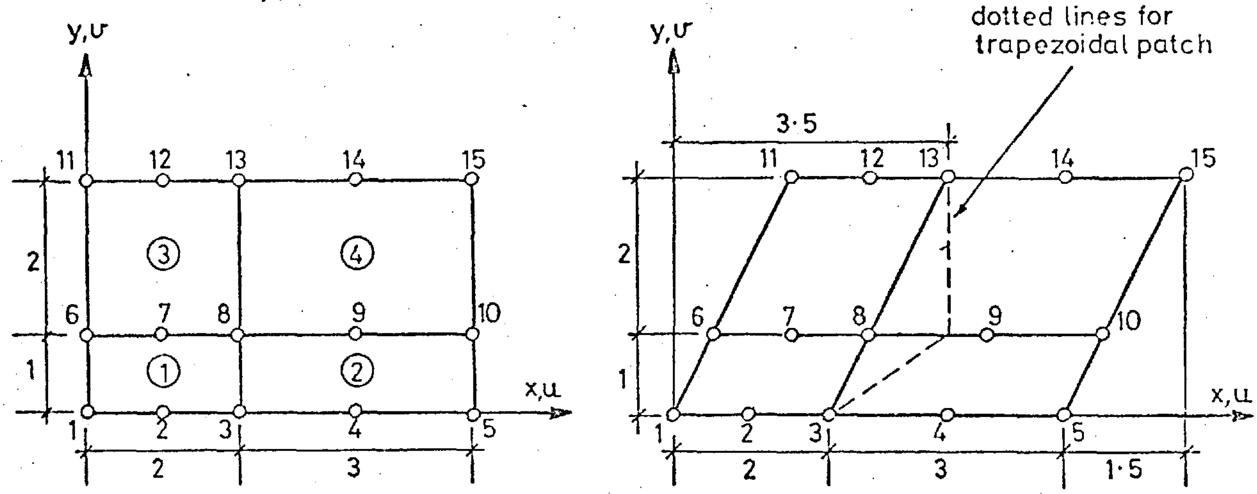

(i) RECTANGULAR PATCH

(ii) PARALLELOGRAM AND TRAPEZOIDAL PATCH

Assumed displacement field

$$u = 1 + 2x + y$$
$$\upsilon = 3 + 5x + 7y$$

Constant strain state

$$\varepsilon_x = 2,\ \varepsilon_y = 7,\ \varepsilon_{xy} = 6$$

Constant stress state with $E = 3000$ $\nu = 0{\cdot}3$

$$\begin{Bmatrix} \sigma_x \\ \sigma_y \\ \sigma_{xy} \end{Bmatrix} = \begin{bmatrix} 3296{\cdot}7 & & 989{\cdot}0 & 0 \\ 989{\cdot}0 & & 3296{\cdot}7 & 0 \\ 0 & 0 & 0 & 1154 \end{bmatrix} \begin{Bmatrix} 2 \\ 7 \\ 6 \end{Bmatrix} = \begin{Bmatrix} 0{\cdot}135165 \times 10^5 \\ 0{\cdot}250549 \times 10^5 \\ 0{\cdot}692308 \times 10^4 \end{Bmatrix}$$

Displacements at node number 8

Rectangle	$u = 6$	$\upsilon = 20$	$\frac{\partial \upsilon}{\partial x} = 5$
Parallelogram	$u = 7$	$u = 22{\cdot}5$	$\frac{\partial \upsilon}{\partial x} = 5$
Trapezium	$u = 9$	$\upsilon = 27{\cdot}5$	$\frac{\partial \upsilon}{\partial x} = 5$

Fig 4·4 Extensional patch test

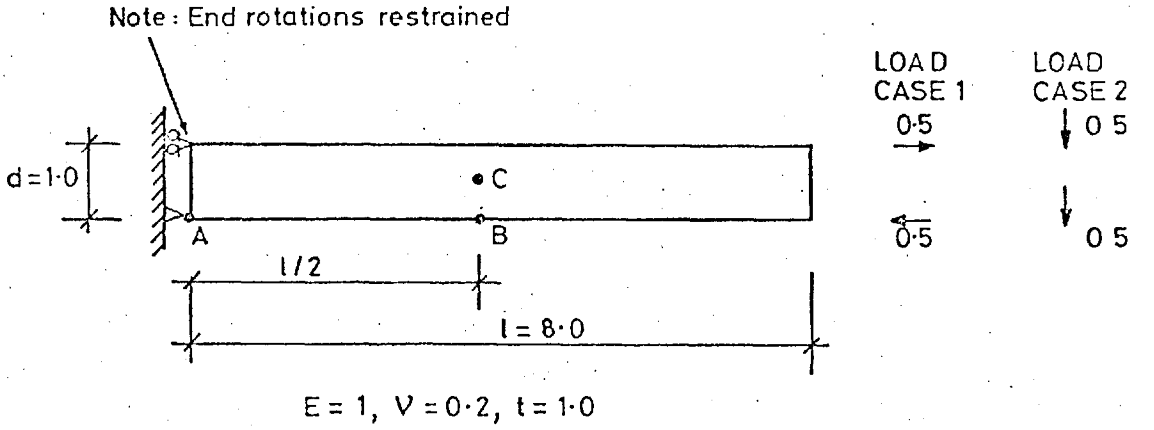

Fig 4·5 Straight cantilever beam

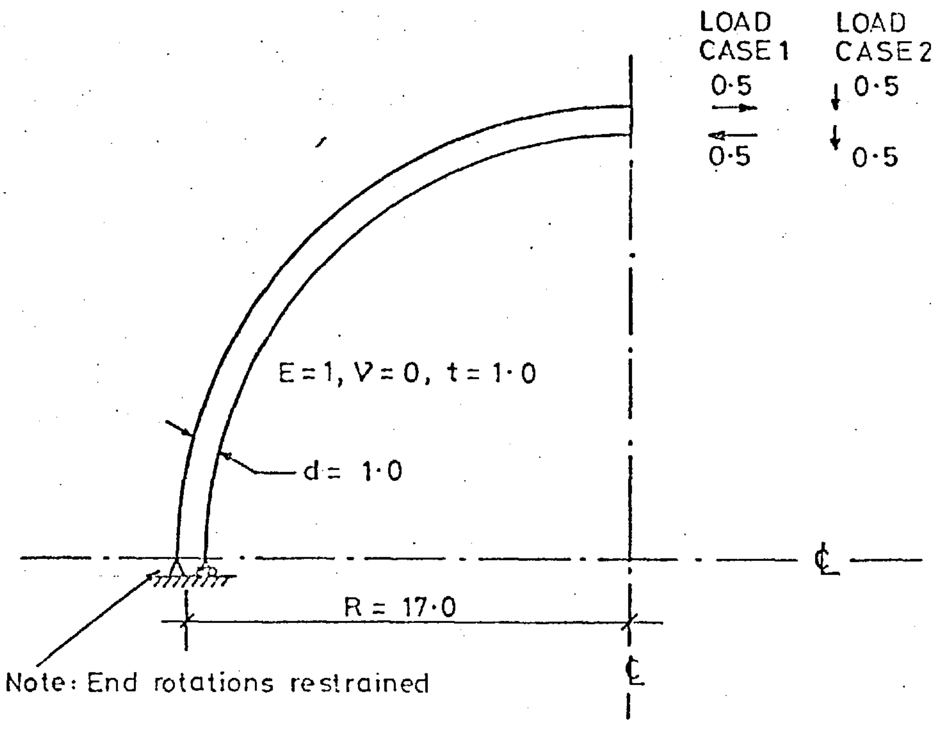

Fig 4·6 Curved cantilever beam

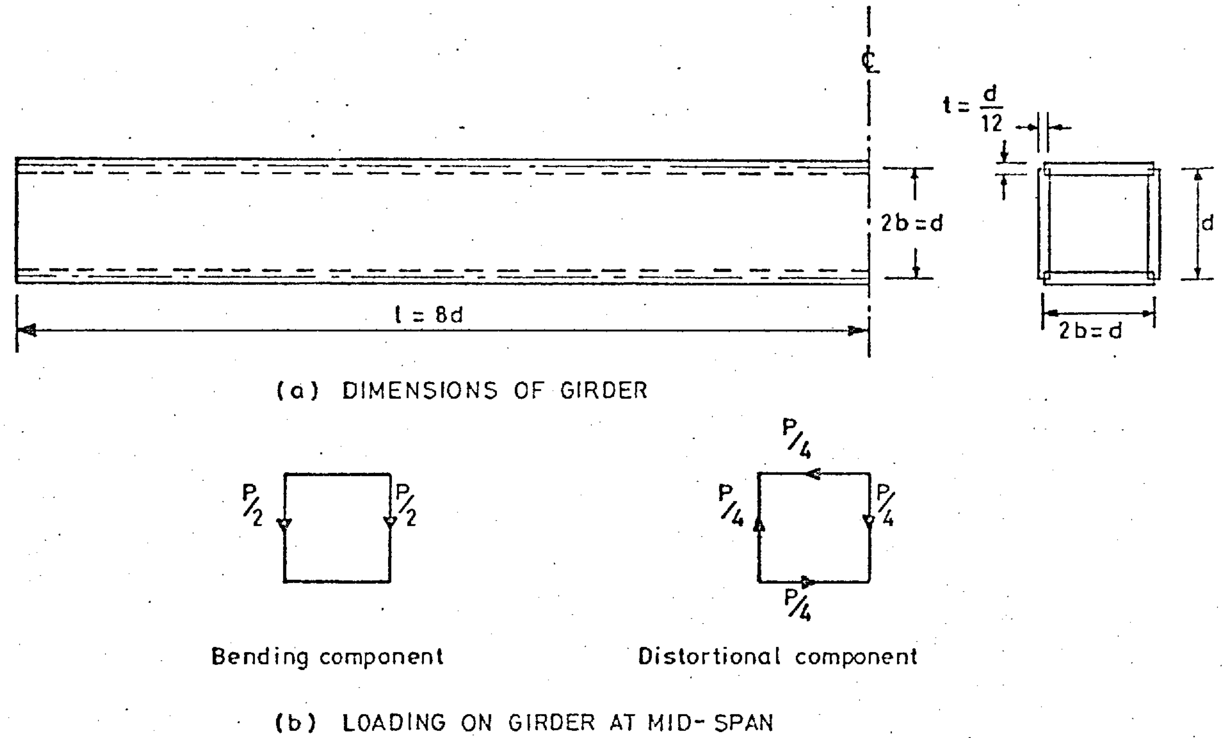

Fig 4·7 Straight single cell box girder
Details of girder ($\nu = 0{\cdot}2$) and loading

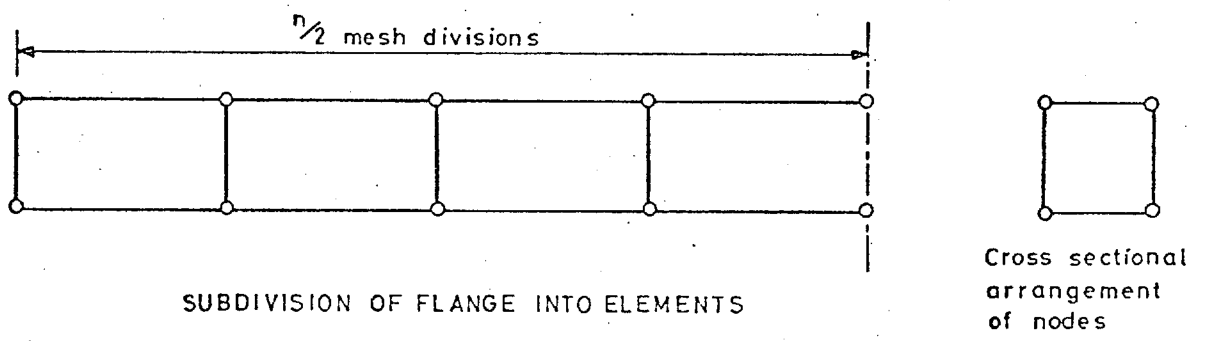

Fig 4·8 Straight single cell box girder
Finite element idealization

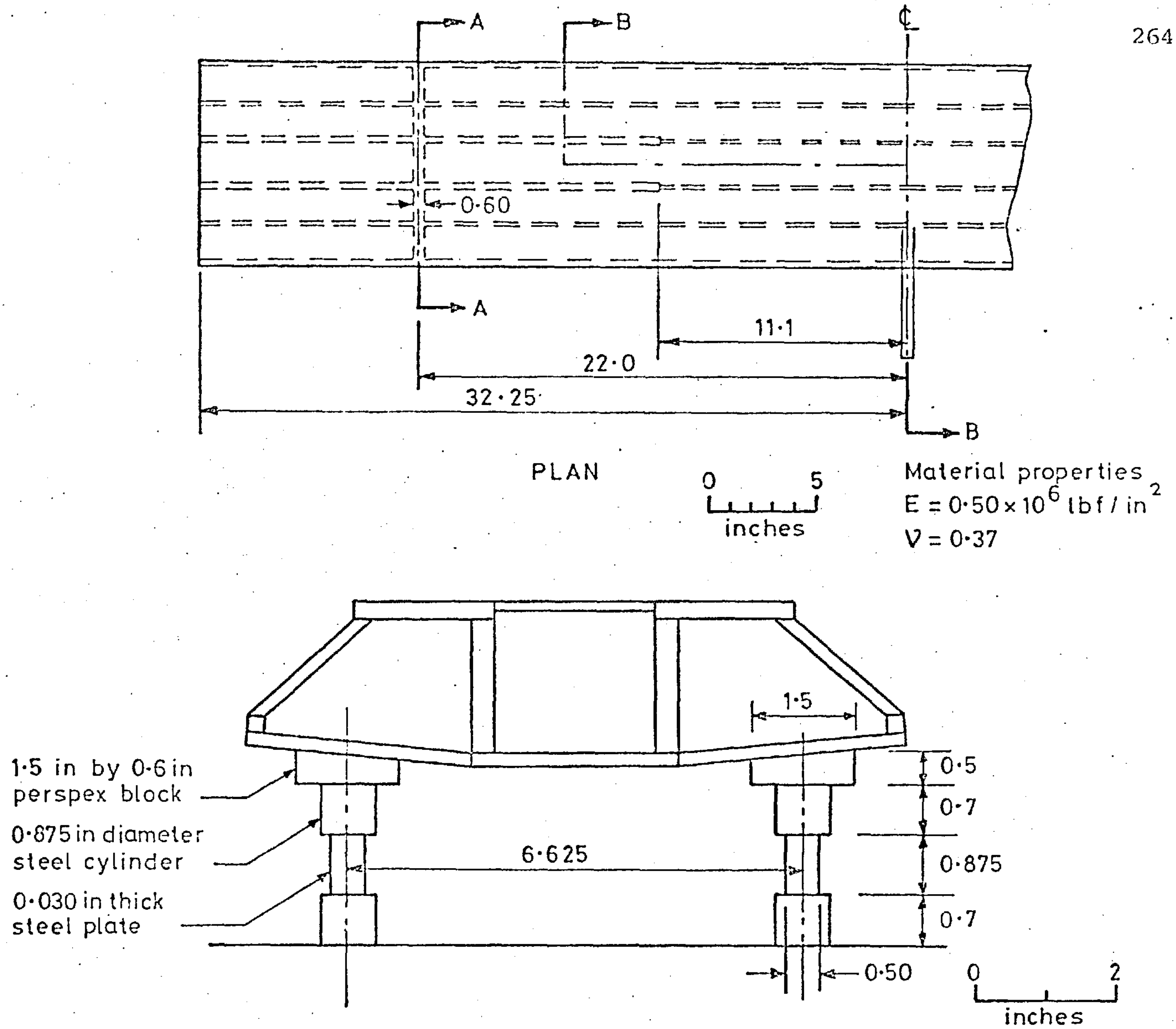

SECTION A – A SHOWING GENERAL ARRANGEMENT OF SUPPORT SYSTEM

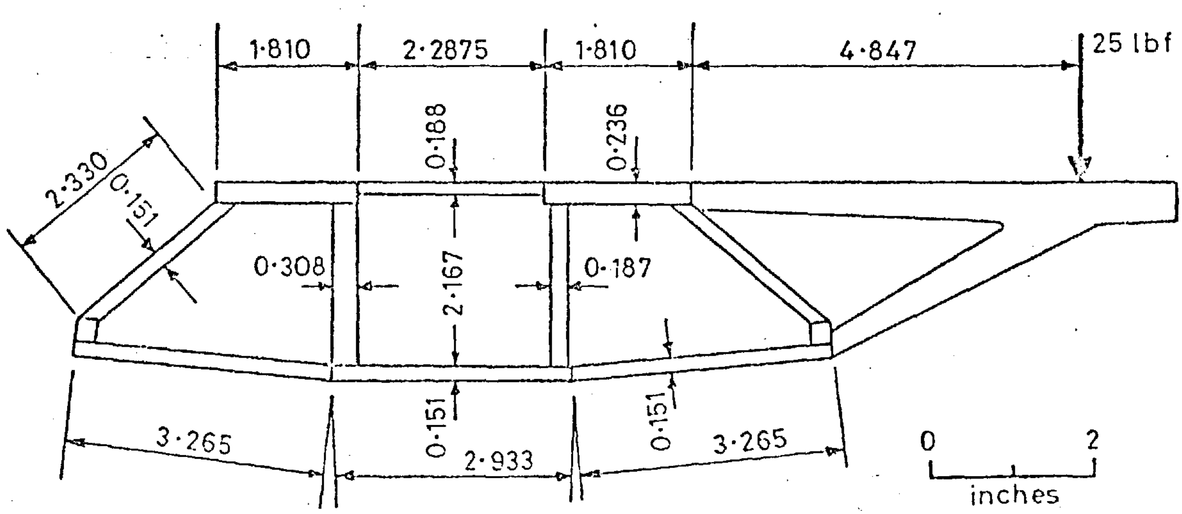

SECTION B – B

Fig 4·9 Straight three cell box girder bridge model. Details of mode and loading.

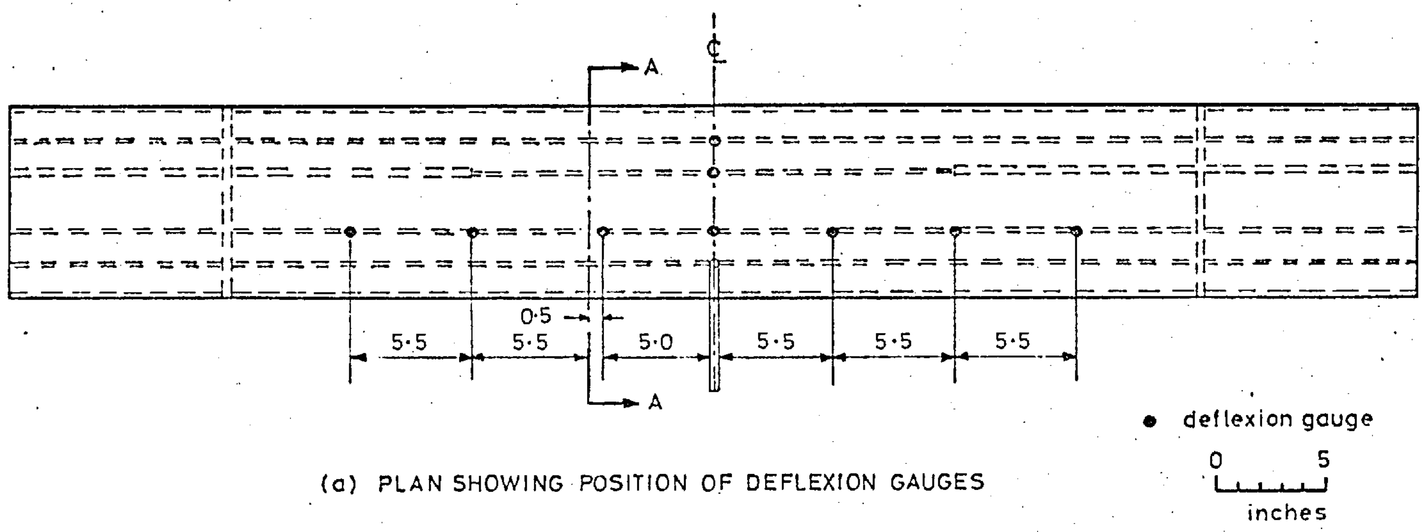

(a) PLAN SHOWING POSITION OF DEFLEXION GAUGES

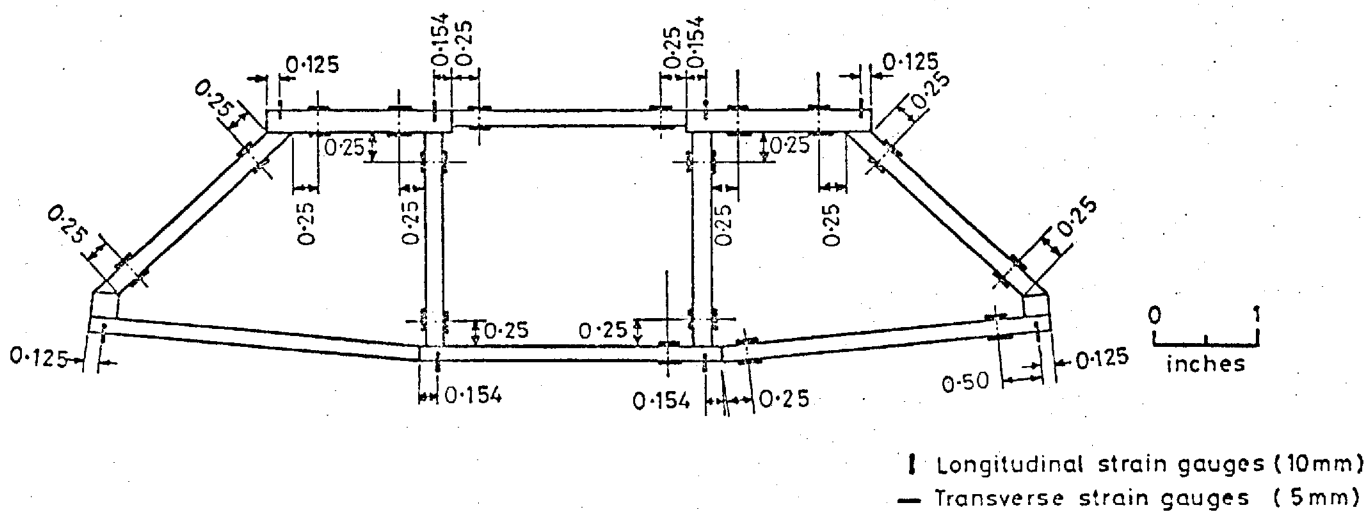

(b) SECTION A-A SHOWING POSITION OF STRAIN GAUGES

Fig 4·10 Straight three cell box girder bridge model. Instrumentation of model

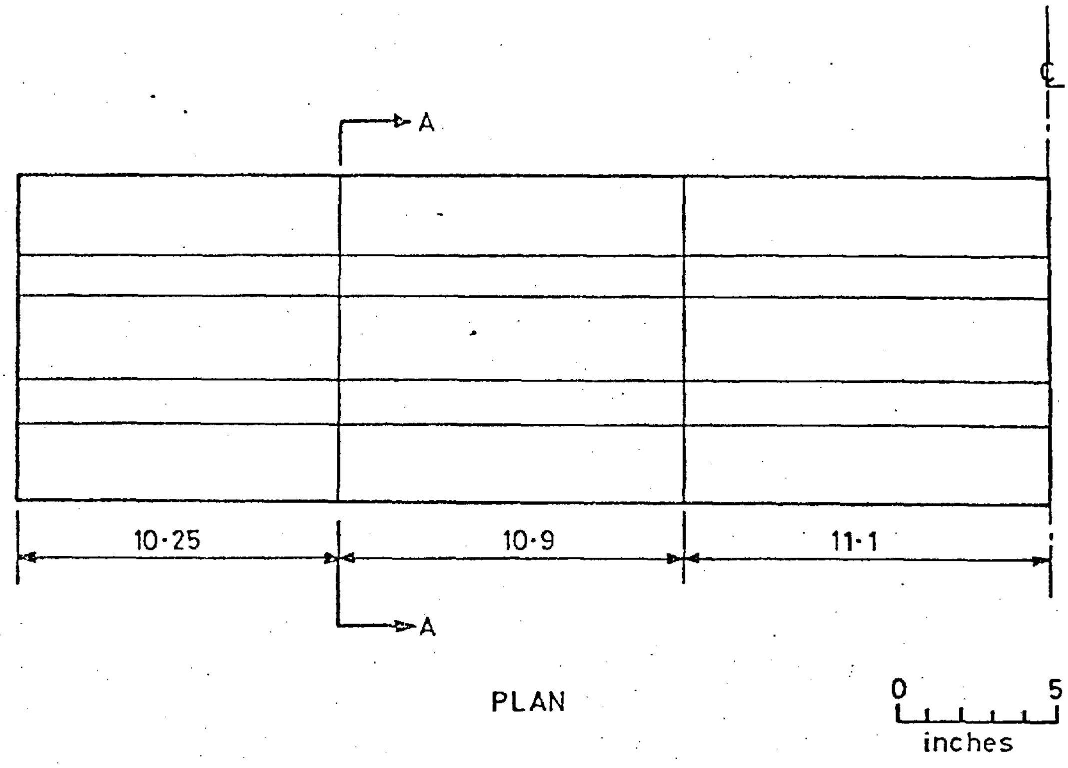

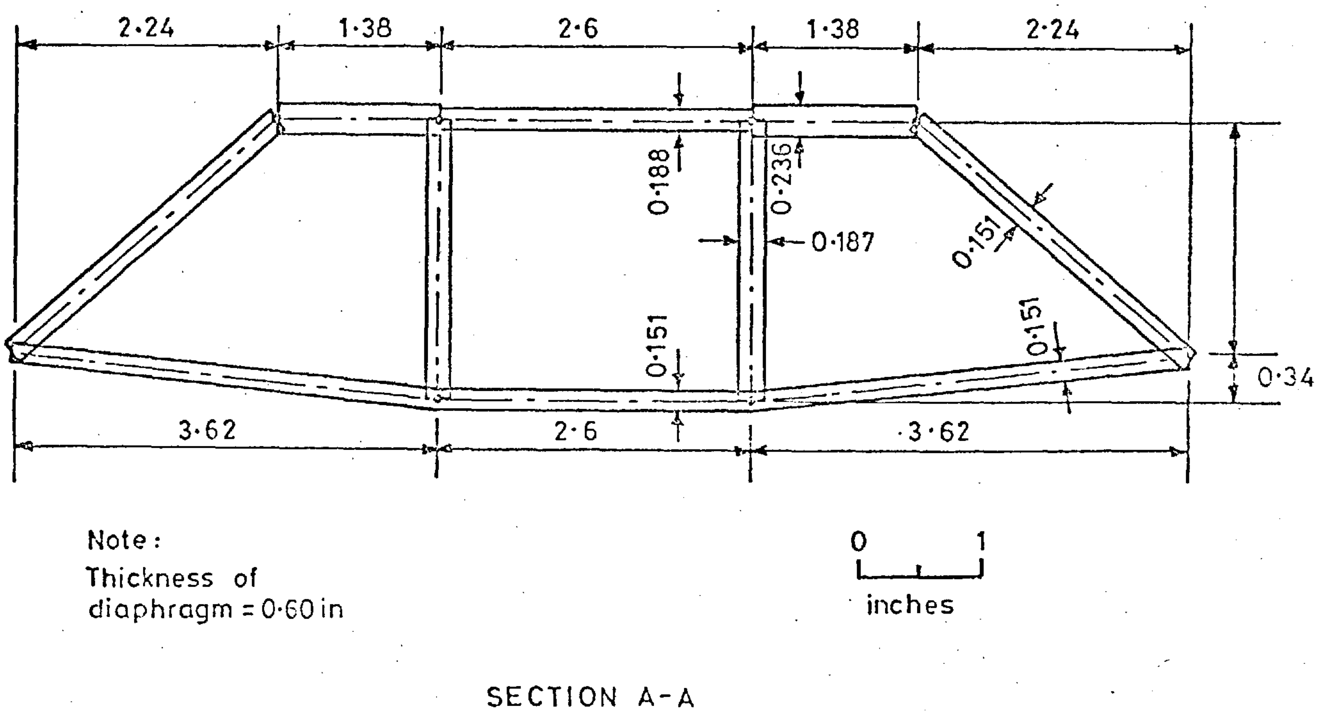

Fig 4·11 Straight three cell box girder bridge model. Finite element idealization

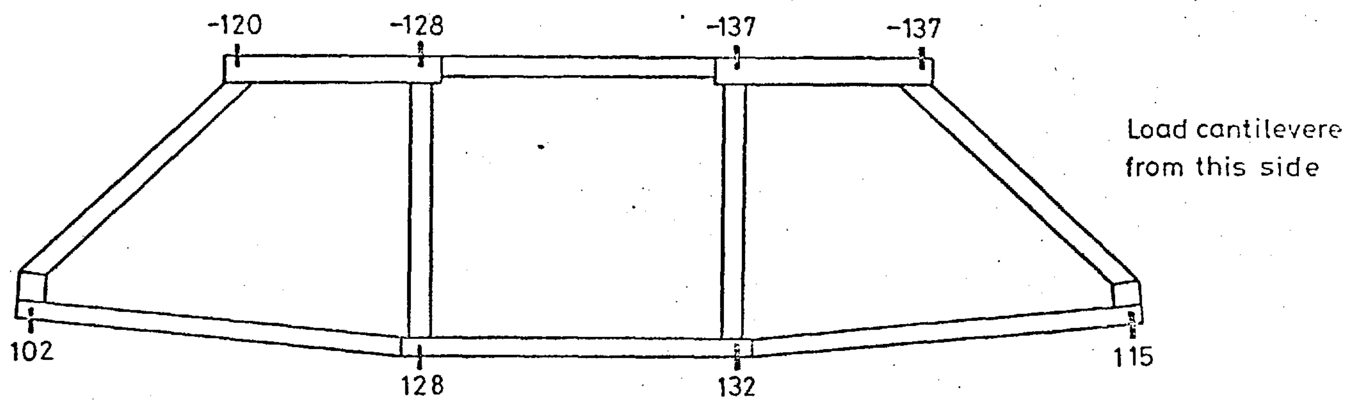

(a) LONGITUDINAL STRAINS ($\times 10^{-6}$)

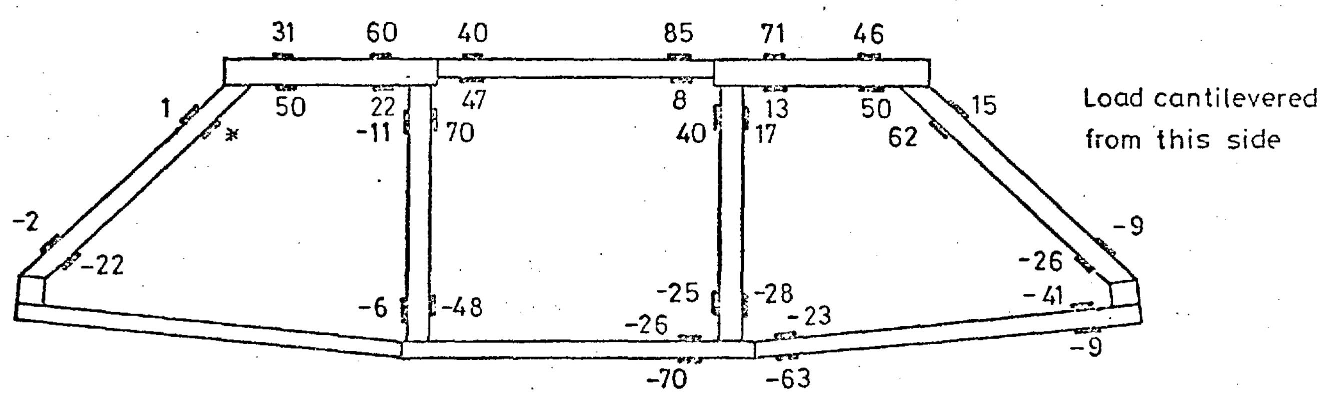

* bad reading

TRANSVERSE STRAINS ($\times 10^{-6}$)

Fig 4·12 Straight three cell box girder bridge model.
Experimental values of strain at section AA
for model under eccentric point load at mid-span

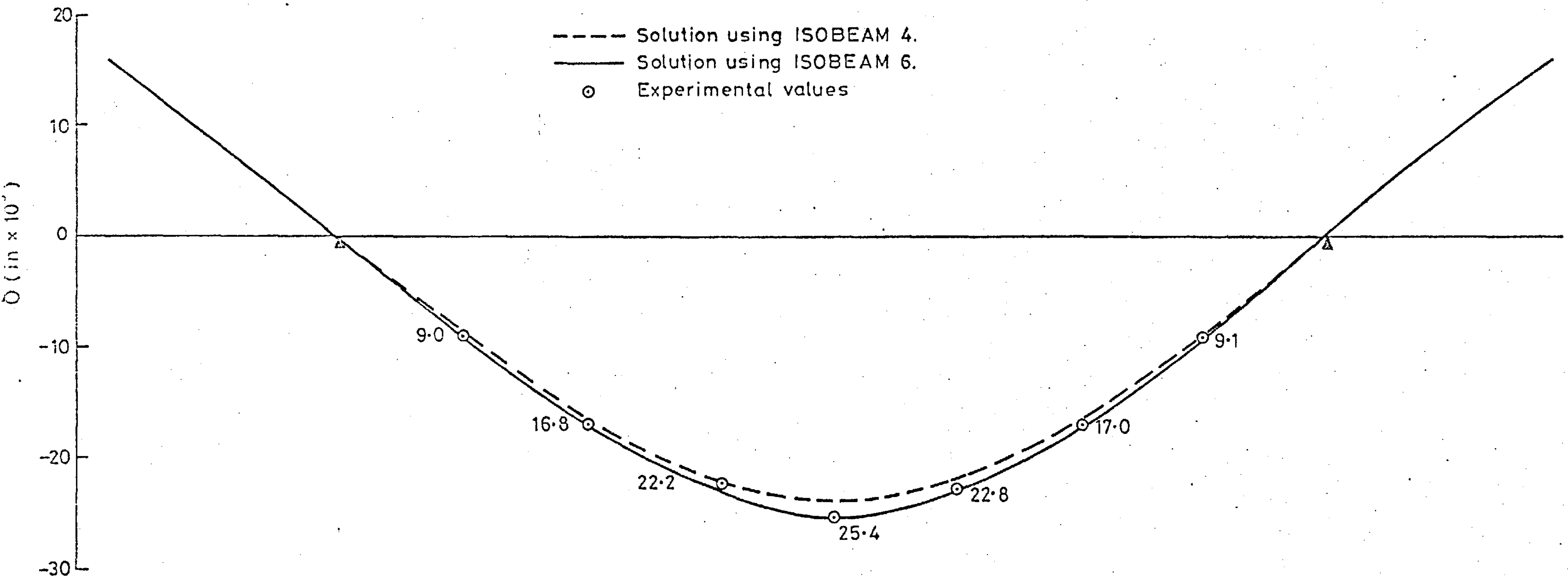

Fig.4·13 Straight three cell box girder bridge model. Longitudinal deflection profile along top of vertical web nearer load for model under eccentric point load at mid-span.

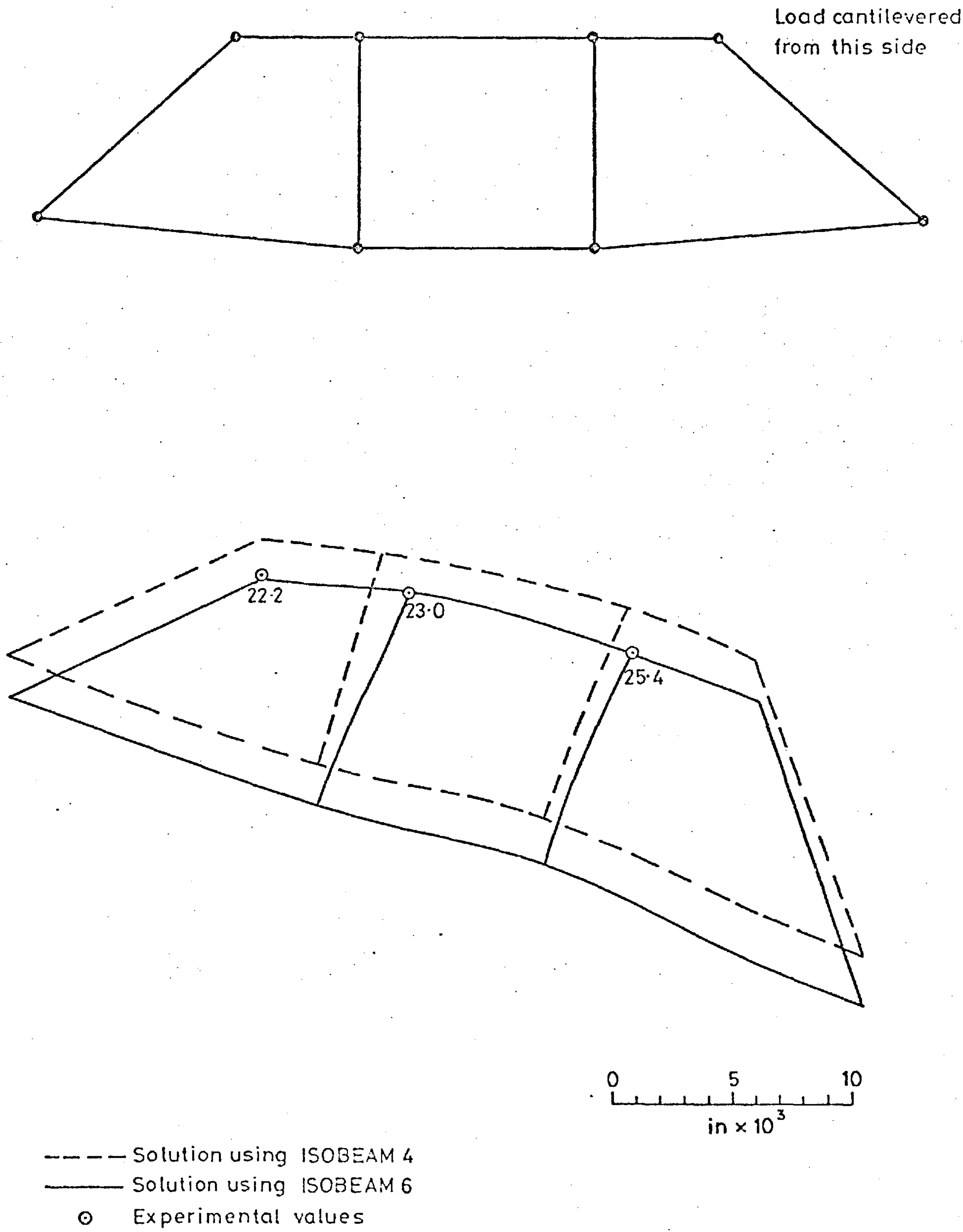

Fig 4·14 Straight three cell box girder bridge model. Displacements at centre cross-section for model under eccentric point load at mid-span

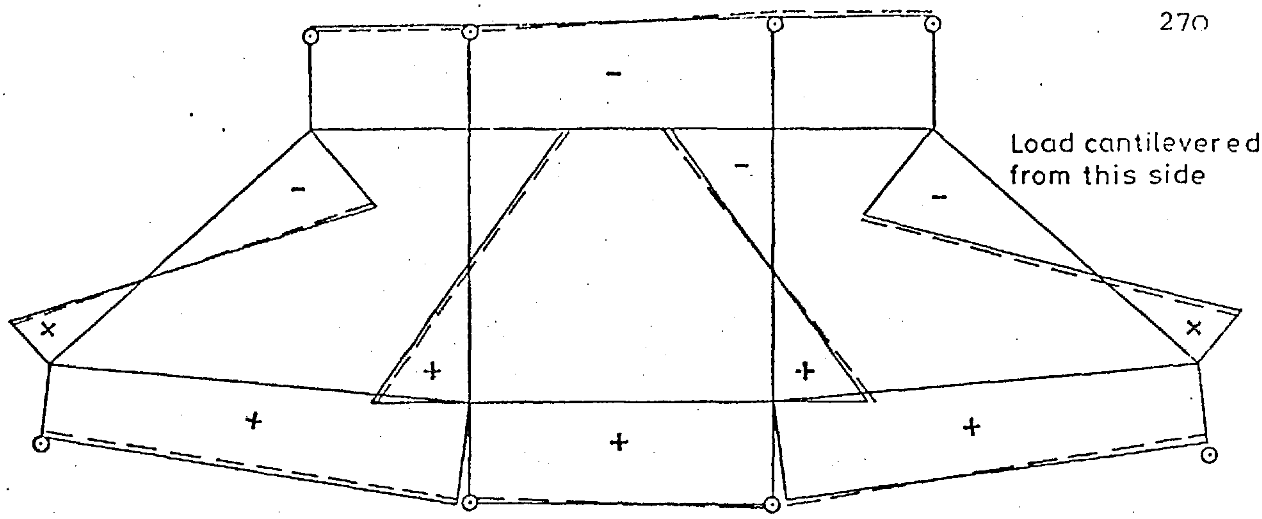

(a) LONGITUDINAL OUTER SURFACE STRAINS

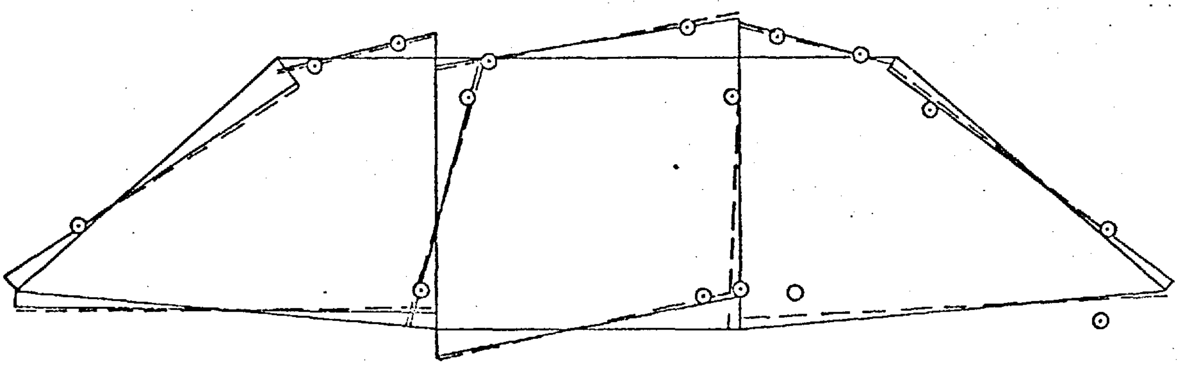

(b) TRANSVERSE FLEXURAL STRAINS

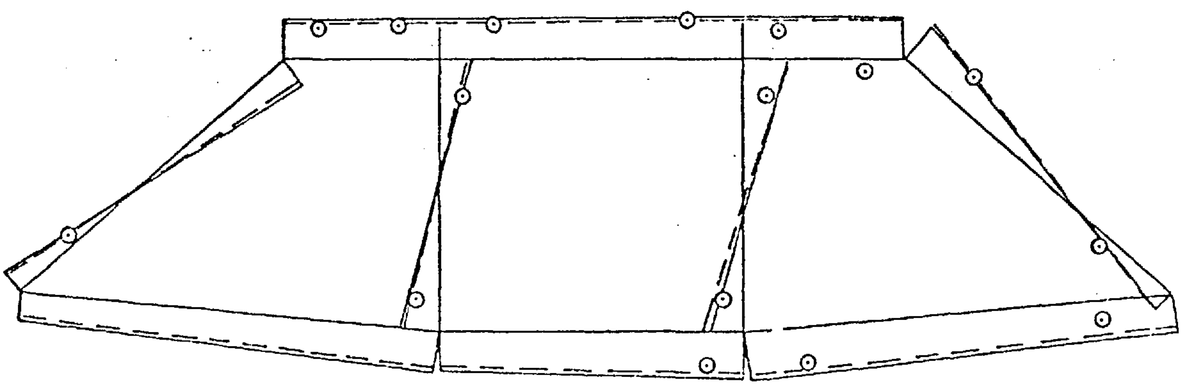

(c) TRANSVERSE EXTENSIONAL STRAINS

Fig 4·15 Straight three cell box girder bridge model.
Distribution of strains at section 5·5in from mid-span
for model under eccentric point load at mid-span.

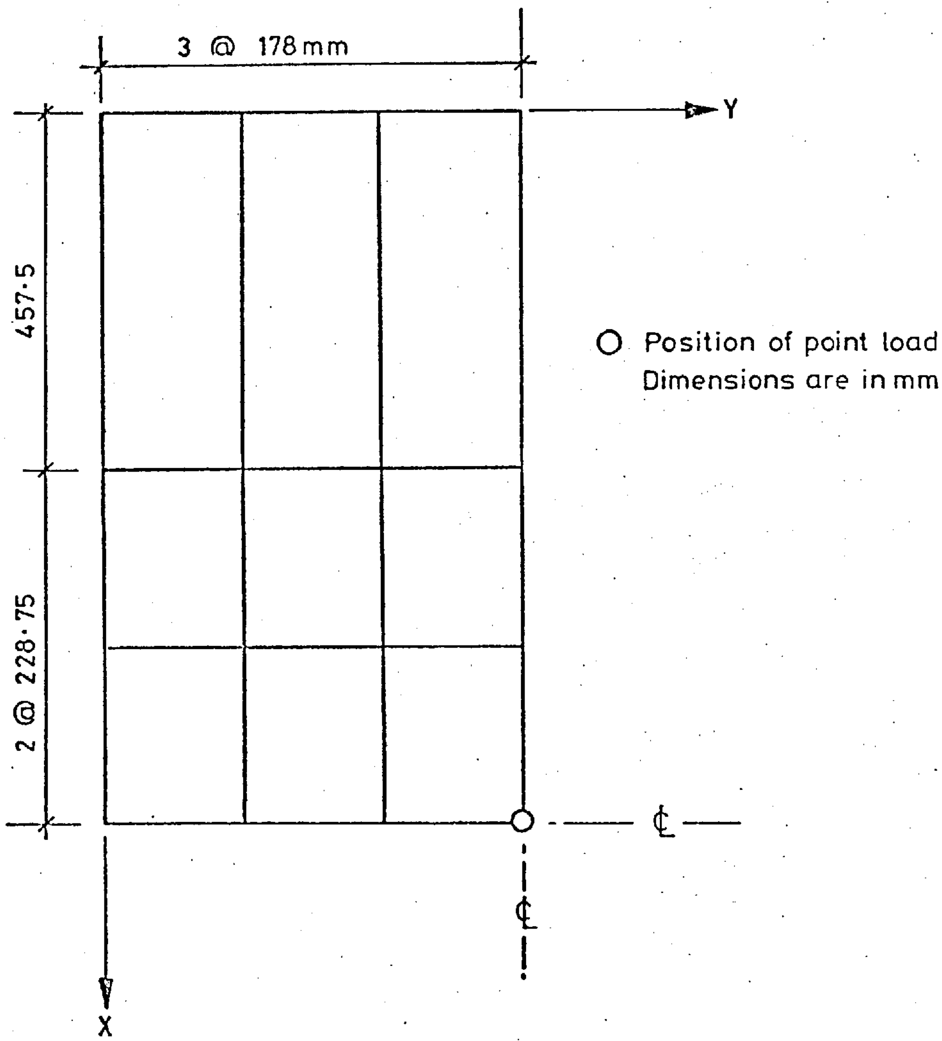

Fig 4·16 Straight multicell bridge model.
Coarse finite element idealization

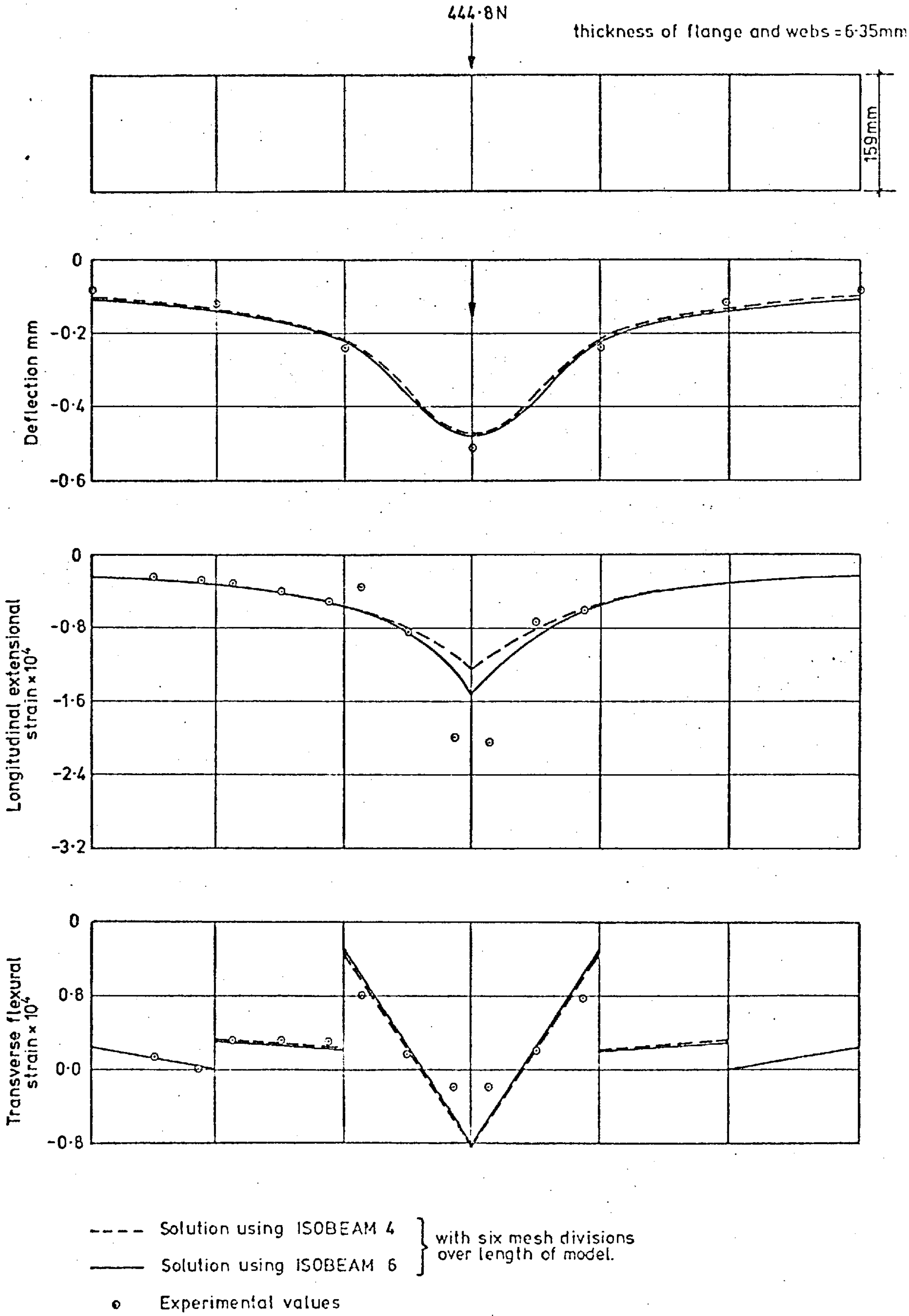

Fig. 4·17 Straight multicell bridge model. Displacements and strains at centre cross-section for model under point load at centre.

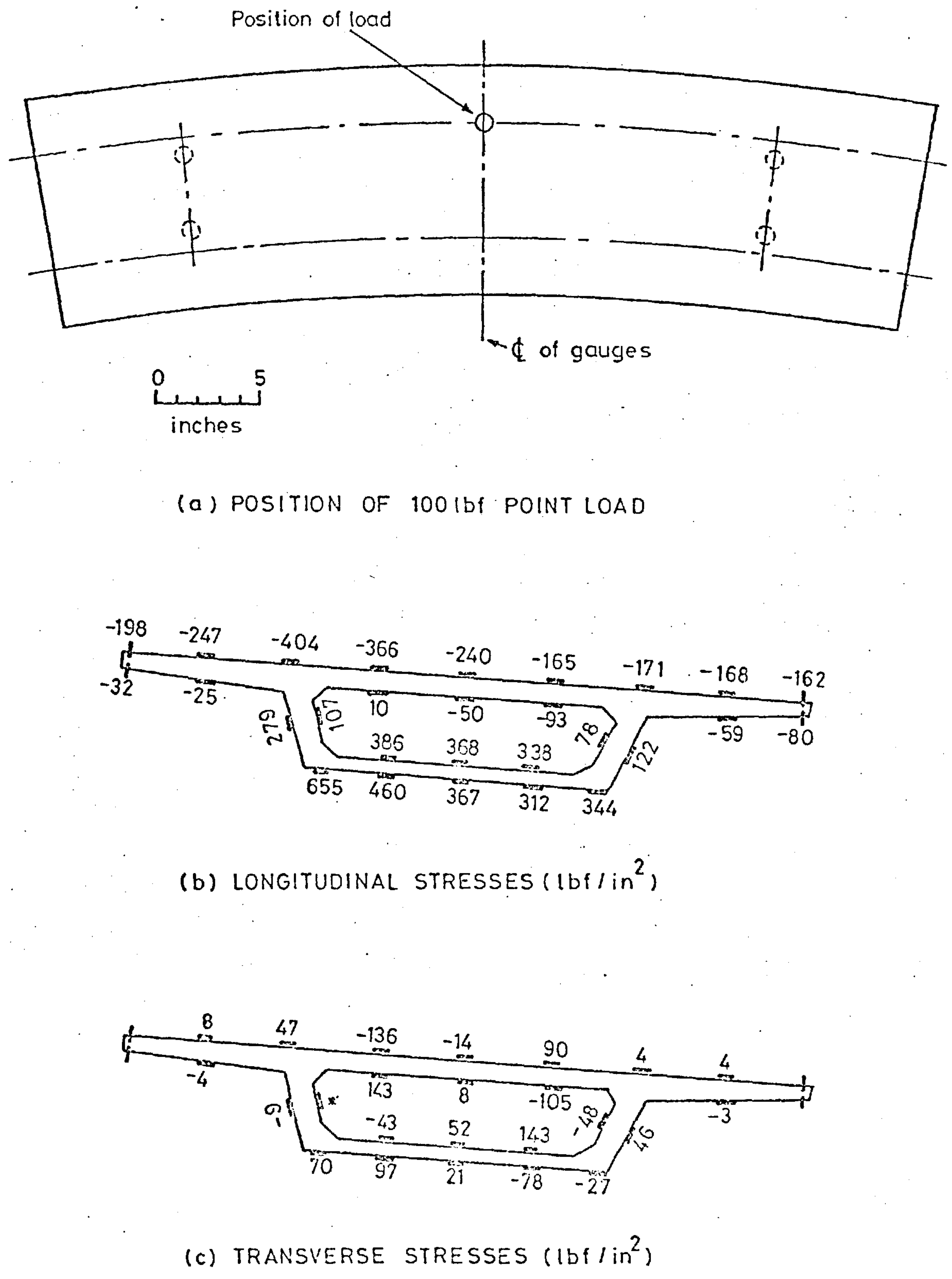

Fig 4·18 Curved single cell box girder bridge model.
Experimental values of stress at centre section
for model under eccentric point load at mid-span

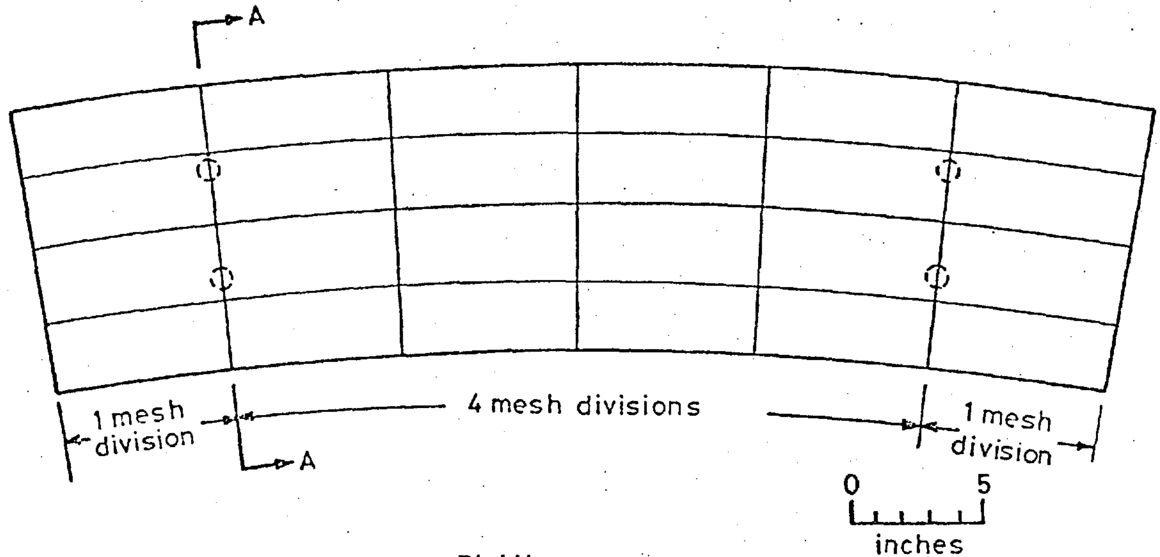

PLAN

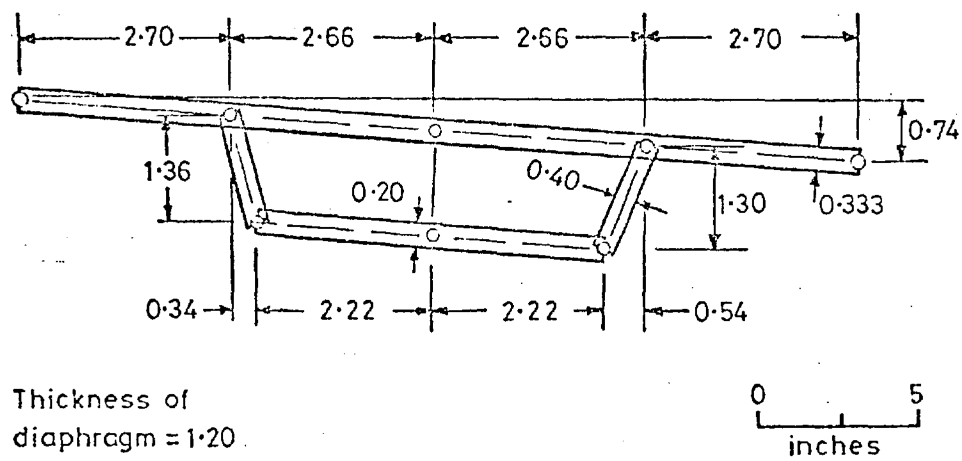

SECTION AA

Fig 4·19 Curved single cell box girder bridge model.
Finite element idealization (n × 3 × 1 mesh)

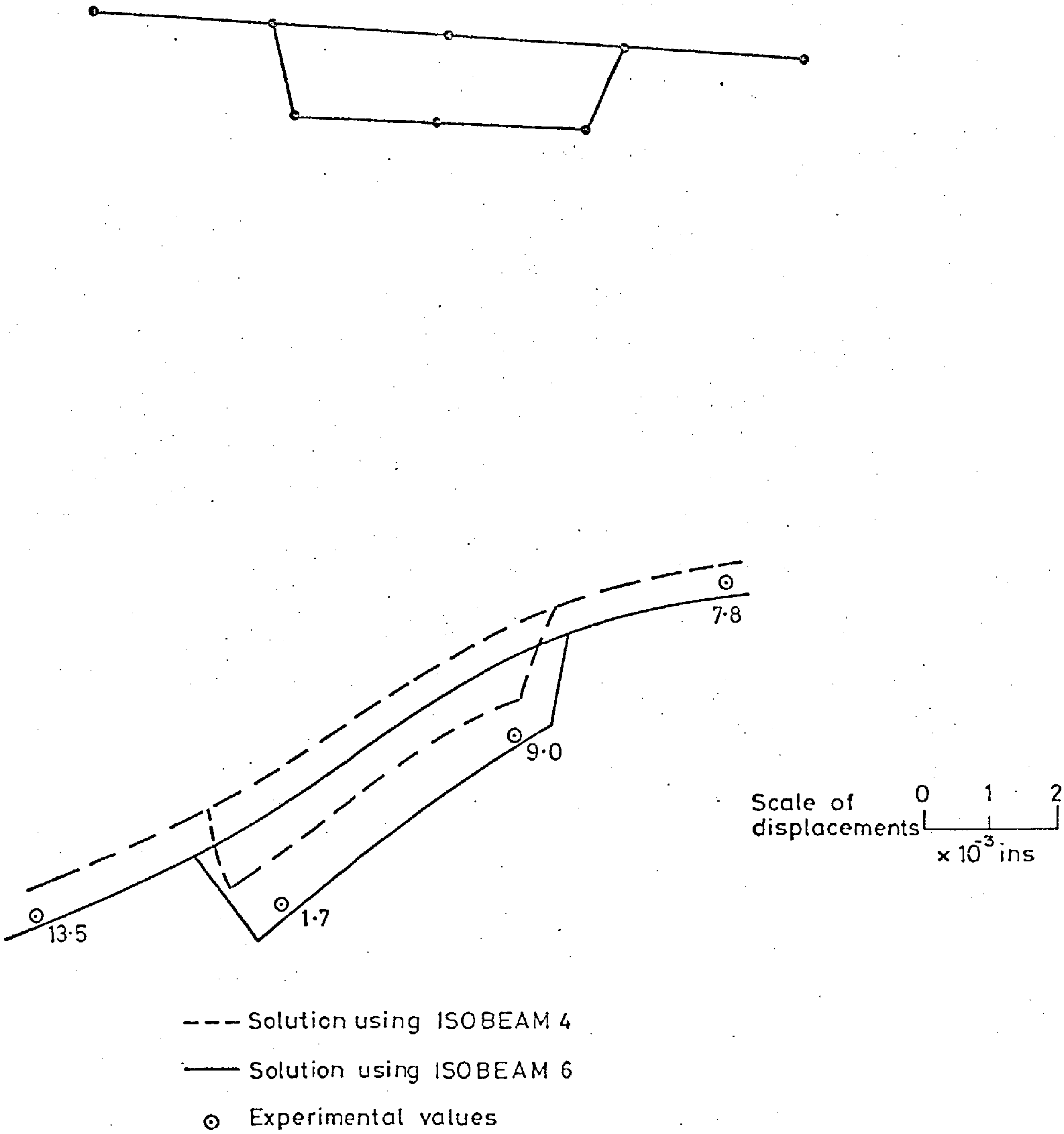

Fig 4·20 Curved single cell box girder bridge model. Displacements at centre cross-section for model under eccentric point load at mid-span

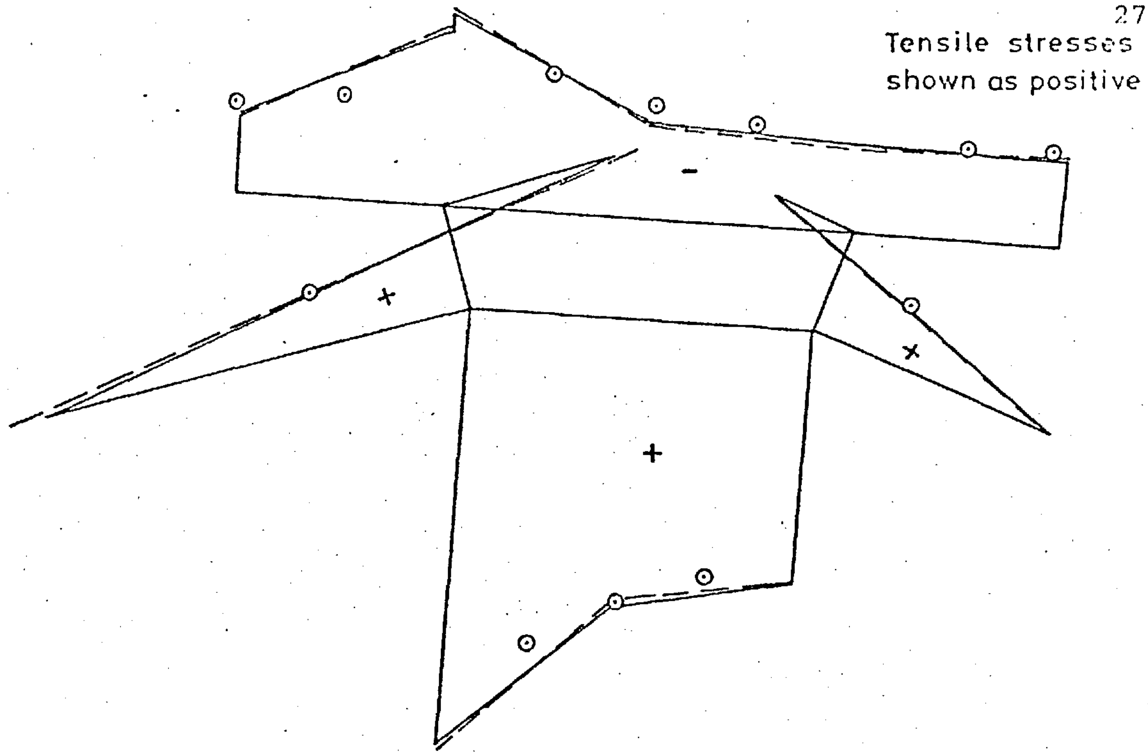

(a) DISTRIBUTION OF LONGITUDINAL EXTENSIONAL STRESSES

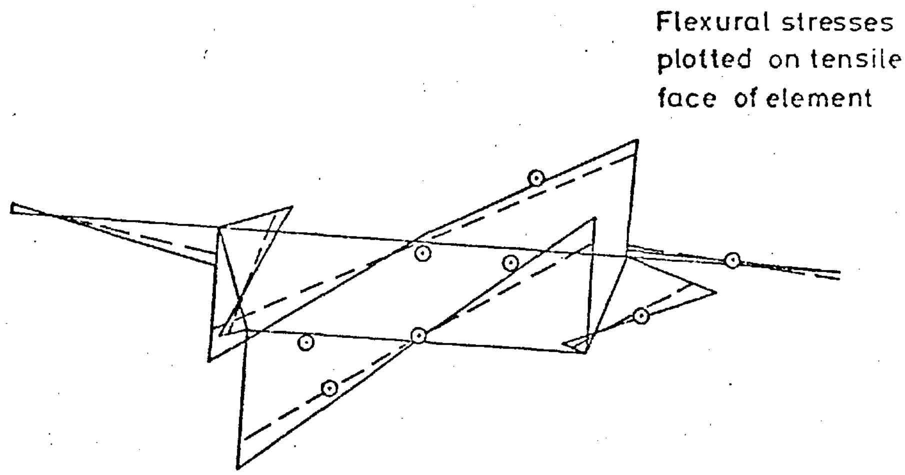

(b) DISTRIBUTION OF TRANSVERSE FLEXURAL STRESSES

---- Solution using ISOBEAM 4. (For (a) values of mid-points of longitudinal sides of elements were extrapolated, and averaged where appropriate. For (b) nodal values were averaged where appropriate)

—— Solution using ISOBEAM 6.

⊙ Experimental values

Scale of stresses 0 200 lbf/in²

Fig 4·21 Curved single cell box girder bridge model.

Distribution of stresses at centre cross-section

… der eccentric point load at mid-span

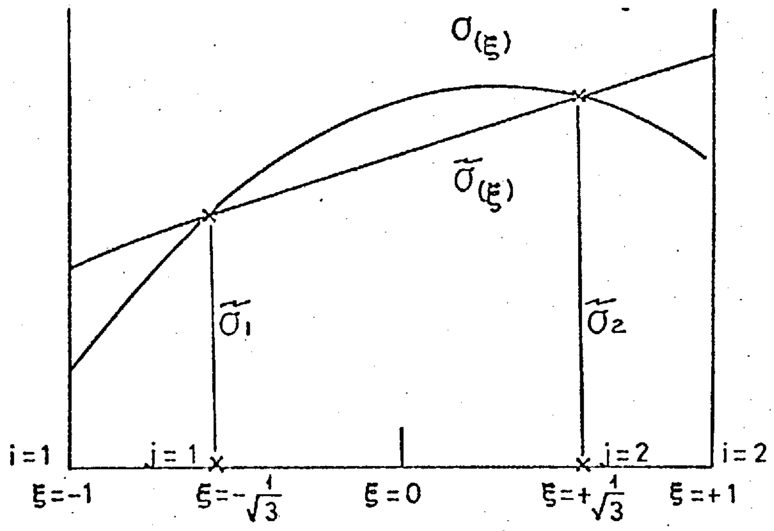

Fig. A 2·1 Smoothed and unsmoothed stress distribution for a 1-D parabolic element

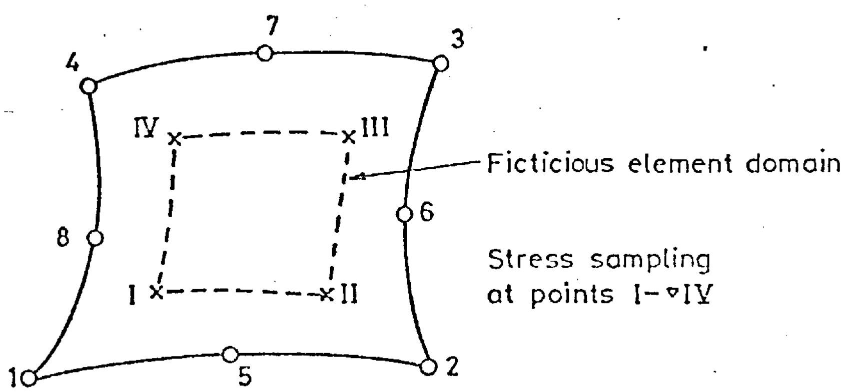

Fig. A 2·2 Stress sampling points for a parabolic quadrilateral and ficticious element domain